**STELLINGEN**

Behorend bij de dissertatie

Hydrodynamische interactie tussen vloeistofstroming en oscillerende slanke cilinders
door M. Shafiee-Far

1.  De mensheid zou beter af zijn wanneer ieder zich aan de volgende twee regels zou houden - hier letterlijk vertaald uit de originele bronnen:
    "Ik geef de voorkeur aan verhoging van kennis boven intensievere aanbidding"
    (Profeet Mohammed (sws))
    "De mate van iemands superioriteit staat in verhouding tot zijn kennis en wijsheid"
    (Imam Ali Ibn Abi-Talib (as))

2.  Hoewel we het vijftig-jarige bestaan van de offshore technologie vieren, is de offshore industrie nog jong!

3.  Hoewel er veel theoretisch en experimenteel onderzoek is gedaan teneinde de vragen omtrent hydrodynamische interactie te beantwoorden, blijft het probleem onopgelost. De situatie kan vergeleken worden met een leger arbeiders die bezig zijn in het duister een muur te bouwen. Hoewel iedere arbeider zijn best doet, wordt er een onverwachte vorm zichtbaar wanneer het licht wordt.

4.  De meeste studies gewijd aan de interactie tussen een vloeistof en vaste materie richten zich op specifieke gevallen van interactie, met een eigen mathematische en fysische wijze van modellering. Er is een meer algemene benadering nodig.

5.  Directe analyses van de data (onafhankelijk van een bepaald belastingmodel) laten zien dat een correct belastingmodel om de hydrodynamische kracht ten gevolge van interactie te voorspellen alle snelheidscomponenten en combinaties van snelheden moet bevatten; de aanname van onafhankelijke snelheidsvelden kan niet tot een juiste oplossing leiden.

6.  Een vergelijking tussen computersimulaties van hydrodynamische krachten en gemeten waarden laat zien dat een model gebaseerd op het concept van relatieve snelheid de hydrodynamische interactie van een cilinder met een gecombineerd snelheidsveld veel beter beschrijft dan een model gebaseerd op het concept van onafhankelijke snelheidsvelden.

7.  In een gecombineerd snelheidsveld is er geen enkele parameter waarmee de hydrodynamische coëfficiënten gecorreleerd zouden kunnen worden zonder de behoefte aan andere parameters. Dimensieloze parameters gebaseerd op de relatieve snelheid meer beter geschikt om hydrodynamische coëfficiënten weer te geven dan de parameters die zijn gerelateerd aan individuele componenten van stroming en beweging.

8.  Bij dynamische analyses van offshore constructies worden, ter wille van een efficiënte berekeningswijze, lineaire belastingmodellen verkozen boven niet-lineaire modellen. Het meenemen van niet-lineariteiten verbetert het resultaat niet altijd. Onder de meeste stromingscondities kan een gelineariseerde versie van het relatieve snelheden model de krachten in de richting van de stroming even nauwkeurig beschrijven als een niet-lineaire versie.

9.  Ieder onderzoek roept onherroepelijk evenveel of meer vragen op dan het beantwoordt.

PROPOSITIONS

Accompanying the dissertation

Hydrodynamic Interaction Between Fluid Flow and Oscillating Slender Cylinders

by M. Shafiee-Far

1. Mankind would be better off if everyone abided by the following two statements - translated here as translations of the original quotations:
   "I cherish increases of knowledge over the increase of worship"
   [Prophet Mohammed (sws)]
   "Your supremacy over others is in proportion to the extent of your knowledge and wisdom"
   [Imam Ali Ibn Abi-Talib (as)]

2. Though we are celebrating the 50th anniversary of offshore technology, the offshore industry is still young!

3. Although many theoretical and experimental investigations have been undertaken to try to resolve the hydrodynamic interaction issue, the problem remains unsolved. The situation may be compared to having an army of workers laying bricks to build a wall in darkness. Even though each worker has done his best, an unexpected form is discovered when it becomes light.

4. Most of the studies on fluid-structure interaction have been targeted on some specific interaction situation with its own mathematical and physical model representation. A more general view has been needed.

5. Direct analyses of the data (regardless of any load model) have shown that a proper load model for predicting the hydrodynamic interaction force in a combined flow field must include all velocity components and combinations of velocities; the assumption of independent flow fields cannot lead to a proper solution.

6. Comparing computer simulations of the hydrodynamic forces with recorded measurements has shown that a model based on the relative velocity concept can describe the hydrodynamic interaction of a cylinder with a combined flow field much better than one which uses the independent flow fields concept.

7. In a combined flow field, there is no single parameter with which the hydrodynamic coefficients may be correlated without the need for other parameters. Nondimensional parameters based on the relative velocity are more appropriate than those related to the individual flow and motion components to represent the hydrodynamic coefficients.

8. For computational efficiency, linear load models are preferred over nonlinear models in dynamic analyses of offshore structures. The inclusion of nonlinearity does not always improve the result. A linearised form of the relative velocity model may predict the inline forces as accurately as the nonlinear form in most flow conditions.

9. Any study inevitably raises as many or more questions than it answers.

# Hydrodynamic Interaction
# Between
# Fluid Flow and Oscillating Slender Cylinders

PROEFSCHRIFT

ter verkrijging van de graad van doctor
aan de Technische Universiteit Delft,
op gezag van de Rector Magnificus, Prof.dr.ir. J. Blaauwendraad,
in het openbaar te verdedigen ten overstaan van een commissie,
door het College van Dekanen aangewezen,
op dinsdag 18 maart 1997 te 10:30 uur

door

**Mehdi SHAFIEE-FAR**

Master of Science in Civil Engineering, Iran University of Science and Technology
Master of Science in Hydraulic Engineering, IHE Delft
geboren te Ghom, Iran

Dit proefschrift is goedgekeurd door de promotor:
Prof.dr.ir. J.H. Vugts

Samenstelling promotiecommissie:

| | |
|---|---|
| Rector Magnificus, | voorzitter |
| Prof.dr.ir. J.H. Vugts, | Technische Universiteit Delft, promotor |
| Prof.dr.ir. J.A. Battjes, | Technische Universiteit Delft |
| Prof.dr.ir. J.A. Pinkster, | Technische Universiteit Delft |
| Prof.dr.ir. J.J.H. Brouwers, | Technische Universiteit Twente |
| Prof. P.W. Bearman, MA., Ph.D., | Imperial College of Science, Technology and Medicine, London |
| W.W. Massie, MSc., P.E., | Technische Universiteit Delft |
| Dr.ir. A. Otter, | Shell International Exploration and Production BV |

# Hydrodynamic Interaction
# Between
# Fluid Flow and Oscillating Slender Cylinders

DISSERTATION

In fulfilment of the requirements for the degree of
Doctor of Technical Science at the Delft University of Technology
under the authority of the
Rector Magnificus, Prof.dr.ir. J. Blaauwendraad
and to be defended in public before a committee appointed by the Board of Deans
on Tuesday March 18, 1997

by

**Mehdi SHAFIEE-FAR**

Master of Science in Civil Engineering, Iran University of Science and Technology
Master of Science in Hydraulic Engineering, IHE Delft
Born in Ghom, Iran

This dissertation has been approved by the major advisor:
Prof.dr.ir. J.H. Vugts

Committee Members:

| | |
|---|---|
| Rector Magnificus, | Chairman |
| Prof.dr.ir. J.H. Vugts | Delft University of Technology |
| Prof.dr.ir. J.A. Battjes, | Delft University of Technology |
| Prof.dr.ir. J.A. Pinkster, | Delft University of Technology |
| Prof.dr.ir. J.J.H. Brouwers, | Delft University of Technology |
| Prof. P.W. Bearman, MA., Ph.D., | Imperial College of Science, Technology and Medicine, London |
| W.W. Massie, MSc., P.E., | Delft University of Technology |
| Dr.ir. A. Otter, | Shell International Exploration and Production BV |

بسم الله الرحمن الرحيم

*In the Name of God
the most compassionate and the most merciful*

*To:
my Parents
my Educators
my Wife*

# Acknowledgments

# SUMMARY

Slender cylindrical members are crucial elements of many types of offshore structure (fixed, compliant and floating) as well as important independent parts of various offshore systems (e.g. risers, cables, umbilicals, wires). Such slender cylindrical members experience excitation as well as reaction forces caused by the movement of the structure as a whole which results from the action of hydrodynamic forces due to waves and current. These forces obviously depend on the fluid properties and flow conditions in the ambient environment, as well as on the geometry and orientation of the cylinder itself. Even when the ambient environment is at rest, the cylinder will nonetheless experience hydrodynamic (reaction) forces when it moves through the fluid. The excitation and reaction forces constitute complex nonlinear hydrodynamic phenomena.

The general case of (large) oscillations of a cylinder through a non-stationary fluid is consequently a very complex nonlinear interaction problem between the hydrodynamic and the mechanical aspects of the problem. That is, the structural response of the cylinder (i.e. its motions) to the loading experienced interacts with the forcing mechanisms to change the loading and thereby in turn change the cylinder motions.

The present work was carried out as a part of an ongoing study of hydrodynamic interaction of slender cylinders conducted by the Workgroup Offshore Technology of the Delft University of Technology. Tests have been carried out to study flow-structure interaction experimentally by oscillating a vertical cylinder in the cross-flow and in-line direction in combination with a steady flow and/or waves. The objective has been to improve the knowledge of the total interaction between the kinematics of the ambient flow on the one hand, and non-stationary slender marine structures on the other. A special objective has been to investigate the validity of Morison equation extensions for combined flow conditions and to establish the governing parameters. A final objective has been to provide the force coefficients for the most appropriate load models. Ideally, this study sought a universal formulation for hydrodynamic interaction which:

- Remains valid for simple as well as complex flow conditions.
- Contains coefficients which can be related to easily determined dimensionless parameters.
- Has stable values of these coefficients for all conditions.

Various existing and postulated load models have been examined within the present work. These models are mostly extensions of the Morison equation based on two well-known ideas: the independent flow fields approach (absolute velocity model) and the relative velocity approach. Furthermore, linearised forms of the extended Morison equation have been evaluated to determine their validity, too.

First the behaviour of the measured in-line forces against various combinations of variables has been studied to see what the data themselves without any recourse to a force model indicate. The statistical values of the measured forces were used for this purpose. The results imply that a proper load model for predicting the hydrodynamic interaction force in a combined flow field

must include all velocity components and combinations of velocities; the assumption of independent flow fields cannot lead to a proper solution.

Even though load models based on the independent flow fields approach were considered improper solutions in the light of direct observations from the data, some extensions of the Morison equation based on this approach have nevertheless been examined. As expected, the results show that these models do not form appropriate load models for a combined flow field. In contrast, models based on the relative velocity approach give a much better quality of fit; they have relatively stable coefficients and the coefficient values resemble those for simpler test cases.

Attempts have also been made to examine linearised forms of the Morison equation for use with various flow fields. The hydrodynamic coefficients for such linearised forms have been determined directly from the data. It has been found that a postulated linear form of the generalised Morison equation based on the relative velocity approach fits as well as (or even better than) the quadratic form.

Evidence has been produced which supports that a universal load model in which the force coefficients depend on some general dimensionless parameters is indeed possible. Both the relative velocity extension of the Morison equation and the linear version of this model satisfy the criteria for a universal model in the flow conditions considered. The results strongly suggest that the linear version of the relative velocity form of the Morison equation extension is applicable to all test cases reported in this dissertation. Besides the quality of fit, this linear model has the following advantages:

- In contrast to common practice in linearised solutions, there is no need for approximation or simplification.
- The velocity terms involved are easy to estimate.
- Since it is linear in application, it simplifies a dynamic analysis of offshore structures.

# SAMENVATTING

Slanke cilinders zijn uiterst belangrijke elementen van vele typen offshore constructies (vast, meegevend en drijvend) alsmede kritieke onafhankelijke onderdelen van verschillende offshore systemen (voorbeelden zijn opkomers (risers), kabels, draden en navelstreng (umbilical)). Zulke slanke cilinders ondervinden excitatiekrachten van stroom en golven, en reactiekrachten als gevolg van de bewegingen van de constructie door de vloeistof; de bewegingen worden op hun beurt weer veroorzaakt door de stroom- en golfkrachten.

Deze krachten hangen af van de eigenschappen van de vloeistof en de stromingscondities aan de ene kant, en de vorm, afmetingen en oriëntatie van de cilinder aan de andere kant. Zelfs als de vloeistof in rust is zal de cilinder (reactie) krachten ondervinden als die zich door de vloeistof beweegt. De excitatie- en reactiekrachten zijn het resultaat van gecompliceerde niet-lineaire hydrodynamische verschijnselen.

Het algemene geval van (grote) oscilaties van cilinders in een niet-stationaire vloeistof is daarom een ingewikkeld niet-lineair interactie probleem tussen de hydrodynamische en de mechanische aspecten van het probleem. De responsie van de cilinder (zijn bewegingen) op de ondervonden krachten beïnvloedt de optredende verschijnselen met als gevolg dat de excitatiekrachten veranderen, waardoor vervolgens weer de bewegingen veranderen.

Het hier gepresenteerde werk is een onderdeel van een doorlopend onderzoek aan de Technische Universiteit van Delft naar de hydrodynamische krachten op slanke cilinders uitgevoerd door de Werkgroep Offshore Technologie. Om de interacties tussen het stromingsveld en de constructie te onderzoeken zijn er proeven uitgevoerd waarbij een cilinder werd geoscilleerd in verschillende combinaties van stroming en golven. Het doel van het onderzoek was het verbeteren van het inzicht in de interacties tussen de kinematica van het stromingveld en niet-stationaire slanke offshore constructies. Hierbij is specifiek gekeken naar de geldigheid van uitbreidingen van de 'Morison vergelijking' voor gecombineerde stromingscondities en het vaststellen van de belangrijkste parameters daarvoor. Er is daarnaast geprobeerd om voor de best toepasbare belastingmodellen de bijbehorende coëfficiënten te bepalen. Idealiter zou deze studie een universele formulering moeten geven voor de hydrodynamische interactie die:
- geldig is voor zowel simpele als voor complexe stromingscondities;
- coëfficiënten bevat die beschreven kunnen worden door eenvoudig te bepalen dimensieloze parameters.
- stabiele waarden heeft van deze coëfficiënten voor alle condities.

In dit werk zijn verscheidene bestaande en voorgestelde belastingmodellen onderzocht. De modellen zijn meestal uitbreidingen van de 'Morison vergelijking', die gebaseerd zijn op één van de twee welbekende ideeën: de onafhankelijke stromingsveld aanpak ('het absolute snelheidsmodel') en de relatieve stromingsveld aanpak ('het relatieve snelheidsmodel'). Daarnaast zijn ook gelineariseerde vormen van uitbreidingen van de 'Morison vergelijking'

bekeken om hun geldigheid te bepalen.

Allereerst zijn, zonder gebruik te maken van enig belastingmodel, de gemeten krachten vergeleken met verschillende combinaties van variabelen, met als doel de kenmerken van een (universeel) belastingmodel uit de data te destilleren. Hiervoor zijn de statistische waarden van de gemeten krachten gebruikt. Uit de resultaten blijkt dat alle snelheidscomponenten en combinaties van snelheden meegenomen moeten worden in een correct model. De aannamc van een absoluut snelheidsmodel kan daardoor niet tot een goede oplossing leiden.

Desondanks zijn enkele uitbreidingen van de 'Morison vergelijking' bekeken die op deze aanpak zijn gebaseerd. Uit vergelijking mct de metingen is nogmaals gebleken dat dergelijke belastingmodellen niet goed blijkbaar zijn. Daar staat tegenover dat de belastingmodellen die gebaseerd zijn op het relatieve snelheidsmodel de hydrodynamische interactiekrachten in een gecombineerd stromingsveld veel beter kunnen beschrijven. De waarden van de bijbehorende coëfficiënten zijn veel stabieler en komen overeen met dc waarden voor enkelvoudige / elementaire stromingsgevallen.

Daarnaast is er geprobeerd om gelineariseerde uitdrukkingen van de 'Morison vergelijking' tc vinden voor verschillende stromingscondities. De bijbehorende hydrodynamische coëfficiënten zijn direct bepaald uit de metingen. Het is gebleken dat een zelf ontwikkelde lineaire vorm van de generaliseerde 'Morison vergelijking' uitgedrukt in de relatieve snelheid daarbij een even goede (zo niet betere) benadering geeft dan een niet-lineaire uitdrukking. Verder wordt het in dit werk aannemelijk gemaakt dat er inderdaad een universeel belastingmodel geformuleerd kan worden met coëfficiënten die afhankelijk zijn van algemene dimensieloze parameters. Zo'n model kan gebaseerd zijn op een van de volgende algemene belastingmodellen:

1. De niet-lineaire vorm van een uitbreiding van de 'Morison vergelijking' uitgedrukt in relatieve snelheiden;
2. De lineaire vorm van een uitbreiding van de 'Morison vergelijking', uitgedrukt in relatieve snelheiden.

Uit de resultaten blijkt dat een lineaire vorm van de 'Morison vergelijking', mits gebaseerd op het relatieve snelheidsmodel, goed te gebruiken is in alle gevallen die beschreven zijn in deze dissertatie. Naast een goede weergave van de optredende krachten heeft het lineaire belastingmodel de volgende voordelen:

- een benadering van het belastingmodel door middel van gelineariseerde oplossingen zoals te doen gebruikelijk is is niet meer nodig;
- de snelheidsafhankelijke termen in het model zijn eenvoudig af te schatten;
- met een belastingmodel dat in zijn toepassingen lineair is, wordt een dynamische analyse van een offshore constructie een stuk minder complex.

# TABLE OF CONTENTS

# CHAPTER 1

# General Introduction

As offshore structures are installed continually in deeper water and more severe environmental conditions, an improved understanding of the interaction of waves and current with these structures remains important as:

- theoretical calculations become more advanced requiring better data and models;
- there is a greater need to demonstrate safety and reliability, again requiring more complete and accurate models;
- costs are to be reduced and one way of achieving that is through the application of better technology.

Analysis for design of these structures requires integration of hydrodynamics and structural mechanics and innovative use of theoretical and experimental techniques.

Offshore structures are usually composed of cylinders; in particular, slender cylinders are essential elements in a great variety of offshore applications and systems. For example, they are found as structural elements in fixed steel offshore structures and jack-up platforms; as pipes (conductors) protecting oil and gas wells from the environment; as conduits for fluid or gas transfer (risers) with fixed and floating production systems and offshore mining installations; as lines (anchor lines) for the positioning of floating vessels; as electrical or hydraulic lines (cables, umbilicals) for the transmission of power or data.

The behaviour of slender cylinders in the marine environment depends on three elements:

- the hydrodynamic interaction between the cylinder and the ambient flow,
- the properties of the mechanical system that is formed by the cylinder,
- the applicable boundary conditions at both its ends - the structure to which it is connected or from which it is suspended.

A seemingly infinite number of individual studies of some aspect of wave-current-structure interaction has already been carried out. Essentially all of these studies, however, have been targeted on some specific interaction situation with its own mathematical and physical model representation. The present work takes a more general view; a universal approach applicable to all types of waves-current interaction with a non-rigid slender circular cylinder has been sought.

The present work was carried out as a part of an ongoing study of hydrodynamic interaction of slender cylinders conducted by the Workgroup Offshore Technology of the Delft University of Technology. Tests have been carried out to study flow-structure interaction experimentally by

oscillating a vertical cylinder in the cross-flow and in-line direction with a steady flow and/or waves. The objective is to increase the detailed knowledge of the total interaction between the hydrodynamics (wave and current) on the one hand, and slender marine structures on the other.

## 1.1 Total Problem Survey

A cylinder experiences hydrodynamic (excitation) forces in a direction perpendicular to its longitudinal axis due to the action of current and/or waves. These forces obviously depend on the fluid properties and flow conditions in the ambient environment, as well as on the geometry and orientation of the cylinder itself. Even when the ambient environment is at rest the cylinder will nonetheless experience hydrodynamic (reaction) forces when it moves through the fluid. The excitation and reaction forces constitute a complex nonlinear hydrodynamic problem.

The dynamic behaviour of the long and slender cylinder mechanical system is similarly a complex nonlinear problem, even when the time varying excitation is fully known. It is influenced by factors such as the large displacements involved, the internal and external fluid pressure, the (variable) mass flow through a pipe and the coupling between axial and torsional deflections.

The general case of cylinder (large) motion through a non-stationary fluid is consequently a very complex nonlinear interaction problem between the hydrodynamic and the mechanical aspects of the problem. That is, the structural response of the cylinder (i.e., its motions) to the loading experienced interacts with the forcing mechanisms to change the loading and thereby in turn change the cylinder motions.

Numerous theoretical and experimental investigations have been undertaken to try and resolve the interaction issue above. However, overall it remains an ill-understood problem. Most researchers and practitioners consider the hydrodynamic interaction problem to be by far the most important issue. This is an important reason for attempting to understand hydrodynamic interaction first.

A comprehensive literature study has already revealed that understanding of the mechanical behaviour as well as fluid-structure interaction are still relatively limited, see Shafiee-Far (1994a, 1994b, 1994c). There is a large body of literature reporting theoretical and experimental investigations into one or more aspects of fluid-structure interaction.

The experimental programs reported in the literature refer almost without exception to laboratory investigations, which are severely hampered by the impossibility to reproduce Reynolds numbers at model scale and the significant practical problems encountered when subjecting long and slender cylinders to conditions in the laboratory scales that reproduce realistic field conditions. Therefore such programs have generally focused on one of two approaches: on the study of particular aspects of the problem only, or on the determination of empirical coefficients in pragmatic force models that are valid for a restricted set of circumstances.

## 1.2 Objective of the Present Work

On the basis of the above background it was further concluded that much of the physics of viscous fluid flow and vortex shedding is still poorly understood and that it would not be realistic to expect that major progress could be made using a theoretical approach. Thus the only way to attempt to make meaningful progress in the relatively near term is to conduct a systematic series of laboratory experiments with a segment of a cylinder. This segment would need to be subjected to known and controlled motions while the hydrodynamic forces in two orthogonal directions would be measured. In this manner a data bank of hydrodynamic force measurements would be set up. This data could be used in a variety of ways such as:

- to analyse the data to detect relationships between the many variables involved;
- to determine the most appropriate of the existing loading models that have been derived theoretically or postulated on the basis of previous experiments for a given set of circumstances;
- to test the adequacy of existing or new force models by comparing computer simulations of the hydrodynamic forces with the recorded measurements.

Ideally, this study sought a universal formulation for hydrodynamic interaction which:

- Remains valid for simple as well as complex flow conditions.
- Contains coefficients which can be related to easily determined dimensionless parameters.
- Has stable values of these coefficients for all conditions.

During 1993 and the early part of 1994 a systematic series of experiments was planned. These were carried out in the Ship Hydromechanics Laboratory of the Faculty of Mechanical Engineering and Marine Technology in the summer and early fall of 1994. The experiments comprised tests with a vertical cylinder, both stationary and subject to forced oscillations, in periodic and random waves with and without current which was simulated by translating the cylinder through the fluid. A list of test cases is given in table 1.

## 1.3 Outline of the Dissertation

While tests have been carried out by oscillating the cylinder in both the in-line and transverse directions, only results for the in-line oscillation tests are included in the present dissertation. Additionally, the author's work has concentrated on the investigation of the in-line force components. However, some results for the transverse force are presented where they are relevant to the discussion.

This dissertation has been organized into 11 chapters. The introductory material thus far comprises the first chapter. The contents of the following chapters are briefly summarized below.

In chapter 2 the physical problem of hydrodynamic interaction is discussed and the significant parameters are reviewed. This discussion gives a general idea about the existing problems and the required experiments.

A survey of various load models and techniques for determination of the force coefficients is provided in chapter 3. Through this, criteria for evaluation of the load models are discussed.

Chapter 4 contains a description of the laboratory systems and the experimental program, as well as the data processing techniques and important formulations used in the subsequent sections.

A number of tests were carried out to establish base cases for situations when other motions were also included. Results of these single mode tests are presented in chapter 5.

Chapters 6 through 9 concern the experimental data analysis and associated results for the following multi mode tests, respectively:

- in-line oscillation while towing the cylinder
- towing the cylinder in waves
- in-line Cylinder Oscillation in Waves
- in-line Oscillation While Towing in Waves

Chapter 10 investigates a universal force model by comparing the results from previous chapters. The main results of the entire work and the conclusions reached, are presented in chapter 11.

| Flow Conditions | Cylinder Oscillations | | |
|---|---|---|---|
| | None | In-line | Transverse |
| Still water | —— | yes | yes |
| Current only | yes | yes | yes |
| Regular waves only | yes | yes | yes |
| Regular waves plus current | yes | yes | yes |
| Irregular waves only | yes | yes | yes |
| Irregular waves plus current | yes | yes | yes |

Table 1   Overview of Flow Conditions and Cylinder Oscillations Considered in Laboratory Experiments

# CHAPTER 2

# The Physical Problem

The state of understanding and the assumptions and uncertainties that are associated with the prediction of the behaviour of slender marine structures have been reviewed in three previous reports by the author, Shafiee-Far (1994a,b,c). The interaction of the fluid and the structure results in a three-dimensional problem even for a vertical cylinder in a unidirectional wave and current field. Analyses of the interaction of waves with currents and the interaction of the modified wave-current combination with slender structures require relevant observations and experiments as well as different mathematical approaches that are applicable to some or all of these physical circumstances. The present analytical, experimental, and operational knowledge is still inadequate to describe the complex realities of fluid loading and dynamic response of slender structures.

From both design and operational points of view, the prediction of forces acting on the slender cylinders is important, just as prediction of the resultant shape and motions of the cylinder are important. It is well known that the motion of the cylinder can significantly alter the flow pattern and amplify the vortex-induced forces. The most important areas for improvement of the representation of hydrodynamic interaction may be considered as follows:

-   Proper description of hydrodynamic forces as inertia, drag and lift force components on a single cylinder cross-section. In this sense, an appropriate (either existing or new) load model is to be adopted for description of the hydrodynamic interaction.

-   Coupling between in-line and crosswise motion. Slender cylinders may undergo oscillations in the in-line and transverse directions. The magnitude of transverse oscillation can be such that ignoring them may yield unconservative estimates of the associated structural loads. The interaction problem can be solved by including vortex-induced forces in the equations governing the motion of the structure, Sarpkaya and Isaacson (1981), Kaplan et al. (1981). The inclusion of these forces results in coupled differential equations. A number of researchers have proposed approximate solutions of the coupled system of equations using various techniques. These approximations often neglect the effect of the coupling between the in-line and transverse oscillations. However, the results associated with the uncoupled equations can be significantly different from those associated with the coupled equations, see Ghanem and Spanos (1992).

-   Characterization of vortex-induced vibration and three-dimensional effects. Developing a general vortex-induced vibration analysis procedure is needed for representing the wide range of vibration behaviour associated with long, slender cylinders in a current and/or waves.

## 2.1 Hydrodynamic Interaction

Since slender cylinders have a large dynamic response to hydrodynamic forces associated with vortex shedding, a complete description of the hydrodynamic interaction must include the effects of this response. This is usually included by using an extension of the Morison equation. Two well-known extensions of the Morison equation are based upon the concepts of:

- *Independent flow fields* (*absolute velocity approach*)
- *Relative flow field* (*relative velocity approach*)

The independent flow fields approach assumes the total force to be a superposition of two unrelated flows, one due to the fluid action on a fixed cylinder, and the other due to the cylinder motion contributions in still water. In the relative velocity approach, the fluid velocity is replaced by the relative velocity between the fluid and the structure. The validity and suitability of each of these extensions has not been examined adequately, however.

The measured data in this study has made it possible to study the validity of existing as well as other postulated load models under a relatively wide range of flow conditions.

## 2.2 Vortex-Induced Vibration and 3D Effects

The concepts presented above are two-dimensional. If a long slender cylinder is considered, the three-dimensional nature of the waves and current and of the cylinder motion cannot necessarily be completely described by a two-dimensional analysis. Some significant areas are addressed below.

Vortex shedding from even a stationary cylinder is not uniform along the span. The flow itself no longer behaves purely two-dimensionally at higher Reynolds numbers. Vortices are then shed in cells. The three-dimensionality of vortex shedding can be characterized by a spanwise correlation length which corresponds to a length of the cell. The cell length depends on many parameters such as Reynolds number, turbulence and shear in the ambient flow, cylinder surface roughness, and cylinder vibration, see e.g. Pantazopoulos (1994).

A vortex-induced vibration analysis procedure has three essential components: a structural model, a flow model (which interacts in some way with the structural model), and a solution technique. For the flow model, the ideal is to solve the Navier-Stokes equations in the presence of the body motion. Theoretical and/or numerical solutions of the Navier-Stokes equations are only available for simplified cases or very low Reynolds numbers, and one has to resort to physical experiments instead to obtain the data required.

There is a class of "wake-oscillator" models between direct Navier-Stokes solutions and physical experiments in which the behaviour of the vortex wake is represented as a nonlinear Van der Pol or Rayleigh oscillator, Hartlen and Currie (1970), Skop and Griffin (1973), Iwan and Blevins (1974). However, most of these models are phenomenological descriptions that do not stem from the underlying physics, Sarpkaya (1979), and therefore need to be calibrated against experimental data. Thus, experimental results could be used directly as the hydrodynamic input to a general

vortex-induced prediction scheme, or indirectly through a wake-oscillator model.

The quasi-steady assumption is frequently used to derive the fluid dynamic forces on an oscillating cylinder for subsequent use in vortex-induced vibration analyses of slender cylinders. The principle of the quasi-steady assumption is that it enables the dynamic fluid forces acting on an oscillating body to be calculated from static forces measured on a stationary body, with the two bodies having otherwise identical conditions. It is assumed that the effect of the oscillating body on the dynamic fluid forces is solely to modify the incident flow velocity vector. A typical example of using the quasi-steady assumption is illustrated in figure 2.1, where it is desired to calculate the dynamic forces on the body in the x and y-directions. If the body is only allowed to oscillate normal to the flow, with velocity $\dot{y}$, then the resultant velocity will be
$V_{rel} = (V^2 + \dot{y}^2)^{1/2}$, inclined at angle $\alpha = \tan^{-1}(\dot{y}/V)$ to the original vector V. The quasi-steady assumption assumes that magnitude of $F_L$ and $F_D$ do not change as the cylinder oscillates, but are merely inclined by a continuously changing angle $\alpha$ relative to their original direction.

Although it is well accepted, and physically reasonable, this assumption of quasi-steady state is only considered to be valid for high values of nondimensional flow velocity (reduced velocity) $V/fD$[1]. This approach seems less appropriate for low reduced velocity values, Price et al. (1988). It is less known how the error associated with the assumption varies with reduced velocity. More research is required to establish when and where a quasi-steady flow assumption is or is not valid.

While all above-mentioned problems are very important for the total hydrodynamic interaction with slender cylinders, the present work is limited to two-dimensional interaction problems.

## 2.3 Significant Parameters

Modelling a slender cylinder behaviour is dependent on a number of empirical parameters such as Strouhal number, correlation length, and force coefficients. These parameters are dependent on other flow parameters such as Reynolds number, surface roughness, Keulegan-Carpenter number, and turbulence intensity. No single test can provide measurements and data for all the parameters involved in hydrodynamic interaction. Most tests provide data for a few parameters, disregarding the effect of others. Selection, interpretation, and evaluation of test data are critical to hydrodynamic interaction of slender marine cylinders.

The in-line hydrodynamic force per unit length acting on an element of a smooth vertical circular cylinder oscillating in a wave plus (uniform) current flow field depends on the following independent parameters:

$$F = \phi(t, D, \rho, \nu, d, z, g, V, H, T_w, A, T_o) \tag{2.1}$$

in which $t$ = time, $D$ = diameter of the cylinder, $\rho$ = density of the fluid, $\nu$ = kinematic viscosity of the fluid, $d$ = water depth, $z$ = elevation of the element below the water surface, $g$ = acceleration due to gravity, $V$ = current velocity, $H$ = wave height, $T_w$ = (intrinsic) wave period, $A$ = amplitude of cylinder displacement, $T_o$ = period of cylinder oscillation.

---

[1]All notations are listed at the end of the main text of the dissertation

Note that there are several other parameters that are used in describing a two-dimensional progressive wave such as: wave length $\lambda$, wave frequency $\omega_w$ and wave number k. However these parameters are interrelated and the independent quantities that are necessary and sufficient to characterise the wave motion are $H$, $d$, $T$ and $g$, Sarpkaya and Isaacson (1981). All other quantities are related to these four independent variables in a manner prescribed by a particular wave theory. For example, the wave length $\lambda$ depends on $T_w$, $d$ and $g$. Thus, $g$ may be replaced by $\lambda$ in equation 2.1.

The amplitude of wave-induced water particle velocity $u_m$ and the amplitude of cylinder velocity $\dot{x}_m$ may also be used to describe the hydrodynamic force due to the combined flow field. Since $u_m$ is a function of elevation, z can be replaced by $u_m$ in equation 2.1 provided that the force concept is considered in a "deep" location where the free surface effects can be neglected. Similarly, the amplitude of cylinder velocity $\dot{x}_m$ is a function of $A$ and $T_o$ and may be exchanged with $A$ in equation 2.1. Using these parameters, the hydrodynamic force may be expressed as the following general function:

$$F = \phi(t,\ D,\ \rho,\ \nu,\ d,\ V,\ H,\ T_w,\ \lambda,\ u_m,\ T_o,\ \dot{x}_m) \tag{2.2}$$

The effect of accelerations of the wave field and the cylinder oscillations are incorporated through the velocity and time parameters. Thus, the dependent variable $F$ is a function of 12 independent variables. Using the Buckingham Pi theorem, in a mass-length-time system, this forms nine (=12-3) independent nondimensional quantities so that the normalised hydrodynamic force per unit length may be expressed in the form of a function of nine nondimensional parameters:

$$\frac{F}{\rho D (Vel)^2} = f\left(\frac{t}{T_w},\ \frac{T_o}{T_w},\ \frac{\pi D}{\lambda},\ \frac{2\pi d}{\lambda},\ \frac{H}{\lambda},\ \frac{\dot{x}_m}{u_m},\ \frac{VD}{\nu},\ \frac{u_m T_w}{D},\ \frac{VT_o}{D}\right) \tag{2.3}$$

where:

| | |
|---|---|
| $Vel$ | = a characteristic velocity for the combined flow field which needs to be defined |
| $t/T_w$, $T_o/T_w$ | = dimensionless time |
| $\pi D/\lambda$ | = diffraction parameter |
| $2\pi d/\lambda$ | = relative depth, kd |
| $H/\lambda$ | = wave steepness |
| $\dot{x}_m/u_m$ | = dimensionless velocity |
| $VD/\nu$ | = Reynolds number based on current velocity ($Re$) |
| $u_m T_w/D$ | = Keulegan-Carpenter number based on wave parameters ($KC_w$) |
| $VT_o/D$ | = reduced velocity - velocity of the steady flow relative to velocity due to the oscillation of the cylinder ($Vr_o$) |

The diffraction effect is not significant for a small diameter cylinder. Therefore, the dependence on the diffraction parameter may be neglected. For linear wave theory, the dependence of force on wave steepness H/$\lambda$ may be waived. Note that the remaining dimensionless parameters are not unique. For example, any two of these quantities may be combined to form a new one; specially the following dimensionless parameters should be mentioned:

$u_m D/\nu$, $\dot{x}_m D/\nu$ = Reynolds number based on orbital velocity and oscillatory velocity, respectively;

$\dot{x}_m T_o /D$    = Keulegan-Carpenter number based on oscillation parameters ($KC_o$);
$VT_w /D$    = reduced velocity - velocity of the steady flow in comparison with flow due to the wave ($Vr_w$).

Besides, there are many possibilities regarding the definitions of the Keulegan-Carpenter number and the Reynolds number. Some possible $KC$ and $Re$ definitions for combined flow fields are presented and discussed in the associated chapters.

One must introduce characteristic values for time, length and velocity ($t_c$, $D$ and $U_c$ respectively) to extend the dimensional numbers to irregular waves. Among these parameters are the Reynolds number $Re = U_c D/\nu$ and the Keulegan-Carpenter number $KC = U_c t_c/D$. Formulations for these dimensional parameters are given when the associated results are discussed.

## 2.4 Laboratory Data Requirements

Many model tests have been conducted to investigate a particular aspect of the hydrodynamic interaction problem or satisfy the needs of a specific numerical or analytical model. Most of these tests were carried out with the objective of establishing empirical coefficients under a narrow range of conditions. Since the objective of the present work was to cover all possible conditions and to cover wide ranges of relevant parameters, an extensive test programme was required.

Experiments for complicated circumstances such as the hydrodynamic interaction of slender cylinders should start with simplified cases and be extended to more complex ones. The following combinations may be required to investigate the matter adequately:

- Current-structure interaction
- Wave-structure interaction
- Wave-current-structure interaction

These different phases of the investigation and the possibility of experiments - using available facilities within the university - for each of these combinations have been reviewed in Shafiee-Far (1995a). Table 3.1 gives a list (matrix) of various experiments that may be carried out to achieve the objectives of the study. However, only combinations of waves and/or currents with forced oscillations were carried out which include the shaded part of table 3.1.

## 2.5 Typical Data Ranges

Typical cross sections for slender cylinders vary for different types of cylinders. There is a large variation of cross sections even for a particular type such as risers or mooring lines. Also, these structures are used in different water depths and various sea states. Thus, the ranges of flow parameters are very wide.

Since combinations of the relevant parameters are very important for comparison of experimental data and real situations, a complete test programme must include a wide range of such combinations. To provide an impression of ranges of the dimensionless parameters in the real offshore environment, figure 2.2 shows combinations of these parameters for a 60 cm riser in 300

m water depth and various sea states.

However, there are some practical restrictions - such as capacity limitations of wave generator, oscillator and force transducers - that restrict the realisable combinations of independent variables. The force transducers only give proper information when the loading stays within acceptable limits. It is only possible to generate certain combinations of wave height and period. The possible simultaneous combinations of dimensionless parameters for various test cases are given in Shafiee-Far (1995a), appendix IV. Such combinations for the test case of in-line oscillation plus current are illustrated in figure 2.3. Considering the possibilities of variables, it appeared that practical data ranges could be achieved except for Reynolds number. The physical limitation of the experimental facilities permits only subcritical - and for some cases critical - flow conditions.

| Test Cases | | Current | Waves | Cylinder Motion | | | |
|---|---|---|---|---|---|---|---|
| | | | | Forced | | Free | |
| | | | | In-line | Cross flow | In-line | Cross flow |
| A1 | 1 | yes | no | yes | no | no | no |
| | 2 | | | no | yes | no | no |
| | 3 | | | yes | yes | no | no |
| A2 | 1 | yes | no | no | no | yes | no |
| | 2 | | | no | no | no | yes |
| | 3 | | | no | no | yes | yes |
| B1 | 1 | no | yes | no | no | no | no |
| | 2 | | | yes | no | no | no |
| | 3 | | | no | yes | no | no |
| B2 | 1 | no | yes | no | no | yes | yes |
| C1 | 1 | yes | yes | yes | no | no | no |
| | 2 | yes | yes | no | yes | no | no |
| C2 | | yes | yes | no | no | yes | yes |

Table 3.1  Basic Experimental Programme
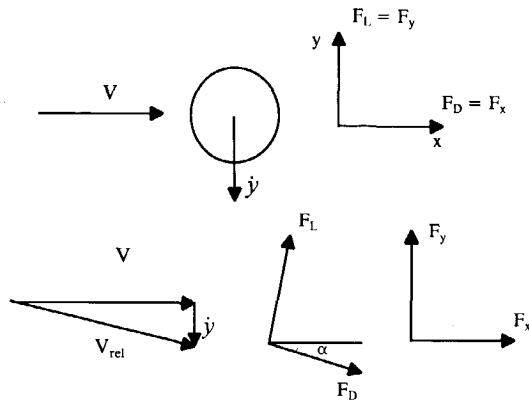
Figure 2.1  Explanation of the quasi-steady assumption
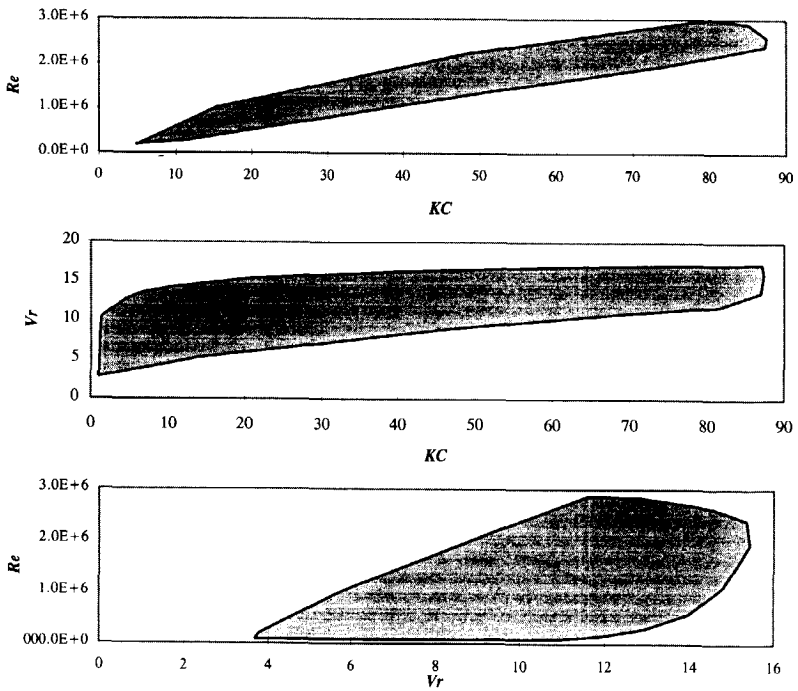


Figure 2.2   An example of combinations of Dimensionless parameters, a
D=60 cm  riser in 300 m water depth and various sea states

11
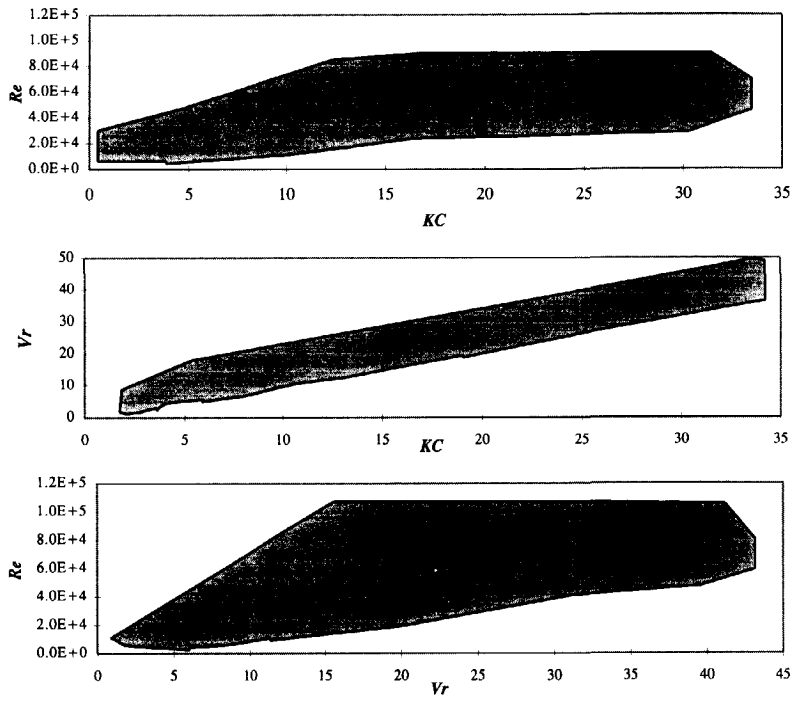
Figure 2.3    Nondimensional parameter ranges for in-line oscillation plus
current that are possible with the experimental facilities used

# CHAPTER 3

# Load Models

Slender cylinder hydrodynamics involves complex interaction between the kinematics of the ambient flow, which may lead to flow separation and the development of vortices, and the response of the cylinder. A load model for such structures must be able to describe this special interaction between the hydrodynamic forces and the response of the structure itself. This is very important both for a coefficient model (Morison equation) and a direct solution of the basic equations (Navier-Stokes). Further, dealing with resonant phenomena can be important for lock-in vibrations where vortices are shed from the structure with a frequency near a natural frequency of the structure.

The calculation of the magnitude of the external hydrodynamic forces may vary depending upon the character of the flow and the type of structure present. Suitable numerical solutions for the viscous flow around slender structural components are highly desirable. In these solutions, besides the possibility of direct evaluation of the acting pressure, the motions of the components could be considered as well. This allows for an integrated numerical treatment of the fluid-structure interaction problem. A numerical solution of the time dependent Navier-Stokes equations coupled with the response of the structure would provide the complete solution. However, the direct integration of the Navier-Stokes equation is not currently feasible due to the large computational effort needed, see Sarpkaya (1989), Moe (1992) and Sarpkaya (1993). Therefore, various approximations need to be made to obtain useful solutions. The objective in formulating approximate mathematical models is to try to find the simplest set of equations of motions whose solutions reflect observed behaviour with an acceptable degree of accuracy. In particular, if the equations are too complex and contain many empirical coefficients then doing enough experiments to compute the values of the coefficients for some wide range conditions will be difficult. On the other hand, if the equations are too simple, they probably cannot describe the observed behaviour adequately.

Various mathematical models proposed for the forces acting on cylinders in oscillatory flow are described in the remainder of this chapter.

## 3.1 Morison Equation and Improvements

Most studies of fluid forces on small bodies that act in-line with an oscillating flow use the Morison approach. Load models for slender marine structures based on the Morison equation are 2D coefficient models. This model is valid for a single length element and can be extended to 3D flow using a strip method. The in-line fluid forces are considered to be the sum of an inertia force and a drag force. The inertia force is due to fluid acceleration and the drag force is associated with velocity, either relative or absolute depending upon the investigator's preference

it seems.

The Morison equation for a fixed cylinder may be written as:

$$F = 0.5 \rho C_D A_p u |u| + \rho C_M \forall \frac{du}{dt} \tag{3.1}$$

in which $C_D$ and $C_M$ are drag and inertia coefficients, $A_p$ represents the projected frontal area; $\forall$, the displaced volume of the structure; and $u$, the velocity of the ambient flow. Velocities and accelerations are components in the plane normal to the cylinder axis.

The Morison equation with inclusion of velocity and acceleration terms from the cylinder itself, describes the in-line force perpendicular to the member. Transverse forces can be included in a similar way. If the proper fluid velocity and appropriate hydrodynamic coefficients can be correctly determined, the use of the Morison equation will yield good results. However, this equation has been subject of a great deal of discussion about appropriate values for its two coefficients. Furthermore, the importance of roughness, rotation of the velocity vector, orientation of the cylinder, spanwise coherence, currents, a free surface, etc., still remains disputed even though a vast amount of experimental work has been published over the past decades.

Since the Morison equation is an approximate solution to a complex problem, many attempts have been made either to improve or to modify the equation, see for example, Barnouin et al. (1979), Sarpkaya and Isaacson (1981), Vugts and Bouquet (1985).

## 3.2 Modified Forms of Morison Equation

Besides the use of the Morison equation for fixed structures in waves, some further extensions of this mathematical model have been used for other flow conditions such as combinations of a current and/or structural oscillations. Particular applications arise when considering the forces on elements of a flexible line structure and when vibrations occur on a fixed platform.

In spite of the differences in the two representative cases of relative motion described above, the usual procedure in offshore engineering is to employ the basic form of the Morison equation for relative motion as the appropriate model representing each case. There are a number of fundamental questions about the correctness of such a representation, but only limited investigations have been made to find out whether such a model is valid under different practical conditions.

If a rigid cylinder is oscillated in otherwise still water, the in-line component of the fluid force acting on the cylinder can be written as:

$$F = -C_{Do}(\frac{1}{2}\rho D) |\dot{x}|\dot{x} - C_A (\rho \frac{\pi}{4} D^2)\ddot{x} \tag{3.2}$$

in which $\dot{x}$ and $\ddot{x}$ are the velocity and acceleration of the cylinder, $C_A$ is the added-mass coefficient and $C_{Do}$ is the drag coefficient for an oscillating cylinder in still water. The reaction force here is taken as the external fluid force experienced by the oscillating cylinder; the inertia

of the cylinder itself due to its acceleration is not included in the reaction forces. Note that the drag coefficient, $C_{Do}$, for an oscillating cylinder is defined independently from the drag coefficient for waves past a fixed cylinder.

The added-mass coefficient is generally assumed to be related to the inertia coefficient by:

$$C_M = C_A + 1 \tag{3.3}$$

The above relation is correct for circular cylinders. Lighthill (1986) explained this relation by introducing Froude-Krylov force component corresponding to the pressure gradient generated by the oscillatory flow. In the present work it will also be assumed that the added-mass and inertia coefficients are related by equation 3.3 in general, even though the definitude of the relationship in the coexisting flow fields will be investigated.

If the cylinder is free to respond or forced to oscillate in an oscillatory flow then some combination of equation 3.1 and 3.2 can be used to approximate the in-line force. As cited in the previous chapter there are two well-known extensions of the Morison equation for these cases; the independent flow field and the relative velocity approach.

The basic assumption of the independent flow fields model is that the wave force acting on an oscillating cylinder is the sum of forces resulting from two independent flow fields: a far field force due to the wave motion and relatively unaffected by the cylinder oscillation and a near field force resulting from the cylinder motion in still water. This gives the in-line force per unit length as:

$$F = +C_D(\frac{1}{2}\rho D)|u|u - C_{Do}(\frac{1}{2}\rho D)|\dot{x}|\dot{x} + C_M(\rho\frac{\pi}{4}D^2)\dot{u} - C_A(\rho\frac{\pi}{4}D^2)\ddot{x} \tag{3.4}$$

In the alternative solution using a relative velocity approach, it is assumed that the drag term in equation 3.4 depends on the relative velocity between the fluid and the body, resulting in an in-line force per unit length given by:

$$F = C_{Dr}(\frac{1}{2}\rho D)|u-\dot{x}|(u-\dot{x}) + C_{Mr}(\rho\frac{\pi}{4}D^2)\dot{u} - C_{Ar}(\rho\frac{\pi}{4}D^2)\ddot{x} \tag{3.5}$$

In this equation the inertia coefficient is separated from the added mass coefficient. Assuming the relation given in equation 3.3 to be valid for a combined flow field, i.e.:

$$C_{Mr} = C_{Ar} + 1 \tag{3.6}$$

the relative velocity model given in equation 3.5 may be written in an alternative form as:

$$F = C_{Dr}(\frac{1}{2}\rho D)|u-\dot{x}|(u-\dot{x}) + C_{Mr}(\rho\frac{\pi}{4}D^2)\dot{u} - (C_{Mr}-1)(\rho\frac{\pi}{4}D^2)\ddot{x} \tag{3.7}$$

This model requires two fewer coefficients than equation 3.4 to determine the fluid force. The value of $C_{Dr}$ used in this case should be based on the amplitude of relative motion rather than the fluid or structural motion alone.

For a structure free to oscillate in the presence of waves and current, the Morison equation may be modified as:

15

$$F = C_{Drc}(\frac{1}{2}\rho D)|V+u-\dot{x}|(V+u-\dot{x}) + C_{Mrc}(\rho\frac{\pi}{4}D^2)\dot{u} - C_{Arc}(\rho\frac{\pi}{4}D^2)\ddot{x} \qquad (3.8)$$

Other forms of equation 3.8 may be proposed as before and have been used in the past.

Beside these modified Morison equations, a number of postulated load models have been used in this study. These models for each flow condition are presented in the relevant chapter where that flow condition is studied.

### 3.3 Harmonic Analysis Models

Harmonic analyses may be carried out to determine Fourier components of the hydrodynamic force on a slender cylinder. If a cylinder oscillation $x(t)$ at the frequency $f_o$ is given by:

$$x(t) = A \sin(2\pi f_o t) \qquad (3.9)$$

then the in-line force may be expressed by a Fourier series having frequencies equal to multiples of the oscillation frequency. Each force component has an amplitude and a phase angle associated with it; thus one may model the in-line force as:

$$F = \sum_{n=1}^{\infty} \hat{F}_{on} \sin(2n\pi f_o t + \phi_{on}) \qquad (3.10)$$

For the case of a cylinder oscillating in still water, analysis of the data has shown that the time variant hydrodynamic force could be represented well by only the first and the second components; higher components had little influence on the accuracy of the results. Thus, for the pure cylinder oscillation in still water the in-line force may be represented by:

$$F = \hat{F}_{o1} \sin(2\pi f_o t + \phi_{o1}) + \hat{F}_{o2} \sin(4\pi f_o t + \phi_{o2}) \qquad (3.11)$$

where $\hat{F}$ is the amplitude of the hydrodynamic force component and $\phi_o$ is a phase angle. $\hat{F}$ can be normalised by the dynamic pressure head factor $\frac{1}{2}\rho D u_m^2$ to obtain the associated force coefficient:

$$C_{dh1} = \frac{\hat{F}_{o1}}{0.5\,\rho D u_m^2} \qquad\qquad C_{dh2} = \frac{\hat{F}_{o2}}{0.5\,\rho D u_m^2} \qquad (3.12)$$

One may instead nondimensionalise $\hat{F}$ in different ways, for example:

$$C_{ah1} = \frac{\hat{F}_{o1}}{0.25\,\pi\,\rho D^2 \dot{u}_m} \qquad (3.13)$$

If the cylinder oscillation is combined with a current (or the cylinder's steady motion), both the Strouhal frequency and the oscillation frequency are introduced in the wake. Depending on the amplitude and frequency of the cylinder oscillations, the wake response may be locked-in where the cylinder motion controls the shedding process and the Strouhal frequency disappears. However, the forces on the cylinder will generally have components at both the Strouhal and body oscillation frequencies. Thus, one may model the in-line force as:

$$F = F_m + \sum_{n=1}^{\infty} \hat{F}_{on} \sin(2\pi n f_o t + \phi_{on}) + \sum_{n=1}^{\infty} \hat{F}_{vn} \sin(2\pi n f_v t + \phi_{vn}) \qquad (3.14)$$

$F_m$ is the magnitude of the mean drag force, $\hat{F}_v$ is the magnitude of the oscillating in-line force at the Strouhal frequency $f_v$ and $\phi_v$ is a corresponding phase angle. Each of the force components can be nondimensionalised in different manners to obtain the appropriate force coefficients.

Applications of the harmonic analysis approach and the examination of various force coefficients for various test conditions are given in later chapters where results for different flow conditions are presented.

## 3.4 Lift Force Models

Vortex shedding causes an additional force acting on the cylinder in a direction perpendicular to the flow direction. This force component is called the lift force or transverse force. The lift force is strongly correlated to the development of the flow field around the cylinder and can induce substantial transverse vibration.
Many investigators have studied the lift force acting on a cylinder in a uniform flow and a recent summary of this work is given by Blevins (1990). The lift force is due to vortex shedding with the frequency of the shedding of pairs of vortices given by

$$f_v = \frac{SV}{D} \qquad (3.15)$$

where S is the Strouhal number and $V$ is the current velocity. A harmonic function with frequency $f_v$ is often used to model the transverse force per unit length as:

$$F_y = \frac{1}{2}\rho V^2 D C_L \sin(2\pi f_v t) \qquad (3.16)$$

Here $C_L$ is a lift coefficient and t is the time in seconds. Many efforts have been directed toward determining the lift coefficients for different geometric and flow conditions.

The lift force also exists in oscillatory flow due to vortex shedding. A very simple model for the lift force would be to use the result from steady flow given by equation (3.16) with the maximum fluid velocity, $u_m$, replacing the current velocity, so that:

$$F_y = \frac{1}{2}\rho u_m^2 D C_L \sin(2\pi f_v t) \qquad (3.17)$$

McConnell and Park (1982) proposed an alternative model for the lift force based on experiments in which a rigid cylinder was oscillated in otherwise still water. This model assumes that the lift force is proportional to the square of the instantaneous velocity rather than $u_m^2$. This results in the lift force being given by:

$$F_y = \frac{1}{2}\rho u^2 D C_L \sin(2\pi f_v t) \qquad (3.18)$$

Thus, with an oscillatory fluid motion given by $u = u_m \sin 2\pi f_o$, where $f_o$ is the forced oscillation frequency, the lift force is given by:

$$F_y = \frac{1}{2}\rho\,(u_m \sin 2\pi f_o t)^2\, D\, C_L \sin(2\,\pi f_v t) \tag{3.19}$$

In this model, the frequency components of $F_y$ occur at $f_v$, $f_v - 2f_o$, and $f_v + 2f_o$. The results of experiments by McConnell and Park also showed a strong tendency for the vortex shedding frequency to assume integer multiples of the oscillation frequency, i.e. $f_v / f_o = n$.

In another formulation, the lift force is represented in terms of its Fourier components; see Chakrabarti et al. (1976). In this case, the lift force is expressed by a Fourier series having frequencies equal to multiples of the wave frequency. Each force component has a lift coefficient and a phase angle associated with it:

$$F_L = A_D\, u_m^2 \sum_{n=1}^{N} C_{L_n} \cos(2\,\pi n f t + \phi_n) \tag{3.20}$$

In which N is the number of Fourier components, $C_{L_n}$ and $\phi_n$ are the nth lift coefficient and corresponding phase angle, respectively.

Using equation 3.16 as a basis, Bearman et al. (1984) have proposed yet another model that is a revision of an earlier model by Verley (1982).This model has not been considered in the present work, which instead focuses on the simple lift force models given above. It must be noted that these models are empirical and that it is very difficult to state conclusively which model is the best one.

Although simple lift models have been used in this study, applications of these models have been extended to the complicated flow conditions such as:

a. fixed cylinders in waves plus current
b. oscillating cylinders in waves
c. oscillating cylinders in wave plus current

Studies on the lift force where waves and currents co-exist are rare, and as far as the author is aware no study concerning the lift force for oscillating cylinders in wave plus current flow condition has been reported.

## 3.5 Coefficient Determination Techniques

Various methods have been suggested to determine force coefficients for load models described in the previous sections. From these suggested methods, two methods are commonly used to determine force coefficients for the Morison equation:

1) Least Squares Method: a least square fitting of the two coefficients to the force over the full length of the measurement,
2) Fourier averaged method: drag and inertia coefficients are related to the first two Fourier coefficients at the fundamental oscillatory frequency.

Formulations for these and other practical methods are summarised in appendix I.

## 3.6 Model Evaluation Criteria

The following criteria have been applied to compare and to evaluate the validity and suitability of various load models in this work:

- Observation from the data itself
- Quality of fit of load models to data
- Stability of the coefficients

### 3.6.1 Direct Observations from the Data

Before trying various load models, the data themselves were observed and studied to see what insight they might yield. To do this, various characteristic forces such as the mean (steady) force and the root mean square of the total measured force were considered. A large number of different checks have been carried out. For example, the RMS value of the in-line forces for all test runs has been plotted against various variables to reveal the presence or absence of dependency.

### 3.6.2 Quality of Fit of Load Models

The quality of fit of load models to data has been another criterion to assess the validity and suitability of various load models. Each of the load models has been used with the input-output data pairs from each of the test runs. The goodness-of-fit parameter, $\epsilon$, given by equation 3.21 has been used in this work to evaluate the quality of the fit of each model to the data.

$$\epsilon = \frac{rms\,(F_{meas} - F_{cal})}{rms\,(F_{meas})} = \left[\frac{\sum (F_{meas} - F_{cal})^2}{\sum (F_{meas})^2}\right]^{\frac{1}{2}} \tag{3.21}$$

where:
$F_{meas}$   is the measured force (corrected for cylinder acceleration)
$F_{cal}$   is the force calculated by the model.

This parameter which has already been used by other investigators, e.g., Sarpkaya (1976) and Stansby et al (1983), is the root mean square error of the force as determined from a load model compared with the measured force; this is normalised by the root mean square of the measured force. The lower this parameter value, the better the quality of the fit. Each test run and each load model will result in a value of $\epsilon$. Statistical information of these $\epsilon$ values will then allow comparison of various load models to assess their validity.

### 3.6.3 Stability of the Coefficients

Even though most of the load models (with appropriate coefficients) can reproduce the measured hydrodynamic force in a more or less reasonable manner, the scattering in the coefficients obtained may differ from one model to another. Thus, scattering in the coefficients is used as an additional criterion to assess suitability of the load models.

# CHAPTER 4

# Laboratory Experiments

A forced oscillation of a vertical cylinder in various flow fields was used to model the vibration of a slender cylinder in waves and current. A wide range of variables in all possible flow situations was required. Especially it was considered important to investigate the hydrodynamic interaction for a lock-in condition. These requirements dictated a large number of test runs.

This chapter provides an overall review of the experimental and data processing methods by which the results were obtained. A detailed description of the laboratory experiments may be found in a separate report, Shafiee-Far (1995b). The topics covered include: test facilities, experimental set up, test program, experimental procedures, measuring techniques and preliminary data processing methods.

## 4.1  Test Facilities

### 4.1.1  Test Cylinder

The experiments were executed using the test cylinder shown in figure 4.1, which has been manufactured by Marintek (Trondheim, Norway). Force transducers measured the hydrodynamic forces on each of the four rings, in two perpendicular directions. Because of shallow submergence resulting from top-end cylinder mounting above the water surface, the upper ring (No. 4) was not used during the experiments. The cylinder is 60 mm in diameter and each ring in the cylinder could represent an element of a full scale slender cylinder.

The force transducers gave a signal by means of a series of strain gages connected in a Wheatstone Bridge. A rubber skin was used to prevent the flow of water into the cylinder. The force transducers were individually calibrated before installation of the cylinder. Details of the calibration programme may be found in Shafiee-Far (1995b). Later calibrations and other checks were carried out in a more direct way to make sure that all transducers were working correctly.

The natural frequency of the cylinder as a whole was determined in air and in water by tapping it with a hammer. It was 31.66 Hz in air and 25.3 Hz in water. The natural frequencies determined for the measuring rings were more than 190 Hz, far above the frequencies of the measured forces.

### 4.1.2  Towing Tank

Experiments for this study were carried out in the Towing Tank II of the Ship Hydromechanics Laboratory of the Marine Technology Department, shown schematically in Fig. 4.2. The tank is

85 m long, 2.75 m wide and 1.25 m deep. Both regular and irregular waves can be generated by a hydraulic wave generator. Waves are damped by a wave damping beach opposite to the wave generator. The beach type is a wooden parabolic arc structure with transverse ribs.

The carriage of the towing tank moves on wheels on rails on top of the tank and can handle towing speeds up to 3 m/s. Although a maximum speed of 1.5 m/s was used for a few cases, the towing speed was often less than 1 m/s.

### 4.1.3 Measuring Probes

The waves were measured by a two-wire conductance wave probe, as normally used in this towing tank. The wave meter was mounted in front of the cylinder so that its record was not affected by the cylinder oscillation.

An electromagnetic velocity meter (EMS) from the Civil Engineering Laboratory of Fluid Mechanics was used to record simultaneous horizontal velocity components in the x and y directions. The calibration factors for this probe are not linear; the recorded signals should be corrected using a given formula to find the velocities in m/s.

### 4.2 Test Set-up

The cylinder is rigidly fixed to the oscillator as a vertical cantilever. Two different configurations were implemented for mounting the cylinder and instruments during the experiments, one for the transverse and the other for the in-line oscillation tests.

Figure 4.3 shows the configuration which was implemented for the in-line oscillation tests in still water and waves. Figure 4.4 shows two pictures taken from this experimental set-up in the towing tank, one of the cylinder and the other of the wave probe and the velocity metre.

### 4.3 Data Recording

Data from the various test runs were recorded in digital form using ASYST software - a data acquisition package.

The following independent (input) variables have been recorded, when executing the model tests in the towing tank:

- Towing speed, $V$ (m/s), in the x direction;
- Oscillation period, $T_o$ (s), in the x or y direction;
- Oscillation amplitude, $A$ (m), in the x or y direction.

The directions were as follows:

- x along the tank, positive toward the wave-maker;
- y perpendicular to this to the left when facing the wave generator.

The wave period, $T_w$ (s), and wave height were set for each test run in waves. Wave elevations

22

were recorded using the wave probe.

In addition, the following output signals were measured as digital time series:

- The forces in the x and y directions on each transducer.
- A reference signal which relates all signals to the oscillatory motion of the cylinder.
- Flow velocities in the x and y directions.

The six measured forces were denoted Fx1, Fy1, Fx2, Fy2, Fx3 and Fy3 respectively. Since the velocity-metre was mounted on the oscillator for the transverse oscillation tests (in still water and in waves), the recorded velocities for these tests are as follows:

$Vx$ = *towing velocity $\pm$ horizontal water particle velocity due to waves*
$Vy$ = $\pm$ *cylinder oscillation velocity*

For other test runs, the velocity-metre was fixed on the carriage. Thus the recorded in-line velocity is again the sum of the towing velocity and the water particle velocity due to waves. A MS-Dos computer was used to record the various signals. The time duration for each run in still water and in regular waves was 20 seconds. This was 150-300 seconds for tests in irregular waves. The sample interval for all test runs except runs in irregular waves was 0.02 seconds. The water temperature was 20-21 degrees Celsius during the experiments.

## 4.4 Testing Procedure

The variables and their values to be used in the experiments have been reviewed in Shafiee-Far (1995a) where the choice of variables and environments is summarized. The test programme involved various flow conditions; the intention was to include all possible combinations of cylinder and fluid motions.

The acceleration of the cylinder introduced an extra force component in the data signals that must be eliminated in order to obtain force signals that represent the hydrodynamic interaction force only. This was achieved by oscillating the cylinder in air. The results could be used to determine the mass of each ring, and using the reference signal, subtracting the calculated mass inertia force from the measured signal data is rather easy.

Towing the cylinder was used to simulate a current. The standard runs of towing the cylinder in still water were done with various towing speeds. These were followed by oscillation of the cylinder in still water; these runs presented the pure oscillation test case. The ratio of oscillation amplitude to cylinder diameter ($A/D$) was chosen as 0.5, 0.75, 1, 1.5, 2, 2.5, 3, 3.5 and for some tests 4 and 4.5. so that a wide range of the Keulegan-Carpenter numbers could be covered. For each of these ratios, the oscillation frequency was changed.

Transverse oscillation while towing the cylinder was the next test case. For each $A/D$ ratio, the towing speed and then the oscillation frequency were changed so that a full matrix of independent variables was generated. This resulted in a combination of flow parameters of practical interest.

23

Next, waves were added to the flow field to have the test case of transverse oscillation while towing the cylinder in waves. In order to decrease the number of runs, only three regular waves were generated for the test runs with waves. These have been denoted as H1, H2 and H3; the other variables have been changed for each of these waves. The characteristics of these waves were as follows:

|     | wave period, $T_w$ | wave height, H |
|-----|--------------------|----------------|
| H1  | 1.0 s              | $\approx 10$ cm |
| H2  | 1.5 s              | $\approx 12$ cm |
| H3  | 2.0 s              | $\approx 18$ cm |

After each test, the water in the tank was allowed to settle until there was no visible movement of the surface. Recording was started after more than 10 waves had passed the cylinder, and continued for 20 seconds for the regular waves. The sampling interval was 20 ms.

For the in-line oscillation tests, the testing procedure was the same as for the transverse oscillation tests described above.

A number of test runs with irregular waves were also carried out for both transverse and in-line oscillations. The generated irregular waves, denoted as H4, had a defined spectrum with $Hs \approx 10$ cm, $T_p \approx 1.7$ s and mean zero-crossing period $T_{01} \approx 1.2$ s. The maximum recording period was 300 seconds due to computer limitations.

A standard run with V=1 m/s was carried out before starting the planned runs each day. Some runs were repeated during the experiments to detect calibration factors' changes and equipment deterioration.

## 4.5  On-line Data Control

Before the analysis of the experiment data, the data had to be evaluated first because the signals possibly contained non-relevant information, or had to be transformed to other coordinates. The instrumentation on the carriage and the data acquisition program made the on-line data analysis possible. Significant representative data were displayed on the computer screen as a check during each experiment; many test runs were repeated in the course of the experiments. Besides, some additional runs were processed to check the suitability of the signals, see Shafiee-Far (1995b) appendix I.

Some zero tests were performed during the experiment. In a zero test the signals were recorded, while the equipment was switched on, but the cylinder was standing still in calm water. The objective of these tests was to check if the signals were constant, and to estimate the zero points of the signals.

## 4.6  Tests Carried Out

All possible combinations of flow condition and cylinder oscillation have been included in this work. Having three independent motions - current (towing), cylinder oscillation, and waves - a

comprehensive combination of flow conditions was gained.

In total, some 907 test runs were carried out for both transverse and in-line directions (including 33 runs for the cylinder oscillation in air). A list of all test runs is given in appendix II; the test runs for a specific series have been grouped together in this list. Table 4.1 gives the number of test runs for each test series.

| Flow Conditions | Cylinder Oscillation | | |
|---|---|---|---|
| | None | In-line | Transverse |
| Air | - | 33 | - |
| Still water | - | 31 | 54 |
| Current only | 43 | 107 | 211 |
| Waves only (regular and irregular) | 30 | 85 | 38 |
| Waves (regular and irregular) plus current | 16 | 158 | 102 |

Table 4.1  Number of Test Runs for Each Test Series

## 4.7  Data Ranges Achieved

As already mentioned, one objective of the present study was to cover a wide range of nondimensional parameters. However, there were some practical limitations on the combinations of independent variables - Reynolds number, Keulegan-Carpenter number and reduced velocity - used in the tests. The range of variable values in the present experiments was just a part of the desired ranges of values, see figure 4.5. Nonetheless, the model size and available facilities allowed coverage of a wide range of Keulegan-Carpenter numbers and reduced velocities.

The physical limitations of the experimental facility permitted only subcritical flow conditions, i.e., the Reynolds number could never exceed $1.3*10^5$. The following comments relate to the low Reynolds numbers in these tests:

1. Many full scale cases involving hydrodynamic interaction and lock-in vibrations of slender cylinders do occur in a subcritical flow regime.

2. Some previous investigations have shown that the lock-in behaviour - which is the most important part of many hydrodynamic interaction studies - is not much different under critical and subcritical Reynolds numbers, see Moe et. al (1994).

3. While the Reynolds number still falls short of practical values in many cases, it is higher than those realized by most other investigators.

The independent variables in an individual test are: the towing speed, oscillation frequency and amplitude, as well as the wave height and period. The ranges of these variables in the experiments were as follows:

| Towing speed: | 0 and 0.05 to 1.50 m/s |
| Oscillation frequency: | 0 and 0.50 to 2.00 Hz |
| Oscillation amplitude: | 0 and 0.03 to 0.275 m |
| Wave period: | 0 and 1.00 to 2.50 s |
| Wave height | 0 and 0.07 to 0.18 m |

These yielded a wide range of derived parameter values. These are given for each test case in the later chapters.

## 4.8  Data Correction

A principal factor in experimental investigations is the dependence of measured quantities on the experimental conditions; all measured values depend on experimental factors such as aspect ratio, end condition, blockage ratio, presence of free surface, and so on. Because of this situation, several researchers have spent a great deal of effort on attempts to quantify the effects of these experimental factors. This is a desirable research goal in itself, but not one that is directly connected with the basic problem of hydrodynamic interaction. Various factors affecting the accuracy of the results are discussed below.

### 4.8.1 Various System Effects

The test cylinder itself is rigidly fixed to the oscillator. With a view to the measurement of forces, it is important that the cylinder does not oscillate in its natural frequency. The first natural frequency of the whole cylinder in water was 25.3 Hz. Because the maximum excitation frequency was 2 Hz, thus much smaller than the natural frequency of the cylinder, the cylinder responds quasi-statically.

The stiffness of the cylinder is important for two further reasons: to keep the flow-field two-dimensional, the deflection of the cylinder must be very small. Second, if the cylinder is too flexible, the phase between the different force-transducers will be different. By structural analysis it was shown that the maximum deflection would be about 0.3 mm; this can be neglected.

Since giving the cylinder an exact rotational orientation was rather difficult, all data should be recalculated if a significant rotation error was detected. The orientation of the cylinder was adjusted by means of the measured forces by carrying out several runs for both transverse and in-line tests. A varying towing speed and no oscillation was used in these runs. It was found that the rotation errors cause such minor errors in the measured forces that they could be neglected in the data analysis; the maximum error was less than 1%.

### 4.8.2  Flow Considerations

### 4.8.2.1  End Effects

Many experiments have shown that disturbances in the flow along the cylinder due to the proximity of the cylinder ends, the free surface, or test tank walls can affect test results. Two methods have been used to ensure two-dimensional flow conditions: 1) providing a sufficiently

long cylinder - where the force measurements are taken far from the ends, and 2) the addition of end plates.

Since the measuring rings of the cylinder are very short (15mm), the three-dimensional effect could not be a problem in this work. However, an end plate was used during transverse oscillations in still water to prevent a possible end effect. Using such a device for tests in waves was not possible. Nonetheless, the dummy parts of the cylinder were relatively long (at least 5 diameters) to reduce the end effect.

One can check the possibility of some influence of the water surface near the upper transducer (no. 3) and the end of the cylinder near the lower transducer (no. 1) by comparing the data from of all three transducers in a single run. The measured force on the middle ring (no. 2) can be used for analysis of most test runs.

### 4.8.2.2 Free-surface Effects

A cylinder in flowing water or a cylinder moving in still water generates a wake on the water surface which disturbs the pressure field in the immediate vicinity of the cylinder and the water surface. This pressure disturbance leads to an additional force acting locally on the cylinder. This additional wake force will, of course, act only near the water surface and will have its greatest influence on a vertical cylinder. However, one might expect its effect to be greatest in a steady flow situation rather than in waves.

For neglecting the free-surface effect, Bishop and Hassan (1964) have used the criterion that the maximum Froude number be much less than unity,

$$Fr_{max} = \frac{V_{max}}{\sqrt{g h_{min}}}$$

where $V_{max}$ is the maximum flow (towing) velocity, g is the acceleration due to gravity, and $h_{min}$ is the minimum depth of submergence of the model.

The $Fr_{max}$ value was 0.375 in the experiment by Bishop and Hassan; they argued that it was sufficiently low. In the present experiment, the $Fr_{max}$ value was less than 0.32 for ring No. 2 in most test runs. This justifies neglecting the effect of the free-surface. It is more than 0.375 for some tests in which the free-surface effect cannot be neglected.

The effect of free-surface wake on the measured forces has been examined for the current only test case in the following chapter. The result shows that this effect for the lower ring is negligible while it is considerable for the upper ring. The data for this upper ring have not been used in this study, however. On the other hand, the free-surface effect is less for the oscillatory flow which form the bulk of the test runs in this study.

### 4.8.2.3 Blockage Effects

Due to the presence of the walls of the channel around the model, the force coefficients measured on a cylinder model in a finite body of water are different from the values expected in an infinite

27

water body; this is referred to as the "blockage effect." Empirical blockage corrections are applied to the measured forces and these corrections depend on the equivalent blocking ratio D/B, or the ratio of the cylinder diameter to the transverse dimension of the test facility. In the present experiment, the blocking ratio was only of the order of 2.2 percent and so no correction was needed.

### 4.8.3 Equipment Deterioration and Long Term Stability

Calibration factors may change during the experiment due to equipment deterioration - especially the rubber skin condition. Since the time interval between the first and the last run was several weeks, the possibility of such an influence on the measured data was realistic. This was checked carrying out some standard runs before conducting tests each day. The results of these runs showed only a minor change in the average recorded force acting on rings in each case, see Shafiee-Far (1995b).

### 4.8.4 Mass Forces

The acceleration of the cylinder and the measuring element itself introduces an extra force component in the forced oscillation tests. This force must be subtracted from the recorded forces to obtain force signals that represent only the hydrodynamic interaction forces. This was done by using the results from the cylinder oscillations in air for a variety of amplitudes and frequencies.

There are two ways to eliminate the inertia forces of the ring from the measured signals:

1.   The mass of the ring could be determined from the runs in air, and assuming that the cylinder oscillation during the experiments in water is a "nice" single harmonic, subtracting the mass force from the measured signals is easy:

$$F_{mass} = m_{ring} \cdot \bar{a}(t)$$

$$F_{hyrodynamic} = F_{measured} - F_{mass}$$

2.   One could subtract the signals from the runs in air directly from the recorded signal of a run in water. Here the frequencies and amplitude must be the same for both runs.

Since the setting of the oscillation frequencies could not be done precisely, the first method had to be applied here.

### 4.9 Preliminary Data Processing

As mentioned in section 4.3, hydrodynamic force components in the x and y direction, cylinder motion trace, wave elevation and velocity signals were sampled at 20 ms intervals (50 Hz). The software used to record the data stored the data in binary format.

The first step in data processing was to translate the binary data to ASCII and spreadsheet forms;

this was accomplished with a program within the data acquisition package. The ASCII files were then played back through a digital lowpass filter to remove unwanted frequencies higher than 8 Hz.

Beside the above initial data processing, some small programs were written to automate further processing such as calibrating velocity signals, removal of ring mass forces, and spectral and statistical analysis. These provided spectra, standard deviation, maxima/minima of force and velocity signals. This is useful information in itself and further served the purpose of quality control.
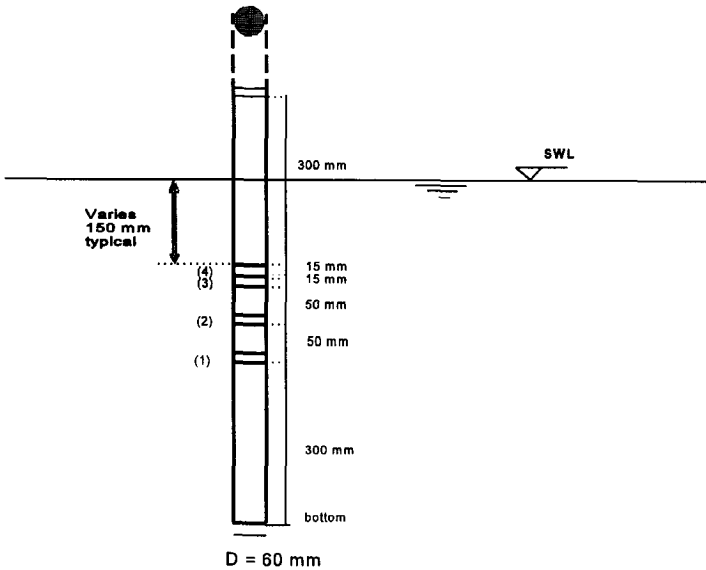


Figure 4.1  Marintek Test Cylinder
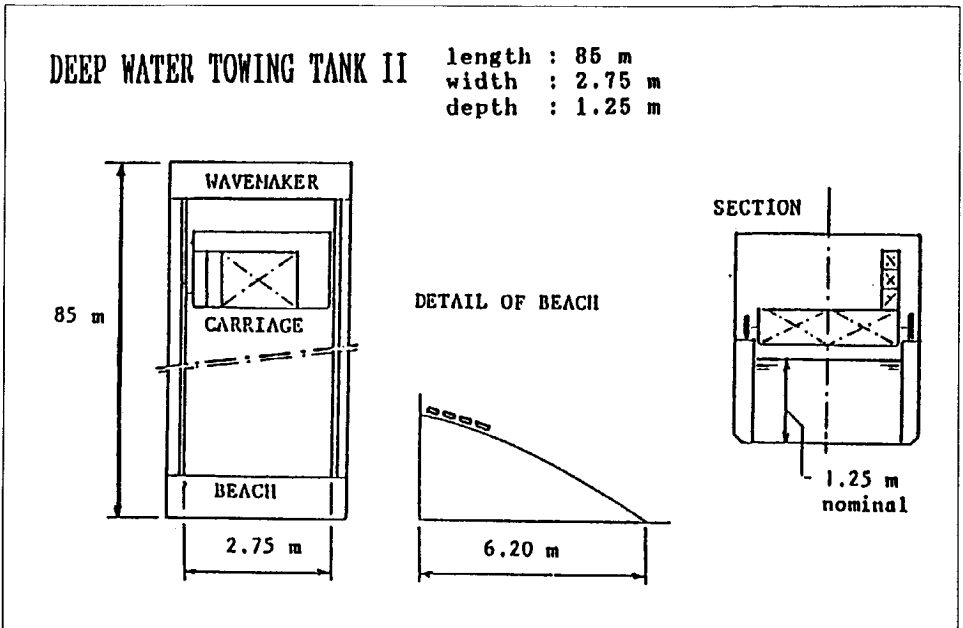
Figure 4.2  Sketch of The Towing Tank Used for Investigation of Hydrodynamic Interaction
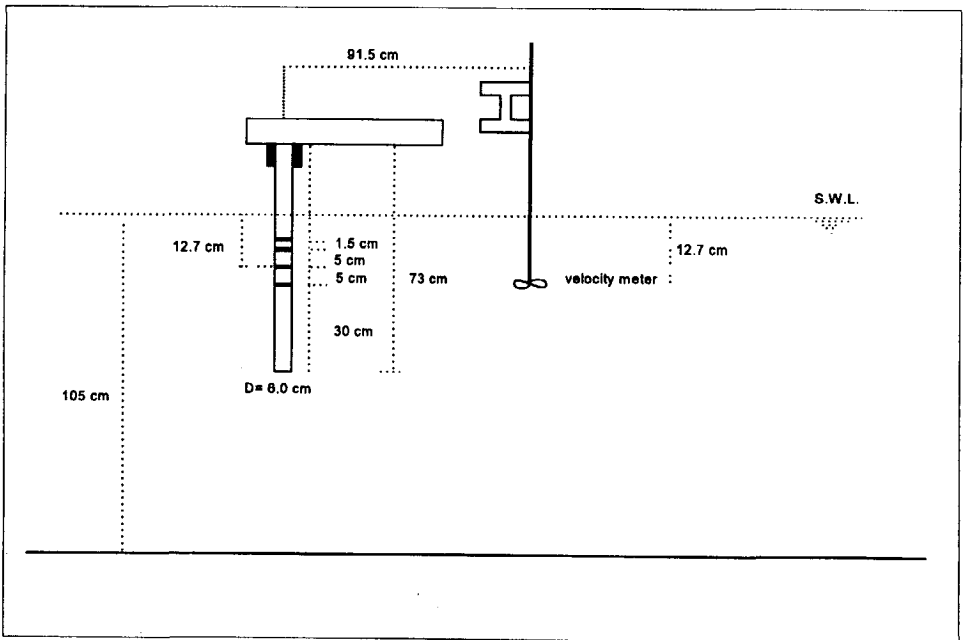


Figure 4.3  Experimental Set-up for In-line Oscillation Tests

30
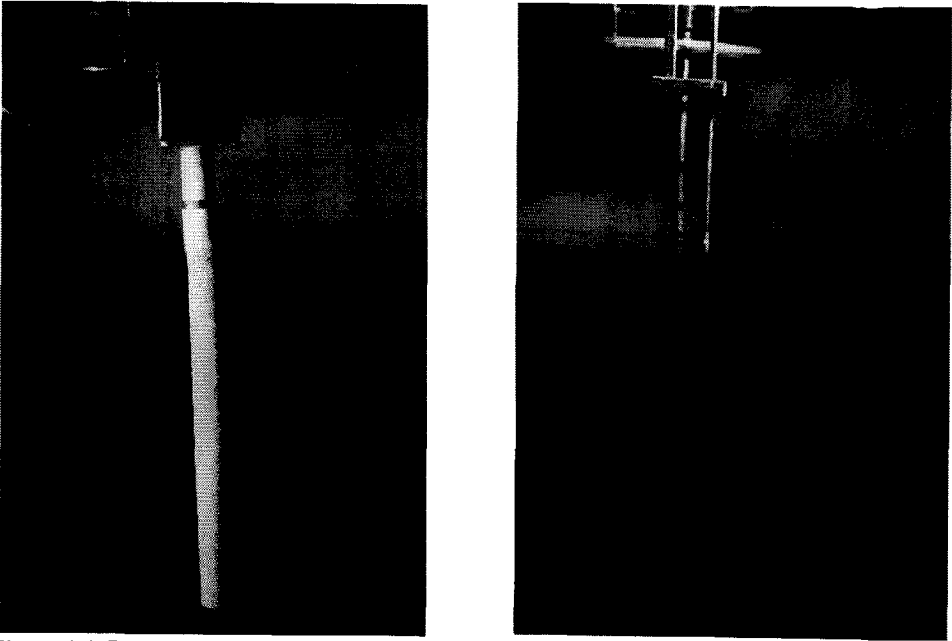
Figure 4.4  Pictures of the Cylinder and Instruments in Experimental Set-up
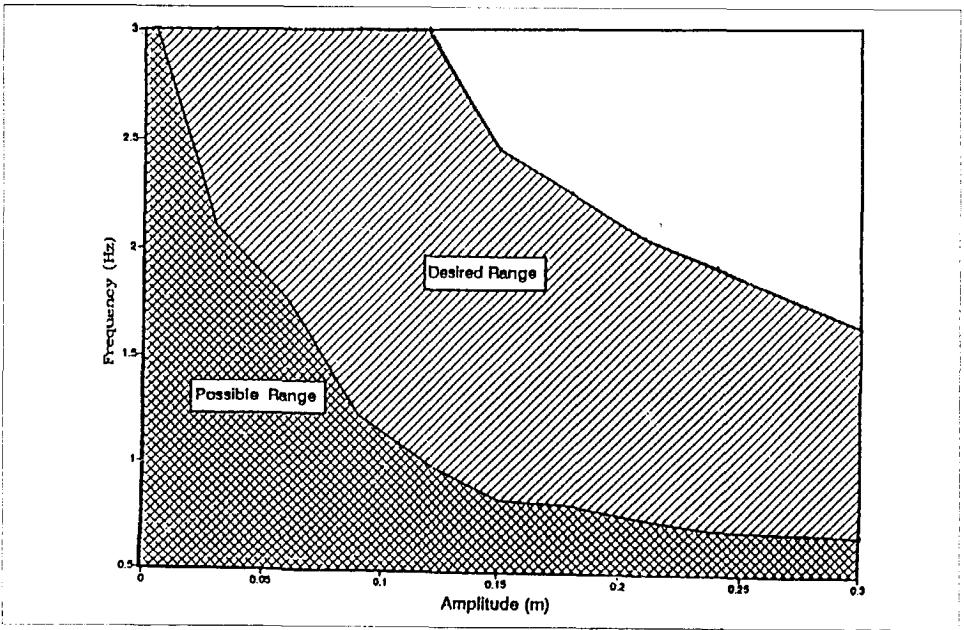

Figure 4.5  Desired and Possible Range for Oscillation Frequency and Amplitude

# CHAPTER 5

# Single Mode Tests

A number of single mode tests were carried out to establish base cases for situations when other motions were also included. Results of these basic tests are presented here. In addition to the scientific benefit of this data, the single mode tests were a valuable way of monitoring the performance of the experimental apparatus and systems in the water.

## 5.1 Towed Cylinder in Still Water

Towing was used to simulate currents in the laboratory; the cylinder was towed with different speeds along the tank. Since the aim here was to produce results for a fixed cylinder in currents, the term 'current' will be used to describe the towing of the cylinder in still water.

### 5.1.1 Specific Load Model Forms

Vortices are shed from a cylinder towed in still water or a fixed cylinder in a current. These are shed at the Strouhal frequency $f_v$ given by the relation:

$$f_v = \frac{St\,V}{D} \tag{5.1}$$

The Strouhal number $St$ is essentially a nondimensional frequency approximately equal to 0.2 over the range of subcritical Reynolds numbers. Due to the vortex shedding, the cylinder experiences an oscillating lift force at the frequency of shedding, an oscillating drag force at twice the frequency of shedding, and a mean drag force. Thus, drag and lift forces per unit length are given as:

$$F_D = F_{Dm} + \hat{F}_{Do}\sin(4\pi f_v t + \phi) \tag{5.2}$$

$$F_L = \hat{F}_L \sin(2\pi f_v t + \psi) \tag{5.3}$$

where $F_{Do}$ and $F_L$ are the magnitudes of the oscillating Strouhal drag and lift forces respectively, $F_{Dm}$ is the magnitude of the mean drag force and $\phi$ and $\psi$ are corresponding phase angles. There is a relation between $\phi$ and $\psi$, however. Each of the force components can be nondimensionalised in the usual manner by the dynamic pressure head factor $\frac{1}{2}\rho D V^2$ to give the associated force coefficients. Thus, the mean and oscillatory drag coefficients are:

$$C_{Dm} = \frac{F_{Dm}}{0.5\,\rho D V^2} \tag{5.4}$$

$$C_{Dv} = \frac{\hat{F}_{Do}}{0.5\,\rho D V^2} \tag{5.5}$$

and the lift coefficient is:

$$C_L = \frac{\hat{F}_L}{0.5\,\rho D V^2} \tag{5.6}$$

## 5.1.2 Specific Processing Methods

Data processing for towing only runs was relatively straightforward. After initial data reduction - transferring data to a separate processing program and lowpass filtering as described in section 4.9 - a spectral analysis was performed on each time record of the transverse force component (1000 points) to determine the shedding frequency. A power spectrum for a typical force trace in the transverse direction (lift force) is shown in figure 5.1 in which the peak in the spectrum is associated with the shedding frequency. The obtained shedding frequency for each test run was then used to calculate the Strouhal number related to that test run.

The magnitudes of the mean drag coefficient $C_{Dm}$ oscillating drag coefficient $C_{Dv}$ and the oscillating lift coefficient $C_L$ were estimated from the time traces. To compute the oscillating drag coefficient $C_{Dv}$, first the mean drag force was subtracted from the force record in the x direction. Then, the least squares method was used to fit the model to the data using the shedding frequency obtained from the spectral analysis. The lift force coefficient $C_L$ was calculated using the first Fourier series component of the transverse force.

## 5.1.3 Results

The average Strouhal number calculated from 43 stationary runs was found to be 0.191, with a standard deviation of less than 2.5%.

The estimated mean drag coefficients $C_{Dm}$ from the 43 tests approximate a normal distribution, with a mean of 1.11 and a standard deviation of 0.044 for ring no. 1. The calculated $C_{Dm}$ values for the middle ring (ring no. 2) are slightly higher. A reason for these differences could be the free surface effect considered in appendix III.

Figure 5.2 shows $C_{Dm}$ versus Reynolds number for these pure-current tests. The lines in this figure are third order polynomial regression lines through data points which have been determined by a least squares method. Such lines in this and most of the following figures are added to show the behaviour of the data more clearly. The obtained mean drag values $C_{Dm}$ are in relatively good agreement with those published in the literature, e.g. Schlichting (1968); this information does serve as a check of the experimental set-up. The estimated oscillating drag coefficients $C_{Dv}$ can be grouped and approximated as a normal distribution; this has a much larger spread than that for the mean drag coefficient. Table 5.1 summarizes results for the in-line force coefficients.

|        | $St$  | $C_{Dm1}$ | $C_{Dv1}$ | $C_{Dm2}$ | $C_{Dv2}$ |
|--------|-------|-----------|-----------|-----------|-----------|
| Mean   | 0.191 | 1.112     | 0.076     | 1.204     | 0.076     |
| STD    | 0.005 | 0.044     | 0.024     | 0.025     | 0.023     |

Table 5.1  Summary of Results for Only-Current Runs

Although there exists a lot of lift force coefficient data in the public literature, however, the degree of scattering in these data is very high. A complete understanding of the assumptions and limitations inherent to each particular data set is required to compile these data. The reported data sets seem to depend on many different factors two of the more important being instrumentation design and end effects.

In figure 5.3, the rms lift force coefficient $C_{Lrms}$ is plotted versus $Re$ and shows a comparison between the present results and two other experiments reported. These are included here even though lift is not the main topic of this dissertation.

The lift force coefficient values are much lower than values for the mean drag force coefficients and higher than the oscillatory drag coefficients.

## 5.2  Forced Oscillation Tests

Forced oscillation tests are often used in the laboratory to model oscillatory flow around fixed cylinders. A kinematically identical flow may be achieved by oscillating the cylinder rather than by oscillating the ambient flow. The forces in the two situations differ because the Froude-Krylov force is zero for the oscillating cylinder. Forced oscillation tests are also used to model hydrodynamic interaction of oscillation and displacement response of the small elements that form flexible cylinders. This approach is based on the philosophy that a short element of a long flexible cylinder may be modelled as a rigid cylinder. The challenge is the accurate modelling of the hydrodynamic interaction of such short elements.

In the present study, the degenerate tests of oscillating the cylinder in still water can be seen as a calibration and to give an indication of the value of the data obtained. Moreover, these tests will be used as a reference for further steps where complex flow conditions are involved.

### 5.2.1  Load Model Forms

In this study, both the Morison equation and harmonic analysis methods were used to model the hydrodynamic forces on the cylinder oscillating in still water. The Morison equation for pure cylinder oscillation is given in equation 3.2. The harmonic model here could be as equation 3.9 with the coefficient given in equations 3.11. If only the first component of the harmonic model given in equation 3.10 is used, the load model for the in-line force may be written as:

$$F_{inline} = 0.5 \, \rho \, D \, C_{DT} \, u_m^2 \sin(2\pi f_o t + \phi_o) \tag{5.7}$$

This is a drag form harmonic model. If the coefficient $C_{AI}$ given in equation 3.13 is applied, one may write a harmonic model in an inertia form as:

35

$$F_{inline} = \rho \frac{\pi D^2}{4} C_{AT} \dot{u}_m \sin(2\pi f_o t + \phi_o) \tag{5.8}$$

It should be noted that there are two unknown parameters in above harmonic models, i.e. a coefficient ($C_{DT}$ or $C_{AT}$) and a phase angle.

Since a linear form of the Morison equation is usually used for frequency domain dynamic analysis of offshore structures, such a linear form of the Morison equation has also been examined as a separate load model in this study. Using only the first term in the Fourier expansion of $|\dot{x}|$, a linear form of the Morison equation may be written as:

$$|\dot{x}| = \frac{8}{3\pi} \dot{x}_m \tag{5.9}$$

$$F = -C_{Dl}(\frac{1}{2}\rho D) \frac{8}{3\pi} \dot{x}_m \dot{x} - C_{Al}(\rho \frac{\pi}{4} D^2) \ddot{x} \tag{5.10}$$

The result of this model is compared with the original form.

Table 5.2 summarizes all load models evaluated for hydrodynamic interaction of oscillating cylinders is still water.

| Load Model | Equation | Code |
|---|---|---|
| Morison equation | $F = -C_D(\frac{1}{2}\rho D) \|\dot{x}\|\dot{x} - C_A(\rho \frac{\pi}{4} D^2)\ddot{x}$ | Model I |
| Harmonic model (drag form) | $F = 0.5 \rho D C_{DT} \dot{x}_m^2 \sin(2\pi f_o t + \phi_o)$ | Model II |
| Harmonic model (inertia form) | $F = \rho \frac{\pi D^2}{4} C_{AT} \ddot{x}_m \sin(2\pi f_o t + \phi_o)$ | Model III |
| Linearised Morison equation | $F = -C_{Dl}(\frac{1}{2}\rho D) \frac{8}{3\pi} \dot{x}_m \dot{x} - C_{Al}(\rho \frac{\pi}{4} D^2)\ddot{x}$ | Model IV |

Table 5.2  List of Load Models Studied for Forced Oscillation Tests

### 5.2.2 Data Range

The cylinder was oscillated with various amplitudes and frequencies; this led to the parameter ranges given in table 5.3. The $Re_o$ and $KC_o$ value combinations are plotted in figure 5.4.

| Parameter | Definition | Range |
|---|---|---|
| Amplitude:Diameter Ratio | $A/D$ | 0.5 - 4.0 |
| Max. Oscillatory Velocity | $\dot{x}_m = 2A\pi f_o$ | 0.09 - 1.01 m/s |
| Reynolds Number | $Re_o = \dot{x}_m D/\nu$ | 5300 - 60300 |
| Keulegan-Carpenter Number | $KC_o = \dot{x}_m T_o/D$ | 3.1 - 25.3 |
| Frequency parameter | $\beta = Re_o/KC_o = D^2/T_o\nu$ | 1680 - 7200 |

Table 5.3  Experimental Variable Ranges

### 5.2.3 Analysis Procedure

The analysis of the pure oscillation data consisted of initial data reduction followed by carrying out a FFT to determine the exact external oscillation frequency. Then, the inertia forces of the test rings were subtracted from the in-line force time trace. This was followed by statistical analysis of the data. The following force values were obtained: mean, standard deviation, maximum over recording time and average of maxima from each cycle. Spectral analysis of the signals was carried out for all runs as well.

Oscillating the cylinder at the frequency $f_o$ the oscillating velocity $\dot{x}$ and the acceleration $\ddot{x}$ are given by:

$$x = A \sin(2\pi f_o t)$$
$$\dot{x} = A(2\pi f_o)\cos(2\pi f_o t)$$
$$\ddot{x} = -A(2\pi f_o)^2 \sin(2\pi f_o t)$$

(5.11)

The cylinder oscillating velocity and acceleration were calculated using the recorded signal for the cylinder motion $x$.

Harmonic analyses were performed to determine Fourier components of the hydrodynamic forces. Results of these analyses were used to compute the in-line force coefficients for the load models given in table 5.2. Reference sine and cosine waveforms were created using the external oscillation frequency; then these were used to calculate the magnitudes of the force coefficients as explained in appendix I.

*Morison Equation, Model I*
Both Fourier analysis and least squares technique were used to calculate the drag and inertia coefficients in the Morison equation. The coefficients for first harmonic components were used to compute the Fourier-averaged force coefficients of the Morison equation, see appendix I.

$$C_D = \frac{3\pi}{8} \cdot \frac{a_1}{0.5\rho D \dot{x}_m^2}$$

(5.12)

$$C_A = \frac{b_1}{0.25 \rho \pi D^2 \ddot{x}_m} \tag{5.13}$$

Besides above method, the in-line Morison equation force coefficients were also computed using a weighted least squares fit over the complete time segment, see appendix I. The velocity required in this analysis was obtained by taking the derivative of the displacement signal.

*Models II and III*

The amplitudes of in-line forces were used to compute $C_{DT}$ and $C_{AT}$ in equations 5.7 and 5.8, model II and III. The phase angle of the in-line force with respect to the externally imposed oscillating motion was calculated as the difference between the phase angle of the force and the phase angle of the motion.

*Model IV*

Only a least squares method was used to compute drag and inertia coefficients for the linear form of the Morison equation.

### 5.2.4 Results and Discussion

#### 5.2.4.1 Force Coefficients

Comparisons between the coefficients obtained from the least squares fit and the Fourier-averaged coefficients have shown that both methods yield approximately the same $C_A$ values. The $C_D$ values differed slightly as shown in figure 5.5. Such a slight difference between drag coefficients obtained from the two methods is comparable with the theoretical relationship between them, see appendix I. Darg coefficients obtained from the least squares method will present and discussed for the present test case as well as for other test cases .

The drag and inertia coefficients are varied with the Keulegan-Carpenter number as shown in figure 5.6. Variations of $C_D$ and $C_A$ versus the Reynolds number $Re_o$ are illustrated in figure 5.7. These figures show, within the range of $Re_o$ and $KC_o$ values encountered, that $C_D$ and $C_A$ depend mainly on $KC_o$.

Dependency of the force coefficients $C_{DT}$ and $C_{AT}$ (in models II and III) on $KC_o$ are shown in figure 5.8. Both coefficients exhibit good correlation with $KC_o$ and the degree of scattering around trend lines is relatively low. The value of $C_{DT}$ decreases with increasing $KC_o$ while the value of $C_{AT}$ increases. The low scatter in the force coefficients for model II and III concurs with earlier observations for the maximum force coefficient, $C_{max} = F_{max} / 0.5 \rho D u_m^2$, or for the RMS force coefficient $C_{rms} = F_{rms} / 0.5 \rho D u_{rms}^2$, see e.g., Bishop (1979), Stansby et al. 1983 and Bearman 1988.

Since the full force trace is needed in a structural analysis, the magnitude of the phase angle has to be determined. The behaviour of the phase angle is illustrated in figure 5.9; increasing $KC_o$ generally results in a decrease in the phase angle. This observation is completely logical due to the fact that at low $KC_o$ values the inertia force is dominant so that $\phi_o \approx 180°$, and at high $KC_o$ values the drag force is dominant and $\phi_o \approx 90°$; in intermediate $KC$ range (drag-inertia

dominated region) there is a gradual transition.

The results for the linear form of the Morison equation, model IV, are presented in figure 5.10. The $C_{Dl}$ and $C_{Al}$ values in this figure have been calculated using a weighted least squares method similar to that used to obtain the original Morison equation coefficients. Comparing figures 5.10 and 5.6, one can observe that the drag coefficients for both models are similar. The average $C_{Dl}$ / $C_D$ ratio is 1.07 with a standard deviation of less than 3%. This suggests that using only the first term in the Fourier expansion of $|\dot{x}|$ will estimate the drag force quite well. The added mass coefficients $C_A$ and $C_{Al}$ are identical - as expected - for the two models.

### 5.2.4.2  Load Model Fitting

Each of the load models given in table 5.2 was used with the input-output data pairs of each of the test runs. As discussed in the preceding section, each of these models has its own distinct set of coefficients. The goodness-of-fit parameter, $\epsilon$, given by equation 3.21 was used to evaluate the quality of fit of each model to the data. The lower this parameter value, the better the quality of the fit.

The $\epsilon$ values for each model were ranked and grouped into histograms. Table 5.4 lists the calculated mean and standard deviation (STD) value of the $\epsilon$ distributions using the load models. Since the load models II and III result in identical $\epsilon$ values by definition, only $\epsilon$ values for model II are given in this table. The fourth and the fifth column in this table show the cumulative distribution of $\epsilon$, i.e. the percentage of runs for which $\epsilon<0.15$ and $\epsilon <0.2$ for each computational model. Sarpkaya (1976) found that the $\epsilon$ value for the Morison equation ranged from 2 to 20 percent with a representative value being on the order of 10 to 12 percent. The representative value for $\epsilon$ is 12 percent for the original Morison equation in the present tests; the $\epsilon$ values for the other models are slightly lower.

Figure 5.11 shows the results for the load models from table 5.2. The cumulative percentage of the 31 test runs is plotted against $\epsilon$ here. High curve values indicate that relatively more of the test runs fitted the chosen model well.

Taking all the information in table 5.4 and figure 5.11 together, one can conclude that all models fit the measured data roughly well; the harmonic load model gives the best fit. The linear form of the Morison equation gives a result similar to that for the harmonic load model and (surprisingly) the quality of fit for this model is better than for the original form of the Morison equation.

|  | Fit quality $\epsilon$ value | | Percentage of runs with: | |
|---|---|---|---|---|
| Load Model | Mean | STD | $\epsilon < 0.15$ | $\epsilon < 0.2$ |
| Model I | 0.120 | 0.047 | 76.0% | 100% |
| Models II & III | 0.108 | 0.039 | 92.0% | 100% |
| Model IV | 0.104 | 0.039 | 88.0% | 100% |

Table 5.4 Forced Oscillation Tests, Model Fitting Statistics

## 5.3  Fixed Cylinder in Regular Waves

The same test set up as before was used to conduct a number of tests for the condition of a fixed cylinder in regular waves. The still water depth was kept constant at 1.05 m. The test cylinder was fixed in a cantilever form and the hydrodynamic forces on two rings were recorded in both in-line and transverse directions.

### 5.3.1  Load Model Forms

The small amplitude wave theory was used to calculate wave kinematics. The potential function of the incident wave is written as:

$$\phi = \frac{gH}{2\omega} \frac{\cosh(ks)}{\cosh(kd)} \sin\theta \tag{5.14}$$

where $\theta = kx - \omega t$ is the wave phase angle.

The displacement of the water surface $\eta$ is written as:

$$\eta = \frac{H}{2} \cos\theta \tag{5.15}$$

The orbital velocity $u$ and acceleration $\dot{u}$ of a fluid particle are written as:

$$u = \frac{\pi H}{T} \frac{\cosh(ks)}{\sinh(kd)} \cos\theta \tag{5.16}$$

$$\dot{u} = \frac{2\pi^2 H}{T^2} \frac{\cosh(ks)}{\sinh(kd)} \sin\theta \tag{5.17}$$

The mathematical formulations used to estimate the hydrodynamic force in the in-line direction are similar to the cylinder oscillation test case except that here the inertia coefficient $C_M$ is used instead of the added mass coefficient $C_A$. These formulations are given in table 5.5.

### 5.3.2  Data Range

The nondimensional parameters on which the hydrodynamic force coefficients depend are mainly the Keulegan-Carpenter number $KC$ and the Reynolds number $Re$. Due to limitations of the wave-maker and the tank, generating waves of large amplitude was impossible; the maximum attainable $KC$ number was less than 10.

Two independent variables were the period and amplitude of the waves. Hydrodynamic forces at two different elevations were recorded. Thus, there were two sets of nondimensional parameters for each test run. The ranges of the nondimensional parameters of the experiments are given in table 5.6.

40

| Load Model | Equation | Code |
|---|---|---|
| Morison equation | $F = C_D(\frac{1}{2}\rho D)\,|u|u + C_M(\rho\frac{\pi}{4}D^2)\dot{u}$ | Model I |
| Harmonic model (drag form) | $F = 0.5\,\rho\,D\,C_{DT}\,u_m^2\,\sin(2\pi f_w t + \phi_w)$ | Model II |
| Harmonic model (inertia form) | $F = \rho\,\frac{\pi D^2}{4}\,C_{MT}\,\dot{u}_m\,\sin(2\pi f_w t + \phi_w)$ | Model III |
| Linearised Morison equation | $F = C_{Dl}(\frac{1}{2}\rho D)\,\frac{8}{3\pi}\,u_m\,u + C_{Ml}(\rho\frac{\pi}{4}D^2)\dot{u}$ | Model IV |

Table 5.5  List of Load Models for Pure Wave Tests

| Parameter | Definition | Range |
|---|---|---|
| Keulegan-Carpenter Number | $KC_w\,(=u_m T_w/D)$ | 2.3 - 9.6 |
| Reynolds Number | $Re_w\,(=u_m\,D/\nu)$ | 8300 - 17400 |

Table 5.6  Parameter Ranges for Pure Wave Tests

### 5.3.3 Analysis Procedure

The analysis procedure was similar to that for the previous tests. After data reduction, the exact amplitude and period of the waves were determined using a FFT analysis. Then the horizontal water particle velocities and accelerations were computed using linear wave theory. The force coefficients for the Morison equation and its linearised form, model IV, were computed using the least squares technique. The coefficients for the harmonic load models were determined using results of a harmonic analysis.

### 5.3.4 Results and Discussion

### 5.3.4.1 Force Coefficients

The calculated hydrodynamic force coefficients using the original Morison equation are discussed in this section. The results show that the coefficients obtained depend mainly on the Keulegan-Carpenter number $KC_w$. The force coefficients are, therefore, shown as a function of $KC_w$ in figure 5.12. The hydrodynamic forces were inertia dominated for all test runs in this series. The obtained coefficients agree well with those reported for wave force measurements in the literature, e.g. Chakrabarti (1980). The scatter in drag coefficients is more than in the inertia coefficients; the average $C_D$ value is 1.05 with a standard deviation of 30% while the average value for $C_M$ is 1.6 with a standard deviation of 10%.

Comparing the results from forced oscillation tests and pure wave tests, one can observe that the force coefficients from both tests have the same tendencies if plotted versus the Keulegan-Carpenter number. However, the degree of scattering for drag coefficients from wave force measurements is more than those from cylinder oscillation tests.

The effect of Reynolds number is not discussed in detail is this work; this would need another experiment with a different experimental set-up and cylinders.

The coefficients $C_{DT}$ and $C_{MT}$ of the harmonic models II and III are shown in figures 5.13, as a function of $KC_w$. As seen from this figure, these total force coefficients turn out to be much more stable than the drag and inertia coefficients for the Morison equation. The $C_{DT}$ decreases as the $KC_w$ increases and tends to a value around 1.5 while the $C_{MT}$ increases with increasing $KC_w$; this also tends to a value around 1.5. However, these force coefficients do not give all the necessary information about the hydrodynamic force, since the phase and the full force traces are usually needed in structural analysis. Thus, the phase angle ($\phi_w$ values) were determined from the harmonic analysis results; they are plotted versus $KC_w$ in figure 5.14. Just as for the total force coefficients, the curve is also smooth and the $\phi_w$ data points show less scatter. Having the results for the total force coefficients ($C_{DT}$ and/or $C_{MT}$) and the phase angle, computing the full force trace is rather easy.

Figure 5.15 illustrates the variation of drag coefficient $C_{Dl}$ against $KC_w$ for the linearised form of the Morison equation (model IV). The results show the same tendencies as $C_D$ for the original Morison equation in figure 5.12. Overall, the drag coefficients obtained from the linearised form are slightly higher than the values for the original form; the average $C_{Dl}/C_D$ ratio is about 1.05.

### 5.3.4.2 Load Model Fitting

The quality of fit of the load models to the data was evaluated using the same procedure as for the previous test case. The statistics of the $\epsilon$ values for each model were used for this purpose. The final results of this evaluation are given in table 5.7. The cumulative probabilities of $\epsilon$ for each load model are given in figure 5.16. Considering all these results, one could draw the same conclusion as for the forced oscillation tests; all load models fit the data pretty well, but the best fit is obtained using the harmonic load model.

Comparing the fit quality between the forced oscillation tests and the wave tests, it is seen that the $\epsilon$ values for the wave tests are lower than those for in the forced oscillation tests. These differences may be related to the vertical component of the orbital velocity; the strength of the vortices formed in waves are lower than those in a corresponding purely two-dimensional flow. In forced oscillation tests, the flow field around the cylinder is nearly two-dimensional and the strengths of the vortices shed by the cylinder are relatively high. Another reason for such differences in $\epsilon$ values for the two test cases is that the wave tests are in the inertia dominated range ($KC_w < 10$); for the same $KC_o$ range the forced oscillation tests give small $\epsilon$ values as well.

| Load model | Fit quality $\epsilon$ value | | Percentage of runs with: | |
|---|---|---|---|---|
| | Mean | STD | $\epsilon < 0.15$ | $\epsilon < 0.2$ |
| Model I | 0.054 | 0.036 | 90.5% | 95.2% |
| Model II & III | 0.030 | 0.019 | 100.0% | 100.0% |
| Model IV | 0.055 | 0.046 | 88.1% | 92.9% |

Table 5.7  Fixed Cylinder in Waves, Model Fitting Statistics

## 5.4  Conclusions From the Single Mode Tests

The results of the single mode tests have been reported in this chapter. The original motivation in conducting these experiments was to lay the basis for the multi-mode tests that are discussed in the following chapters. The single mode tests support the following conclusions:

1.      The long term durability of the measuring devices was acceptable.

2.      The drag coefficients obtained for the towed cylinder in still water agree well with those reported in the literature. This indicates that the equipment worked correctly.

3.      The added mass coefficient $C_A$ obtained by a least squares fitting to the data and by a Fourier average method (see appendix I) are almost identical while the drag coefficient $C_D$ values are slightly different; $C_D$ values using the Fourier average method are about 10% less than those using the least squares method.

4.      Force coefficients for pure wave tests are in good agreement with those for forced cylinder oscillation tests at a corresponding Keulegan-Carpenter number over the range of $KC$ - values over which the data extend ($KC \leq 10$). However, the degree of scattering in drag coefficients obtained from wave tests is more than that obtained from forced oscillation tests.

5.      Overall, a harmonic load model fits the data as well as does the Morison equation if the corresponding phase angle is determined correctly. Observations indicated that there is a correlation between the phase angle and the Keulegan-Carpenter number.

6.      A linear form of the Morison equation can also be used to reproduce the in-line force; the computed signals fit the measured signals as closely as the original Morison equation does, provided that the associated value of the linearised drag coefficient is used.
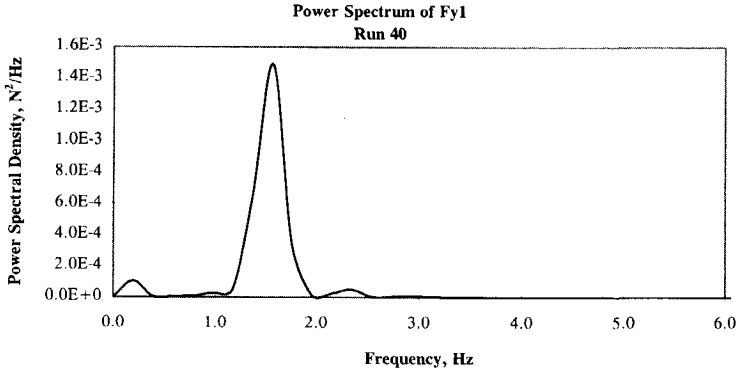
Figure 5.1 Towing the cylinder in still water, power spectrum of a typical transverse force
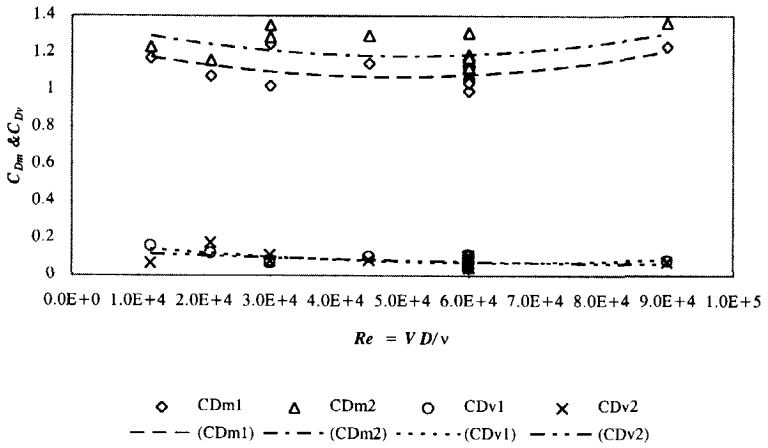


Figure 5.2 Towing the cylinder in still water, mean and oscillating drag force coefficients plotted versus $Re$; lines: 3rd order polynomial regression lines
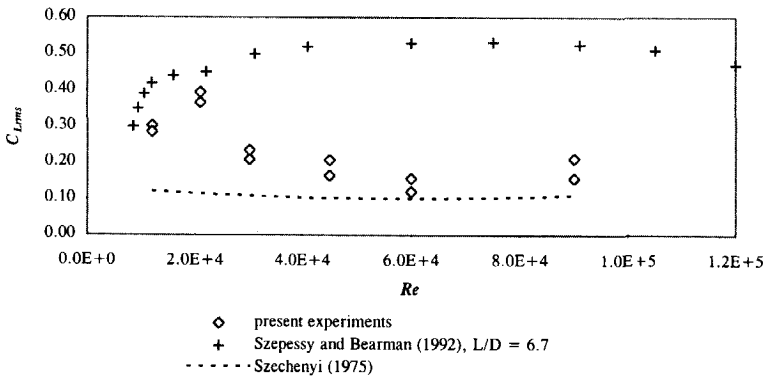


Figure 5.3 Towing the cylinder in still water, lift force coefficient versus $Re$

44
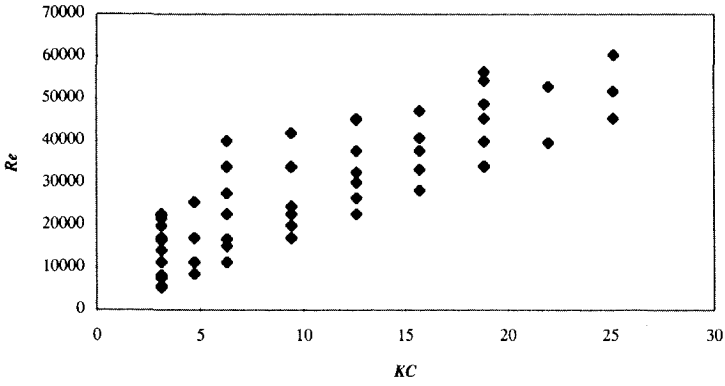
Figure 5.4  Forced cylinder oscillation tests, covered parameter combinations



$$C_{Dh} = 1.0398\ C_{Dls}$$
$$R^2 = 0.876$$



$$C_{Ah} = 1.0002\ C_{Als}$$
$$R^2 = 0.98$$
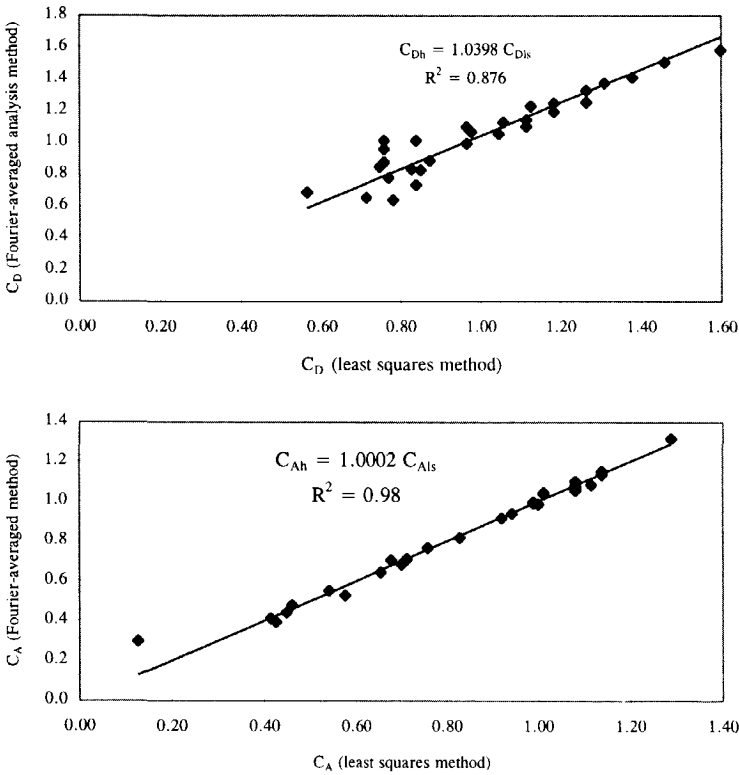
Figure  5.5  Forced oscillation tests,  coefficients obtained by least squares method
versus those obtained by Fourier  method
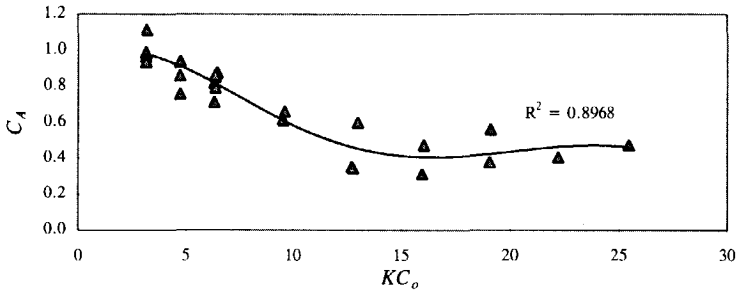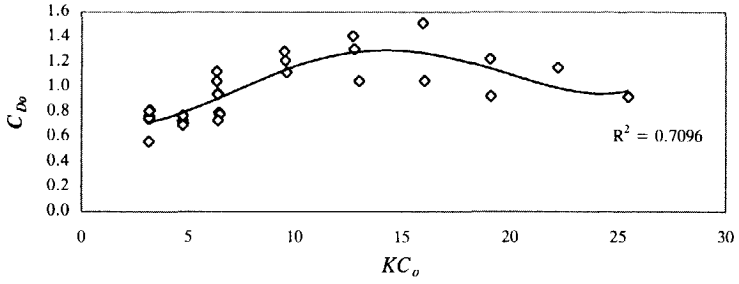
Figure 5.6  Forced oscillation in still water, $C_{Do}$ and $C_A$ plotted versus $KC_o$;  solid lines:
3rd order polynomial regression lines
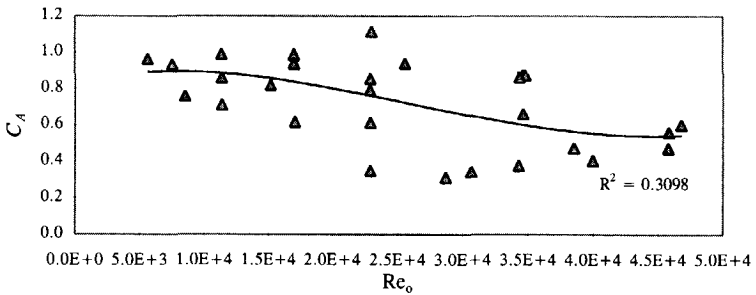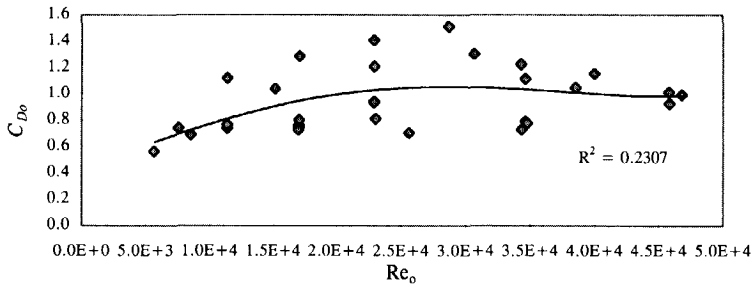


Figure 5.7  Forced oscillation in still water, $C_{Do}$ and $C_A$ plotted versus $Re_o$; solid lines:
3rd order polynomial regression lines
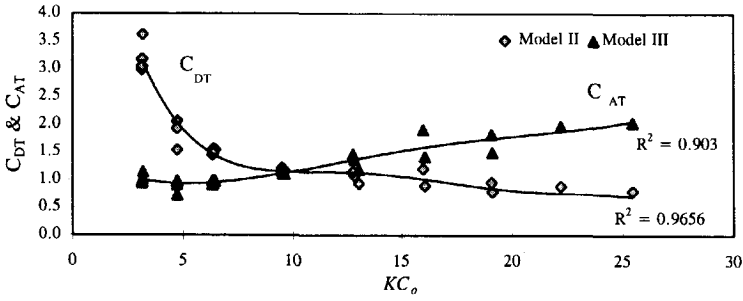
Figure 5.8  Forced oscillation in still water, $C_{DT}$ and $C_{AT}$ plotted versus $KC_o$; solid lines: 3rd order polynomial regression lines though data points
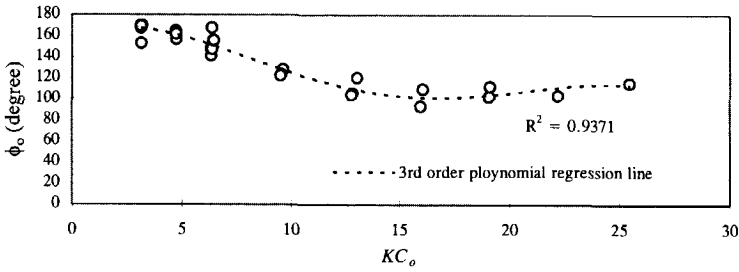


Figure 5.9  Forced oscillation in still water, variation of phase angle, $\phi_o$, versus $KC_o$
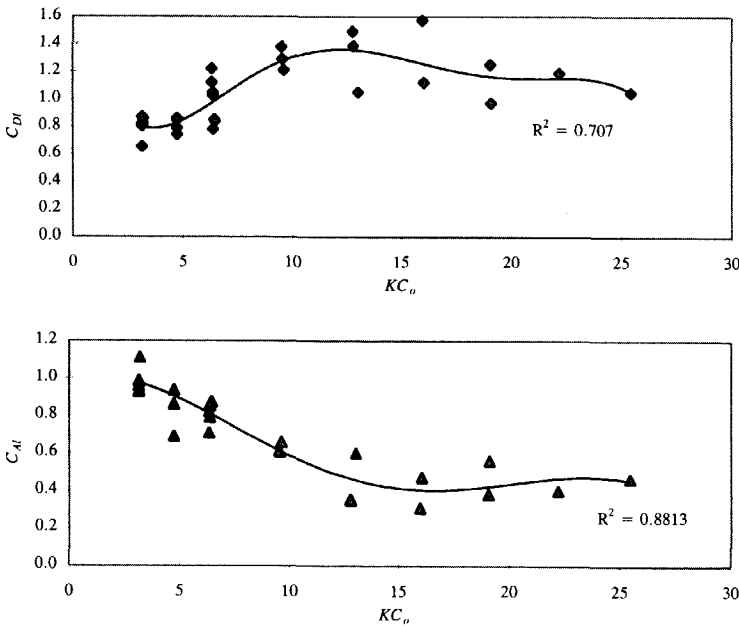




Figure 5.10  Forced oscillation in still water, $C_{DI}$ and $C_{AI}$ plotted versus $KC_o$; solid lines: 3rd order polynomial regression lines through data points

—△— Original Morison equation —○— Linearised Morison equation —✕— Harmonic model
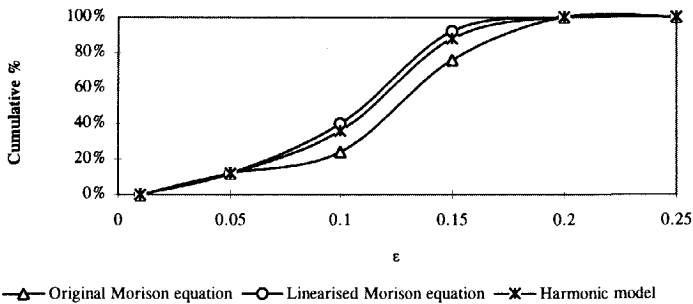
Figure 5.11  Forced oscillation in still water, comparison of goodness-of-fit parameter ε
for given load models



$$R^2 = 0.3013$$

$$R^2 = 0.449$$
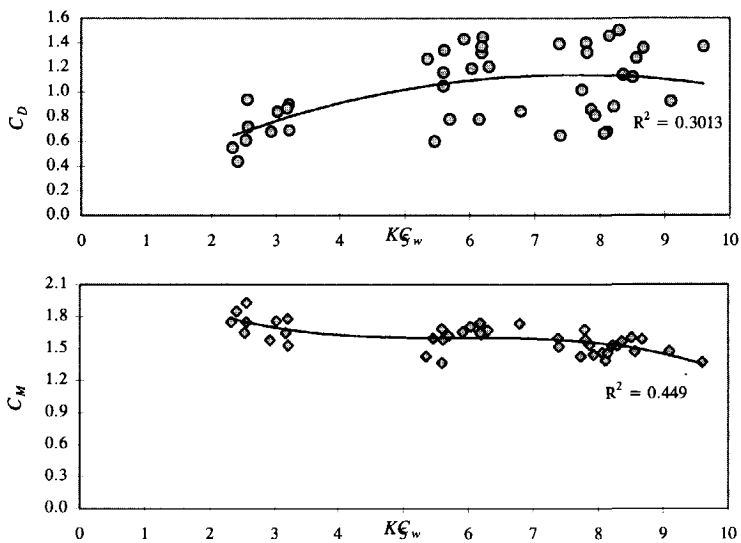
Figure 5.12  Fixed cylinder in waves, $C_D$ and $C_M$ plotted versus $KC_w$; lines: 3rd order
polynomial regression lines through data points



○ Model II
△ Model III
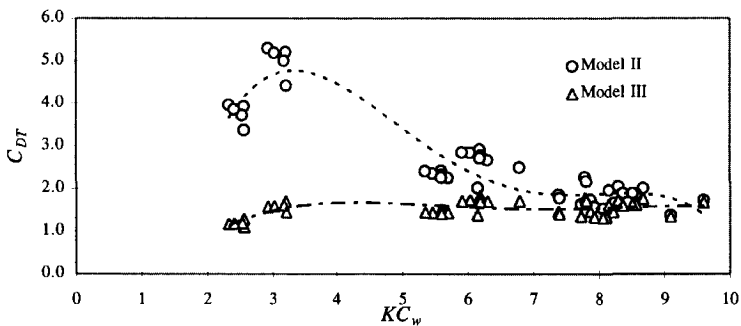
Figure 5.13  Fixed cylinder in waves, total force coefficients, $C_{DT}$ and $C_{AT}$ plotted versus $KC_w$;
lines: 3rd order polynomial regression lines though data points

48
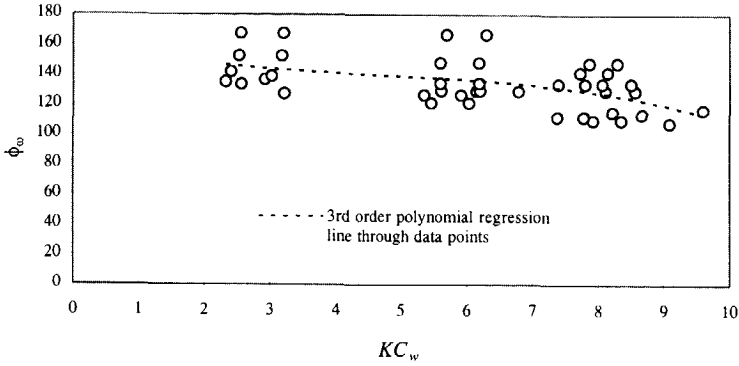
Figure 5.14  Fixed cylinder in waves, the phase angle $\phi_w$  plotted versus $KC_w$
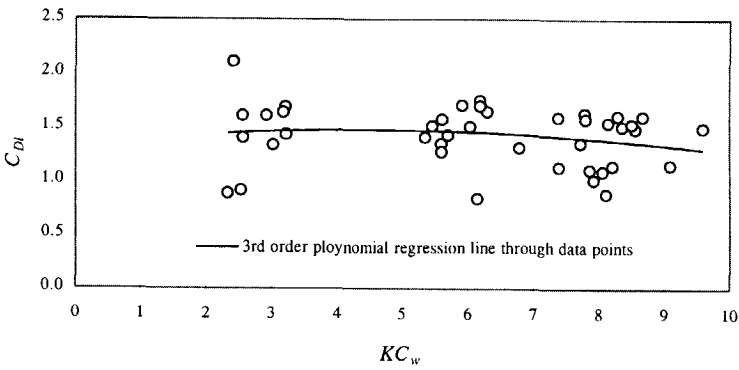


Figure 5.15  Fixed cylinder in waves, the linearised drag coefficient, $C_{Dl}$, plotted versus $KC_w$
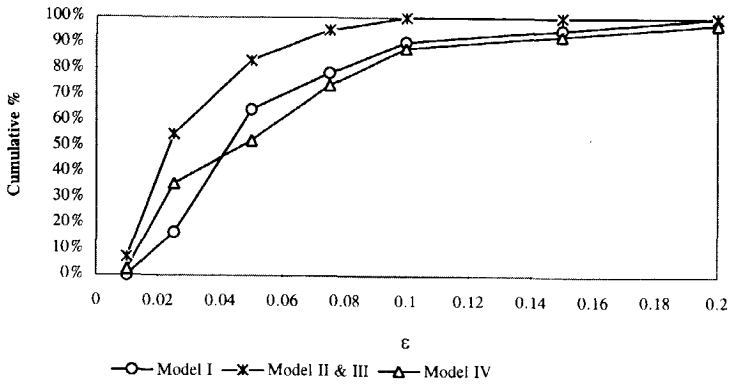


Figure 5.16  Fixed cylinder in waves, comparison of goodness-of-fit parameter ε  for given
load models

# CHAPTER 6

# In-line Oscillations in Uniform Flow

## 6.1 Introduction

This chapter will be devoted to the presentation and discussion of the results of the tests of in-line harmonic oscillations of a cylinder in a uniform flow. Elements of offshore structures are often exposed to flows which are a combination of an oscillatory flow (due to waves) and a mean flow (due to current) around a stationary cylinder. The flow situation considered in this chapter is complementary to this case, the difference being that in the present situation the cylinder is oscillating. The flow situation discussed here is expected to have practical relevance to the understanding of wave and current forces on offshore structures; however, the hydrodynamic interaction between a fixed cylinder and a current superimposed on the waves will be discussed more specially in the next chapter. Results for other multi-mode flow conditions will be presented in subsequent chapters.

From a practical point of view, in-line oscillation of a cylinder in a current is important, partly because of the superposition of waves with currents and partly because of the damaging vortex-induced oscillations encountered in currents. Since from a kinematics point of view, the phenomenon is identical to that where the cylinder is subjected to a time-dependent flow characterised by $u = V - u_m \cos \omega t$, the evaluation of the forces might shed some light on the combined effect of waves and currents on slender cylinders.

It is ordinarily assumed that the Morison equation applies equally well to oscillatory flow with a mean velocity and that the drag and inertia coefficients are independent of the current. This would imply that drag and inertia coefficients are independent of vortex-shedding and its attendant consequences. However, the shedding of the vortices by the current causes significant changes in vortex motion and in both the drag and inertia coefficients, compared with their no-current values, see Sarpkaya and Isaacson (1981). The value of $C_D$ and $C_M$ may vary considerably from one half of the wave cycle to the next because of the current induced biassing of the wake and vortex formation. Also, neither set of coefficients may be identical to those obtained without current. Thus, the hydrodynamic interaction of combined flows must be carefully examined in the light of available data.

The purpose of this series of experiments is to examine the validity of existing load models and to find a better description if possible. An additional purpose is to obtain useful force coefficient values over a wide range of offshore conditions.

## 6.2 Previous Work

Relatively few studies have been carried out on superposed oscillatory and mean flow past a fixed cylinder, or on a cylinder oscillating in-line with a current. An extensive review of the previous investigations is given by Sarpkaya and Isaacson (1981). Here only the more recent and most relevant investigations are briefly described.

Iwagaki et al. (1983) have carried out experiments with two relatively small vertical cantilevered cylinders. The force coefficients were calculated by two approximate methods using the total moment acting on the entire cantilever. They have plotted $C_D$ and $C_M$ versus various $KC$ numbers and claimed that a new $KC$ number based on the relative displacement of the fluid correlates quite well with the force coefficients.

Kato et al. (1983) have subjected a cylinder to a combined flow field by means of a carriage which oscillated in either the in-line or the transverse direction while moving forward at a constant speed. They have concluded that the drag coefficient increases with increasing $Vr=VT/D$. This result is in contradiction to that obtained by Moe and Verley (1980) and Iwagaki et al. (1983). An explanation for this apparent contradiction is that KC and $Vr$ were implicitly linked by the experimental set-up and procedure used by Kato et al. (1983). This linking makes it impossible to draw conclusions about the behaviour of the drag coefficient as a function of any single parameter.

An extensive evaluation of the drag and inertia coefficients for an oscillating cylinder in steady flow has been conducted by Koterayama (1984). The $KC$ number was varied up to 100 and the reduced velocity up to 60. It is concluded that the drag and inertia coefficients depend mainly on the reduced velocity $Vr$ when $Vr < 20$ and weakly on the $KC$ number for larger $Vr$. The fluid forces in this experiment have been measured over a 6.7 diameter long portion of the test cylinder which is not expected to clarify the individual effects of current, wave and cylinder motion on force coefficients.

Sarpkaya and Storm (1985) have conducted experiments with cylinders moving at constant velocity in a sinusoidally oscillating flow to determine the drag and inertia coefficients and to examine the effect of wake biasing on the modified Morison equation. They have reported that the drag coefficient decreases with increasing current for a given Reynolds number and Keulegan-Carpenter number; the two-term Morison equation with force coefficients obtained under no-current conditions is not applicable to the prediction of wave and current induced loads.

Low et al (1989) investigated the drag and inertia coefficients of an oscillating cylinder in a steady current at large reduced velocity (up to 100). The experiments were conducted at $Re$ numbers, based on the current velocity, of 27 000 to 54 000 and at $KC$ numbers of 2.5 to 15. It is shown that the drag coefficient is dependent on the $KC$ number even at large reduced velocities. At small $KC$ the $C_D$ approaches its steady flow value of about 1.2. At large $KC$ the $C_D$ is reduced. They found that a two-term Morison equation suffices to describe the force.

Although pragmatic approaches have been adopted in the foregoing investigations and useful results have been produced by some of them, more laboratory and field investigations remain to

be carried out for a better understanding and quantifying of these wave-current-structure interactions.

## 6.3  Present Tests

Returning now to the present tests, the in-line oscillation while towing the cylinder in still water is the first multi-mode test series in which the effects of a mean flow and an oscillatory flow are combined. The flow situation is different from that of the pure cylinder oscillation tests; forces on the oscillating cylinder obviously are modified by current action. Important parameters and the data range for the present test series are summarized below.

### 6.3.1 Important Parameters

A general consideration of governing parameters for different flow conditions is given in section 2.3 where it is shown that the hydrodynamic forces depend on a Keulegan-Carpenter number, a Reynolds number, and a parameter involving current velocity such as $V/f_oD$ or $V/\dot{x}_m$. The dimensionless velocity, $Vr = V/f_oD$, is the ratio of the length of the path travelled by a water particle due to the current during one cycle of cylinder oscillation and the cylinder diameter and referred to as the reduced velocity.

There are many possibilities for the definitions of the Keulegan-Carpenter number and the Reynolds number in coexisting flow fields. A partial list of possible $KC$ and $Re$ definitions can be given as follows:

a) in terms of maximum cylinder velocity, $\dot{x}_m$, as:

$$KC_o = \frac{\dot{x}_m T}{D}, \qquad Re_o = \frac{\dot{x}_m D}{\nu} \qquad (6.1)$$

b) in terms of total velocity, $\dot{x}_m + V$, as:

$$KC_{ov} = \frac{(\dot{x}_m + V)T}{D}, \qquad Re_{ov} = \frac{(\dot{x}_m + V)D}{\nu} \qquad (6.2)$$

c) By introducing suitable characteristic values of time, velocity, etc. in the Navier-Stokes equation, Sarpkaya et al. (1984) have introduced Keulegan-Carpenter number and Reynolds number definitions as:

$$KC_3 = \frac{\dot{x}_m T}{D}(1 + |\frac{V}{\dot{x}_m}|)^2, \qquad Re_3 = \frac{\dot{x}_m D}{\nu}(1 + |\frac{V}{\dot{x}_m}|)^2 \qquad (6.3)$$

$KC_3$ represents the ratio of the maximum convective acceleration to the maximum local acceleration.

d) Iwagaki et al. (1983) tried to find a new definition for the Keulegan-Carpenter number so that $KC$ and $Vr$ could be combined into one parameter. They found that the best expression for the Keulegan-Carpenter number then was:

53

$$KC_4 = (2\pi/D) \int_{t^*}^{T/2} (V + \dot{x})dt \quad , \qquad V \le \dot{x}_m \qquad\qquad (6.4)$$

where

$$t^* = Arc\cos(V/\dot{x}_m)/(2\pi f_o)$$

and:

$$KC_5 = \pi VT/D \quad , \qquad\qquad V > \dot{x}_m$$

The Reynolds numbers throughout these tests were subcritical. Force coefficients due to a current or a pure oscillatory flow show little dependence upon Reynolds numbers in this range. Thus, the present results are suitable for investigating the influence of $KC$ and $Vr$. In the present study, an investigation was conducted to find more suitable nondimensional parameters by examining the correlation of the data.

### 6.3.2 Tests Conducted and Data Range

An extensive experimental programme was conducted to achieve the objective of this test series, see Shafiee-far (1995a). Tests involving in-line oscillations while towing the model cylinder were carried out using different combinations of towing speed, $V$, oscillation period, $T_o$, and oscillation amplitude, $A$. These independent parameters were varied over the following ranges:

$$A : \quad 30 - 270 \text{ mm}$$
$$T_o : \quad 0.5 - 2 \text{ sec.}$$
$$V : \quad 0.2 - 1 \text{ m/s}$$

| Parameter | Definition | Range |
|---|---|---|
| Amplitude:Diameter Ratio | $A/D$ | 0.5 - 4.5 |
| Max. Oscillatory Velocity | $\dot{x}_m = 2A\pi f_o$ | 0.09 - 1.13 m/s |
| Reynolds Number based on current | $Re = V D/\nu$ | 12000 - 60000 |
| Reynolds Number based on oscillatory flow | $Re_o = \dot{x}_m D/\nu$ | 5650 - 67900 |
| Reynolds Number based on total flow | $Re_{ov} = (V + \dot{x}_m)D/\nu$ | 17650 - 95900 |
| Keulegan-Carpenter number, oscillatory flow | $KC_o = \dot{x}_m T_o/D$ | 3.1 - 28.3 |
| Keulegan-Carpenter number, total flow | $KC_{ov} = (\dot{x}_m + V)T_o/D$ | 4.8 - 53.3 |
| Reduced velocity | $Vr = VT_o/D$ | 1.7 - 33.3 |
| Velocity parameter | $V/\dot{x}_m$ | 0.17 - 6.0 |

Table 6.1 Ranges of Experimental Variables for In-line Oscillation Plus Current Tests

The degenerate cases - for example with $A = 0.0$ - have already been discussed in chapter 5. Figure 6.1 shows the parameter combinations covered for the in-line oscillation plus current tests. These combinations led to the nondimensional parameter ranges given in table 6.1.

## 6.4 Load Models

Various load models which were thought to be applicable to the description of the hydrodynamic forces on an oscillating cylinder in a current were formulated and the corresponding analysis procedures were developed. These models are described below.

Simultaneous time series of cylinder motion and hydrodynamic forces make it possible to study the validity and suitability of these load models. The measured forces are compared with simulations based upon the various load models.

### 6.4.1 Harmonic Load Models

Similar to the harmonic load models formulated for single mode tests (see sections 5.2.1, 5.3.1 and 3.3) the oscillatory component of the hydrodynamic force may be written in terms of harmonic components. Assuming that the steady force component is only due to the steady current, one may write the total (combined) force per unit length of an oscillating cylinder in a steady current as:

$$F = 0.5 \rho D C_{Dm} V^2 + 0.5 \rho D \dot{x}_m^2 \sum_{n=1}^{N} C_{dhn} \sin(n \omega t + \phi_n) \tag{6.5}$$

### 6.4.2 Generalisation of Morison Equation

An extension of the Morison equation is usually used to describe hydrodynamic forces on slender cylinders in combined flow fields. Eight different forms of Morison equation extensions have already been evaluated by Shafiee-far et al. (1996). These extended forms are given in table 6.2. Model I and II in this table are the relative and absolute velocity models, respectively, see Verley and Johns (1983), Laya et al. (1984), Chakrabarti and Cotter (1984) and Bearman et al. (1992).

Models III to V are different postulates. Model III is another form of the relative velocity model. Model IV is a combined model in which the steady force component is separated from the total force, and the oscillatory component is treated using a relative velocity approach. Model V is a modified form with four force coefficients. Model VI is a linearised form of the independent flow fields approach in which the oscillatory drag component is linearised using the Fourier series expansion methods, Borgman (1972). Model VII is a linearised form of the relative velocity model in which the drag component is written in a linear form using expansion of the relative velocity, Gudmestad and Connor (1983). Model VIII is another postulated and linearised form of the relative velocity model.

### 6.4.3 Energy Balance Model

Barnouin et al. (1979) have examined a model based on energy balance consideration for pure cylinder oscillation in still water. That load model was extended to a combined flow field using

a relative flow concept which leads to:

$$F = \frac{1}{2}\rho D \, K_1 (V - \dot{x}) \, |(V - \dot{x})| + K_2 \, \tau \, \rho \, D \, (V - \dot{x})\ddot{x} \tag{6.6}$$

where $K_1$ and $K_2$ are two constants to be calculated and $\tau$ is a time scale of dissipation. $\tau$ is taken equal to the period, $T_o$, for sinusoidal oscillations.

| Models | Equation |
|---|---|
| Model I<br>Relative Velocity | $F = \frac{1}{2}\rho D \, C_{Dr} |V - \dot{x}|(V - \dot{x}) - \rho\frac{\pi D^2}{4} C_{Ar} \ddot{x}$ |
| Model II<br>Absolute Velocity | $F = \frac{1}{2}\rho D \, C_{Dm} V^2 - \frac{1}{2}\rho D \, C_{Da} |\dot{x}|\dot{x} - \rho\frac{\pi D^2}{4} C_{Aa} \ddot{x}$ |
| Model III | $F = \frac{1}{2}\rho D \, C_{D3} (V - \dot{x})|\dot{x}| - \rho\frac{\pi D^2}{4} C_{A3} \ddot{x}$ |
| Model IV | $F = \frac{1}{2}\rho D \, C_{Dm} V^2 + \frac{1}{2}\rho D \, C_{D4} (V - \dot{x})|\dot{x}| - \rho\frac{\pi D^2}{4} C_{A4} \ddot{x}$ |
| Model V | $F = \frac{1}{2}\rho D \, C_{Dm} V^2 - \frac{1}{2}\rho D \, C_{dvo} V\dot{x} - \frac{1}{2}\rho D \, C_{doo} |\dot{x}|\dot{x} - \rho\frac{\pi D^2}{4} C_{A5} \ddot{x}$ |
| Model VI<br>Linearised Absolute<br>Velocity | $F = \frac{1}{2}\rho D \, C_{Dm} (V^2) - \frac{1}{2}\rho D \, C_{D6} \frac{8}{3\pi} \sigma_{\dot{x}} \dot{x} - \rho\frac{\pi D^2}{4} C_{Ai} \ddot{x}$ |
| Model VII<br>Linearised Relative<br>Velocity | $F = \frac{1}{2}\rho \, C_{D7} (V\cdot\beta + \dot{x}_m \cos\beta)(V - \dot{x}) - \rho\frac{\pi D^2}{4} C_{Ar} \ddot{x}$<br><br>where $\sin\beta = V/\dot{x}_m$ |
| Model VIII | $F = \frac{1}{2}\rho D \, C_{D8} (V + \dot{x}_m)(V - \dot{x}) - \rho\frac{\pi D^2}{4} C_{A8} \ddot{x}$ |

Table 6.2   List of Modified Morison Equation Forms

### 6.4.5  Lift Force

The lift force for a combined flow condition has not been studied extensively. There are indications from previous works that a current can produce significant changes. Verley (1980), Sarpkaya and Storm (1985), and Bearman and Obasaju (1989) have reported instances when a small current produced major changes in the vortex shedding pattern.

When the cylinder is forced to oscillate in a current, the frequency ratio $f_v / f_o$ (vortex shedding

frequency / frequency of cylinder oscillation) and the amplitude parameter ($\hat{x} = A/D$) play a very important role in determining various fluid mechanics phenomena and the fluid forces acting on the cylinder. At specific parameter combinations, $f_v / f_o$ and $A/D$, the "lock-in" phenomenon can be observed.

The Strouhal number ($St$) is widely used to describe both steady and unsteady vortex shedding phenomena. For a cylinder in a periodic fluid flow, the Strouhal number ($St$) is usually defined as:

$$St = \frac{f_v D}{u_m} = \frac{f_v}{f KC} \tag{6.7}$$

where $u_m$ is the maximum oscillatory velocity. This definition may be used for the Strouhal number of an oscillating cylinder in a current but with different definitions for the Keulegan-Carpenter number, for example:

$$St_o = \frac{f_v D}{\dot{x}_m} = \frac{f_v}{f_o KC_o}$$

$$St_{ov} = \frac{f_v D}{V + \dot{x}_m} = \frac{f_v}{f_o KC_{ov}}$$

The following lift force coefficients have calculated studying transverse forces on the cylinder oscillating in-line with a steady current.

$$C_{Lmax} = \frac{F_{Ymax}}{0.5 \rho D (V + \dot{x}_m)^2} \quad , \quad C_{Lrms} = \frac{F_{Yrms}}{0.5 \rho D (V + \dot{x}_m)^2} \tag{6.8}$$

The intent is to examine how vortex shedding and corresponding lift force observed in oscillatory flow are modified by the presence of a current.

## 6.5 Results and Discussion

The results are presented and discussed in this section. First the indications from the data themselves without regarding a load model are demonstrated. Results for evaluations of validity and suitability of the in-line load models are presented after that. The last part deals with the lift forces.

### 6.5.1 Direct Observations from the Data

Before trying modified forms of the Morison equation, the data were studied to see what insight they might yield. The behaviour of the force on a measuring element for various combinations of variable values was studied.

The following characteristic forces have been used for this evaluation:

1. $F_{max}$, the maximum of the measured force in each test run,
2. $F_{rms}$, the root mean square of the measured total force defined as:

$$F_{rmsT} = \sqrt{\frac{\sum F_{meas}^2}{n}} \qquad (6.9)$$

3. $Fm$, the mean (steady) force, and

4. $F_{rmsO}$, the root mean square of the oscillatory force component:

$$F_{rmsO} = \sigma_F = \sqrt{\frac{\sum (F_{meas} - F_m)^2}{n}} \qquad (6.10)$$

The values of these characteristic forces for all test runs have been plotted against various variables to detect the presence (or absence) of dependency.

### 6.5.1.1 Maximum Values of the In-line Force

The variation of the maximum values of the in-line force as a function of various variables was investigated. The first row in table 6.3 gives $R^2$ correlation coefficient values for linear regression of data when various combinations of $V^2$, $\dot{x}_m^2$ and $V \cdot \dot{x}_m$ are used as the independent variable. The highest $R^2$ value is obtained when $F_{max}$ is plotted versus $V^2 + 2V \dot{x}_m$ parameter.

### 6.5.1.2 RMS Values of the In-line Force

The variation of $F_{rmsT}$ was plotted against various combinations of $V^2$ and $\dot{x}_m^2$ and $V \dot{x}_m$. It was found that $F_{rmsT}$ can also best be related to $(V^2 + 2V\dot{x}_m)$ for all test runs with different values of steady velocity, oscillation frequency and oscillation amplitude, see figure 6.2. The second row in table 6.3 gives $R^2$ correlation coefficient values for linear regression of data when this and other combinations of $V^2$, $\dot{x}_m^2$ and $V \cdot \dot{x}_m$ are used as the independent variable.

Results of four tests deviated significantly from the trend in figure 6.2. These four points are associated with runs in which the oscillation frequency is close to the natural vortex shedding frequency, the region where lock-in occurs. These four tests are still included in table 6.3 and figure 6.2. Removing these points from the data gives a still better fit with a correlation coefficient $R^2 = 0.96$.

Figure 6.3 shows the variation of

$$C_{Frms} = \frac{F_{rmsT}}{0.5 \rho D (V^2 + 2 V \dot{x}_m)} \qquad (6.11)$$

as a function of $KC_{ov}$. Despite the high correlation coefficient between $F_{rmsT}$ and $(V^2 + 2V\dot{x}_m)$ the scatter in figure 6.3 is still large. The reason for such a result may be explained as follows. The contribution of $F_{rmsT}$ variations for small $F_{rmsT}$ values is not significant in overall correlation between the two variables. However, even a small $F_{rmsT}$ may result in a large $C_{Frms}$ value since then the value of $(V^2 + 2V\dot{x}_m)$ is small too.

|  | $V^2$ | $\dot{x}_m^{\,2}$ | $V\dot{x}_m$ | $(V+\dot{x}_m)^2$ | $V^2+2V\dot{x}_m$ |
|---|---|---|---|---|---|
| $F_{max}$ | 0.49 | 0.19 | 0.84 | 0.85 | 0.87 |
| $F_{rms T}$ | 0.69 | 0.10 | 0.77 | 0.82 | 0.93 |
| $Fm$ | 0.79 | 0.02 | 0.54 | 0.89 | 0.94 |
| $F_{rms O}$ | 0.28 | 0.41 | 0.92 | 0.86 | 0.71 |

Table 6.3  $R^2$ Values for the Characteristic Forces Fitted to Different Velocity Components

### 6.5.1.3 Mean Drag Force

The variation of mean force, $Fm$, as a function of various variables was investigated as was done above for the RMS values of the total forces. The third row of the values in table 6.3 gives the calculated correlation coefficient $R^2$ values between $Fm$ and various combinations of independent variables such as $V^2$, $\dot{x}_m^{\,2}$ and $V\cdot\dot{x}_m$.

Figure 6.4 shows how $Fm$ varies as a function of $(V^2 + 2V\cdot\dot{x}_m)$. The mean drag force correlates well with the combined velocity. The dependence of the steady force on the oscillatory velocity demonstrates that this force component depends on the cylinder oscillation velocity in addition to the current velocity. One could conclude that the steady and oscillatory flows interact in generating the force.

It has been reported in the literature that the mean force $Fm$ normalised by the square of current velocity $V$,

$$C_{Dm} = \frac{Fm}{0.5\,\rho D V^2} \tag{6.12}$$

exhibits large values and a high degree of scattering. $C_{Dm}$ values do not correspond to those obtained under current-only conditions, Mercier (1973) and Verley (1980). Based on the above observation, however, the mean drag force, $Fm$, could be normalised by $(V^2+2V\dot{x}_m)$ to get a new drag coefficient:

$$C_{Dmc} = \frac{Fm}{0.5\,\rho D(V^2 +2\,V\dot{x}_m)} \tag{6.13}$$

Figure 6.5 shows how $C_{Dmc}$ varies as a function of the reduced velocity, $Vr$. The mean drag coefficient, $C_{Dmc}$, obtained in this way is relatively stable, unless the reduced velocity, $Vr$, is near 5. These jumps around $Vr = 5$ are associated with the 'lock-in' phenomenon. This is the case when the vortex shedding frequency, $f_v$ is close to the forced oscillation frequency, $f_o$.

### 6.5.1.4 The RMS Values of the Oscillatory Force Component

The best linear fit for the oscillatory force component, $F_{rms O}$, was obtained by plotting it against $V\cdot\dot{x}_m$ as shown in figure 6.6. As listed in table 6.3, the $R^2$ value for $\dot{x}_m^{\,2}$ (not plotted here) is relatively low; a high value would confirm an absolute velocity approach. The dependence of the oscillatory force on the current velocity proves that the non-steady in-line force component (associated with the cylinder oscillation) also depends on the current; there must be an interaction

59

between the two flow fields. This should be included in the load model; the independent flow field does not seem suitable for estimating the hydrodynamic force on an oscillating cylinder in a current.

### 6.5.2 Fitting Load Models to Data

This section discusses the quality of fit of the various load models. The quality and interpretation of the force coefficients obtained is treated in section 6.5.3.

The same procedure as described for single mode tests was used to evaluate the quality of fit of the given load models. The results of this evaluation for the load models based on an extension of the Morison equation may be found in Shafiee-far et al. (1996). It has been concluded that the relative velocity model (two-term Morison equation) and a linearised form of this approach fit the data better than the other modified forms of the Morison equation. Therefore, only results for these two models along with the results for the harmonic load model (equation 6.5) and the energy balance model (equation 6.6) are presented here.

Before trying these models, an attempt was made to examine the effect of higher harmonic components on the quality of fit of the harmonic load models. The following harmonic load models were evaluated to examine the consequence of adding higher harmonic components:

- Harmonic model with the first component,
- Harmonic model with the first two components, and
- Harmonic model with the first three components.

The goodness-of-fit parameter, $\epsilon$, (see equation 3.21) was calculated for each test run and each of the above harmonic load models. The 107 $\epsilon$ values for each model were subsequently ranked and grouped into histograms. Figure 6.7 shows the cumulative probabilities of $\epsilon$ for these three harmonic forms. High curve values indicate that relatively more of the test runs fitted the chosen model well. As seen from this figure, adding higher harmonic components improves the quality of fit of the models, but the improvement is not very significant beyond the second component.

### 6.5.2.1 Fitting Using Individual Run Coefficients

Figure 6.8 shows the results for the harmonic load model (with only the first component) and other given load models. The cumulative percentage of the 107 test runs is plotted against $\epsilon$ here. Table 6.4 lists the statistics of the $\epsilon$ using the given models. Note that the best possible (individual) coefficient values for each run were used here. Taking all information in this table and figure 6.8 together, one can conclude that all models but the energy balance model fit the measured data equally well.

Both the relative velocity model (two-term Morison equation, model I) and a linearised form of this approach (model VIII) give a reasonable fit; the relative velocity model gives a closer fit for some runs while the linearised form fits better to others.

60

| Load Model | Fit quality ε value | | Percentage of runs with: |
| --- | --- | --- | --- |
| | Mean | STD | ε < 0.2 |
| Harmonic model (the first component) | 0.101 | 0.098 | 87.0% |
| Harmonic model (two components) | 0.085 | 0.094 | 88.9% |
| Harmonic model (three components) | 0.076 | 0.091 | 90.7% |
| Relative velocity Morison equation | 0.105 | 0.080 | 88.7% |
| Linearised relative velocity Morison equation | 0.112 | 0.142 | 92.5% |
| Energy balance model | 0.171 | 0.174 | 72.6% |

Table 6.4 In-line Oscillation Plus Current Tests, Model Fitting Statistics

## 6.5.2.2 Fitting Using Smoothed Coefficients

The results shown in figure 6.8 and table 6.4 were obtained by using coefficients obtained separately for each individual test run. This would never be done in practice. Using each model with a smoothed coefficient value to predict the interaction force is much more realistic.

If the individually determined coefficients are only slightly scattered around the smoothed value, then one would expect the computed results using this latter value to be about the same as with the individual coefficients. More coefficient spreading will show up as a poorer fit when a smoothed coefficient value is used.

This evaluation has been carried out for the three best equation models above. Figure 6.9 shows the end results of this work with smoothed coefficients plotted in the same way as in figure 6.8. Table 6.5 lists salient values for each model.

The lower rating of the harmonic model is consistent with the relatively large scatter of its coefficients which are discussed below.

| Load Models | Fit quality ε value | | Percentage of runs with: |
| --- | --- | --- | --- |
| | Mean | STD | ε < 0.2 |
| Harmonic model (three components) | 0.215 | 0.196 | 49.4% |
| Relative velocity Morison equation | 0.175 | 0.162 | 68.9% |
| Linearised relative velocity Morison equation | 0.151 | 0.090 | 74.5% |

Table 6.5 Summary of Model Fitting Statistics with Smoothed Coefficients

## 6.5.3 Force Coefficient Values Obtained

The force fitting just discussed has yielded force coefficients. Their quality and interpretation are discussed here.

### 6.5.3.1 Harmonic Coefficients

Harmonic components of the in-line force are calculated with a harmonic analysis program. Results for harmonic coefficients in equation 6.5, $C_{dhn}$, are plotted versus the Keulegan-Carpenter number $KC_o$ and the reduced velocity $Vr$ in figure 6.10 through 6.13 using contour maps. In these plots, the contour lines represent lines of equal force coefficient magnitude. The numbers marked on the contour lines are the values of the relevant coefficient. Each figure contains results for all of the in-line oscillation plus current tests conducted, i.e. each figure represents data collected for a total of 107 data points. A brief description of each contour plot is given below.

*Mean Drag Coefficient*: Results for the mean drag coefficients $C_{Dm}$ are presented in figure 6.10. The amplification of the mean drag in the region $5 < Vr < 7$ is clearly seen, with a $C_{Dm}$ value of about 2.8 for a $KC_o$ value of 3. Such an amplification of the mean drag in this region has already been reported by Koterayama (1984). It should be noted that the amplification of the mean drag for transverse cylinder oscillations (lock-in) does also occur in this region. However, one expects, for transverse cylinder oscillations, the amplification of mean drag force in the in-line direction happens at $Vr = 2.5$.

The mean drag coefficient values for higher reduced velocity $Vr$ and moderate $KC_o$ are in the range of those for current-only tests. However, the mean drag coefficient values are much higher than expected for $Vr < 15$ and $KC_o > 9$; the mean drag coefficient is apparently strongly affected by the oscillatory flow in this area.

*Oscillating Drag Coefficient of the First Harmonic*: Contours of the oscillating drag coefficient at the first harmonic, $C_{dh1}$, are presented in figure 6.11. The magnitude of $C_{dh1}$ is large at low $KC$; it agrees with the values obtained from the oscillation-only tests when $KC_o > 11$ and $Vr < 12$. A high $KC$ represents a high oscillatory velocity $\dot{x}_m$ and a high $Vr$ is proportional to a high steady velocity $V$. Thus, the observation from this figure shows that the steady velocity $V$ affects the oscillatory force considerably. This observation agrees completely with those made earlier in section 6.5.1. An oscillating drag coefficient normalised by a combination of two velocities ( $\dot{x}_m$ and $V$) may improve the results.

*Oscillating Drag Coefficient of the Higher Harmonics*: The results for the oscillating drag coefficients for the second and the third harmonics ($C_{dh2}$ and $C_{dh3}$) are presented in figures 6.12 and 6.13 respectively. The maximum $C_{dh2}$ value is 1.7 for $KC_o \approx 3$ and $Vr \approx 8$. The $C_{dh2}$ value decreases by increasing $KC_o$ for a constant $Vr$; in general, it increases first and then decreases with increasing $Vr$ for a constant $KC_o$. This suggests that the second harmonic also depends on the steady current velocity $V$. The third harmonic results are presented here even though the contribution of this component is universally negligible. A similar tendency as for $C_{dh2}$ is observed for $C_{dh3}$ values.

### 6.5.3.2 Modified Morison Equation Coefficients

Results for hydrodynamic force coefficients of the relative velocity Morison equation are presented and discussed here. As in existing studies, first the variations of these coefficients versus traditional nondimensioal parameters ($KC$ and $Vr$) are discussed. This is followed by a

presentation of the outcome of an attempt to find some better parameters for correlating the hydrodynamic coefficients.

The drag coefficient for the relative velocity approach, $C_{Dr}$, is plotted versus $KC_o$ in figure 6.14. As shown in this figure, the drag coefficient $C_{Dr}$, is affected by the current; for $KC_o < 9$ the $C_{Dr}$ value is larger with current than for the no-current case while for higher $KC_o$ values, it is smaller than those for the no-current case. For example, the $C_{Dr}$ for $KC_o = 25.1$ and $Vr = 12.5$ (corresponding to $V/\dot{x}_m \approx 0.5$) is approximately 38 percent smaller than that for the no-current case. Comparing figure 6.14 and 5.6 it is clear that $C_{Dr}$ is not equal to its no-current value and strongly depends on $KC_o$ and $Vr$.

The $C_{Dr}$ values are re-plotted versus reduced velocity $Vr$ and velocity ratio $V/\dot{x}_m$ in figures 6.15 and 6.16, respectively, to show the effect of a current in other ways. Figure 6.15 shows sharp changes around $Vr = 5$ and $KC_o \le 6.3$ while values for $KC_o > 6.4$ do not. This 'instability' near $Vr = 5$ is associated with the 'lock-in' phenomenon; the force frequency due to vortex shedding is the same as the oscillation frequency. Considering figure 6.16, the $C_{Dr}$ increases with increasing velocity ratio for $V/\dot{x}_m < 2$, then it decreases with increasing $V/\dot{x}_m$. For a higher velocity ratio, the $C_{Dr}$ values approach the drag coefficient value for current-only tests.

Figures 6.17 and 6.18 show the inertia coefficient, $C_{Mr} = C_{Ar} + 1$, for the same model plotted in a way similar to figures 6.14 and 6.15. These figures show that $C_{Mr}$ depends on both $KC_o$ and $Vr$ and is strongly affected by the current. For small $Vr$ values, $C_{Mr}$ is smaller than for the no-current case for all $KC_o$ values; it increases with increasing $Vr$, and is larger than the no-current case for $Vr = 25$. A relatively low value of $C_{Mr}$ in figure 6.18 occurs at about the same reduced velocity value as is associated with the maximum of the $C_{Dr}$ value in figure 6.15.

**Suitable Parameters for Expressing Hydrodynamic Force Coefficients**
Various proposed definitions given in section 6.3.1 as well as some new ones for Keulegan-Carpenter number were examined to find more suitable parameters and to provide a better representation of the current effect on hydrodynamic force coefficients. The results (for the drag coefficient) arranged by $KC_{ov}$, $KC_3$, $KC_4$ are shown in figures 6.19 through 6.21. I It is clear from these figures that the drag coefficient cannot be correlated with Keulegan-Carpenter number alone without the need for an additional parameter involving the current velocity, e.g. reduced velocity $Vr$ or velocity ratio $V/\dot{x}_m$.

There are some fundamental ideas which help to explain the phenomena observed. For values of $V/\dot{x}_m \le 1$ flow reversal occurs twice in each oscillation cycle. Thus, each cycle may be divided into two parts: one part in which the cylinder is travelling with the flow and is faster than the flow and the other part in which the cylinder is travelling slower than or against the flow. For a given value of $V/\dot{x}_m$, the higher the $Vr$ value, the greater the differences between the relative distance travelled in each cycle. Looked at in another way, for a given $Vr$, as $KC_o$ is decreased ($V/\dot{x}_m$ increased), the relative distance travelled in both parts decreases. The lower the value of $V/\dot{x}_m$, the more nearly equal the two parts of the cycle. Note also that:

$$\frac{V}{\dot{x}_m} = \frac{Vr}{KC_o}$$

From the foregoing, it is evident that the velocity ratio $V/\dot{x}_m$ is an important parameter for

expressing the drag coefficients in a coexisting flow field.

The inertia coefficient $C_{Mr}$ is plotted versus $KC_{ov}$, $KC_i$, $KC_i$ in figure 6.22 through 6.24. The degree of scattering in $C_{Mr}$ exhibits similar behaviour to that for drag. The phenomenon is relatively complex and the effect of current on the force coefficient cannot be explained simply in terms of an increased Keulegan-Carpenter number.

A variety of forms of combined nondimensional parameters were tried in an attempt to improve the correlation. The nondimensional parameter

$$K_{AC} = \frac{KC_o}{Vr^2 + Vr\,KC_o}$$

results in a better correlation for the inertia coefficient as shown in figure 6.25. The concept of this parameter came from considering the ratio of the inertia force to the steady drag force. Using $K_{AC}$, the behaviour of $C_{Mr}$ is quite similar to that for the inertia coefficients for the no-current test case.

### 6.5.3.3 Lift Force Coefficients

As with single mode tests, a spectral analysis was carried out on each time record of the transverse force component to determine the shedding frequency assuming that the peak in the spectrum is associated with the shedding frequency. The obtained vortex shedding frequencies for all runs were used to determine the Strouhal number as per equation 6.7 and an appropriate definition for the Keulegan-Carpenter number as discussed after equation 6.7. It was found that $KC_{ov}$ is a better parameter to define the vortex shedding frequency for co-existing flow fields.

The obtained $f_v/f_o$ ratio was plotted as function of $KC_{ov}$ for all test runs with different towing velocity, oscillation frequency and oscillation amplitude in figure 6.26. From equation 6.7, it is seen that a constant Strouhal number plots as a straight line. Two constant Strouhal number ($St_{ov}$) lines of 0.09 and 0.18 are drawn in this figure for reference. Two important facts can be observed from this figure: First, the Strouhal number is bounded in the range from 0.09 to 0.18 for most tests. The linear trend line fitted to the data is equal to $St_{ov}=0.125$. Second, the vortex shedding frequency $f_v$ increases with increasing values of the $KC_{ov}$ number.

The calculated lift force coefficients, $C_{Lmax}$ and $C_{Lrms}$, are plotted against the reduced velocity $Vr$ in figures 6.27 and 6.28. As seen in the figures, the rms force coefficients exhibit the same functional dependence as the maximum values. Both the peak lift coefficient, $C_{Lmax}$ and the rms lift force coefficient, $C_{Lmax}$, depend on the Keulegan-Carpenter number and the reduced velocity. High coefficient values - as high as $C_{Lmax} = 2.5$ - were observed in the reduced velocity range $5 \le Vr \le 8$ for small $KC_o$ values. However, the lift force coefficient values are small for large values of the reduced velocity and Keulegan-Carpenter number; no peaks appear in the curve of $C_{Lmax}$ and $C_{Lrms}$ versus $Vr$ at $KC_o > 10$.

Comparing with no-current case results, the present rms lift force coefficient is about half of that for a no-current case, except in the reduced velocity range $5 \le Vr \le 8$ in which the $C_{Lrms}$ values for a co-existing flow field are larger than for no-current tests.

## 6.6 Conclusions from In-line Oscillation Plus Current Tests

The hydrodynamic forces acting on an oscillating cylinder in-line with a uniform flow have been investigated experimentally. The suitability of different load models for describing hydrodynamic interaction between an oscillating cylinder and a uniform flow have been examined using the laboratory data. The main conclusions obtained are as follows:

1. Analysis of the data indicates that there is a distinct correlation between the constant component of the drag force and the amplitude of the oscillatory flow velocity when the cylinder is oscillating in-line with the flow direction. Also, there is an obvious correlation between the oscillatory component of the drag force and the steady flow velocity. These tend to refute the independent flow fields approach for the prediction of interaction forces.

2. Each of the computational load models was fitted to the measured data from 107 test runs covering a wide range of $KC$ and $Vr$ values. The qualities of fit of these models are almost the same, provided that each equation form used its own distinct set of coefficients.

3. A harmonic load model (with the first two harmonic components) fits the data as well as does a two-term form of the Morison equation, if the corresponding phase angle is determined correctly. Observations indicate that higher harmonics give no significant improvement of the results.

4. It is very obvious that significant errors can result from the indiscriminate use of hydrodynamic coefficients in a different computational model than the one for which the coefficients are determined.

5. In the light of conclusions 2 and 4, additional criteria must be used to select a 'best' form of computational model. One such criterion can be the degree by which the coefficients are consistent over wide ranges of dimensionless parameters. Another criterion may perform a check on the computed forces using each selected model and corresponding but smoothed coefficients. Both these criteria have been used in the present work.

6. Both the two-term relative velocity Morison equation and a linearised form of this equation seem to satisfy these additional criteria well.

7. The hydrodynamic coefficients for co-existing flow fields are not identical with those for no-current tests; the drag and inertia coefficients are strongly affected by a current. The variation of the force coefficients depends on both the Keulegan-Carpenter number and the velocity ratio $V/\dot{x}_m$ (or the reduced velocity).

8. The frequency of the lift force ($f_v$) in oscillatory flow plus current depends on $KC_{ov}$ (relative velocity), and increases with increasing values of the $KC_{ov}$ number.

9. The peak lift coefficient $C_{Lmax}$ and the rms lift force coefficient $C_{Lrms}$ depend also on the Keulegan-Carpenter number and the reduced velocity.

10. The rms lift force coefficients for in-line oscillations plus current are about half of those for no-current tests, except in the reduced velocity range $5 \le Vr \le 8$ in which the $C_{Lrms}$ values for the co-existing flow field are larger than for no-current tests.

65
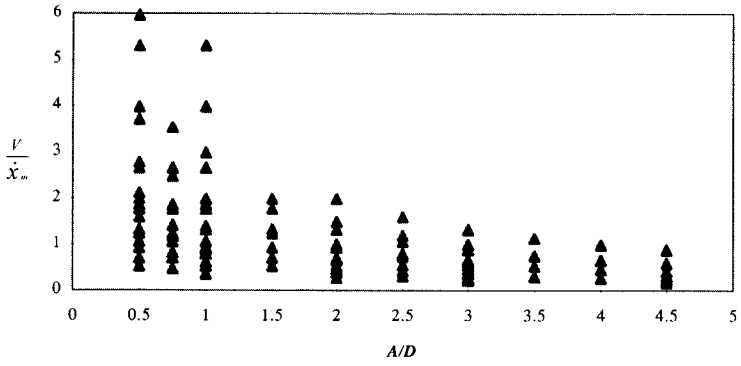
Figure 6.1   Parameter combinations covered for tests with in-line oscillation plus current
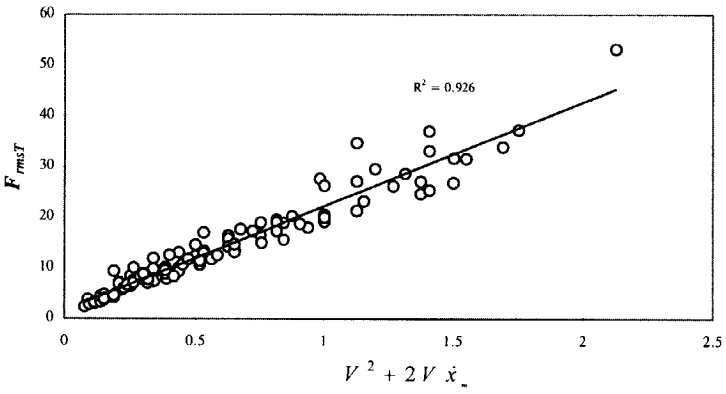


Figure 6.2  In-line oscillation plus current, *Frms*  plotted  versus $(V^2 + 2\,V\dot{x}_m)$
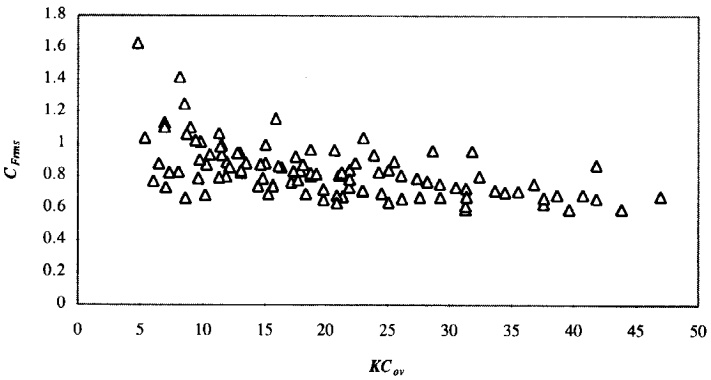


Figure 6.3   In-line oscillation plus current, $C_{Frms}$ plotted versus $KC_{ov}$
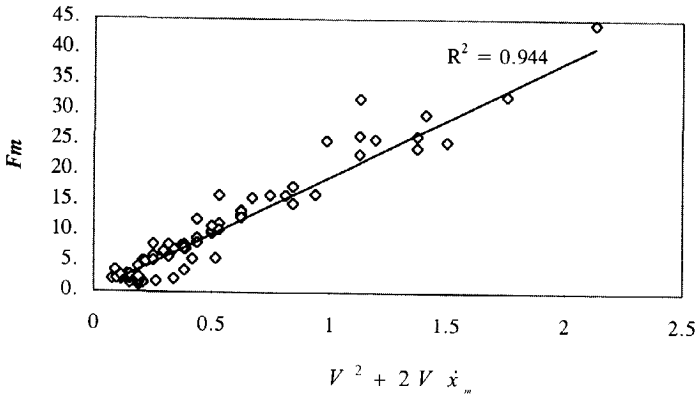
Figure 6.4 In-line oscillation plus current, mean drag force plotted versus $(V^2 + 2\ V\dot{x}_m)$



$$Vr = V\,T_o\ /\ D$$

o A/D = .5   □ A/D = .75   △ A/D = 1   × A/D = 1.5
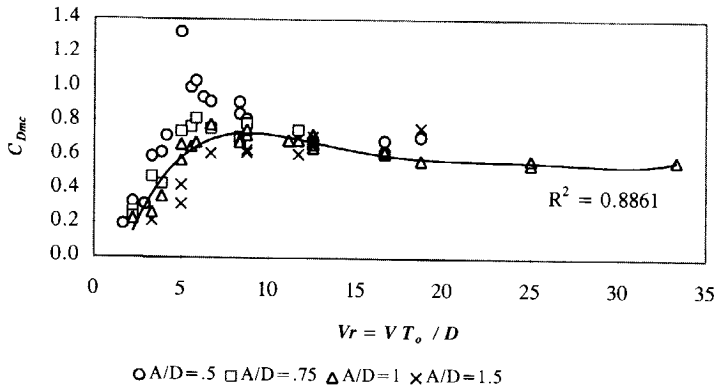
Figure 6.5  In-line oscillation plus current, $C_{Dmc}$ versus reduced velocity Vr, solid line: fourth order polynomial regression line through the data for $A/D = 1$



$$V\,\dot{x}_m$$
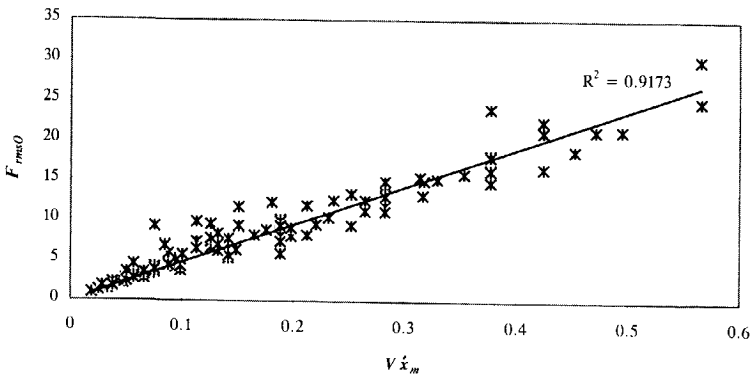
Figure 6.6  In-line oscillation plus current, standard deviation value of the in-line force plotted versus $V.\dot{x}_m$

67
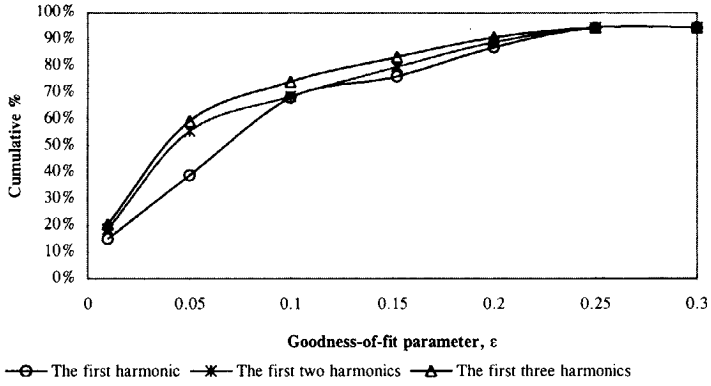
Figure 6.7 Comparison of goodness-of-fit parameter, ε, for harmonic load models
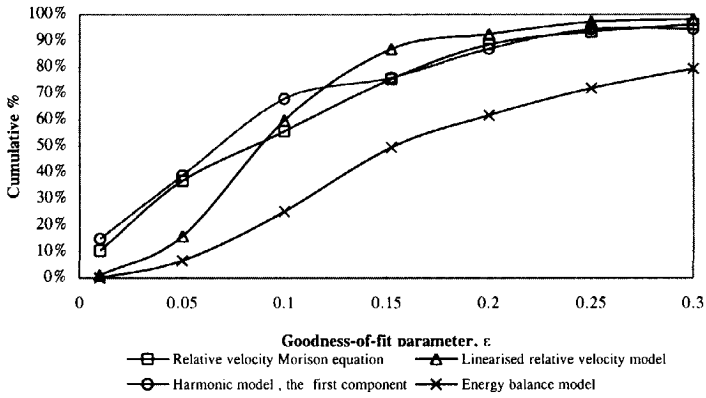


Figure 6.8 Comparison of goodness-of-fit parameter, ε, for given load models using the best individual coefficients
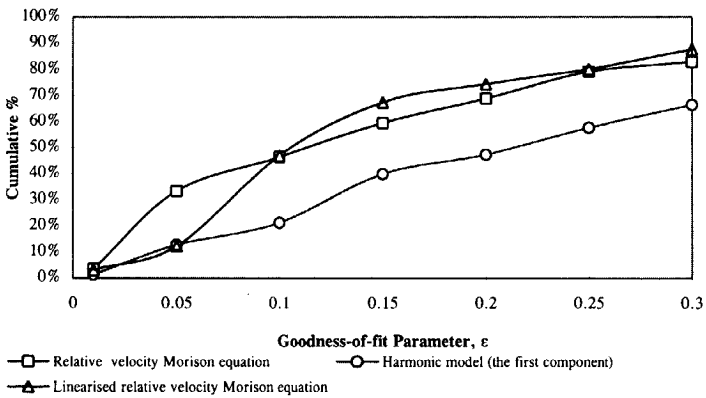


Figure 6.9 Comparison of Goodness-of-fit parameter, ε, for given load models using smoothed coefficients
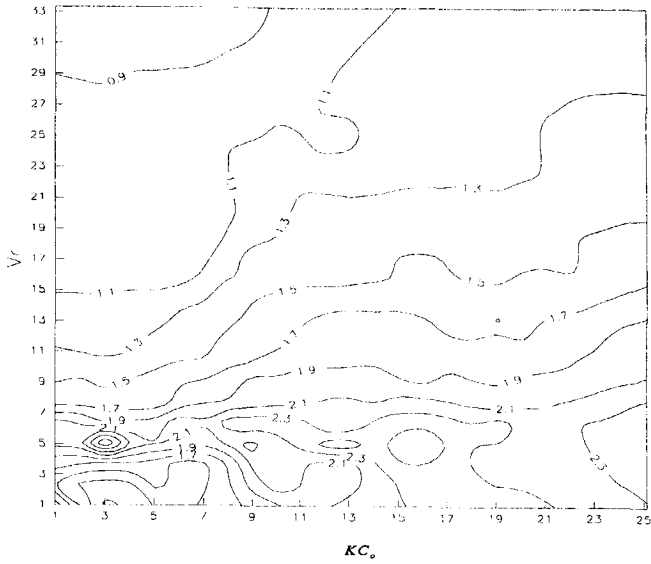
Figure 6.10  In-line oscillation Plus Current Tests, Contours of the Mean Drag
Coefficient $C_{Dm}$
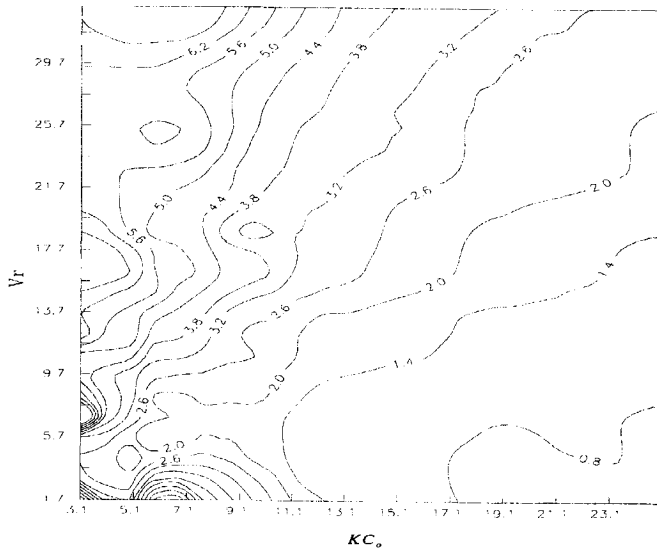


Figure 6.11 In-line Oscillation Plus Current Tests, Contours of $C_{dhl}$
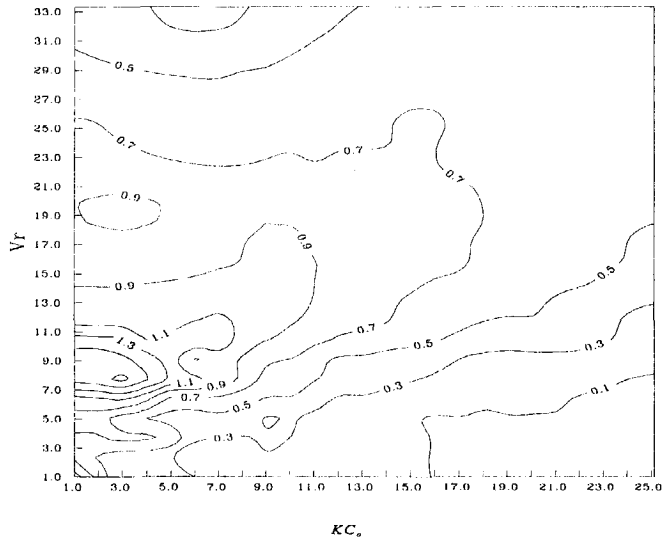
Figure 6.12  In-line Oscillation Plus Current Tests, Contours of $C_{dh2}$
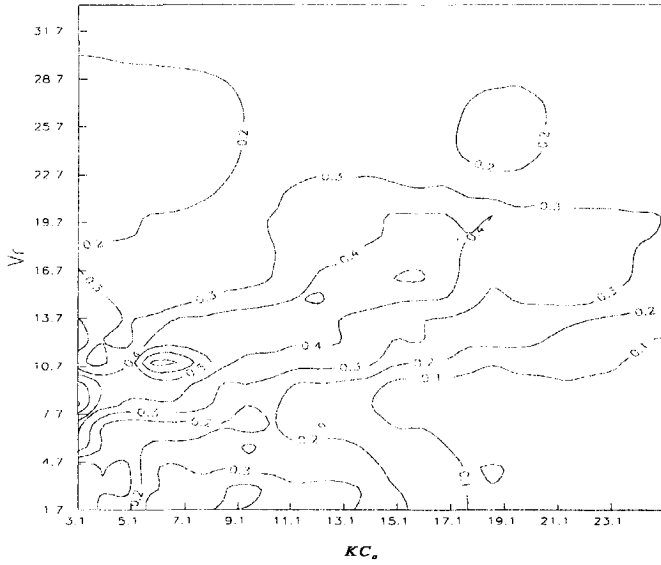


Figure 6.13  In-line Oscillation Plus Current, Contours of $C_{dh3}$

70
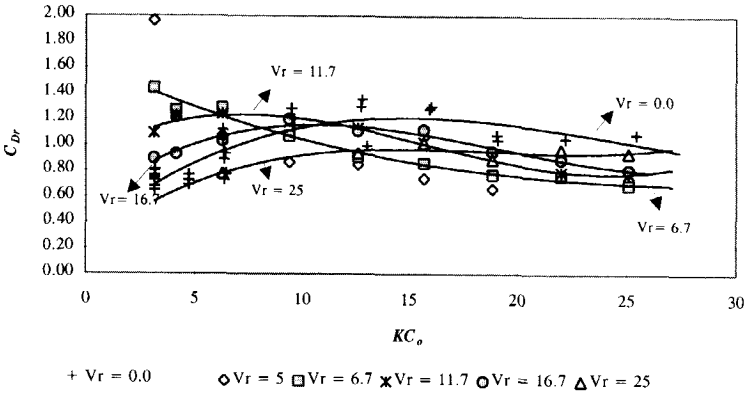
Figure 6.14 In-line Oscillation plus current tests, $C_{Dr}$ plotted versus $KC_o$
lines: 3rd order polynomial regression line through the data points
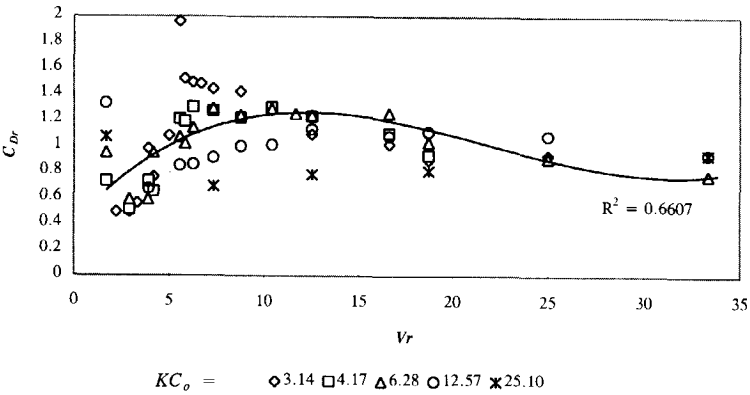


Figure 6.15 In-line oscillation plus current tests, $C_{Dr}$ plotted versus $Vr$; solid line:
3rd order polynomial regression line through the data for $KC_o - 6.28$
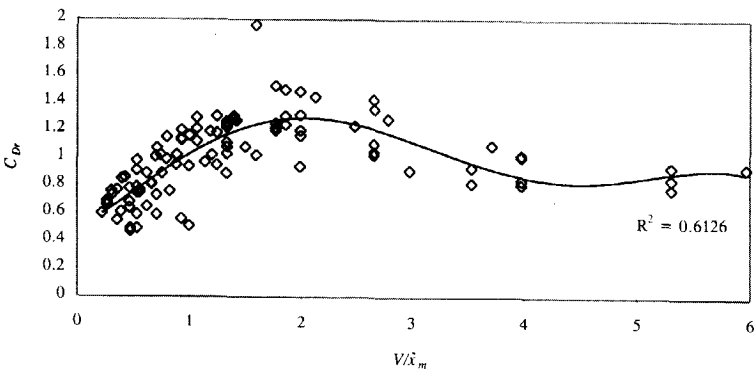


Figure 6.16 In-line oscillation plus current tests, $C_{Dr}$ plotted versus velocity ratio $V/\dot{x}_m$;
solid line: 3rd order polynomial regression line through the data

71
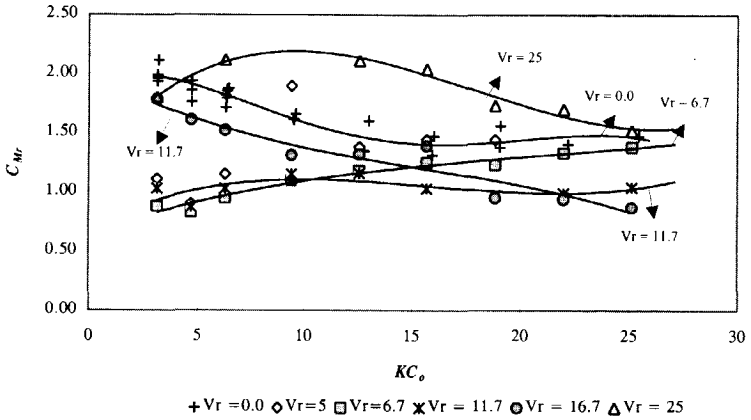
Figure 6.17  In-line oscillation plus current tests, $C_{Mr}$ plotted versus $KC_o$
lines: 3rd order polynomial regression line through the data points
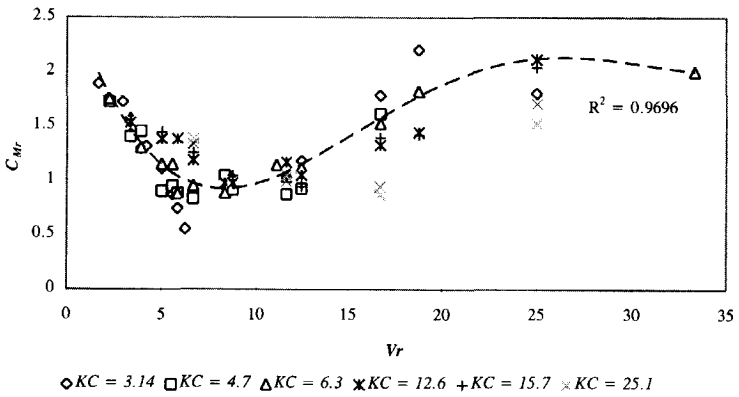


Figure 6.18  In-line oscillation plus current tests, $C_{Mr}$ plotted versus $Vr$; dash line:
3rd order polynomial regression line through the data for $KC_o = 6.3$
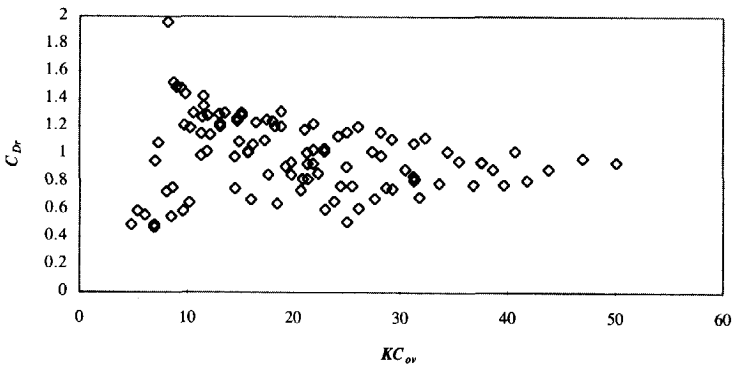


Figure 6.19  In-line oscillation plus current tests, $C_{Dr}$ plotted versus $KC_{ov}$
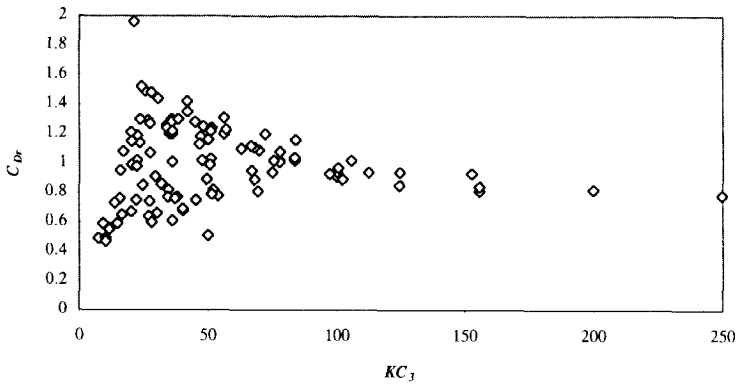
Figure 6.20 In-line oscillation plus current tests, $C_{Dr}$ plotted versus $KC_3$
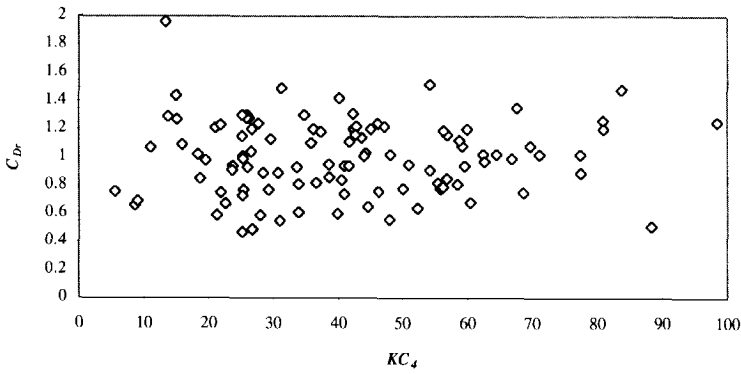


Figure 6.21 In-line oscillation plus current tests, $C_{Dr}$ plotted versus $KC_4$
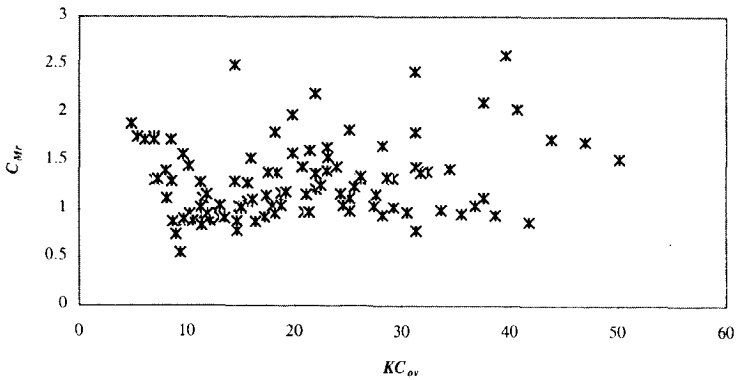


Figure 6.22 In-line oscillation plus current tests, $C_{Mr}$ plotted versus $KC_{ov}$
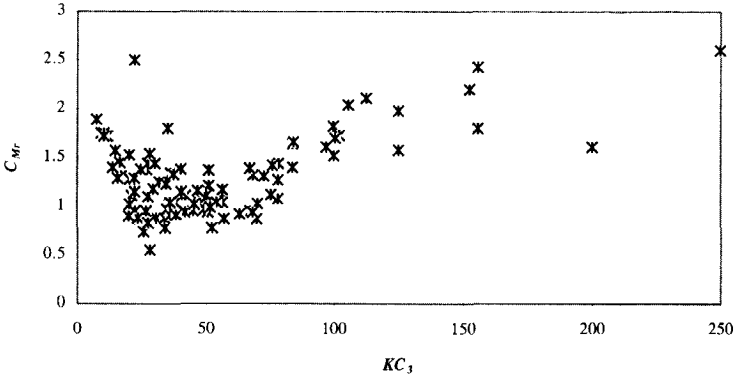
Figure 6.23 In-line oscillation plus current tests, $C_{Mr}$ plotted versus $KC_3$
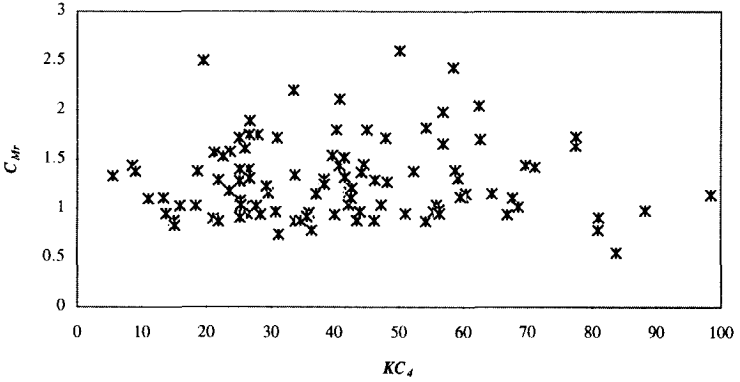


Figure 6.24 In-line oscillation plus current, $C_{Mr}$ plotted versus $KC_4$
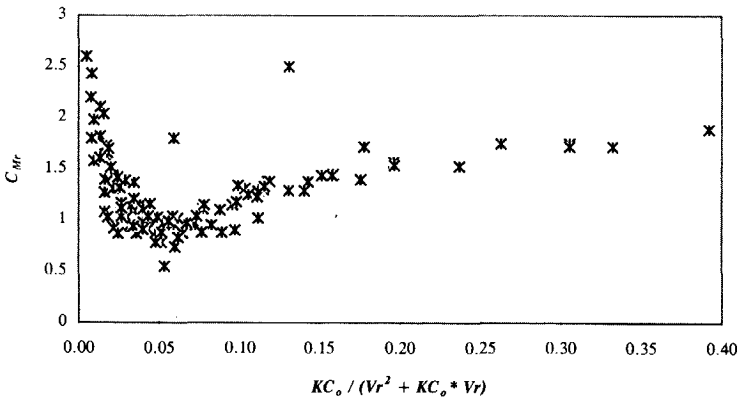


Figure 6.25 In-line oscillation plus current tests, $C_{Mr}$ plotted versus $K_{AC}$

74
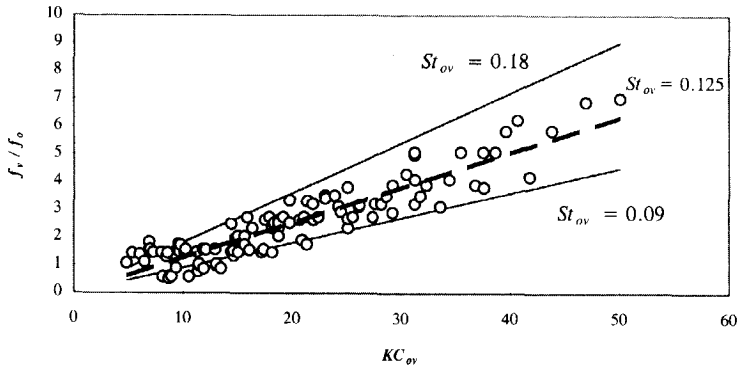
Figure 6.26 In-line oscillation plus current tests, $f_v/f_o$ plotted versus $K_{ov}$
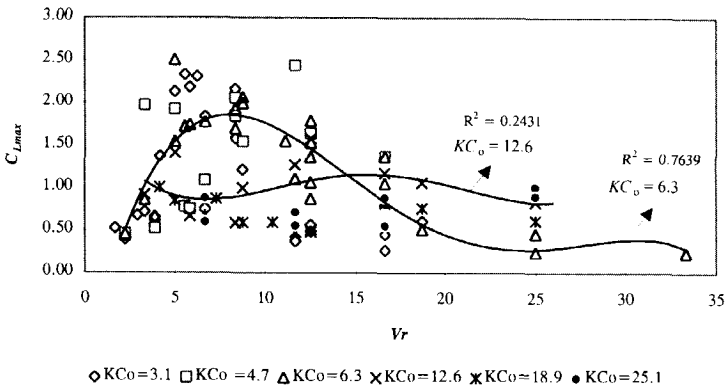
Figure 6.27 In-line oscillation plus current tests, peak lift force coefficient $C_{Lmax}$ plotted versus $Vr$, lines: 3rd order polynomial regression line through the data points
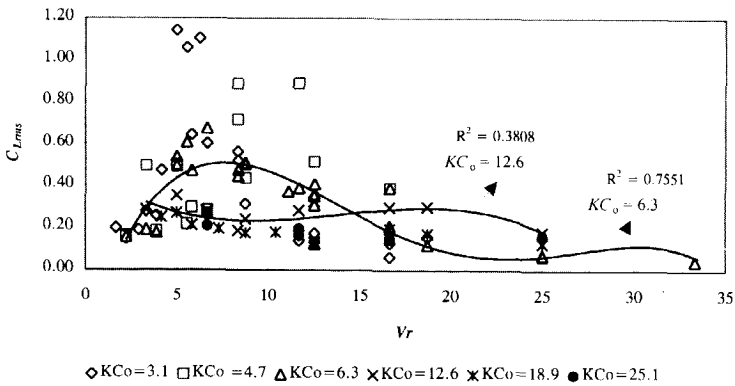
Figure 6.28 In-line oscillation plus current tests, rms lift force coefficient $C_{Lrms}$ plotted versus $Vr$, lines: 3rd order polynomial regression line through the data points

# CHAPTER 7

# Towing the Cylinder in Waves

## 7.1 Introduction

The research on fluid forces in the combined flow field caused by co-existing waves and current is scarce. Although considerable attention has been given to this subject, no consistent understanding has developed yet.

The present chapter presents and discusses the results of the waves plus current tests. Since slender marine structures are usually subjected to waves together with a current in an actual environment, the results presented here are significant for the design of offshore structures.

To calculate the in-line forces on a fixed cylinder in a combined wave and current flow field the Morison equation is normally used. From the view point of particle motion, however, it seems clear that the situation of a cylinder in a wave field is very different from that in a wave and current flow field. However, in some references and engineering practices, the value of the drag coefficient in a wave and current field is considered the same as that in a wave field alone. This may not be justified. It is necessary to determine the value of the associated coefficients based on the motion mechanism in the combined wave and current field.

In this work, as in the previous chapters, the Morison equation will not be taken for granted.

## 7.2 Specific Details of the Wave and Current Flow Field

The present test series is a multi-mode test series which combines two previously considered single mode tests, i.e. wave-only tests and current-only tests. However, the hydrodynamic interaction of a cylinder in the combined waves and current flow field is totally different from that for the single mode tests. The specific phenomena and flow situations for the present test series are summarized in the following paragraphs.

### 7.2.1 Wave-Current Interaction

Due to interaction between waves and current, the characteristics of a wave are changed in the presence of a current; especially the wave height and the wave length are modified. If the current is in the direction of wave propagation, the wave slope decreases and its length increases. On the other hand, if the current opposes the wave, the wave slope increases in magnitude and the wave length shortens. This effect of wave-current interaction is usually neglected; an interactive term in the description of the wave and current field is omitted; the resulting velocity field is simply written as a linear superposition of wave and current terms.

The general problem of modelling wave-current interactions, either analytically or numerically, is fraught with difficulties, see Thomas (1979). However, solutions for different flow conditions, especially for the simple case of a wave propagating on a uniform in-line current, have been implemented in the past, see e.g. Peregrine (1976) and Li and Kang (1992).

The physical interaction between waves and currents will not be considered in this study and is not present in the experiments performed in this work where the cylinder is towed in waves generated on water being at rest. Therefore, only knowledge of Doppler shift due to towing is required to estimate the flow kinematics.

The flow condition for the present test case is illustrated in figure 7.1. The towing speed $V$ is positive when the carriage is towed with the (regular) wave, and negative when it opposes the wave. The regular wave has an (intrinsic) frequency of $\omega_w$:

$$\omega_w^2 = g\,k\,\tanh\,kd \tag{7.1}$$

The wave frequency relative to the moving coordinate (carriage) - the so-called 'encounter frequency' or 'apparent wave frequency' $\omega_{app}$ - is related to the intrinsic wave frequency through the relationship:

$$\omega_{app} = \omega_w + kV \tag{7.2}$$

in which the last term is the Doppler shift. Then the dispersion relation in a frame of reference moving with the carriage has the form:

$$(\omega_{app} - kV)^2 = g\,k\,\tanh\,kd \tag{7.3}$$

Thus, for a given wave (intrinsic) frequency $\omega_w$, it is possible to link $k$ (and thus the wave length) with the towing speed $V$ and to determine the apparent wave frequency.

A horizontal distance along the wave propagation $x_w$ with respect to the moving coordinate system is related to $x$ by (see figure 7.1):

$$x_w = x - Vt \tag{7.4}$$

with $x_w = x$ at $t = 0$. Using linear wave theory, the water surface elevation as observed in the moving coordinate is given by:

$$\eta = \frac{H}{2}\cos(kx_w - \omega_w t) \tag{7.5}$$

Combining equations 7.2, 7.4 and 7.5, one may obtain:

$$\eta = \frac{H}{2}\cos(kx - \omega_{app}t) \tag{7.6}$$

Superimposing the towing speed and wave particle velocity, the total velocity in the fixed frame of reference is given as:

$$u_T = V + u = V + \frac{H}{2}\omega_w\frac{\cosh k(z+d)}{\sinh kd}\cos(kx - \omega_{app}t) \tag{7.7}$$
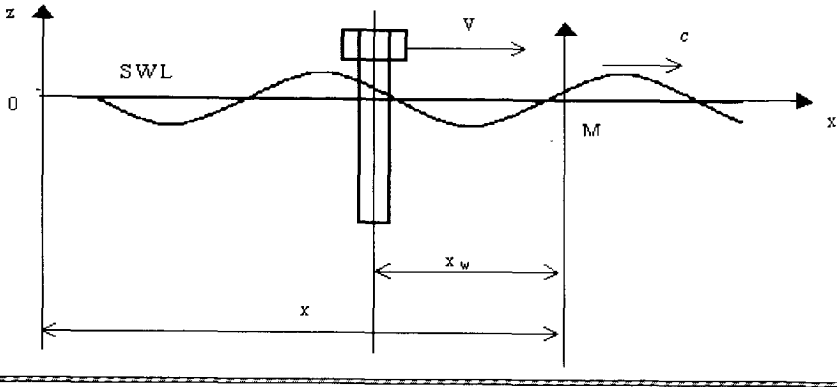
Figure 7.1 Definition sketch for towing the cylinder in regular waves

The amplitude of wave particle velocity becomes:

$$u_m = \frac{H\omega_w}{2} \cdot \frac{\cosh k(z+d)}{\sinh kd} = \frac{Hgk}{2(\omega_{app} - kV)} \cdot \frac{\cosh k(z+d)}{\cosh kd} \qquad (7.8)$$

## 7.2.2 Orbital Velocity Effects

When compared with the earlier multi-mode test case (forced in-line oscillation in a current), the oscillatory flow around a vertical cylinder in waves has a vertical component of the orbital velocity and a horizontal component of the orbital velocity which varies along the cylinder axis. Several investigations have been published on the effects of orbital flow when a cylinder is in the plane of the particle velocity ellipse. However, the effects of orbital flow in a coexisting flow field have not been investigated completely yet. Common practice is to neglect the orbital flow effect and to assume that the cross flow principle is correct when the cylinder axis is in the plane of the velocity ellipse, see for example API (1993). The data for the present test series may make it possible to study effects of the orbital velocity in a combined flow field.

## 7.2.3 Vortex Properties

There is an essential difference between the mechanisms of generating hydrodynamic forces in the wave-current co-existing field and in the wave-only field. In the wave-only field, the water particles move almost symmetrically in the phases of wave crest and wave trough, whereas these movements are distinctly asymmetric in the co-existing field. Consequently, the development and shedding of vortices become different from the wave-only field; they produce different characteristics in the hydrodynamic forces, too.

## 7.2.4 Important Parameters

Just as for the in-line oscillation plus current test series, the governing nondimensional

parameters are a Reynolds number, a Keulegan-Carpenter number, and a parameter involving current velocity such as reduced velocity $Vr = VT/D$, or velocity ratio $u_m/V$. Various definitions given in section 6.3.1 for these parameters may be used for the present test series by replacing $\dot{x}_m$ with $u_m$:

$$KC_w = \frac{u_m T}{D}, \qquad\qquad Re_w = \frac{u_m D}{\nu} \qquad\qquad\qquad (7.9)$$

$$KC_{wv} = \frac{(u_m + V)T}{D}, \qquad\qquad Re_{wv} = \frac{(u_m + V)D}{\nu} \qquad\qquad (7.10)$$

$$KC_3 = \frac{u_m T}{D}(1 + |\frac{V}{u_m}|)^2, \qquad Re_3 = \frac{u_m D}{\nu}(1 + |\frac{V}{u_m}|)^2 \qquad (7.11)$$

Another form of Keulegan-Carpenter number is based upon the wave-current interaction concept by using the apparent wave period, $T_{app} = 2\pi/\omega_{app}$ as:

$$KC_{app} = \frac{(u_m + V) T_{app}}{D} \qquad\qquad\qquad\qquad (7.12)$$

According to theoretical analysis as well as experimental study, the water particle path in a wave and current field is dependent on the ratio of the maximum horizontal velocity $u_m$ due to wave action to that of the steady flow, i.e. $u_m/V$. When $u_m/V > 1$, the maximum horizontal velocity due to wave motion is larger than that of the steady flow, see figure 7.2a. When $u_m/V < 1$, the velocity of the steady current is larger than that of wave motion, see figure 7.2b.



(a) $u_m/V > 1$             (b) $u_m/V < 1$
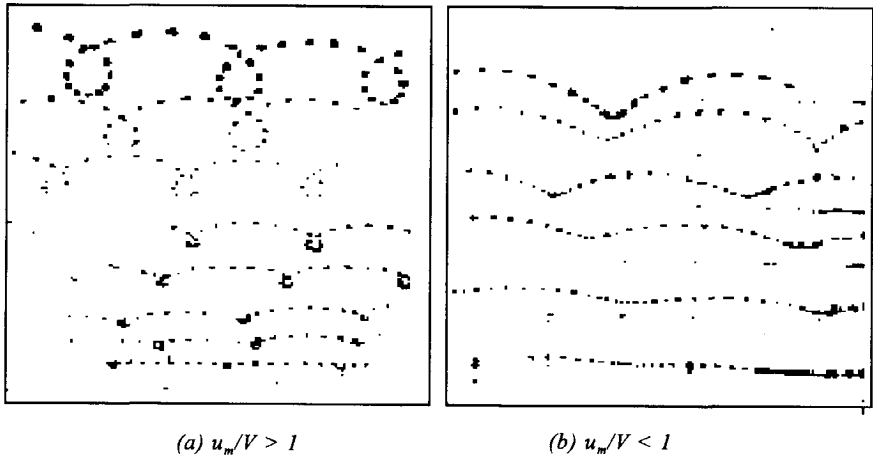
Figure 7.2 Pictures of Flow Pattern for a Combined Waves and Current Field (Ren and He 1986)

### 7.2.5 Tests Conducted and Data Range

The present test series is a two-mode test case which combines the current-only tests and wave-only tests. The cylinder was towed with different speeds in given waves. Table 7.1 gives the nondimensional parameter ranges for the test case under consideration.

| Parameter | Definition | Range |
|---|---|---|
| Reynolds number based on current | $Re = V D/\nu$ | 12000 - 45000 |
| Reynolds number based on oscillatory flow | $Re_w = u_m D/\nu$ | 5300 - 55000 |
| Reynolds number based on total flow | $Re_{wv} = (V + u_m)D/\nu$ | 19500 - 60760 |
| Keulegan-Carpenter number, oscillatory flow | $KC_w = u_m T/D$ | 3.1 - 9.2 |
| Keulegan-Carpenter number, total flow | $KC_{wv} = (u_m + V)T/D$ | 7.5 - 25.7 |
| Reduced velocity | $Vr = VT/D$ | 3.3 - 18.75 |
| Velocity ratio | $u_m/V$ | 0.23 - 1.33 |

Table 7.1  Experimental Variable Ranges for Waves Plus Current Tests

## 7.3 Load Models

Based on the results of the previous test series, only a harmonic load model and two modified forms of the Morison equation have been examined for the present test series. Even though these models are similar to those given in section 6.4, they are summarized here with their specific forms for the test series under consideration.

### 7.3.1 Harmonic Load Models

Just as the harmonic load model formulated for the in-line oscillation plus current tests (see section 6.4.1) the hydrodynamic force on a cylinder in the combined wave and current flow field may be written as:

$$F = 0.5 \, \rho \, D \, C_{Dm} \, V^2 + 0.5 \, \rho \, D \, u_m^2 \sum_{n=1}^{N} C_{dhwn} \, \sin(n \, \omega_{app} \, t + \phi_n) \qquad (7.13)$$

### 7.3.2 Generalisation of the Morison Equation

Two well-known extensions of the Morison equation in a waves plus current flow field are based upon the independent flow fields approach and the relative (total) velocity approach. These extensions may be written as:

$$F = C_{Dm}(\frac{1}{2}\rho D) V^2 + C_{Da}(\frac{1}{2}\rho D)|u|u + C_{Ma}(\rho \frac{\pi}{4} D^2) \dot{u} \qquad (7.14)$$

$$F = C_{Dr}(\frac{1}{2}\rho D)|V+u|(V+u) + C_{Mr}(\rho\frac{\pi}{4}D^2)\dot{u} \qquad (7.15)$$

The inertia coefficients in the two models are expected to be equal, $C_{Ma} = C_{Mr}$. However, different symbols are used to test such a relation using the data.

### 7.3.3 Lift Force Model

One can similarly determine the lift force coefficients and vortex shedding frequency using different models and techniques. It is interesting to observe the influence of current on the maximum and the rms lift force coefficients:

$$C_{Lmax} = \frac{Fy_{max}}{0.5\rho D(V+u_m)^2} \qquad (7.16)$$

$$C_{Lrms} = \frac{Fy_{rms}}{0.5\rho D(V+u_m)^2} \qquad (7.17)$$

Two different definitions may be used for the Strouhal number of a combined wave plus current flow field:

$$St_w = \frac{f_v D}{u_m} = \frac{f_v}{f_w KC_w} \qquad (7.18)$$

$$St_{wv} = \frac{f_v D}{V+u_m} = \frac{f_v}{f_w KC_{wv}} \qquad (7.19)$$

Another definition may also be proposed for Strouhal number by including the convective term and using the apparent wave frequency $f_{app} = \omega_{app}/2\pi$ instead of $f_w$ in equation 7.19 as:

$$St_{app} = \frac{f_v D}{V+u_m} = \frac{f_v}{f_{app} KC_{app}} \qquad (7.20)$$

### 7.4 Analysis Procedure

The analysis procedure was similar to that for the waves-only tests. After data reduction, the exact amplitude and period of the waves were determined using a FFT analysis. The wave probe was installed on the carriage in such a way that the measured water surface elevation was the instantaneous displacement of the water surface in the measuring point. In other words, the wave elevation was measured in the moving coordinate system. Therefore, the frequencies obtained by FFT analysis were the apparent frequencies and different from those set at the wave generator.

Applying linear wave theory, results of the FFT analysis were used to compute the horizontal water particle velocities and accelerations. The force coefficients for the extended Morison equation forms were computed using the least squares technique. The coefficients for the harmonic load models were determined using results from the FFT analysis.

The lift force frequencies were obtained through FFT analysis of the measured transverse forces.

## 7.5 Results and Discussion

### 7.5.1 Direct Observations from the Data

Behaviour of the measured in-line forces against various combinations of variable values was studied to see what relationships between kinematics and forces would fit the data best. The characteristic forces listed in section 6.5.1 were used for this purpose.

The variations of these characteristic forces as a function of various variables were investigated as was done for the in-line oscillation plus current tests. Table 7.2 gives the values of the calculated correlation coefficient $R^2$ between the characteristic forces and various combinations of independent variables such as $V^2$, $u_m^2$ and $V \cdot u_m$. These results are discussed in the following paragraphs.

| | $V^2$ | $u_m^2$ | $Vu_m$ | $(V+u_m)^2$ | $V^2 + u_m^2$ | $V^2 + 2Vu_m$ | $V^2 + Vu_m$ |
|---|---|---|---|---|---|---|---|
| $F_{max}$ | 0.60 | 0.16 | 0.90 | 0.93 | 0.80 | 0.95 | 0.85 |
| $F_{rmsT}$ | 0.68 | 0.08 | 0.91 | 0.93 | 0.85 | 0.92 | 0.88 |
| $Fm$ | 0.77 | 0.10 | 0.86 | 0.91 | 0.90 | 0.93 | 0.91 |
| $F_{rmsO}$ | 0.56 | 0.24 | 0.93 | 0.89 | 0.76 | 0.85 | 0.78 |

Table 7.2    $R^2$ Correlation Coefficient Values for Linear Regression of Characteristic Forces to Different Velocity Components

### 7.5.1.1 Maximum Values of the In-line Force

The second row in table 7.2 gives $R^2$ correlation coefficient values for linear regression of maximum values of the in-line force $F_{max}$ when different combinations of $V^2$, $u_m^2$ and $V \cdot u_m$ are used as independent variables. As listed in this table, the best correlation can be obtained using $(V^2 + 2V \cdot u_m)$ as independent variable, however, other combinations such as $(V+u_m)^2$ also correlate very well. Figure 7.3 shows how $F_{max}$ varies as a function of $(V^2 + 2V \cdot u_m)$.

Using this observation, a maximum drag coefficient may be defined as:

$$C_{Dmax} = \frac{F_{max}}{0.5 \rho D (V^2 + 2 V u_m)} \tag{7.21}$$

Figure 7.4 shows the variation of $C_{Dmax}$ as a function of $u_m/V$.

### 7.5.1.2 RMS Values of the In-line Force

Correlation coefficient values $R^2$ between root mean square values of the total in-line force $F_{rmsT}$ and various variables are listed in the third row of table 7.2. As seen from this table $F_{rmsT}$ is equally well related to $(V+u_m)^2$ and $(V^2 + 2Vu_m)$ for all test runs. Figure 7.5 shows $F_{rmsT}$ as a function of $(V+u_m)^2$.

### 7.5.1.3 Mean Drag Force

As listed in the third row of table 7.2, the best linear fit for the mean steady force component $Fm$ is obtained by plotting it against $(V^2 + 2V \cdot u_m)$, see figure 7.6. The $R^2$ value for $V^2$ is relatively low; a high value would confirm an absolute velocity approach. The dependence of the steady force on the oscillatory velocity proves that the steady in-line force component depends on waves; there must be an interaction between the two flow fields. The independent flow field does not seem a proper solution for estimating the hydrodynamic force on a cylinder in waves plus current flow field.

Based on the above observation, the mean drag force $Fm$ can be normalized by $(V^2+2Vu_m)$ to get a mean drag coefficient:

$$C_{Dmc} = \frac{F_m}{0.5\,\rho\,D(V^2 + 2\,Vu_m)} \tag{7.22}$$

Values of $C_{Dmc}$ are plotted versus the velocity ratio $u_m/V$ in figure 7.7.

### 7.5.1.4 The RMS Values of the Oscillatory Force Component

The fourth row of the values in table 7.2 gives the calculated $R^2$ values between $F_{rms0}$ and various combinations of independent variables. Figure 7.8 shows how $F_{rms0}$ varies as a function of $V \cdot u_m$. Similar to the earlier test series (in-line oscillation plus current), the oscillatory force correlates well with the product of the velocities indicating interaction between the steady and oscillatory flows. The conclusion in section 7.5.1.3 is again confirmed.

### 7.5.2 Fitting the Load Models to Data

The quality of fit using various load models will be discussed in this section. The interpretation of the force coefficients obtained is considered in the next section. The same procedure as described for previous test cases was used to evaluate the quality of fit of the given load models.

### 7.5.2.1 Quality of Fit Using Individual Run Coefficients

It has been shown that only keeping the first two terms in the harmonic load model given in equation 7.13 leads to a good approximation; more than 96% of signal variances are described by the amplitudes of first two harmonics.

The goodness-of-fit parameter $\epsilon$ (see equation 3.21) was calculated for each test run and each of the load models for in-line forces given in sections 7.3.1 and 7.3.2. The cumulative probability of $\epsilon$ for these three load models is shown in figure 7.9. Table 7.3 lists the statistics for $\epsilon$ using the models. Note that the best possible (individual) coefficient values for each run were used here. Taking all information in this table and figure 7.9 together, one can conclude that all three load models fit the data pretty well and that these load models all seem suitable to describe hydrodynamic forces on a fixed cylinder in a co-existing flow field if their individually obtained coefficients are used.

84

The variation of $\epsilon$ is plotted versus the velocity ratio $V/u_m$ in figure 7.10 to illustrate the effect of this ratio on the quality of fit of the load models. As seen from this figure, $\epsilon$ decreases as $V/u_m$ increases. Both extensions of the Morison equation do not fit to the data well when $V/u_m \leq 1$. However, this conclusion is not well-supported since the amount of data for $V/u_m < 1$ is insufficient.

| Load Models | Fit quality $\epsilon$ value | | Percentage of runs with: |
|---|---|---|---|
| | Mean | STD | $\epsilon < 0.2$ |
| Absolute Velocity Model | 0.072 | 0.045 | 100.0% |
| Total (relative) Velocity Model | 0.081 | 0.055 | 95.8% |
| Harmonic Model | 0.082 | 0.058 | 91.7% |

Table 7.3  Summary of Model Fitting Results with Individual Coefficients

## 7.5.2.2 Quality of Fit Using Smoothed Coefficients

Since in practice it is almost impossible to use coefficients separately obtained for each individual test run, using each model with a smoothed coefficient value to predict the interaction force is much more realistic. The load models have also been evaluated using smoothed coefficients. Even though harmonic load models are very sensitive to the phase angle values, these values in equation 7.13 have not been smoothed in this evaluation.

Figure 7.11 shows the final results of this work with smoothed coefficients plotted in the same way as in figure 7.9. Table 7.4 lists the statistical values of $\epsilon$ for each model using the smoothed coefficients. Considering information in this table and figure 7.11, one can conclude that the relative velocity model gives better results than the two other models. This was expected in view of the observations discussed earlier in section 7.5.1. The quality of fit for the harmonic load model is low in comparison to the results obtained using 'best' individual coefficients. More error shows up as a poorer fit when a smoothed coefficient value is used.

| Load Models | Fit quality $\epsilon$ value | | Percentage of runs with: |
|---|---|---|---|
| | mean | STD | $\epsilon < 0.2$ |
| Absolute Velocity Model | 0.137 | 0.093 | 86.4% |
| Total (relative) Velocity Model | 0.109 | 0.069 | 87.5% |
| Harmonic Model | 0.148 | 0.062 | 84.5% |

Table 7.4  Summary of Model Fitting Results with Smoothed Coefficients

## 7.5.3 Force Coefficients

From the foregoing discussion it is noticed that both extended forms of the Morison equation (with appropriate coefficients) could reproduce the measured hydrodynamic force. However, the scattering in the obtained coefficients was greater for the absolute velocity model. Thus, scattering in the coefficients may be used as an additional criterion to assess suitability of the load models. The quality and interpretation of force coefficients for both extended forms of the

Morison equation as well as lift force coefficients are discussed here.

### 7.5.3.1 Modified Morison Equation Coefficients

*Absolute Velocity Model*:

The extended form of Morison equation based on absolute velocities (see equation 7.14) has three coefficients; i.e. the mean drag coefficient $C_{Dm}$, the oscillatory drag coefficient $C_{Da}$ and the inertia coefficient $C_{Ma}$. Figure 7.12 shows the mean drag coefficient versus $u_m/V$. $C_{Dm}$ has an average value of $C_{Dm} = 1.1$. This is comparable to the average value of the steady drag coefficient obtained for current-only tests. For small $u_m/V$ values, $C_{Dm}$ is smaller than the steady drag coefficient for the current-only tests. $C_{Dm}$ increases when $u_m/V$ increases, approaching the current-only coefficient values.

In figure 7.13, the oscillatory drag coefficient $C_{Da}$ is shown as a function of $u_m/V$; $C_{Da}$ exhibits a significant scatter. As $u_m/V$ increases from 0 (no waves), the value of $C_{Da}$ increases, approaching a value as high as 4.4 for $u_m/V \approx 0.5$ and then decreases for $u_m/V > 0.5$, approaching the value of 1.5, which is slightly larger than that of the wave-only tests.

To compare $C_{Da}$ with the oscillatory drag coefficients for wave-only tests, $C_{Da}$ and $C_D$ are plotted versus $KC_w$ in figure 7.14. It is seen that the oscillatory drag coefficient is significantly affected by a current; $C_{Da}$ values are generally much higher than $C_D$ values and there is more scatter in $C_{Da}$.

The inertia coefficient $C_{Ma}$ is plotted versus $u_m/V$ in figure 7.15. As can be seen in this figure, the scatter for $C_{Ma}$ is small compared with $C_{Da}$, and $C_{Ma}$ decreases as $u_m/V$ increases approaching a value as low as 0.6. Figure 7.16 shows $C_{Ma}$ and $C_M$ (inertia coefficient for wave-only tests) plotted versus $KC_w$. The effect of current is to decrease the inertia coefficient (by about 50%) when the absolute velocity model is employed as the load model.

From the above results one can conclude that neither the oscillatory drag coefficient $C_{Da}$ nor the inertia coefficient $C_{Ma}$ is identical to those obtained for waves-only tests. Furthermore, $C_{Da}$ exhibits large values which do not correspond to those obtained under no-current conditions.

*Relative Velocity Model*:

Extensive examination of force coefficients $C_{Dr}$ and $C_{Mr}$ in equation 7.16 with various nondimensional parameters have shown that these coefficients correlate relatively well with the velocity ratio $u_m/V$ as shown in figures 7.17 and 7.18. As this ratio increases, $C_{Dr}$ increases in the region of small $u_m/V$ (<0.8) then it decreases for $u_m/V > 0.8$. As expected, this is just opposite to the trend for the inertia coefficient $C_{Mr}$ in figure 7.18.

The $C_{Dr}$ values are shown as a function of $KC_w$ in figure 7.19. The results obtained under wave-only conditions are also shown in this figure. It shows again that the drag coefficient (using a relative velocity approach) for a cylinder in waves plus current flow field is affected by the current. Overall, the drag coefficients (for relative velocity model) obtained from waves plus

current tests are smaller than those from wave-only tests: $C_{Dr} < C_D$. This result is opposite to that of the oscillatory drag coefficient for the absolute velocity model: $C_{Da} > C_D$. Such a result can be expected; assuming $C_{Dm} \leq C_{Da}$ (which is true for the present test series), $C_{Dr}$ should be smaller than $C_{Da}$ due to the fact that $(V+u_m)^2 > (V^2 + u_m^2)$.

Since the inertia coefficients obtained from the relative velocity model $C_{Mr}$ are identical to those obtained from the absolute velocity model, one may refer to figure 7.16 to compare $C_{Mr}$ with $C_M$.

### 7.5.3.2 Lift Force Coefficients

The lift force acts on the cylinder in a combined waves plus current field perpendicularly to the direction of the incident wave (and current).

An extensive examination of various nondimensional parameters has shown that the lift force coefficients do not correlate well with any single nondimensional parameter. However, they correlate roughly well with the total Reynolds number $Re_{wv}$. Since $Re_{wv}$ is a function of $(V+u_m)$ in the present experiment, it can be argued that the lift force coefficients depend on the total velocity. In figure 7.20, the lift force coefficients ($C_{Lmax}$ and $C_{Lrms}$) are shown as a function of the total Reynolds number $Re_{wv}$. This figure shows that $C_{Lmax}$ and $C_{Lrms}$ are large when $Re_{wv}$ is between 30 000 and 40 000. The values of $C_{Lmax}$ and $C_{Lrms}$ become smaller as $Re_{wv}$ increases.

The relation between the maximum lift force coefficient $C_{Lmax}$ and the maximum drag coefficient $C_{Dmax}$ is shown in figure 7.21. In general, the maximum drag coefficient is much larger than the maximum lift force coefficient.

The frequency of the lift force has been calculated by carrying out a spectral analysis on the data. In figure 7.22, the ratio of the frequency of the lift force $f_L$ to that of the incident wave $f_w$ is shown as a function of $KC_w$. The $f_L/f_w$ exhibits a large scatter in this figure. However, the ratio of the lift force frequency to the apparent wave frequency $f_{app}$ exhibits less scatter if plotted versus $KC_{app}$ as shown in figure 7.23. In the small $KC_{app}$ region ($KC_{app} < 15$), the ratio is 0.5 or 1 and becomes 2, 3 and even 4 as $KC_{app}$ increases. This observation suggests that the apparent frequency has to be used in the lift force computation for a fixed cylinder in a combined wave and current flow field.

## 7.6 Conclusions

The following specific conclusions can be drawn from the above results and discussions:

1. Direct analysis of the data indicates that both the steady and the oscillatory components of the measured hydrodynamic force depend on both the steady current velocity and the orbital velocity. This suggests that the combined flow kinematics has to be used in modelling the hydrodynamic forces on a fixed cylinder in a wave and current co-existing flow field. This discredits the concept of an independent flow fields approach in which the total force is a superposition of two independent forces caused by two unrelated flows, one due to the wave and one due to the current.

2. The use of Morison's equation for the combined wave and current flow field is a speculative extension of the original Morison equation which was formulated for a fixed cylinder in waves only. It has been shown with the data from the present test series that the relative velocity formulation can be applied to extend the Morison equation for a combined wave and current flow field. However, the drag and inertia coefficients for the combined flow field are significantly different from those from the waves-only test series. This implies that the extension of the Morison equation is not simply a choice of a reference system alone; a totally different set of coefficients would have to be used to reflect the effects due to the combination of the two separate flows.

3. In the light of conclusion 2, it is obvious that the engineering practice of using the coefficients for regular waves only to describe hydrodynamic forces on a combined wave and current flow field cannot be justified.

4. The hydrodynamic coefficients $C_{Dr}$ and $C_{Mr}$ (in the relative velocity model) for a cylinder in a waves plus current flow field are strongly affected by the current. These coefficients depend mainly on the velocity ratio $u_m/V$ or the reduced velocity $Vr$.

5. Overall, the drag coefficients obtained from waves plus current tests are smaller and the inertia coefficients are larger than those from wave-only tests in the rage of Keulegan-Carpenter number considered.

6. The maximum and the rms lift force coefficients ($C_{L,max}$ and $C_{L,rms}$) depend on the total velocity. They are generally smaller than the in-line force coefficients, $C_{Dmax}$ and $C_{Drms}$.

7. The frequency of the lift force depends on the nondimensional parameter $KC_{app}$. In the small $KC_{app}$ region ($KC_{app} < 15$), the ratio is 0.5 or 1 and becomes 2, 3 and even 4 as $KC_{app}$ increases.

88
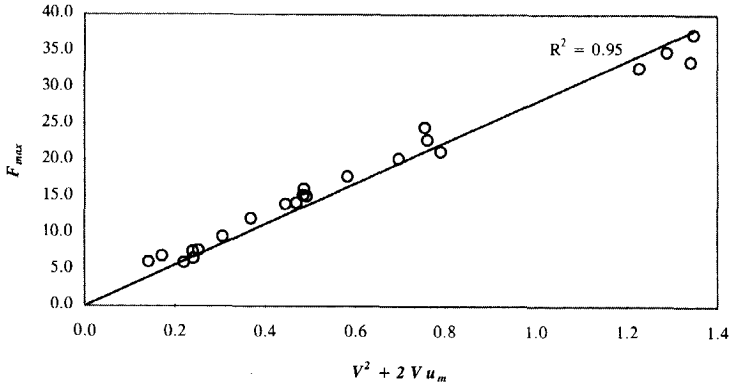
Figure 7.3 Fixed cylinder in waves plus current flow field, $F_{max}$ plotted versus $(V^2+2Vu_m)$
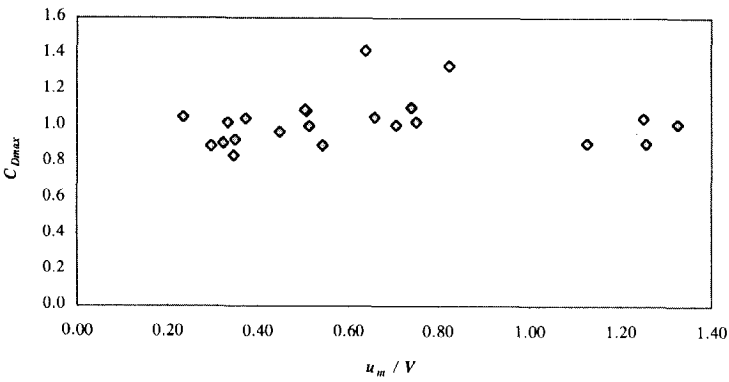


Figure 7.4 Fixed cylinder in waves plus current flow field, $C_{Dmax}$ plotted versus $u_m/V$
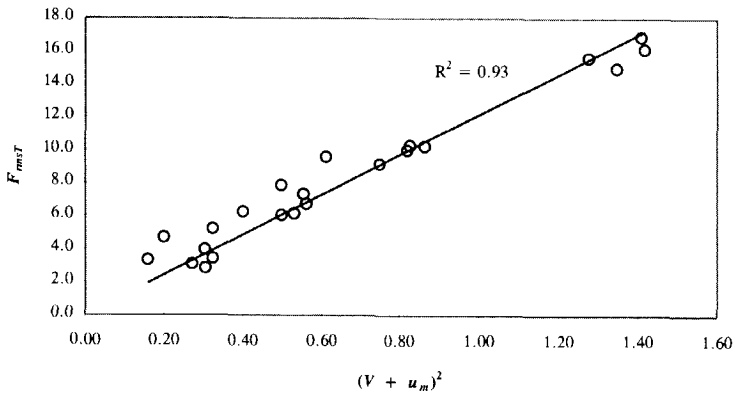


Figure 7.5 Fixed cylinder in waves plus current flow field, $F_{rmsT}$ plotted versus $(V+u_m)^2$

89
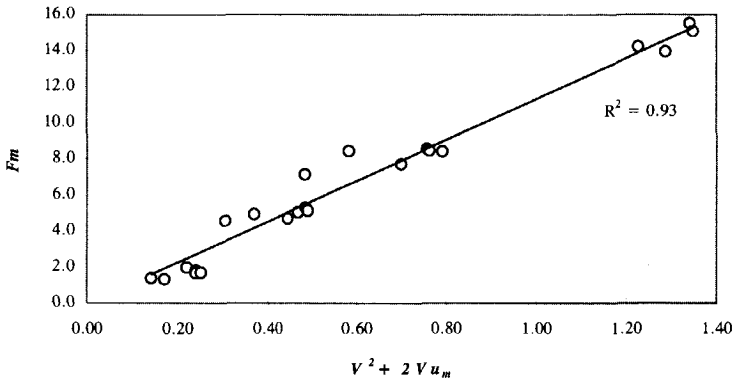
Figure 7.6 Fixed cylinder in waves plus current flow field, $Fm$ plotted versus $V^2 + 2V u_m$
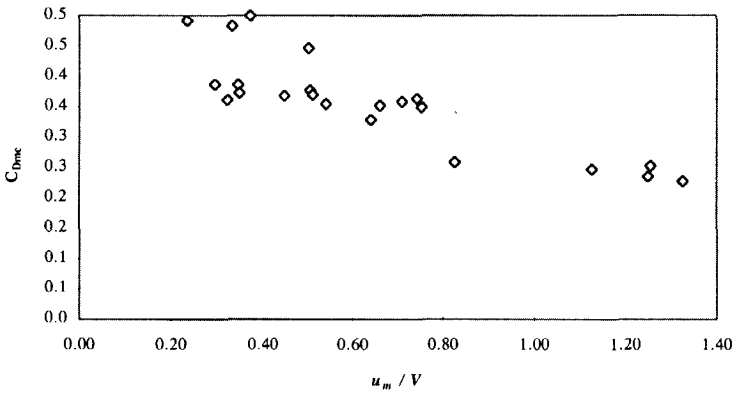


Figure 7.7 Fixed cylinder in waves plus current flow field, $C_{Dm}$ plotted versus $u_m/V$
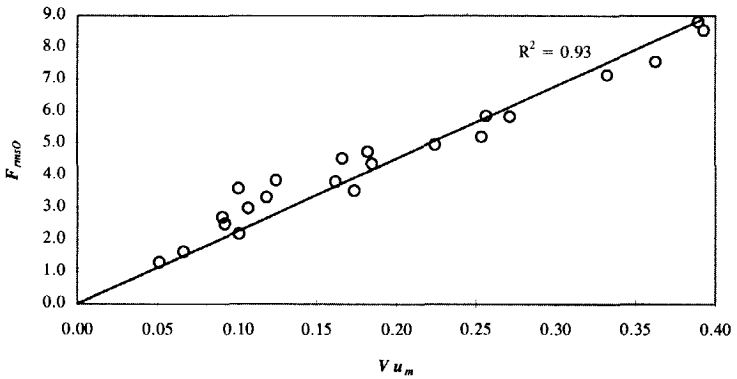


Figure 7.8 Fixed cylinder in waves plus current flow field, $F_{rms0}$ plotted versus $V.u_m$

90
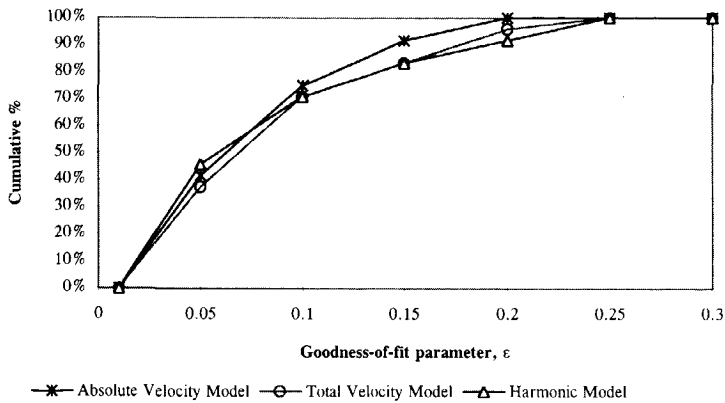
Figure 7.9 Fixed cylinder in waves plus current flow field, goodness-of-fit parameter $\varepsilon$
for three load models using best individual coefficients
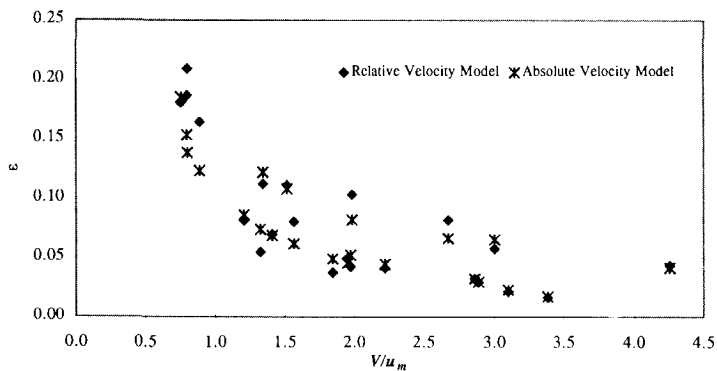


Figure 7.10 Variation of goodness-of-fit parameter $\varepsilon$ for Morison equation extensions plotted
versus $V/u_m$, (best individual coefficients used)
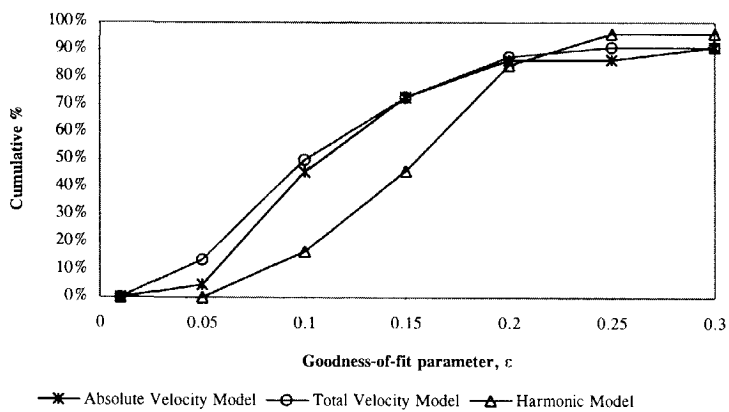


Figure 7.11 Fixed cylinder in waves plus current flow field, goodness-of-fit parameter $\varepsilon$
for three load models using smoothed coefficients

91
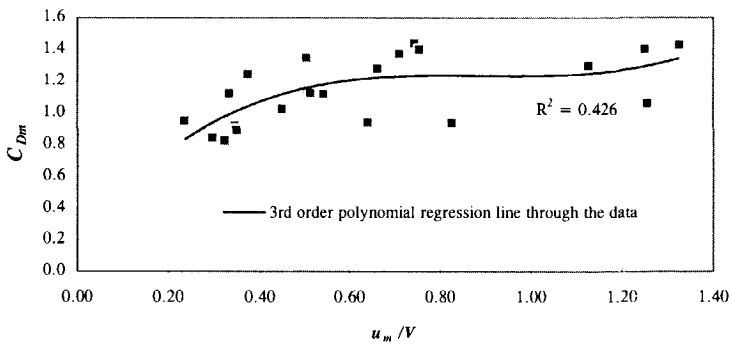
Figure 7.12 Fixed cylinder in waves plus current flow field, the mean drag coefficient $C_{Dm}$ plotted versus $u_m/V$ (absolute velocity model)
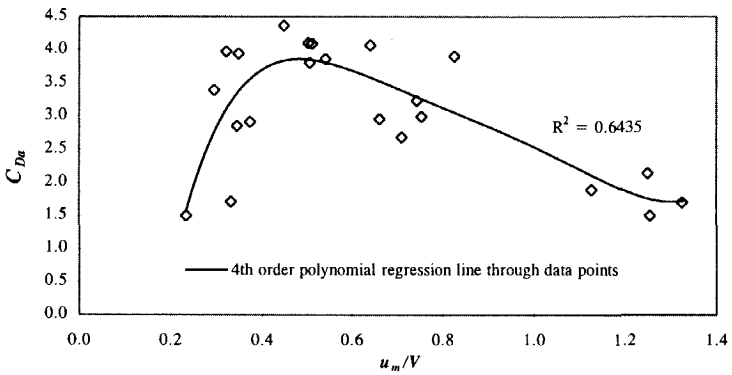


Figure 7.13 Fixed cylinder in waves and current flow field, the oscillatory drag coefficient $C_{Da}$ plotted versus $u_m/V$ (absolute velocity model)
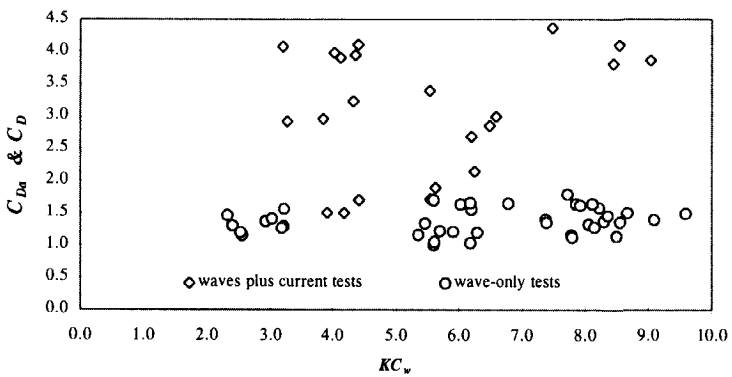


Figure 7.14 Oscillatory drag coefficient for waves plus current tests and wave-only tests plotted versus $KC_w$ (absolute velocity model)

92
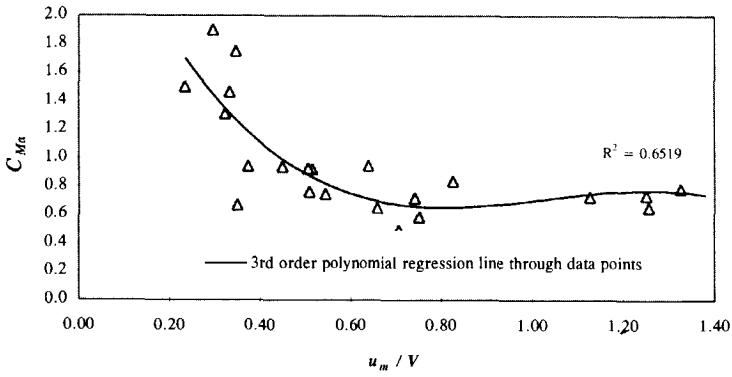
Figure 7.15 Fixed cylinder in waves plus current flow field, the inertia coefficient $C_{Ma}$ plotted versus $u_m/V$ (absolute velocity model)
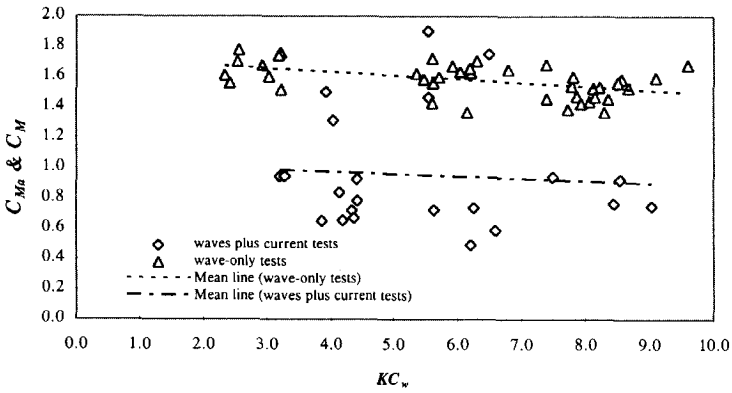


Figure 7.16 Inertia coefficient for waves plus current tests and wave-only tests plotted versus $KC_w$ (absolute velocity model)
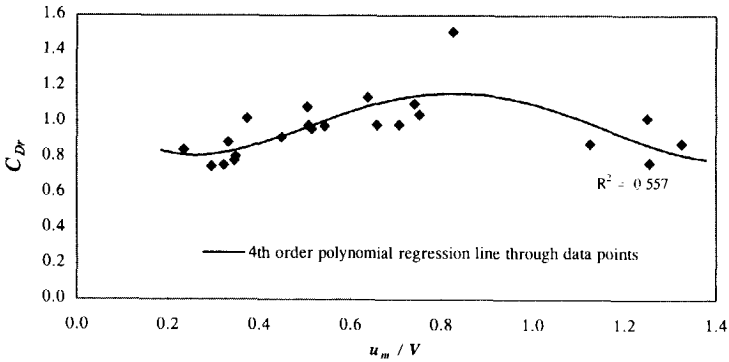


Figure 7.17 Fixed cylinder in waves plus current flow field, drag coefficient $C_{Dr}$ plotted versus $u_m/V$ (relative velocity model)

93
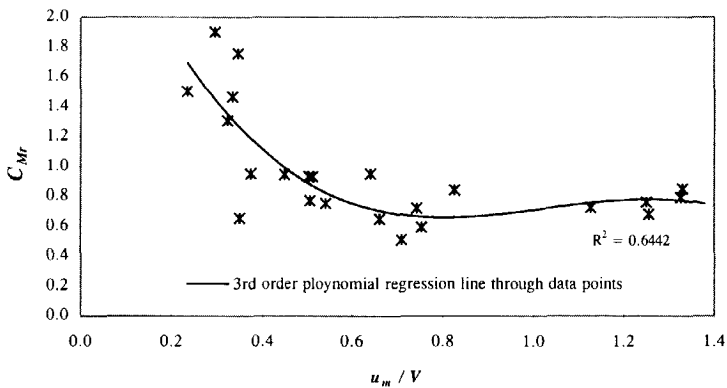
Figure 7.18  Fixed cylinder in waves plus current flow field, inertia coefficient $C_{Mr}$ plotted versus $u_m/V$ (relative velocity model)



x waves plus current tests  ◇ wave-only tests
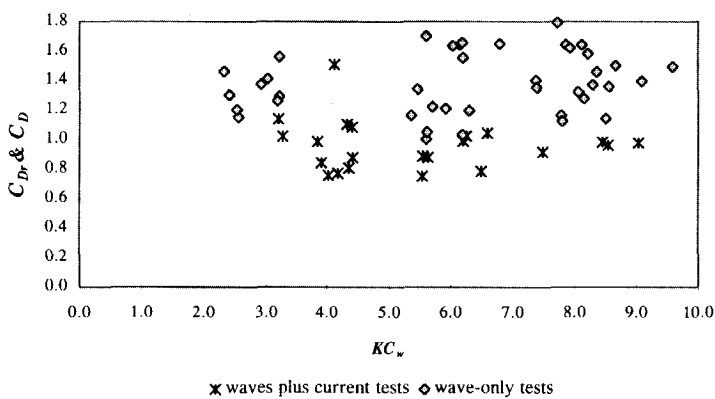
Figure 7.19  Drag coefficient for waves plus current tests and wave-only tests plotted versus $KC_w$ (relative velocity model)
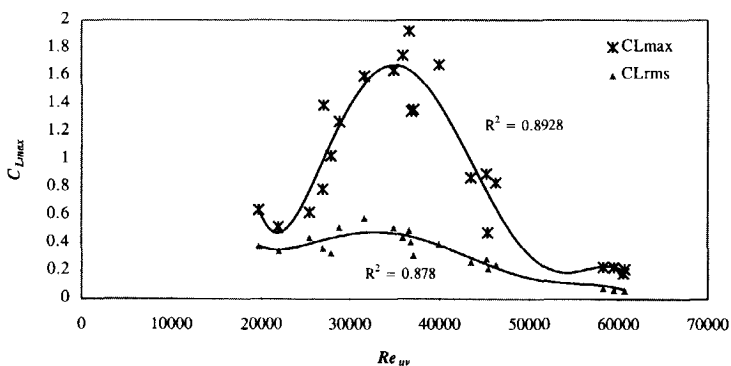


Figure 7.20  Fixed cylinder in waves plus current flow field, maximum and rms lift force coefficients  plotted versus $Re_{uv}$; lines: 3rd order regression lines through data
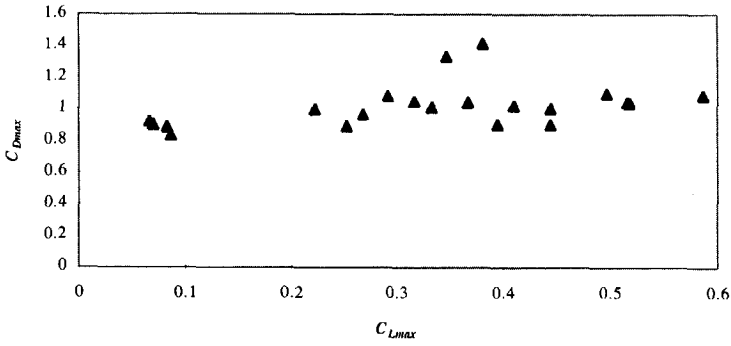
Figure 7.21   Fixed cylinder in waves plus current flow field, maximum drag force coefficient $C_{Dmax}$ plotted versus maximum lift force coefficient $C_{Lmax}$
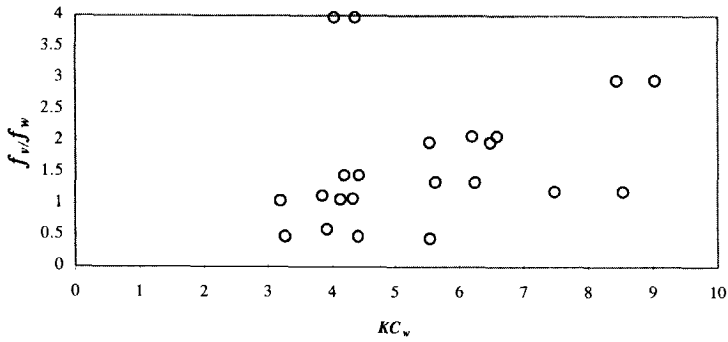


Figure 7.22   Fixed cylinder in waves plus current flow field, the ratio of the lift force frequency $f_v$ to the incident wave frequency $f_w$ plotted versus $KC_w$
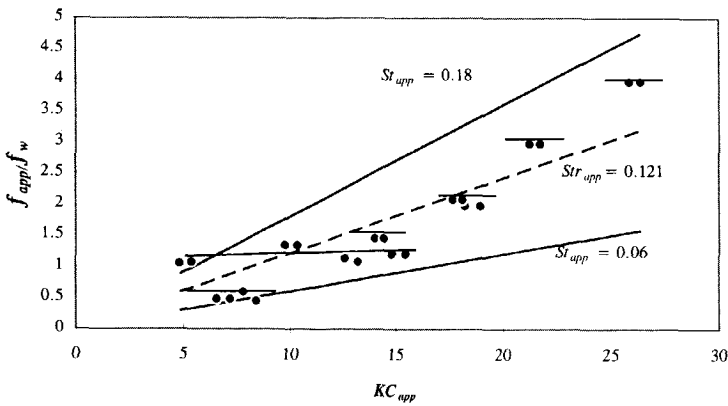


Figure 7.23   Fixed cylinder in waves plus current flow field, the ratio of the lift force frequency $f_v$ to the apparent wave frequency $f_{app}$ plotted versus $KC_{app}$

# CHAPTER 8

# In-line Cylinder Oscillation in Waves

## 8.1 General

This chapter presents the results and discussion of the experiments with the in-line cylinder oscillations in waves. Comparing with the earlier test cases, two acceleration terms are involved in the present test series making it more complicated.

Accurate prediction of wave loads and responses of slender offshore structures are very important for the design and operation of these structures in a natural environment. The present results have practical application when considering the wave forces acting on a flexible cylinder such as a riser and also when structural vibrations occur on a fixed platform.

For the flexible cylinders, the motion is fairly large and proportional with the incident fluid particle motions, while for the vibratory motion of a fixed platform the structure's motion is much smaller than that of the surrounding fluid. Furthermore, for the vibratory case, the motion occurs at a higher frequency than the wave motion, while for flexible cylinders both motions generally include the same frequency band.

Beside the two above cases, the results of this test series may shed some light on the understanding of the motion of a floating structure in waves. Both the water particles and the structure are moving and the wave force and the hydrodynamic damping are very important for calculating the motion, especially near the resonant frequencies.

The major reason for undertaking the experiments described in this chapter was the desire to investigate the validity of existing mathematical models for hydrodynamic interaction of an oscillating cylinder in waves as well as to provide appropriate force coefficients values for the best mathematical model. The latter objective would contribute to accurate hydrodynamic force evaluations on oscillating cylinders and to specifying the damping of vibrations of slender offshore structures.

## 8.2 Specific Details of the Experiments

The present test series is a two-mode test in which there are two simultaneous accelerated motions. Specific phenomena and test conditions for this test case are briefly discussed in the following sections. All motions - of the water or of the cylinder - are considered to be sinusoidal in this discussion.

### 8.2.1 Structure-Waves Interaction

When the structural motion is not negligible, fluid-structure interaction needs to be considered. Several investigators have attempted to take into account the effect of structural flexibility in force evaluation by modifying the original Morison equation to include interactive terms that involve both the fluid and the structural velocities and accelerations. In this process it is usually assumed that the interaction between the ambient fluid flow and the flow around the cylinder resulting from the structural motion is linear, i.e. the resulting flow field kinematics are equal to the algebraic difference between the kinematics of the incident fluid flow and the resulting kinematics of the structure, both measured relative to a fixed axis system. However, as discussed by Vugts (1979) and Chakrabarti (1987) among others, the validity of this assumption, which determines the level of hydrodynamic drag damping, is questionable; it is still rather arbitrary and should be interpreted as an entirely new empirical formula that needs separate verification.

### 8.2.2 Dynamic Analysis

The results of the present test series may be used in the dynamic analysis of slender offshore structures by accounting for the hydrodynamic damping as well as the exciting forces. Giving a brief description of the present methods used to account for damping in the dynamic analysis of such structures would therefore seem appropriate here.

In the design of slender offshore structures, particularly in deep waters, dynamic response of the entire structure to waves, currents and wave and/or current-induced vortex forces must be considered. A dynamic analysis is particularly important for waves of moderate sea states since these frequently occurring sea states may make the greatest contribution to fatigue damage. When the sea state dominant frequency coincides with the structure natural frequency, the magnification due to dynamic response will be greatest and will depend on the damping of the system.

Dynamic analysis turns out to be complex because of the interactions of the sea, structure and the foundation. Damping becomes more important when offshore structures are designed and installed in deeper water because the natural frequencies of the structure approach the wave frequencies.

The first essential step in a dynamic analysis is the formulation of an appropriate mathematical model representing the structure by suitably defined mass, damping, and stiffness matrices together with a mathematical model for the hydrodynamic excitation - usually a modified form of Morison equation.

The equation of motion for a cylinder in-line with the direction of wave propagation may in general be written as:

$$m\ddot{x} + c\dot{x} + kx = F(t) \tag{8.1}$$

where $m$, $c$ and $k$ are the mass, structural damping and stiffness.

The hydrodynamic damping in most investigations is derived from the modified Morison

98

equation using the relative velocity formulation (equation 3.5).

$$m\ddot{x} + c\dot{x} + kx = C_{Dr}(\frac{1}{2}\rho D)|u - \dot{x}|(u - \dot{x}) + C_{Mr}(\rho\frac{\pi}{4}D^2)\dot{u} - C_{Ar}(\rho\frac{\pi}{4}D^2)\ddot{x} \qquad (8.2)$$

There are three approaches to solve this equation of motion:

1. Direct numerical solutions obtained by time-history integration (time domain simulation)
2. Linearisation of the equation to make possible a frequency domain solution
3. Static solutions obtained by neglecting the structural motion terms $\dot{x}$ and $\ddot{x}$

Examination and discussion of these solutions is beyond the present work. However, a linearised form the equation is briefly examined here to see the effect of structural motion on the dynamic analysis of slender offshore structures. Other extended forms of the Morison equation are discussed in section 8.3.2.

If $u_m \gg \dot{x}_m$, as is usually the case for fixed structures, the drag term may be approximated as:

$$\frac{1}{2}\rho D C_{Dr}(u - \dot{x})|u - \dot{x}| = \frac{1}{2}\rho D C_{Dr}[u|u| - 2|u|\dot{x}] \qquad (8.3)$$

Applying this approximation to equation 8.2 under the assumption that $u_m \gg \dot{x}_m$, collecting $\dot{x}$ and $\ddot{x}$ on the left-hand side and introducing the added mass per unit length $m_a = 0.25\rho\pi D^2 C_{Ar}$, one may write:

$$(m + m_a) + (c + \rho D C_{Dr}|u|)\dot{x} + kx = 0.5\rho DC_{Dr}u|u| + 0.25\rho\pi D^2 C_{Mr}\dot{u} \qquad (8.4)$$

The right-hand side of equation (8.4) is identical to the original Morison equation and thus the effect of introducing a relative term into Morison equation has been to introduce the added mass and the hydrodynamic damping on the left in equation 8.4. The hydrodynamic damping coefficient then is $\rho D C_{Dr}|u|$. A constant damping coefficient could be obtained by using the average value of $\bar{u} = 2u_m/\pi$, (if $u(t)$ is sinusoidal).

It should be noted that even if the $2|u|\dot{x}$ term in equation (8.3) is extremely small compared to the $u|u|$ term (that is $u_m \gg \dot{x}$), it is still very important for responses near resonance as it is a damping term, and at resonance damping provides the sole limitation to the response.

Linearising the nonlinear drag force and the use of the above form of Morison equation is a common practice. Although this procedure may not violate the basic principles, uncertainty stems partly from the linearisation and partly from the use of force coefficients derived from conditions in which the behaviour of the cylinder is (quasi-) static rather than dynamic. The force coefficients under static conditions are not the same as under dynamic conditions. The force coefficients depend generally on the velocity ratio $u_m/\dot{x}$ in addition to other nondimensional parameters. Existing analyses do not consider this, primarily because of lack of reliable data. This procedure can lead to high damping values if the drag coefficient value for static conditions ($C_D$) is used.

### 8.2.3 Important Parameters

Since the present test series can be seen as a combination of two already considered degenerate test cases of "fixed cylinder in waves" and "oscillating cylinder in still water," all nondimensional parameters for these cases are relevant here too. Due to the fact that the two motions occur simultaneously in the present test series, considering any combination of parameter sets of those two motions is also essential. Thus, beside those parameters for single mode tests, the following additional nondimensional parameters have been studied:

a) in terms of total maximum velocity, $\dot{x}_m + u_m$, as:

$$KC_T = \frac{(\dot{x}_m + u_m)T}{D}, \qquad Re_T = \frac{(\dot{x}_m + u_m)D}{\nu} \qquad (8.5)$$

The period $T$ here could be either the wave period, $T_w$, or the cylinder oscillation period, $T_o$.

b) in terms of the maximum relative velocity, $(\dot{x} - u)_{max}$, as:

$$KC_r = \frac{(u - \dot{x})_{max}T_r}{D}, \qquad Re_r = \frac{(u - \dot{x})_{max}D}{\nu} \qquad (8.6)$$

The relative velocity between two motions $(\dot{x} - u)$ is usually composed of two sinusoidal signals, thus it is also a periodic function. A solution to determine the period of the relative motion $T_r$ is presented in appendix IV.

c) The sum of Keulegan-Carpenter numbers for degenerate cases, i.e.:

$$KC_{ow} = KC_o + KC_w = \frac{\dot{x}_m T_o + u_m T_w}{D} \qquad (8.7)$$

### 8.2.4 Tests Conducted and Data Range

The variable values for this combined test series were chosen the same as those for the single mode tests of "a fixed cylinder in waves" and "cylinder oscillation in still water." This has allowed direct comparison of the present test series with results of those degenerate tests. Various load models can further be checked.

There are five independent variables in this test series:

- Cylinder motion amplitude and period, $A$ and $T_o$
- Wave height and period, $H$, $T_w$
- Phase differences between the two motions

Setting the first four variables for each test run was possible, while the phase difference between the two motions was a random variable. Thus, the phase difference in each test run is not predetermined because the starter button of the measurement was pushed manually. However, in order to study the effect of the phase difference, a number of test runs were carried out in which the first four variables were constant but the phase difference had distinct (random) values.

100

The influence of the phase difference on the in-line force is undeniably significant. To be convinced, one should consider for instance a situation with u and $\dot{x}$ having the same amplitude and same frequency. A phase difference of $180°$ can obviously lead to a relative velocity equal to zero. In such a fictitious case, the water particle would in a horizontal direction seem to be standing still relative to the cylinder; the cylinder would not experience any drag force. Ranges of some relevant nondimensional parameters are given in table 8.1.

It is expected that the inertia coefficient should depend on a nondimensional parameter proportional to an acceleration term. Thus, several possibilities may be tried leading to a suitable parameter. One may express the maximum acceleration terms, $\dot{u}_m$ and $\ddot{x}_m$, by relating them to the associated velocities as:

$$\dot{u}_m = \frac{2\pi}{T_w} u_m \quad \text{and} \quad \ddot{x}_m = \frac{2\pi}{T_o} \dot{x}_m \tag{8.8}$$

Two approaches can lead to nondimensional forms of these accelerations. On the one hand, multiplying the acceleration by a length and then dividing it by the square of a velocity is possible. On the other hand, one could divide the acceleration by a length and multiply it by a time squared. A partial list of the possible dimensionless parameters based on the above approaches is given in table 8.2.

| Parameter | Definition | Range |
|---|---|---|
| Amplitude:Diameter Ratio | $A/D$ | 0.5 - 4.0 |
| Max. Oscillatory Velocity | $\dot{x}_m = 2A\pi f_o$ | 0.09 - 0.75 m/s |
| Reynolds Number based on cylinder oscillation | $Re_o = \dot{x} D/\nu$ | 5 650 - 45 260 |
| Reynolds Number based on wave oscillatory flow | $Re_w = u_m D/\nu$ | 8 360 - 16 720 |
| Reynolds Number based on total flow | $Re_{nw} = (u_m + \dot{x}_m)D/\nu$ | 14 100 - 60 020 |
| Reynolds Number based on relative velocity | $Re_r = (u - \dot{x})_{max} D/\nu$ | 4 870 - 59 840 |
| Keulegan-Carpenter number wave flow | $KC_w = u_m T_w /D$ | 2.3 - 9.3 |
| Keulegan-Carpenter number, cylinder oscillation | $KC_o = \dot{x}_m T_o /D$ | 3.1 - 25.1 |
| Keulegan-Carpenter number, total flow | $KC_T = (u_m + \dot{x}_m)T_o /D$ | 4.4 - 33.3 |
| Sum Keulegan-Carpenter numbers | $KC_S = (u_m T_w + \dot{x}_m T_o) /D$ | 5.4 - 58.4 |
| Keulegan-Carpenter number, relative velocity | $KC_r = (u - \dot{x})_{max} T_r /D$ | 3.4 - 97.1 |
| Velocity parameter | $u_m / \dot{x}_m$ | 0.26 - 2.6 |

Table 8.1 Experimental Variable Ranges for the In-line Oscillation in Waves

| Parameter | $K_1$ | $K_2$ | $K_3$ | $K_4 = K_{ac}$ | $K_5$ | $K_6$ | $K_-$ |
|---|---|---|---|---|---|---|---|
| Definition | $\ddot{x}_m D/u_m^2$ | $\dot{u}_m D/\dot{x}_m^2$ | $\ddot{x}_m T_w^2/D$ | $\dot{u}_m T_o^2/D$ | $\ddot{x}_m D/(u+\dot{x}_m)^2$ | $\dot{u}_m D/(u_m+\dot{x}_m)^2$ | $(\dot{u}_m+\ddot{x}_m)T_r^2/D$ |

Table 8.2 Nondimensional Parameter Proportional to Acceleration Terms of the Flows

## 8.3  Load Models

### 8.3.1  Morison Equation Generalisation

When a cylinder is moving in waves, the force and the motion are dependent upon the water particle kinematics as well as the velocity and acceleration of the structure itself. In this case several alternate forms of the modified Morison equation are used. As stated in section 3.2, however, two extensions based on the concepts of the "independent flow fields" and the "relative flow field" are well-known and are considered here. One of the objectives of the present test series is to verify these forms.

The basic assumption of the independent flow fields approach is that the force acting in an oscillating cylinder is the sum of the forces that would act on a fixed cylinder, which are the "far field" effects, plus the fluid forces that the cylinder would experience if it were oscillating in still water, which are the "near field" effects. A load model based on this approach is referred to as the "absolute velocity" model and is written as:

$$F = \frac{1}{2}\rho D C_{Dw}|u|u + \frac{\pi D^2}{4}\rho C_{Mw}\dot{u} - \frac{1}{2}\rho D C_{Do}|\dot{x}|\dot{x} - \frac{\pi D^2}{4}\rho C_{Ao}\ddot{x} \qquad (8.9)$$

The values of $C_{Dw}$ and $C_{Mw}$ used in this equation should be taken from the data for a fixed cylinder in the same flow. Also, $C_{Do}$ and $C_{Ao}$ should be taken from data corresponding to a cylinder oscillating in the still water at the amplitude of cylinder motion. Note that here $C_{Mw}$ is not equal to $C_{Ao}+1$ as they are related to two different flows.

However, the force coefficients in equation 8.9 may be calculated directly from the measured data by applying the least squares method. The coefficients obtained are not necessarily identical to those for the degenerate cases.

Alternatively, the drag force can be assumed to depend on the relative velocity between the fluid and the body, resulting in an in-line fluid force given by:

$$F = \frac{1}{2}\rho D C_{Dr}|u-\dot{x}|(u-\dot{x}) + \frac{\pi D^2}{4}\rho C_{Mr}\dot{u} - \frac{\pi D^2}{4}\rho(C_{Mr}-1)\ddot{x} \qquad (8.10)$$

The value of the force coefficients $C_{Dr}$ and $C_{Mr}$ should be based on the amplitude of the relative motion rather than on the fluid or structural motions alone. Thus, these coefficients may not necessarily be equal to the stationary values. However, because of the lack of data in this area, the hydrodynamic coefficients for the analysis of moving structures in waves are normally chosen from studies on a fixed cylinder in waves or from an oscillating cylinder in still water.

### 8.3.2  Linearised Forms

Linear analysis is highly desirable in the study of the structural dynamics of offshore structures,

102

if possible. Unfortunately, the force as expressed by extended forms of the Morison equation is nonlinear with respect to the drag term. However, various techniques have been proposed to linearise the drag term; the nonlinear terms are then expanded in a power series or in a Fourier series.

The linearisation of the absolute velocity model is rather easy because each drag term may be linearised separately similar to the linearisation for the single mode test cases, see in sections 5.2.1 and 5.3.1. This will lead to the following linear form of the absolute velocity model:

$$F = \frac{1}{2}\rho D C_{Dwl}\frac{8}{3\pi}u_m u + \frac{\pi D^2}{4}C_{Mwl}\dot{u} - \frac{1}{2}\rho D C_{Dol}\frac{8}{3\pi}\dot{x}_m \dot{x} - \frac{\pi D^2}{4}C_{Aol}\ddot{x}$$ (8.11)

For the relative velocity model, if the wave velocity is much larger than the structural velocity, as is often the case ($u \gg \dot{x}$), then the nonlinear terms of the relative velocity model can be approximated as equation 8.3. Applying that approximation to the relative velocity gives:

$$F = \frac{1}{2}\rho D C_{Drl}[u|u| - 2|u|\dot{x}] + \frac{\pi D^2}{4}\rho C_{Mr}\dot{u} - \frac{\pi D^2}{4}\rho(C_{Mr}-1)\ddot{x}$$ (8.12)

Besides above technique for linearisation of the drag term (in a relative velocity approach), various other linearisation techniques have been discussed in the literature; see for example Blevins (1990), Leira (1987), Langley (1984), Gudmestad and Connor (1983), Malhotra and Penzien (1970).

A linear form of the relative velocity may be obtained by linearising the drag term directly using the same procedure as for degenerate cases:

$$F = \frac{1}{2}\rho D C_{Drl}\frac{8}{3\pi}(u-\dot{x})_{max}(u-\dot{x}) + \frac{\pi D^2}{4}\rho C_{Mrl}\dot{u} - \frac{\pi D^2}{4}\rho(C_{Mrl}-1)\ddot{x}$$ (8.13)

This linear solution does not require the assumption of $u \gg \dot{x}$. However, the maximum of the relative velocity is unknown and should be calculated using an iterative solution.

Also, another postulated linear form of the relative velocity model has been considered in the present work. It can be expressed as:

$$F = \frac{1}{2}\rho D C_{Drs}(u_m + \dot{x}_m)(u-\dot{x}) + \frac{\pi D^2}{4}\rho C_{Mrs}\dot{u} - \frac{\pi D^2}{4}\rho(C_{Mrs}-1)\ddot{x}$$ (8.14)

This is a linear model which requires only easily determined coefficient values.

### 8.3.3 Summary of the Tested Models

Table 8.3 summarizes five different load models evaluated within the present work.

### 8.3.4 Lift Force

Evaluation of the lift force is very complicated for the test series under consideration in which two motions are involved. Lift force models are not discussed here and just as with other test series, only the maximum and the RMS lift force coefficients are evaluated. However, for each coefficient two different definitions may be introduced:

$$C_{LmaxT} = \frac{Fy_{max}}{0.5\rho D(u_m + \dot{x}_m)^2} \tag{8.15}$$

$$C_{LmaxR} = \frac{Fy_{max}}{0.5\rho D(u - \dot{x})^2_{max}} \tag{8.16}$$

$$C_{LrmsT} = \frac{Fy_{rms}}{0.5\rho D(u_m + \dot{x}_m)^2} \tag{8.17}$$

$$C_{LrmsR} = \frac{Fy_{rms}}{0.5\rho D(u - \dot{x})^2_{max}} \tag{8.18}$$

| No | Name | Equation |
|----|------|----------|
| I | Relative velocity | $F = \frac{1}{2}\rho D C_{Dr}|u-\dot{x}|(u-\dot{x}) + \frac{\pi D^2}{4}\rho C_{Mr}\dot{u} - \frac{\pi D^2}{4}\rho(C_{Mr}-1)\ddot{x}$ |
| II | Absolute velocity | $F = \frac{1}{2}\rho D C_{Dw}|u|u + \frac{\pi D^2}{4}\rho C_{Mw}\dot{u} - \frac{1}{2}\rho D C_{Do}|\dot{x}|\dot{x} - \frac{\pi D^2}{4}\rho C_{Ao}\ddot{x}$ |
| III | Linearised relative velocity | $F = \frac{1}{2}\rho D C_{Drl}\frac{8}{3\pi}(u-\dot{x})_{max}(u-\dot{x}) + \frac{\pi D^2}{4}\rho C_{Mrl}\dot{u} - \frac{\pi D^2}{4}\rho(C_{Mrl}-1)\ddot{x}$ |
| IV | Linearised absolute velocity | $F = \frac{1}{2}\rho D C_{Dwl}\frac{8}{3\pi}u_m u + \frac{\pi D^2}{4}C_{Mwl}\dot{u} - \frac{1}{2}\rho D C_{Dol}\frac{8}{3\pi}\dot{x}_m \dot{x} - \frac{\pi D^2}{4}C_{Aol}\ddot{x}$ |
| V | Postulated linear relative velocity | $F = \frac{1}{2}\rho D C_{Drs}(u_m + \dot{x}_m)(u-\dot{x}) + \frac{\pi D^2}{4}\rho C_{Mrs}\dot{u} - \frac{\pi D^2}{4}\rho(C_{Mrs}-1)\ddot{x}$ |

Table 8.3  Modified Morison Equation Forms Evaluated

## 8.4  Results and Discussion

### 8.4.1  Direct Observations from the Data

The statistical values of the force signals were used to find any linear relationship between these values and the flow kinematics. Various combinations of $u_m^2$ and $\dot{x}_m^2$ as well as $(u-\dot{x})_{max}^2$ were tried. The results of this evaluation have revealed that the relative velocity term $(u-\dot{x})$ is a better variable for estimating the hydrodynamic forces. It was found that $F_{max}$ and $F_{rms}$ can best be related to $(u-\dot{x})_{max}^2$ for all test runs with different values of oscillation frequency, oscillation amplitude and different waves as shown in figures 8.1 and 8.2, see also table 8.4.

| | $\dot{x}_m^2$ | $u_m^2$ | $\dot{x}_m u_m$ | $(\dot{x}_m + u_m)^2$ | $\dot{x}_m^2 + u_m^2$ | $\dot{x}_m^2 + 2\dot{x}_m u_m$ | $(u-\dot{x})_{max}^2$ |
|---|---|---|---|---|---|---|---|
| $F_{max}$ | 0.47 | 0.36 | 0.75 | 0.74 | 0.65 | 0.68 | 0.82 |
| $F_{rms}$ | 0.40 | 0.31 | 0.69 | 0.70 | 0.60 | 0.63 | 0.72 |

Table 8.4  $R^2$ Correlation Coefficient Values for Linear Regression of Characteristic Forces to Different Velocity Components

The importance of the velocity ratio can be seen in figures 8.3 and 8.4 where $F_{max}$ and $F_{rms}$ are plotted versus $u_m/(u-\dot{x})_{max}$. These results show that even a small velocity change in one motion may result in a significant change in the hydrodynamic forces.

Using results for the single mode tests of wave-only and oscillation-only (the same waves and the same cylinder oscillations were used), it is possible to compare the sum of the maximum measured forces for those tests, with the maximum measured force for the combined test series. In figure 8.5, $F_{maxA}$ is plotted versus $F_{max}$ where:

$F_{maxA}$ = Maximum measured force for wave-only tests + Maximum measured force for oscillation-only tests.

This figure shows that the maximum in-line force values for the oscillating cylinder in waves are not equal to the calculated maximum in-line force values based on the independent flow field approach. $F_{max}$ is generally greater than $F_{maxA}$.

The variation of the maximum transverse force $Fy_{max}$ with various nondimensional parameters is almost similar to that of the maximum in-line force. For example $Fy_{max}$ exhibits a good correlation if plotted versus $(u-\dot{x})_{max}^2$ as shown in figure 8.6. The dependency of $Fy_{max}$ on the velocity ratio of $u_m/(u-\dot{x})_{max}$ can be seen in figure 8.7; $Fy_{max}$ decreases as this ratio increases.

### 8.4.2 Phase Difference Effect

As discussed earlier in section 8.2.4 the phase difference $\Delta\Phi$ between two motions may have a great effect on hydrodynamic interaction forces. To take into account the effect of $\Delta\Phi$ during the experiments, the cylinder motion and the waves were kept constant for 15 test runs. The phase difference for these runs varies from - 180° to +180°. To present the results in a more convenient way, $F_{max}$ has been plotted versus $\cos(\Delta\Phi)$ in fig 8.8. This figure shows how strongly the phase differences may affect the hydrodynamic force.

The phase difference has an even stronger effect on the maximum transverse force $Fy_{max}$ as shown in figure 8.9. The possible variation around the mean value is ±80%.

### 8.4.3 Suitability of the Load Models

### 8.4.3.1 Criteria

Appropriate coefficients have been determined for each load model, by minimizing the goodness-of-fit parameters $\epsilon$ (equation 3.21). However, the minimised values of $\epsilon$ are different for each load model. Just as for the previous test cases, statistics of $\epsilon$ values have been used to evaluate the load models.

105

As discussed before, this criterion is not sufficient to ascertain the suitability of a model. A load model used in a design process must be stable and have easily determined coefficients. Therefore, the following additional criteria have been successively considered to evaluate the suitability of the five models given in table 8.3:

- The goodness-of-fit parameter obtained with best individual coefficients
- Scattering in the force coefficients
- The goodness-of-fit parameter obtained with smoothed coefficients

The work and results corresponding to these three criteria are summarised in the following paragraphs.

### 8.4.3.2 Quality of Fit Using Best Individual Coefficients

Using the input-output data pairs of each of the 66 test runs, each load model results in an $\epsilon$ value. Table 8.5 lists the calculated mean and standard deviation values for the $\epsilon$ distributions using the five models given. The fourth column in this table shows the percentage of runs for which $\epsilon < 0.20$ for each computational model.

The cumulative percentage of $\epsilon$ for each load model is plotted in figure 8.10. High curve values indicate that relatively more of the test runs fitted the chosen model well.

Note that the results of model V are not plotted on figure 8.10 because it gives similar results to model III. Indeed, for a given run, the expression of the force is almost the same. The only difference is the coefficient used in the drag term.

All four remaining models seem to be of about equal quality; the four curves are too close to assert that one model is better than another.

| Load Models | Fit quality $\epsilon$ value | | Percentage of runs with: |
|---|---|---|---|
| | Mean | STD | $\epsilon < 0.2$ |
| I. Relative Velocity | 0.123 | 0.049 | 96.9% |
| II. Absolute Velocity | 0.119 | 0.060 | 93.9% |
| III. Linearised Relative Velocity | 0.113 | 0.048 | 95.4% |
| IV. Linearised Absolute Velocity | 0.108 | 0.044 | 96.9% |
| V. Postulated Linear Relative Velocity | 0.113 | 0.048 | 95.4% |

Table 8.5 Summary of Model Fitting Results with Best Individual Coefficients

### 8.4.3.3 Coefficient Stability

Though most of these models (with appropriate coefficients) could reproduce the measured hydrodynamic force, the scattering in the obtained coefficients is greater for some computational models than for others.

106

The force coefficients for model I, III and V (all based on the relative velocity approach) show a similar tendency if they are plotted versus an appropriate nondimensional parameter such as $KC_r$. Also, the force coefficients for model II and IV (based on the absolute velocity approach) show corresponding behaviour. Thus, studying only the coefficient scattering in models I and II, the relative velocity and the absolute velocity forms, respectively, is adequate.

The coefficients for model I and II will be presented and discussed in section 8.4.4. Considering those results, one can notice greater coefficient scattering for the absolute velocity model.

### 8.4.3.4 Quality of Fit Using Smoothed Coefficients

The results shown in figure 8.10 and table 8.5 were obtained by using the best coefficients separately calculated for each individual test run. In a design process, the main environmental conditions are known and the required coefficients for Morison equation must be determined consistent with those conditions. Using each model with a smoothed coefficient value to predict the hydrodynamic forces is then much more realistic. Therefore, the individually obtained coefficients were smoothed and used to determine new $\epsilon$ values. This third criterion is, in turn, an alternate approach to quantifying the second one discussed in section 8.4.3.1.

This evaluation has been carried out for the five given models; the best individual coefficients obtained for the previous stage have been plotted against the relevant Keulegan-Carpenter numbers ($KC_o$, $KC_w$ and $KC_{ow}$). Then, for each $KC$ value, the smoothed coefficients were determined. The $\epsilon$ values resulting from the use of those smoothed coefficients have been calculated for each run. Figure 8.11 shows the end results of this work with smoothed coefficients plotted in the same way as figure 8.10. Table 8.6 lists the percentage of runs for which $\epsilon < 0.20$.

| Load Models | Fit quality $\epsilon$ value | | Percentage of runs with: |
|---|---|---|---|
| | Mean | STD | $\epsilon < 0.2$ |
| I.   Relative Velocity | 0.166 | 0.091 | 75.7% |
| II.  Absolute Velocity | 0.248 | 0.307 | 66.6% |
| III. Linearised Relative Velocity | 0.167 | 0.103 | 78.8% |
| IV. Linearised Absolute Velocity | 0.28 | 0.180 | 51.5% |
| V.  Postulated Linear Relative Velocity | 0.173 | 0.117 | 75.7% |

Table 8.6  Summary of Model Fitting Results with Smoothed Coefficients

The results shown in table 8.5 reveal that Model II and IV provide higher $\epsilon$ mean values (more than 0.24) whereas model I, III and V give lower values ($\approx 0.17$). Taking the information in this table and figure 8.11 together, it is obvious that models based on the relative velocity approach give a better quality of fit; the linearised form of the absolute velocity model (model IV) is not an adequate model.

*Further Evaluation of the Absolute Velocity Approach*:
As already mentioned, the absolute velocity form of Morison equation is based on an assumption

that the flow consists of a superposition of two independent flow fields: a far field due to waves and relatively unaffected by the structure motion and a near field resulting from the structure's motion. This theoretical split of the flow field comes down to assuming that $C_{Dw}$ and $C_{Mw}$ correspond to a situation with a fixed cylinder in waves, i.e. $C_D$ and $C_M$ whereas $C_{Do}$ and $C_{ao}$ correspond to an oscillating cylinder in still water. The validation of this assumption has been studied by using degenerate coefficients for these cases in the absolute velocity model.

There are two possibilities to determine the coefficients for those two independent situations: First, the literature provides many results, both for an oscillating cylinder in still water and for a fixed cylinder in waves. However, using the results obtained for the present single mode cases would be more consistent because they utilise the same experimental apparatus.

Figure 8.12 shows the cumulative percentage of $\epsilon$ for the absolute velocity model when degenerate case coefficients are used. The results of previous evaluations (using the best individual coefficients and smoothed coefficients) are also included in this figure. Table 8.7 summarises the results.

Considering all these results, it is obvious that the fit obtained by using the absolute approach with degenerate coefficients is quite bad. This tends to refute the original and basic assumption of the absolute approach. The force due to the total flow field cannot be considered as the superposition of force for two independent flow fields; on the contrary, it contains complex interactions.

| Coefficient Sets Used | Fit quality $\epsilon$ value | | Percentage of runs with: |
|---|---|---|---|
| | Mean | STD | $\epsilon < 0.2$ |
| Best Individual | 0.119 | 0.060 | 93.9% |
| Smoothed | 0.248 | 0.307 | 66.6% |
| Degenerate | 0.279 | 0.159 | 42.4% |

Table 8.7   Summary of Model Fitting Results for the Independent Flow Fields Approach with Various Sources of Coefficients

### 8.4.4 In-line Force Coefficients

The quality of fit of various load models has revealed that each model may produce the hydrodynamic forces if appropriate coefficients are used. The feature and interpretation of force coefficients for the given load models are discussed in the following paragraphs.

### 8.4.4.1 Relative Velocity Model (model I)

Many evaluations were carried out to investigate if a good correlation could be found between the drag and inertia coefficients and the relevant nondimensional parameters.

*Drag coefficient, $C_{Dr}$*
The drag coefficient for the relative velocity model ($C_{Dr}$) should not depend on the phase difference because this influence is clearly reflected in the relative velocity term ($u - \dot{x}$). Initially,

a relation between $C_{Dr}$ and $KC_o$ or $KC_w$ was sought, but no obvious correlation was discovered. However, as shown in figure 8.13, a better result was obtained when $C_{Dr}$ is plotted versus $KC_o$ for fixed $KC_w$ values. Considering the regression lines in this figure, one can observe that the higher $KC_w$ is, the higher $C_{Dr}$ is. In other words, one would expect a higher drag coefficient for a higher wave amplitude.

In the second stage, $C_{Dr}$ was plotted versus the combined nondimensional parameters such as $KC_{ow}$ and $KC_r$. Figures 8.14 and 8.15 show the dependency of $C_{Dr}$ on $KC_{ow}$ and $KC_r$ respectively. Both dimensionless parameters $KC_{ow}$ and $KC_r$ show a good correlation with $C_{Dr}$ values. However, using $KC_{ow}$ is preferred because it has some advantages; the tendency of the coefficient is similar to those of previous test cases and concerning practical application of the data, estimating $KC_{ow}$ is rather easy compared with $KC_r$.

Beside trying the above nondimensional parameters, various combinations of them such as $KC_S$ ($= KC_o + KC_w$) and $KC_1$ were also examined but no better results were obtained.

### Inertia coefficient, $C_{Mr}$
The same method was used to evaluate the inertia coefficient for the relative velocity model. Figures 8.16 and 8.17 present $C_{Mr}$ versus $KC_{ow}$ and $KC_r$. The scattering of the inertia coefficient $C_{Mr}$ is much less than that for the drag coefficient; all values are between 1.18 and 2.14. The inertia coefficient correlates well with the nondimensional accelerations given in table 8.2, in particular with $K_{ac} = \dot{u}_m T_o^2/D$, see figure 8.18. The inertia coefficient generally decreases as this parameter increases.

### Comparison of measured and calculated in-line forces:
Figures 8.19 compares measured and calculated force time histories (from the relative velocity model) for randomly selected test runs. These examples indicate that the relative velocity model can reproduce the hydrodynamic forces very well if the phase difference and the force coefficients are chosen correctly.

### 8.4.4.2 Absolute Velocity Model (model II)

The force coefficients of the absolute velocity model ($C_{Dw}$, $C_{Do}$ and $C_{Mw}$) should normally be plotted versus corresponding Keulegan-Carpenter numbers, i.e. $KC_w$ and $KC_o$. However, they are plotted versus $KC_{ow}$ in order to make comparison of the results for these coefficients with those for the relative velocity model possible.

The drag coefficient for wave flow, $C_{Dw}$, is plotted versus $KC_{ow}$ in figure 8.20. One can notice significant scattering in this figure; $C_{Dw}$ varies from 0.3 to 2.9. The drag coefficient for cylinder oscillation, $C_{Do}$, exhibits a large scattering too as seen in figure 8.21; the coefficient value ranges from 0.5 to 5.6.

Figure 8.22 presents the values of the inertia coefficient $C_{Mw}$ plotted versus $KC_{ow}$. Here again, there is scattering and $C_{Mw}$ varies from 0.84 to 2.20.

Comparing the drag force coefficients for the absolute velocity model with those for the degenerate test series, one can observe very high coefficient values for this more complex

condition; generally these do not resemble the degenerate case coefficient values.

### 8.4.5 Lift Force Coefficients

Before evaluating the lift force coefficients, it may be interesting to compare the measured in-line forces with the transverse measured forces. This is done by comparing the maximum forces in each direction as shown in figure 8.23. The maximum transverse force $Fy_{max}$ is plotted versus the maximum in-line force $F_{max}$ in this figure. A 45° line is included here for better comparing of the forces; the data points near this line indicate that both forces are about equal. Even though the maximum lift force $Fy_{max}$ is greater than the maximum in-line force, $F_{max}$ for some runs, overall $Fy_{max}$ is smaller than $F_{max}$. Figure 8.24 shows ratios of $Fy_{max}/F_{max}$ as a function of $KC_{ow}$. The ratios are typically less than unity. However, they are more than one for some runs especially between $10 < KC_{ow} < 15$.

The above comparisons show that the transverse force in a combined flow field is significant and should not be neglected as a force on an element.

One objective has been to find, if possible, a correlation between the maximum lift force coefficients, $C_{L,maxT}$ or $C_{L,maxR}$ (see equations 8.15 and 8.16), and various nondimensional parameters; this has not been successful. However, the maximum lift force coefficient $C_{L,maxT}$ is plotted versus $KC_{ow}$, $KC_r$ and the velocity ratio $u_m/(u\text{-}\dot{x})_{max}$ in figures 8.25 through 8.27, respectively. As seen from these figures, $C_{L,maxT}$ scatters in the range of 0.25 to 2.7. Nevertheless, the variation of $C_{L,maxT}$ with the velocity ratio of $u_m/(u\text{-}\dot{x})_{max}$ is interesting (figure 8.27); the maximum $C_{L,maxT}$ values are concentrated around $u_m/(u\text{-}\dot{x})_{max} = 0.5$. This shows that the velocity ratio is a significant parameter for the lift force in a combined flow field.

Figure 8.28 and 8.29 show the maximum lift force coefficient $C_{L,rmsR}$ plotted versus $KC_r$ and the velocity ratio $u_m/(u\text{-}\dot{x})_{max}$. As seen from figure 8.29, the $C_{L,rmsR}$ increases with increasing velocity ratio. Comparing these figures with those corresponding to $C_{L,maxT}$ (figures 8.26 and 8.27) one may conclude that $C_{L,maxR}$ shows somewhat smaller scattering and is therefore a better coefficient for representing the maximum lift force.

The rms lift force coefficient defined in equation 8.18, $C_{L,rmsR}$, presents a better correlation if plotted versus $KC_r$ as shown in figure 8.30. The coefficient value is less than 0.5 for most of the test runs.

### 8.6  Conclusions

The main conclusions from the experiments with cylinder oscillations in waves are summarised in the following paragraphs.

*Important parameters*

1. Nondimensional parameters based on the relative velocity $(KC_r, Re_r)$ have been introduced. These parameters are more appropriate than the independent parameters to study the hydrodynamic forces.
2. The velocity ratio of the two motions is a very important parameter.

110

3. A number of dimensionless parameters have been introduced to relate to the acceleration terms of the flows. It has been found that correlation between $K_{ac} = \dot{u}_m T_o^2 / D$ and the inertia force coefficient is quite good.
4. The phase difference between the cylinder velocity and the horizontal water particle velocity has a significant effect on the hydrodynamic forces.

## In-line Forces

1. The characteristic in-line forces exhibit better correlation when plotted versus a relative velocity term.
2. The maximum in-line force on the oscillating cylinder in waves is not equal to the sum of the maximum in-line forces resulting from the cases of the oscillating cylinder in still water and the fixed cylinder in waves. This tends to disprove the independent flow field approach.
3. Five extended forms of Morison equation have been considered: two result from the relative velocity approach (model I and III), two result from the absolute velocity approach (model II and IV) and a further postulated form also based on the relative velocity approach (model V). These models fit the measured data quite well if their own sets of coefficients are used.
4. Load models based on the independent flow field approach (absolute velocity models) are not appropriate mathematical models to predict hydrodynamic forces for the following reasons:

   - The basic assumption underlying the absolute form of the modified Morison equation does not seem valid. Indeed, using degenerate coefficients corresponding to two independent flow fields leads to a bad fitting. This remark tends to refute the theoretical background of the absolute approach and thus the validity of models based on this approach, i.e. model II and IV.
   - Model II and IV predict the measured forces much less consistently than the other models when smoothed coefficients are used.
   - A relatively larger scattering in the coefficients has been noticed for model II and IV.

5. Load models based on the relative velocity approach (Model I, III and V) are of about the same quality.
6. Linearised forms of the relative velocity model predict the in-line forces as well as the nonlinear form. Especially model V appears to be very interesting since it is linear in use and contains well known velocity terms.

## Transverse Forces

1. The lift force has the same range of value as the in-line force for intermediate $KC_{ow}$.
2. Relative flow parameters are appropriate to study the transverse force as well. $Fy_{max}$ shows good correlation with the velocity ratio $u_m/(u-\dot{x})_{max}$.
3. With respect to the phase difference between the cylinder motion and the waves, the measured variations of $F_{y\,max}$ around its mean value are very large (80%) and even greater than the variations noted for the maximum in-line force $F_{max}$.
4. Various maximum and rms lift force coefficients have been calculated by normalising the measured transverse forces. The coefficient normalised by the relative velocity term $(u - \dot{x})_{max}$ shows smaller scattering and is a better parameter for representing the lift force than other possible choices.

111
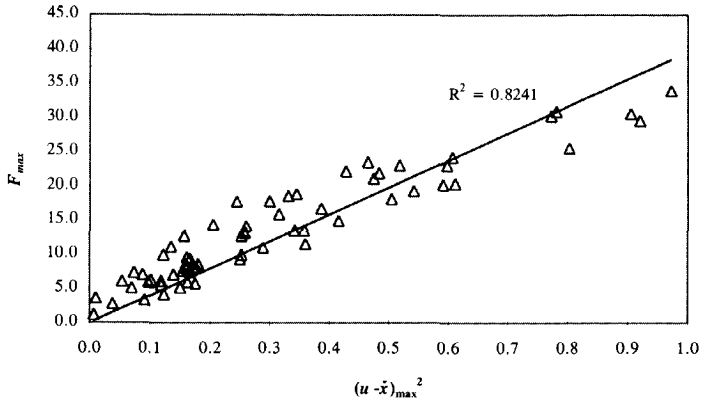
Figure 8.1 In-line cylinder oscillation in waves, $F_{max}$ plotted versus $(u - \overset{\bullet}{x})_{max}^{2}$
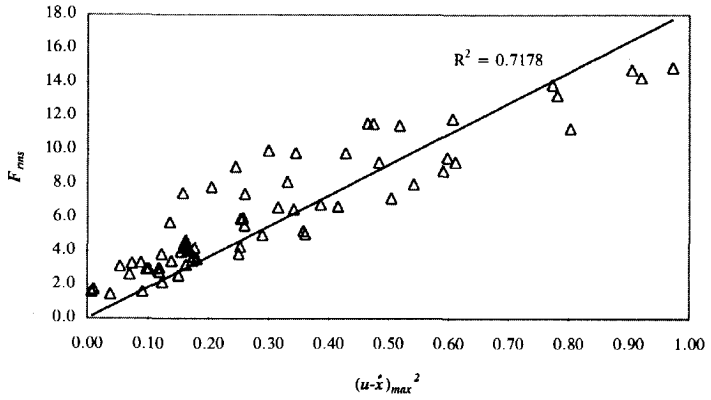


Figure 8.2 In-line cylinder oscillation in waves, $F_{rms}$ plotted versus $(u - \overset{\bullet}{x})_{max}^{2}$
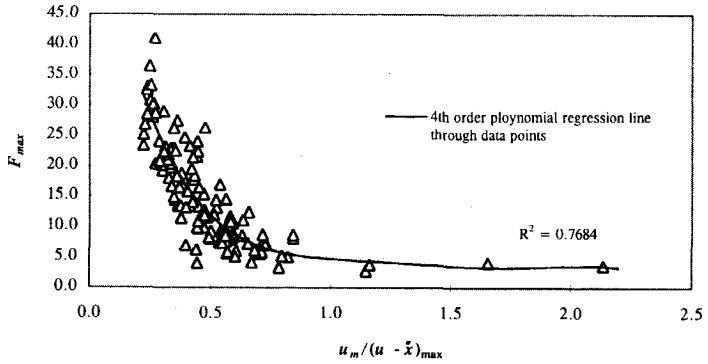


Figure 8.3 In-line cylinder oscillation in waves, $F_{max}$ plotted versus $u_{m}/(u - \overset{\bullet}{x})_{max}$

112
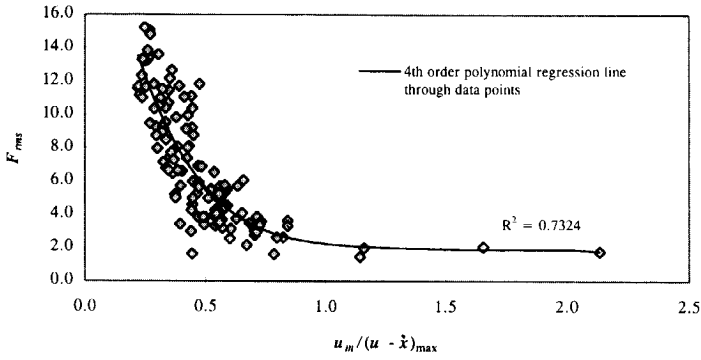
Figure 8.4  In-line cylinder oscillation in waves, $F_{rms}$ plotted versus $u_m / (u- \dot{x})_{max}$
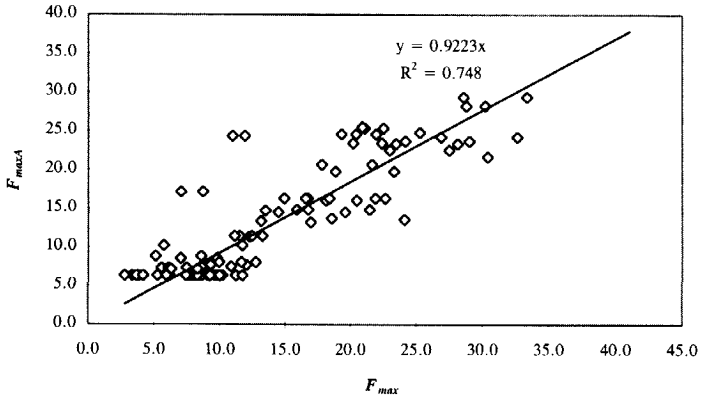


Figure 8.5  Correlation between total maximum in-line forces of degenerate tests, $F_{maxA}$ and the maximum forces of cylinder oscillation in waves, $F_{max}$
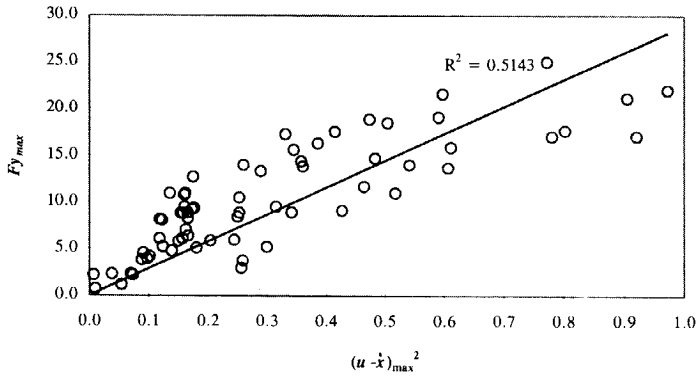


Figure 8.6  In-line cylinder oscillation in waves, $Fy_{max}$ plotted versus $(u- \dot{x})_{max}^{2}$

113
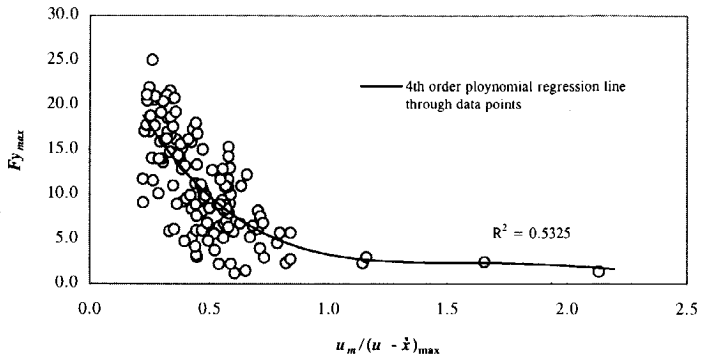
Figure 8.7  In-line cylinder oscillation in waves, $Fy_{max}$ plotted versus $u_m / (u-\dot{x})_{max}$
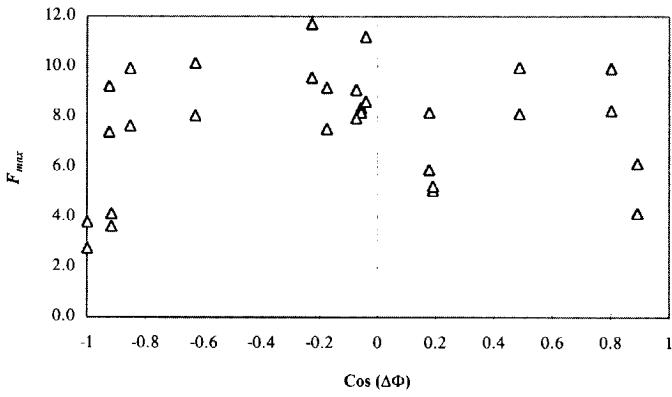


Figure 8.8  Maximum measured in-line forces versus $\cos(\Delta \Phi)$
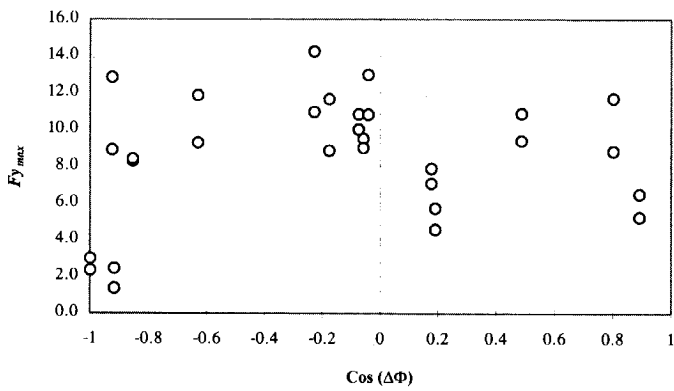


Figure 8.9  Maximum measured transverse forces versus $\cos(\Delta \Phi)$

114

— Model I, Rel. Velocity —✳— Model II, Abs. Velocity △ Model III —◇— Model IV
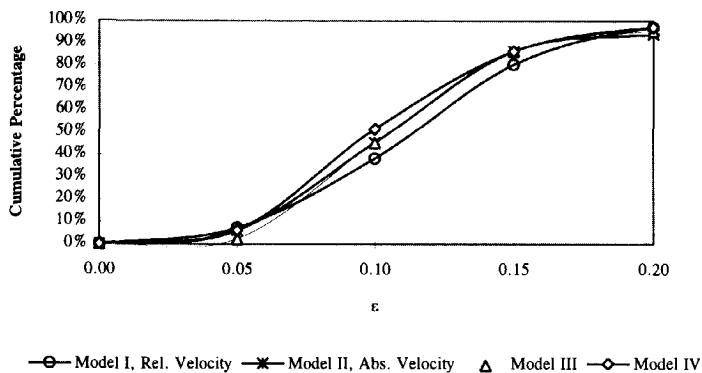
Figure 8.10  In-line cylinder oscillation in waves, comparison of goodness-of-fit
parameter for given load models using best force coefficients



— Model I, Rel. Velocity —✳— Model II, Abs. Velocitty —△— Model III —◇— Model IV
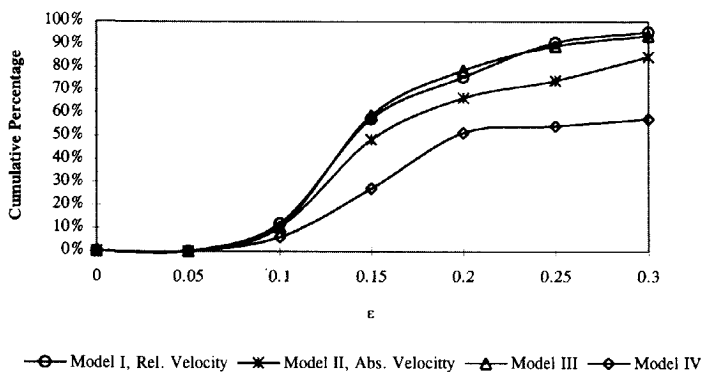
Figure 8.11  In-line cylinder oscillation in waves, comparison of goodness-of-fit
for load models using smoothed force coefficients



—◆— Individual Coefficients —■— Smoothed Coeffcients —▲— Degenerate Case Coefficients
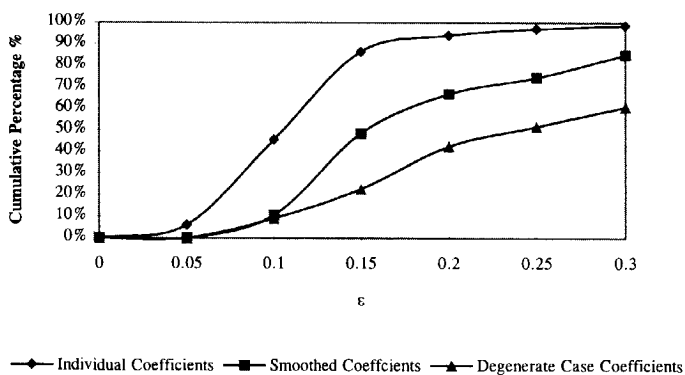
Figure 8.12  In-line cylinder oscillation in waves, cumulative percentage of ε for the absolute
velocity model using best individual, smoothed, and degenerate case coefficients

115
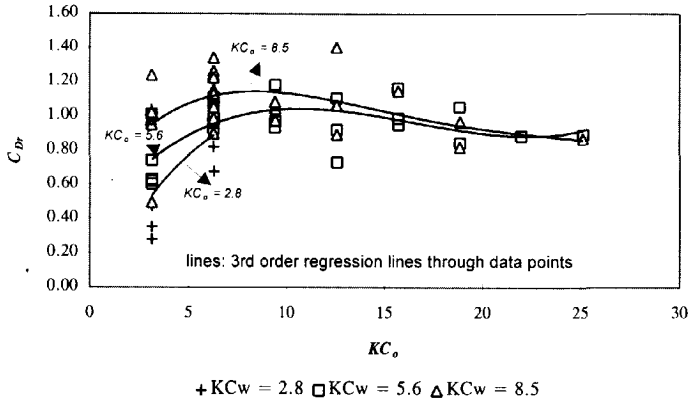
Figure 8.13  In-line cylinder oscillation in waves, drag coefficient for the relative velocity model, $C_{Dr}$ versus $KC_o$
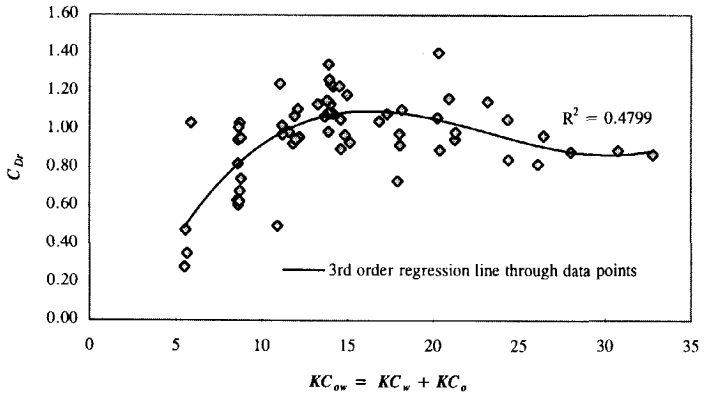


Figure 8.14  In-line cylinder oscillation in waves, drag coefficient for the relative velocity model, $C_{Dr}$ versus $KC_{ow}$
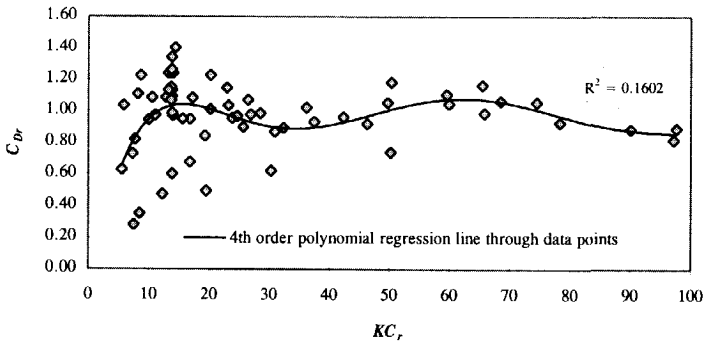


Figure 8.15  In-line cylinder oscillation in waves, drag coefficient for the relative velocity model, $C_{Dr}$ versus $KC_r$
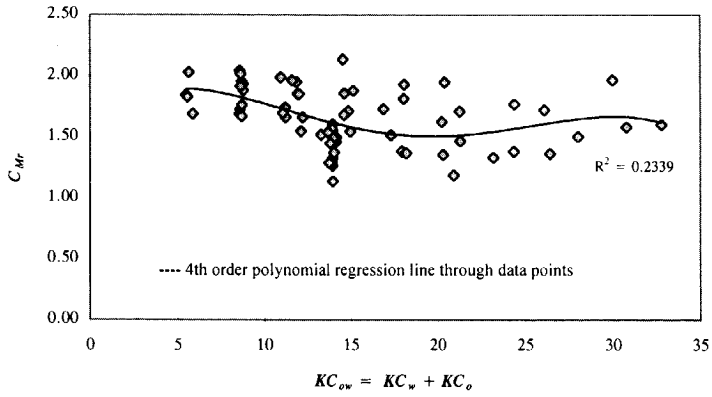
116

Figure 8.17   In-line cylinder oscillation in waves, inertia coefficient for the relative
velocity model, $C_{Mr}$ versus $KC_{ow}$
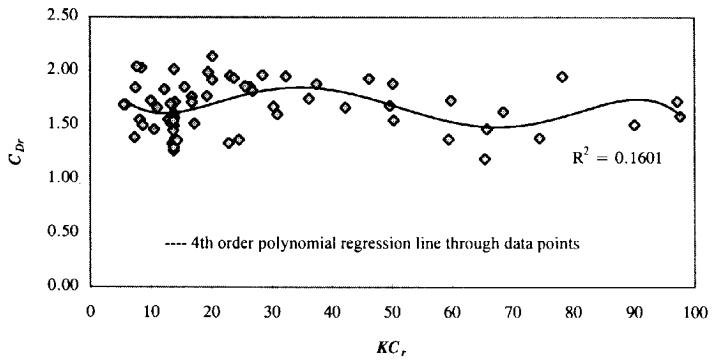


Figure 8.17   In-line cylinder oscillation in waves, inertia coefficient for the relative
velocity model, $C_{Mr}$ versus $KC_r$
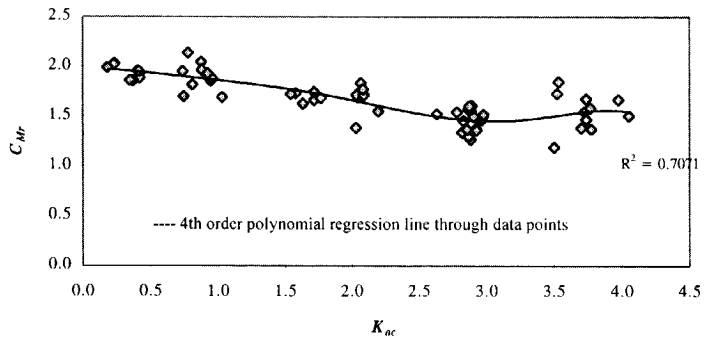


Figure 8.18   In-line cylinder oscillation in waves, inertia coefficient for the relative
velocity model, $C_{Mr}$ versus $K_{ac}$

117
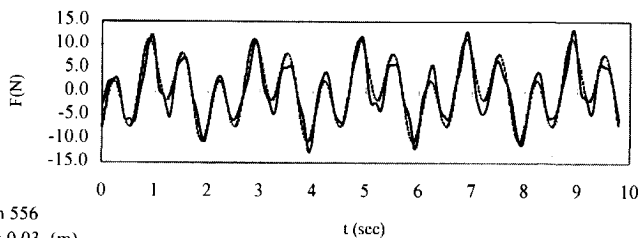
Run 556
A = 0.03 (m)
To = 0.667 (sec)
Tw = 2 (sec)          ———— Measured force — — — Calculated force
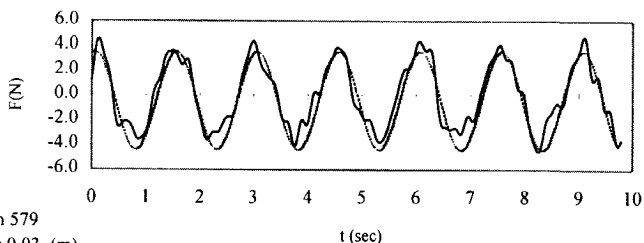
Run 579
A = 0.03 (m)
$T_o$ = 1.5 (sec)
$T_w$ = 1.5 (sec)     ———— Measured force — — — Calculated force
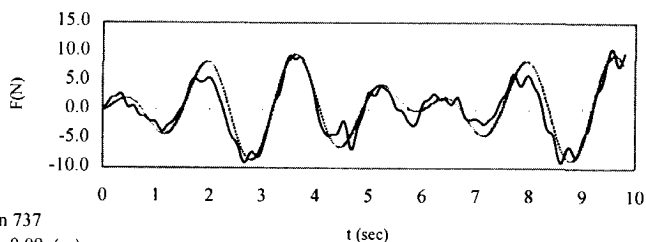
Run 737
A = 0.09 (m)
To = 2.0 (sec)
Tw = 1.5 (sec)        ———— Measured force — — — Calculated force
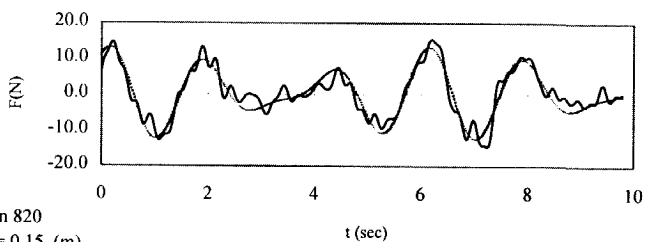
Run 820
A = 0.15 (m)
To = 2 .0 (sec)
Tw = 1.5 (sec)        ———— Measured force — — — Calculated force

Figure 8.19   Example of measured and predicted hydrodynamic force time histories using
the relative velocity model

118
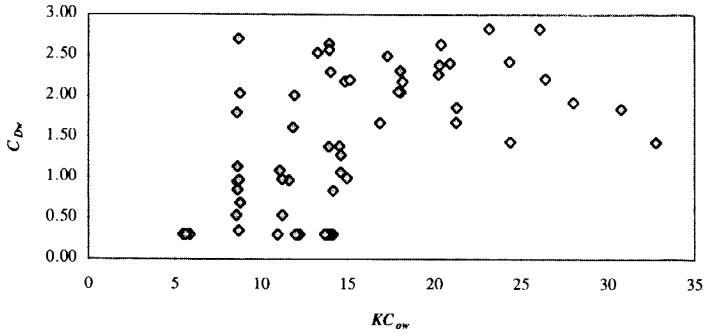
Figure 8.20 In-line cylinder oscillation in waves, drag coefficient due to waves for the absolute velocity model, $C_{Dw}$, versus $KC_{ow}$
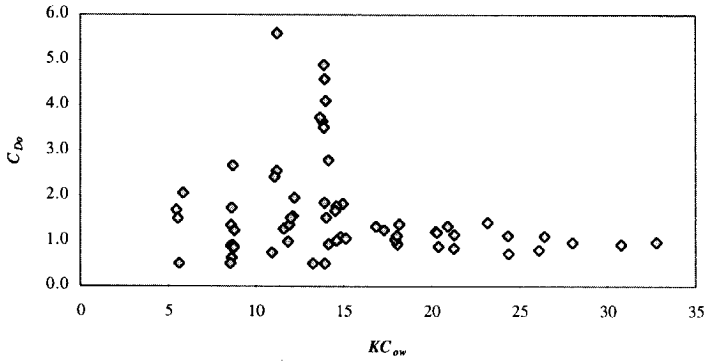


Figure 8.21 In-line cylinder oscillation in waves, drag coefficient due to cylinder oscillation for the absolute velocity model, $C_{Do}$, versus $KC_{ow}$
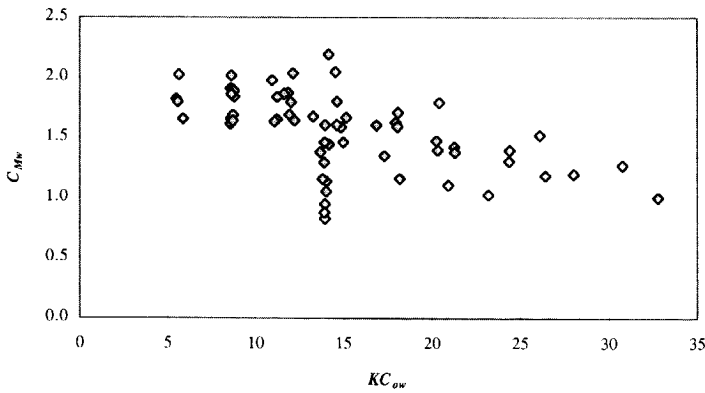


Figure 8.22 In-line cylinder oscillation in waves, inertia coefficient due to waves for the absolute velocity model $C_{Mw}$ versus $KC_{ow}$
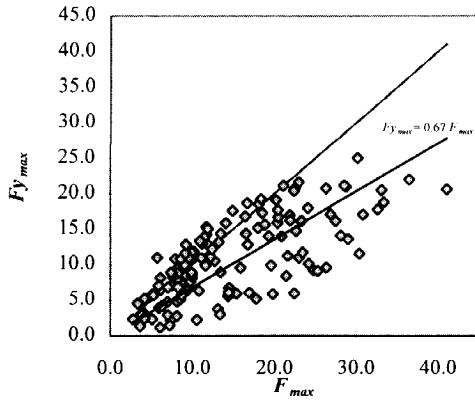
Figure 8.23   In-line cylinder oscillation in waves, correlation of measured  transverse and
in-line maximum forces
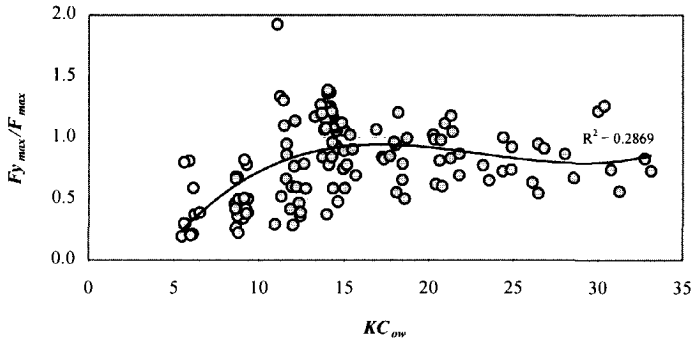


Figure 8.24  In-line cylinder oscillation in waves, ratio of  measured transverse and
in-line forces
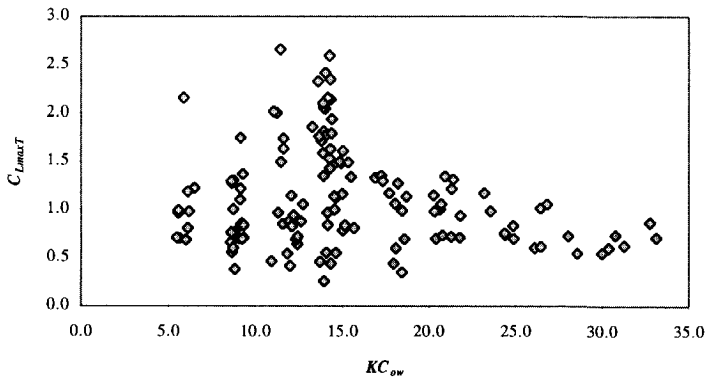


Figure 8.25   In-line cylinder oscillation in waves, maximum lift force coefficient $C_{l,maxT}$
plotted versus $KC_{ow}$
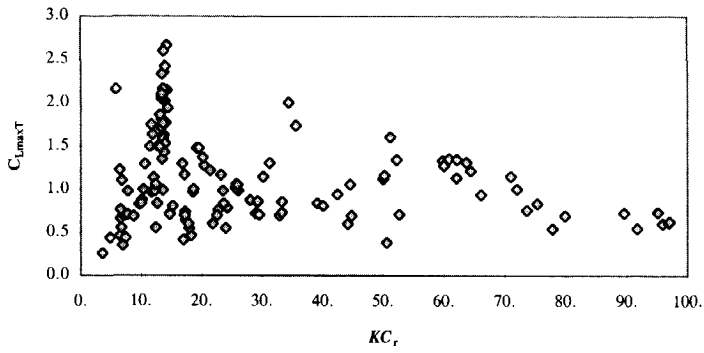
Figure 8.26  In-line cylinder oscillation in waves, maximum lift force coefficient $C_{L,maxT}$ plotted versus $KC_r$
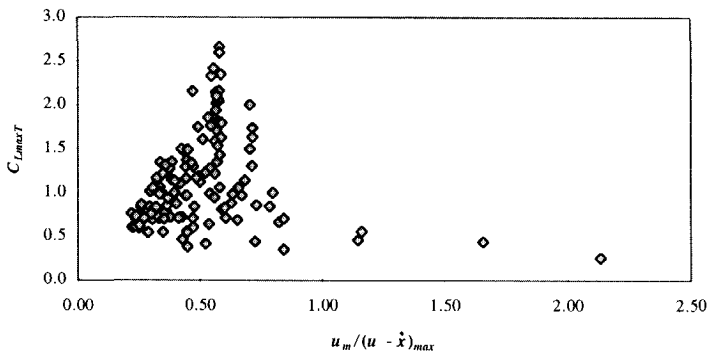


Figure 8.27  In-line cylinder oscillation in waves, maximum lift force coefficient $C_{L,maxT}$ plotted versus $u_m/(u - \dot{x})_{max}$
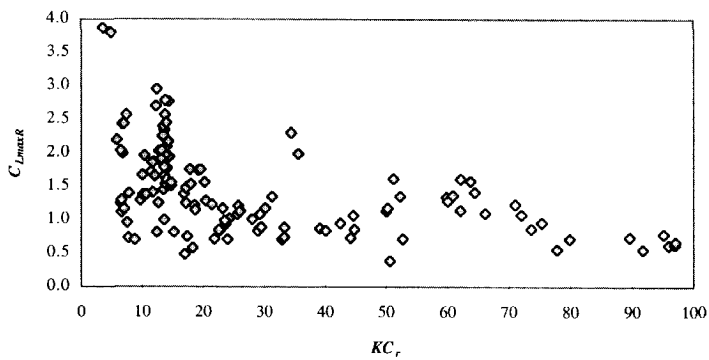


Figure 8.28  In-line cylinder oscillation in waves, maximum lift force coefficient $C_{L,maxR}$ plotted versus $KC_r$
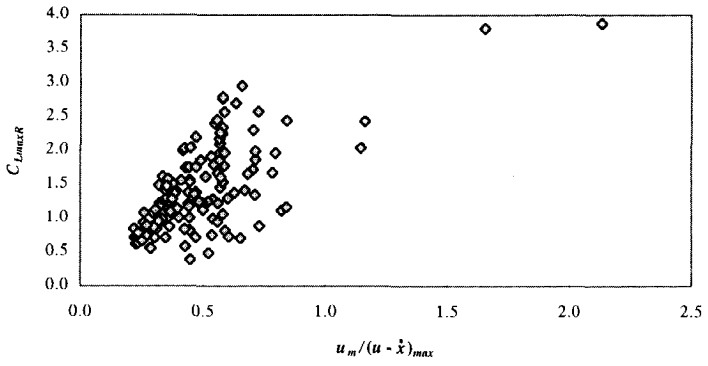
Figure 8.29 In-line cylinder oscillation in waves, maximum lift force coefficient $C_{L,maxR}$ plotted versus $u_m/(u-\dot{x})_{max}$
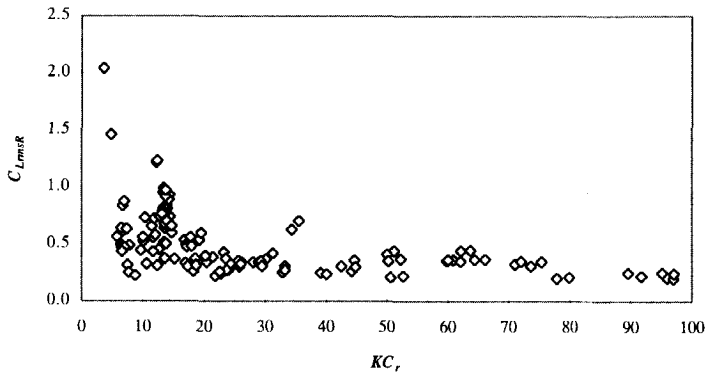


Figure 8.30 In-line cylinder oscillation in waves, rms lift force coefficient $C_{L,rmsR}$ plotted versus $KC_r$

# CHAPTER 9

# In-line Cylinder Oscillation in Waves Plus Current Flow Field

## 9.1 General

A variety of offshore structures such as compliant and floating structures and slender members of fixed offshore structures experience fluid loading as well as reaction forces caused by the movement of the structure as a whole due to the action of hydrodynamic forces from waves and current. Generally, the fluid-structure interaction for such structures has been studied either in a steady flow (mostly) or in waves (barely). To the best of the author's knowledge, a comprehensive experiment including all motions has not been carried out before the present work.

The results of tests with in-line cylinder oscillations in waves while towing the cylinder are discussed in this chapter. The flow condition is similar to that of a cylinder oscillating in a combined waves plus current flow field.

## 9.2 Specific Details of the Experiments

This test series is a combination of all previous test cases associated with the three possible separate flow conditions. These experiments occupy the space shown in figure 9.1, while the single mode tests fall along the axes and the combined tests discussed earlier fall in one of the planes through two axes. Thus, the test series under consideration is the most complicated test case within this work, involving many parameters and phenomena. Specific phenomena and test conditions are briefly addressed in the following sections.
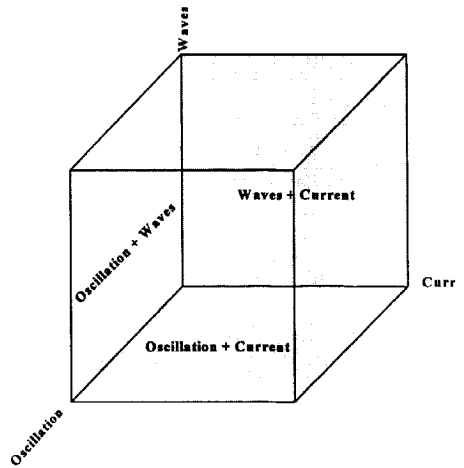


Figure 9.1 The Tests Cases Studied

## 9.2.1 Wave-Current-Structure Interaction

The interaction between waves and current on the one hand and the oscillating (flexible or floating) structures on the other hand is a very complex problem. Test results are scarce for such

a flow condition. The forces and the motions are dependent upon the water particle kinematics as well as the velocities and accelerations of the structure itself.

The waves-current, current-structure and waves-structure interactions have already been discussed in the previous chapters. The problem of waves-current-structure interaction is of much greater complexity, due to the fact that the role of various factors such as the orbital motion, wake structure, relative motion, etc. is not obvious. For example, the combination of regular waves and sinusoidal cylinder oscillations will result in a modulated relative motion in which prediction of hydrodynamic forces is very difficult.

Schematically, waves-current-structure interaction involves the following stages:

1. Waves and current interaction results in a flow field in which the flow kinematics may be assumed to be vectorial summation of the two separate flows (ignoring the physical interaction between waves and currents).
2. The combined flow field will then initiate forces on the structure. Compliant and floating structures and slender components such as risers respond to the action of the hydrodynamic forces.
3. As a result of this response, fluid reaction forces are generated leading to interactions between the motion and the loading.

In general, the process is iterative, since the interaction will change the structure's motion and hence the flow around the structure.

Many laboratory and field investigations remain to be carried out for a better understanding and quantification of wave-current-structure interaction. This need has long been recognized but it has not been possible to obtain systematic data over a broad range of parameters. The present investigation was carried out to shed some light on wave-current-structure interaction, to determine the forces acting on an oscillating cylinder in a co-existing waves plus current flow field, and to examine the applicability of the Morison equation to the flow situation under consideration.

## 9.2.2 Important Parameters

Investigation of the most important parameters is a significant task. As demonstrated in the dimensional analysis in section 2.3, various nondimensional parameters may be considered. Besides the earlier definitions, the following definitions for the Reynolds number, the Keulegan-Carpenter number and the reduced velocity may be used:

$$KC_{owvo} = \frac{(V+u_m+\dot{x}_m)T_o}{D}, \qquad Re_{owv} = \frac{(V+u_m+\dot{x}_m)D}{\nu} \qquad (9.1)$$

$$KC_{owvw} = \frac{(V+u_m+\dot{x}_m)T_w}{D} \qquad (9.2)$$

124

$$Vr_{ow} = Vr_o + Vr_w = \frac{V(T_o + T_w)}{D} \tag{9.3}$$

In the forgoing relations the apparent wave period $T_{app} = 2\pi/\omega_{app}$ may be used instead of the true incident wave period resulting in another set of Keulegan-Carpenter numbers and reduced velocity.

Since the water particle path in a combined waves plus current field is dependent on the ratio of the maximum horizontal velocity $u_m$ due to wave action to that of the steady flow $(u_m/V)$, this ratio could be an important parameter. The ratio of the maximum cylinder velocity $\dot{x}_m$ to $u_m$ is also considered to be important. An additional velocity ratio may be defined as:

$$V_{ratio} = \frac{u_m + \dot{x}_m}{V} \tag{9.4}$$

which is the ratio of the maximum (total) oscillatory velocity to the steady velocity.

### 9.2.3 Tests Conducted

The present test series is a three-mode test case which combines all single- and two-mode tests. The cylinder has been oscillated with different amplitudes and frequencies while towing with different speeds in given waves. To make it possible to study each motion effect, the values of various independent parameters were made to coincide with those of simpler tests discussed in the earlier chapters.

There were five independent variables in these tests:
- Towing (current) velocity, $V$
- Oscillation amplitude and period, $A_o$ and $T_o$
- Wave height and period, $H_w$ and $T_w$

The selected ranges of these variables were similar to those in the previous test cases. For each oscillation amplitude, first the towing speed and then the oscillation frequency was changed in various waves. In total, some 156 test runs were carried out for the present test series so that a reasonably full matrix of independent variables was generated.

### 9.3 Load Models

### 9.3.1 In-line Force

Several extended forms of the Morison equation may be considered for the combined flow field caused by co-existing waves, current and cylinder oscillations. However, only results for the following forms are reported here:

Model I. The relative velocity model:

$$F = \frac{1}{2}\rho D C_{Dr}|V + u - \dot{x}|(V + u - \dot{x}) + \frac{\pi D^2}{4}\rho C_{Mr}\dot{u} - \frac{\pi D^2}{4}\rho(C_{Mr} - 1)\ddot{x} \tag{9.5}$$

125

Model II. A postulated linear version of this relative velocity model:

$$F = \frac{1}{2}\rho D C_{Drl}(V + u_m + \dot{x}_m)(V + u - \dot{x}) + \frac{\pi D^2}{4}\rho C_{Mrl}\dot{u} - \frac{\pi D^2}{4}\rho(C_{Mrl} - 1)\ddot{x} \qquad (9.6)$$

Model III. A hybrid model in which the steady force component is related to the steady current and the oscillatory force component is related to the relative oscillatory velocity:

$$F = \frac{1}{2}\rho D C_{Dm}V^2 + \frac{1}{2}\rho D C_{Dh}|u - \dot{x}|(u - \dot{x}) + \frac{\pi D^2}{4}\rho C_{Mh}\dot{u} - \frac{\pi D^2}{4}\rho(C_{Mh} - 1)\ddot{x} \qquad (9.7)$$

Model IV. An absolute velocity model in which the drag force is split into three components:

$$F = \frac{1}{2}\rho D C_{Dm}V^2 + \frac{1}{2}\rho D C_{Dw}|u|u - \frac{1}{2}\rho D C_{Da}|\dot{x}|\dot{x} + \frac{\pi D^2}{4}\rho C_{Ma}\dot{u} - \frac{\pi D^2}{4}\rho(C_{Ma} - 1)\ddot{x} \qquad (9.8)$$

Even though other extended forms have been evaluated in this study, their results are not reported here because they did not satisfy the criteria for a suitable model.

## 9.3.2 Lift Force

The amplitude of the lift force on a unit length of an oscillating cylinder in a combined waves plus current flow field may be written in a simple form - based on the relative velocity approach - as:

$$Fy = 0.5\rho D C_L (V + u - \dot{x})^2 \qquad (9.9)$$

Since the lift force coefficients are generally presented for the maximum or root-mean-square value of the lift force, only the maximum and rms lift force coefficient have been evaluated in this work. However, various lift force coefficients may be obtained by normalising the maximum or rms value of the lift force with various velocity combinations, such as:

$$C_{LmaxT} = \frac{Fy_{max}}{0.5\rho D(V + u_m + \dot{x}_m)^2} \qquad (9.10)$$

$$C_{LmaxR} = \frac{Fy_{max}}{0.5\rho D(V + u - \dot{x})^2_{max}} \qquad (9.11)$$

$$C_{LrmsT1} = \frac{Fy_{rms}}{0.5\rho D(V + u_m + \dot{x}_m)^2} \qquad (9.12)$$

$$C_{LrmsT2} = \frac{Fy_{rms}}{0.5\rho D(V + u_{rms} + \dot{x}_{rms})^2} \qquad (9.13)$$

$$C_{LrmsR1} = \frac{Fy_{rms}}{0.5\rho D(V + u - \dot{x})^2_{max}} \qquad (9.14)$$

126

$$C_{LrmsR2} = \frac{Fy_{rms}}{0.5\rho D(V + u - \dot{x})^2_{rms}}$$

<div style="text-align:right">(9.15)</div>

## 9.4  Results and Discussion

### 9.4.1  Direct Observations from the Data

The characteristic forces described in section 6.5.1 have been used to examine the behaviour of the force on a measuring element against various combinations of variables. Table 9.1 lists the correlation coefficient $R^2$ between the characteristic forces and some velocity combinations. These results are discussed for each characteristic force in the following paragraphs.

| No. | $R^2$ | $F_{max}$ | $F_{rms1}$ | $Fm$ | $F_{rms0}$ |
|---|---|---|---|---|---|
| 1 | $V^2$ | 0.376 | 0.593 | 0.761 | 0.139 |
| 2 | $\dot{x}_m^2$ | 0.134 | 0.120 | 0.010 | 0.492 |
| 3 | $u_m^2$ | 0.079 | 0.057 | 0.031 | 0.074 |
| 4 | $(V + \dot{x}_m)^2$ | 0.635 | 0.676 | 0.364 | 0.839 |
| 5 | $(V + u_m)^2$ | 0.462 | 0.582 | 0.823 | 0.156 |
| 6 | $(u_m + \dot{x}_m)^2$ | 0.167 | 0.136 | 0.000 | 0.755 |
| 7 | $V^2 + 2V\dot{x}_m + 2\dot{x}_m u_m$ | 0.666 | 0.820 | 0.576 | 0.406 |
| 8 | $V^2 + V\dot{x}_m + \dot{x}_m u_m$ | 0.713 | 0.918 | 0.752 | 0.803 |
| 9 | $V^2 + V u_m + V\dot{x}_m$ | 0.738 | 0.832 | 0.908 | 0.793 |
| 10 | $V^2 + V u_m + \dot{x}_m u_m$ | 0.583 | 0.736 | 0.811 | 0.651 |
| 11 | $V^2 + 2V\dot{x}_m + 2 V u_m$ | 0.796 | 0.844 | 0.866 | 0.551 |
| 12 | $V^2 + 2V u_w + 2 \dot{x}_m u_m$ | 0.653 | 0.737 | 0.763 | 0.404 |
| 13 | $V^2 + u_m^2 + \dot{x}_m^2$ | 0.523 | 0.669 | 0.320 | 0.753 |
| 14 | $(V + \dot{x}_m)^2 + u_m^2$ | 0.649 | 0.686 | 0.370 | 0.847 |
| 15 | $(V + u_m)^2 + \dot{x}_m^2$ | 0.678 | 0.784 | 0.574 | 0.697 |
| 16 | $(\dot{x}_m + u_m)^2 + V^2$ | 0.483 | 0.541 | 0.194 | 0.789 |
| 17 | $(V\dot{x}_m + V u_m + u_m \dot{x}_m)$ | 0.739 | 0.619 | 0.436 | 0.771 |
| 18 | $(V^2 + 2 V u_m + 2 V\dot{x}_m + 2 u_m \dot{x}_m)$ | 0.862 | 0.889 | 0.714 | 0.695 |
| 19 | $(V + u_m + \dot{x}_m)^2$ | 0.705 | 0.699 | 0.418 | 0.866 |
| 20 | $u_m^2 + 2 V u_m + 2\dot{x}_m u_m$ | 0.817 | 0.413 | 0.169 | 0.489 |
| 21 | $V^2 + u_m^2 + 2V\dot{x}_m$ | 0.821 | 0.891 | 0.775 | 0.668 |

Table 9.1  $R^2$ Correlation Coefficient Values for Linear Regression of the Characteristic Forces

### 9.4.1.1  Maximum Value of the In-line Force

The third column of the values in table 9.1 gives the $R^2$ correlation coefficient values for $F_{max}$. As listed in this table, the best correlation can be obtained using $(V^2 + 2V u_m + 2V\dot{x}_m + 2 u_m\dot{x}_m)$ as independent variable. Figure 9.2 shows how $F_{max}$ varies as a function of this variable. This

observation is quite interesting as it agrees with the earlier observations for other test cases. In fact, it is a generalised form which can be used for the degenerate cases as well.

Using this observation, a maximum drag coefficient may be defined as:

$$C_{Dmax} = \frac{F_{max}}{0.5 \rho D (V^2 + 2 V u_m + 2 V \dot{x}_m + 2 \dot{x}_m u_m)}$$ (9.16)

Figure 9.3 shown the variation of $C_{Dmax}$ as a function of the velocity ratio $\dfrac{u_m + \dot{x}_m}{V}$ .

### 9.4.1.2  RMS Values of the In-line Force

The values in the fourth column of table 9.1 are $R^2$ correlation coefficient values between the root mean square values of the total in-line force, $F_{rmsT}$, and various variable combinations. As seen from this table and figure 9.4, the highest $R^2$ value is found if $F_{rmsT}$ is plotted versus $(V^2 + V\dot{x}_m + u_m \dot{x}_m)$, line 8. There is also still a good correlation between $F_{rmsT}$ and $(V^2 + 2V\dot{x}_m + 2V\dot{u}_m + 2 u_m \dot{x}_m)$, line 18 and $(V^2 + u_m^2 + 2V\dot{x}_m)$, line 21.

### 9.4.1.2 Mean Drag Force

The correlation coefficient values between the mean steady force component, $Fm$, and various variables are listed in the fifth column of table 9.1. As listed in this column, the $R^2$ value for $V^2$ (line 1) is lower than $R^2$ for some other combinations; the highest $R^2$ value has been obtained for $(V^2 + V u_m + V \dot{x}_m)$ (line 9), see also figure 9.5. The dependence of the steady force on the oscillatory velocities demonstrates that the steady in-line force component depends on both waves and the cylinder oscillation; there must be an interaction of the three flow fields. As with earlier test cases, the independent flow field approach does not seem to offer a proper basis for estimating the hydrodynamic force here.

If the mean drag force $Fm$ is normalised by the steady current velocity $V$ then the normally used mean drag coefficient:

$$C_{Dm} = \frac{Fm}{0.5\rho D V^2}$$ (9.17)

will exhibit large values which bear no resemblance to those obtained under current only conditions. As shown in figure 9.6, $C_{Dm}$ increases as the $V_{ratio}$ - the ratio between the total oscillatory velocity $(u_m + \dot{x}_m)$ and the steady current velocity $V$ - increases. One can observe a large scatter in the $C_{Dm}$ values in this figure.

Based on the above observation, however, a new mean drag coefficient may be introduced by normalising $Fm$ as:

$$C_{Dmc} = \frac{Fm}{0.5\rho D(V^2 + Vu_m + V\dot{x}_m)}$$ (9.18)

Figure 9.6 also shows that the values of this new drag coefficient $C_{Dmc}$ correlate well with the

velocity ratio $V_{ratio}$; $C_{Dmc}$ decreases as the velocity ratio increases.

## 9.4.1.2  The RMS Values of the Oscillatory Force Component

The sixth column in table 9.1 gives the calculated $R^2$ values between the rms values of the oscillatory force component $F_{rmsO}$ and the combinations of independent variables. The $R^2$ values are fairly low for the velocity variables that exclude the steady current velocity component, whereas better correlations are obtained against some combinations in which the steady current component is included. This indicates that the oscillatory force component is also affected by the steady current; as expected, there is an interaction between the oscillatory flows and the steady current.

The best correlation coefficient value is obtained if $F_{rmsO}$ is plotted versus the relative velocity $(V+u_m+\dot{x}_m)^2$ (line 19 in table 9.1) as shown in figure 9.7.

## 9.4.2  Load Models Evaluations

The observations just discussed indicate that there is an interaction among the three motions (cylinder oscillation, waves and current) and that a load model for describing hydrodynamic forces must include all components involved. Therefore, an extension of the Morison equation based on the relative velocity approach seems to be a suitable model. However, the hybrid load model and the absolute velocity model have also been evaluated. The evaluation procedure is the same as for the earlier test cases.

Values of the goodness-of-fit parameter $\epsilon$ have been used to evaluate the quality of fit of the four load models given in section 9.3.1. The input-output data pairs of 156 test runs have been used to calculate the values of $\epsilon$ for each load model. Both best individual coefficients as well as the smoothed coefficients have been used for the evaluation.

***Individual Coefficients***:
Table 9.2 lists the calculated mean and standard deviation values for the $\epsilon$ distributions using the best individual coefficients. This table also includes the percentage of runs for which $\epsilon < 0.20$ for each computational model.

The cumulative probability of $\epsilon$ for the four load models is shown in figure 9.8. Having all information in this figure and table 9.2, one can infer that all four load models fit the data well if their individually obtained coefficients are used. The quality of fit of the extended Morison equation based on the absolute velocity is slightly better than the others. However, having such a result for the absolute velocity model can be expected; this model contains five coefficients providing more curve fitting flexibility.

Although the model based on the absolute velocity as well as the hybrid model could reproduce each measured hydrodynamic force, the scattering in the coefficients obtained with these models is relatively great, especially for the absolute velocity model. The coefficients for these models exhibit unrealistically large values that do not compare to those obtained for degenerate conditions. The effect of such scattering in force coefficients will show up as a poorer fit when

129

the individually determined coefficients are smoothed and used in the computational models. The results of this latter evaluation are given in the following paragraph.

| Model | name | Mean of $\epsilon$ value | STD of $\epsilon$ value | P ( $\epsilon$ < 0.20) |
|-------|------|--------------------------|-------------------------|------------------------|
| I | Relative Velocity | 0.12 | 0.06 | 88.89% |
| II | Linearised Relative Velocity | 0.101 | 0.056 | 96.73% |
| III | Hybrid Model | 0.130 | 0.094 | 86.93% |
| IV | Absolute Velocity | 0.091 | 0.061 | 97.39% |

Table 9.2 Summary of Model Fitting Results with Individual Coefficients

***Smoothed Coefficients***:
The individually obtained coefficients were smoothed and used in the computational models to obtain a new series of $\epsilon$ values. Figure 9.9 shows the cumulative percentage of $\epsilon$ using smoothed coefficients plotted in the same way as in figure 9.8. Table 9.3 summarises the statistical values of $\epsilon$.

The results shown in table 9.3 and figure 9.9 reveal that the extended Morison equation based on the relative velocity approach (Model I) and especially the linear version of this model (model II) now provide a much better fit than the others. The lower rating of the two other models is consistent with the relatively large scatter of their coefficients. Finding the best quality of fit for the linear relative velocity model is very significant since application of this model in dynamic analysis of offshore structures is much more convenient than the use of the quadratic form.

The fact that models based on the relative velocity approach require only two force coefficients is another advantage of these models. The behaviour of these coefficients as a function of various nondimensional parameters is discussed in the following section.

| Model | name | Mean of $\epsilon$ value | STD of $\epsilon$ value | P ($\epsilon$ < 0.20) |
|-------|------|--------------------------|-------------------------|-----------------------|
| I | Relative Velocity | 0.170 | 0.121 | 74.51% |
| II | Linearised Relative Velocity | 0.144 | 0.102 | 88.24% |
| III | Hybrid Model | 0.289 | 0.399 | 64.71% |
| IV | Absolute Velocity | 0.396 | 0.611 | 59.48% |

Table 9.3 Summary of Model Fitting Results with Smoothed Coefficients

### 9.4.3 In-line Force Coefficients

From the above evaluations it has been concluded that the two models based on the relative velocity approach are the most suitable load models. The feature and interpretation of the force coefficients for these models are discussed below.

130

### 9.4.3.1 Relative Velocity Model (Model I)

Extensive analysis of the force coefficients in terms of this load model has been carried out to seek a good correlation between the drag and inertia coefficients on the one hand and the relevant nondimensional parameters on the other. The effect of phase differences between the two oscillatory motions (wave and cylinder oscillation) could not be studied because the data were too limited for that purpose. However, the phase difference should not affect the force coefficients because this influence is already reflected in the relative velocity term $(V + u - \dot{x})$.

Many attempts have been made to find a relation between the force coefficients ($C_{Dr}$ and $C_{Mr}$) and various nondimensional parameters. The results of this investigation have revealed that there is no single parameter with which the drag and inertia coefficients may be correlated without the need for other parameters. However, the force coefficients correlate better with some parameters than with others. The behaviour of the force coefficients versus the more promising parameters is reported here.

The variations of $C_{Dr}$ and $C_{Mr}$ plotted against the combined reduced velocity $Vr_{ow}$ values are presented in figure 9.10. The solid line in each plot in figure 9.10 (and the following figures) is a third order polynomial regression line which has been determined by a least squares method. At low $Vr_{ow}$ values, the inertia coefficient is large; it decreases as $Vr_{ow}$ increases reaching its minimum value for $Vr_{ow} \approx 10$. For $Vr_{ow} > 10$, $C_{Mr}$ increases as $Vr_{ow}$ increases. The inverse is true for the drag coefficient; $C_{Dr}$ is small at small $Vr_{ow}$ values, but rises for moderate $Vr_{ow}$ values and decreases again.

Comparing the values of the hydrodynamic coefficients for the combined flow field with those for a fixed cylinder in oscillatory flow, one will notice that, overall, the drag coefficient values here are smaller and the inertia coefficient values are slightly higher than corresponding values for the fixed cylinder.

In order to illustrate the effect of cylinder oscillations, the variations of the force coefficients $C_{Dr}$ and $C_{Mr}$ are re-plotted in figure 9.11 for various $A/D$ values. Considering the regression lines in this figure, it is clear that for various $A/D$ the drag coefficients $C_{Dr}$ exhibit almost similar behaviour versus $Vr_{ow}$ and that $C_{Dr}$ decreases as $A/D$ increases for comparable data range, i.e. $Vr_{ow} < 20$. This is just opposite for the inertia coefficient when $Vr_{ow} < 12$; afterwards $C_{Mr}$ decreases as $A/D$ increases, as does $C_{Dr}$.

Figure 9.12 illustrates the behaviour of the force coefficients, $C_{Dr}$ and $C_{Mr}$ versus the velocity ratio: $V_{ratio} = (u_m + \dot{x}_m)/V$. Both coefficients are fairly stable around the polynomial regression lines in this figure. The reasonably good correlations between the force coefficients and the velocity ratio $V_{ratio}$ indicate that this parameter is a significant variable for a flow field consisting of combined waves, current and cylinder oscillation. The effect of $A/D$ (which is proportional to $KC_o$) can be seen in figure 9.13; for the relationship of the hydrodynamic coefficients with $V_{ratio}$, increasing $A/D$ generally increases $C_{Dr}$ and decreases $C_{Mr}$.

### *Comparison of Measured and Calculated In-line Forces*:
For the purpose of comparison, the measured and calculated (from the relative velocity model)

force time histories are shown for randomly selected test runs in figures 9.14, using smoothed coefficients. These examples show that the relative velocity model can reproduce the hydrodynamic forces well if the flow kinematics and force coefficients are specified properly. The model underpredicts some peaks, however.

### 9.4.3.2  Linear Relative Velocity Model (model II)

Figures 9.15 and 9.16 compare the force coefficients for the relative velocity model, $C_{Dr}$ and $C_{Mr}$, and those for the linear relative velocity model, $C_{Drl}$, $C_{Mrl}$. As expected, the inertia coefficients for both models are almost identical $C_{Mrl} \approx C_{Mr}$, and there is a linear relationship between the drag coefficients; $C_{Drl} \approx 0.73 C_{Dr}$. Because of these linear relationships, the behaviours of the force coefficients as function of their nondimensional parameters are alike. Therefore, separate results for the linear relative velocity model are not reported.

### 9.4.4  Lift Force Coefficients

The maximum lift force coefficient $C_{LmaxT}$ is plotted versus the velocity ratio $V_{ratio}$ in figure 9.17. At low values of the velocity ratio, $C_{LmaxT}$ is small, but rises sharply and peaks around $V_{ratio} \approx 1$; then it drops to very small values for large velocity ratio values.

Figures 9.18 and 9.19 show the variation of $C_{LrmsT1}$ and $C_{LrmsT2}$ versus $V_{ratio}$. Comparing the results for the maximum and the rms lift force coefficients, it is apparent that all coefficients show similar behaviour if plotted versus $V_{ratio}$; the maxima occur around $V_{ratio} \approx 1$. All have a relatively large scatter, however.

### 9.5  Conclusions From the In-line Cylinder Oscillation in Waves Plus Current Tests

The test case under consideration is the most complex combination of structural motion and conditions of fluid flow within this research work. The main objective of this study has been to investigate the validity of Morison equation extensions to such combined flow conditions and to introduce the governing parameters. An additional objective has been to provide the force coefficients for the most appropriate load models. The data analysis for the present test series resulted in the following specific conclusions:

*Direct Observations from the Data*

Direct analyses of the data (regardless of any load model) have shown that the statistical values of the measured force components depend upon the combined velocity variables:

1. There is not a very good correlation between the steady component of the measured forces $Fm$ and the steady velocity component $V^2$; correlations between $Fm$ and the combined velocity variables, e.g. $(V^2 + V u_m + V \dot{x}_m)$, are distinctly better.

2. Good correlations are obtained between $F_{rms0}$ - the root mean square of the oscillatory component of the in-line measured force - and velocity components that include the steady current velocity. The highest correlation coefficient value $R^2$ is obtained if $F_{rms0}$ is plotted

versus the maximum relative velocity squared, i.e. $(V+u_m+\dot{x}_m)^2$.

3. The above conclusions and other observations imply that the proper load model for predicting the hydrodynamic interaction force in the combined flow field must include all velocity components; the independent flow field approach cannot lead to a proper solution.

## *Evaluations of the In-line Load Models*

1. Though an assumption of the independent flow fields provides improper solutions in the light of direct observations from the data, two extensions of the Morison equation based on this approach (model III and IV) have been examined. As expected, the results have shown that these models do not form appropriate load models for the combined flow field; the coefficients for these models exhibit considerably more scatter than for the relative velocity models I and II and require generally large values that do not resemble the coefficients for degenerate flow conditions.

2. Two extensions of the Morison equation based on the relative velocity approach (model I and II) are more appropriate models for predicting the hydrodynamic interaction forces. Both models have relatively stable coefficients and the values resemble those for the simpler flow conditions. Model II is in applications a linear form of model I and the force histories calculated with this model fit the measured force histories even better than the well-known quadratic form of the relative velocity model.

## *Force Coefficients*

1. There is a linear relationship between the drag coefficient for the quadratic relative velocity $C_{Dr}$ and the drag coefficient for the linear relative velocity $C_{Drl}$ ($C_{Drl} \approx 0.73\ C_{Dr}$). As expected, the inertia coefficients for the two models are almost identical ($C_{Mlr} \approx C_{Mr}$).

2. There is no single parameter with which the drag and inertia coefficients may be correlated without the need for other parameters.

3. The ratio between total oscillatory velocity ($u_m+\dot{x}_m$) and the steady velocity ($V$) is a very significant parameter for an oscillating cylinder in a waves plus current flow field. Both the drag and the inertia coefficients ($C_{Dr}$ and $C_{Mr}$) are fairly stable when plotted versus this ratio.

4. Large drag coefficient values correspond to $V_{ratio} = \dfrac{u_m + \dot{x}_m}{V} \approx 1$; whereas the inertia coefficient values are then small.

5. The maximum and rms lift force coefficients show similar behaviour if plotted versus the velocity ratio $V_{ratio}$. Peaks of the maximum and rms lift force coefficients also occur around $V_{ratio} \approx 1$.
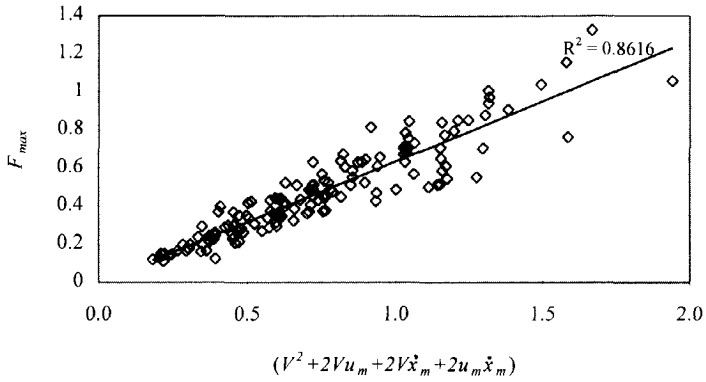
Figure 9.2   In-line Cylinder Oscillation in Waves and Current, $F_{max}$ Plotted Versus $(V^2+2Vu_m+2Vx_m+2u_m\dot{x}_m)$
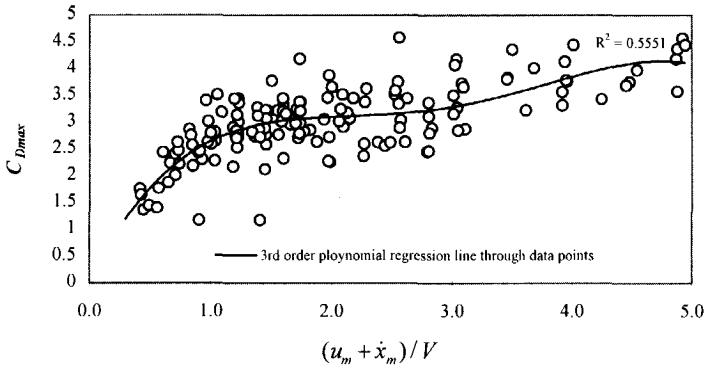


Figure 9.3   In-line Cylinder Oscillation in Waves and Current, $C_{Dmax}$ Plotted Versus $V_{ratio}$
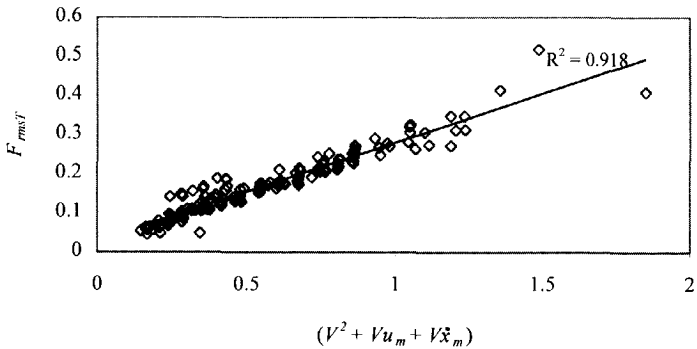


Figure 9.4   In-line Cylinder Oscillation in Waves and Current, $F_{rmsT}$ Plotted Versus $(V^2+Vu_m+V\dot{x}_m)$
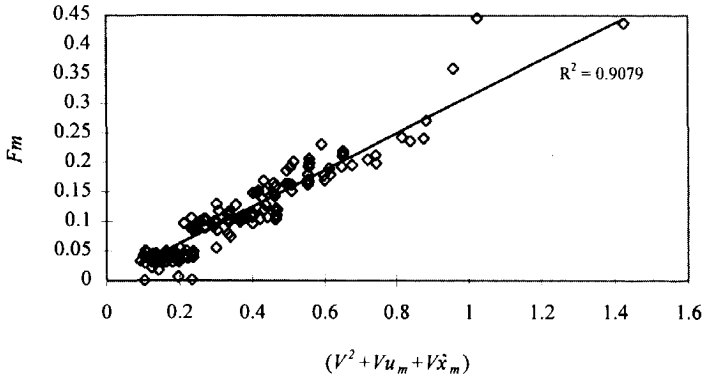
Figure 9.5  In-line Cylinder Oscillation in Waves and Current, $Fm$ Plotted Versus $(V^2 + Vu_m + V\dot{x}_m)$
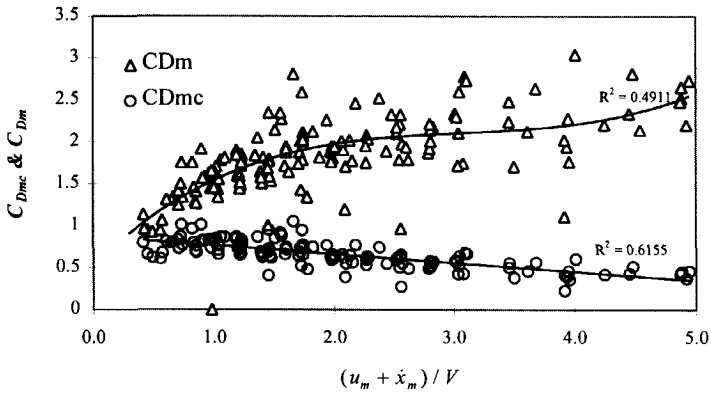


Figure 9.6  In-line Cylinder Oscillation in Waves and Current, $C_{Dmc}$ and $C_{Dm}$ Plotted Versus $V_{ratio}$
Solid Lines: 3rd Order Polynomial Regression Lines Through Data Points
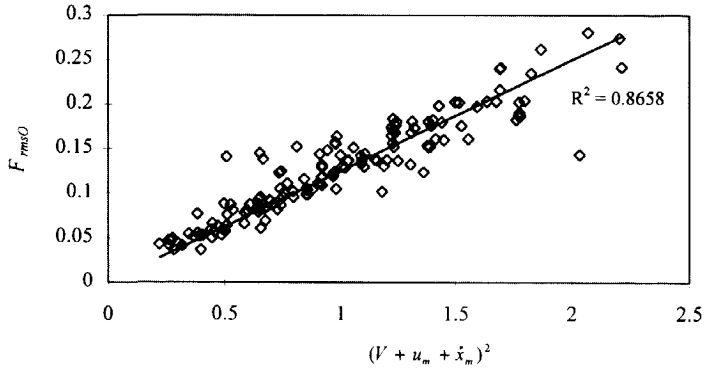


Figure 9.7  In-line Cylinder Oscillation in Waves and Current, $F_{rmsO}$ Plotted Versus $(V + u_m + \dot{x}_m)^2$

135
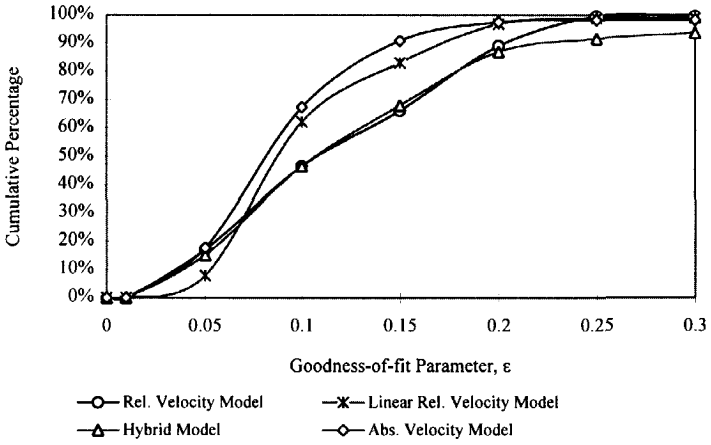
Figure 9.8   In-line Cylinder Oscillation in Waves and Current, Comparison of Quality of Fit for Given Load Models Using Best Coefficients
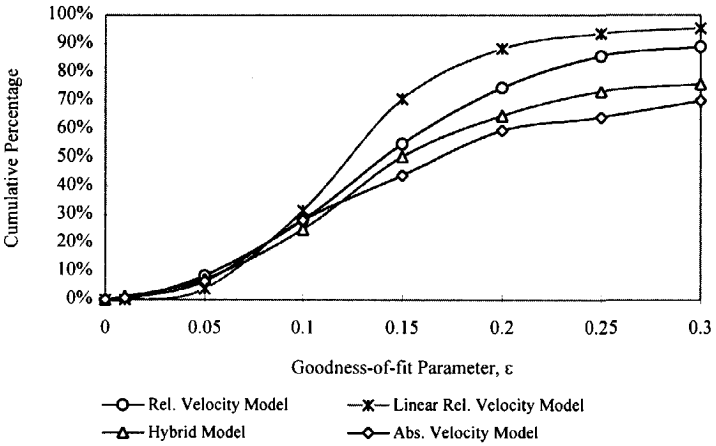


Figure 9.9   In-line Cylinder Oscillation in Waves and Current, Comparison of Quality of Fit for Given Load Models Using Smoothed Coefficients
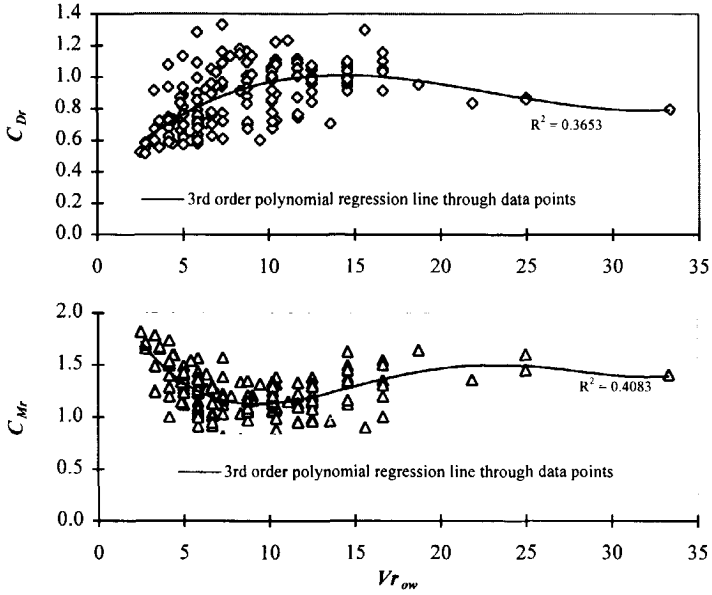
Figure 9.10  In-line Cylinder Oscillation in Waves and Current, $C_{Dr}$ and $C_{Mr}$ Plotted Versus $Vr_{ow}$
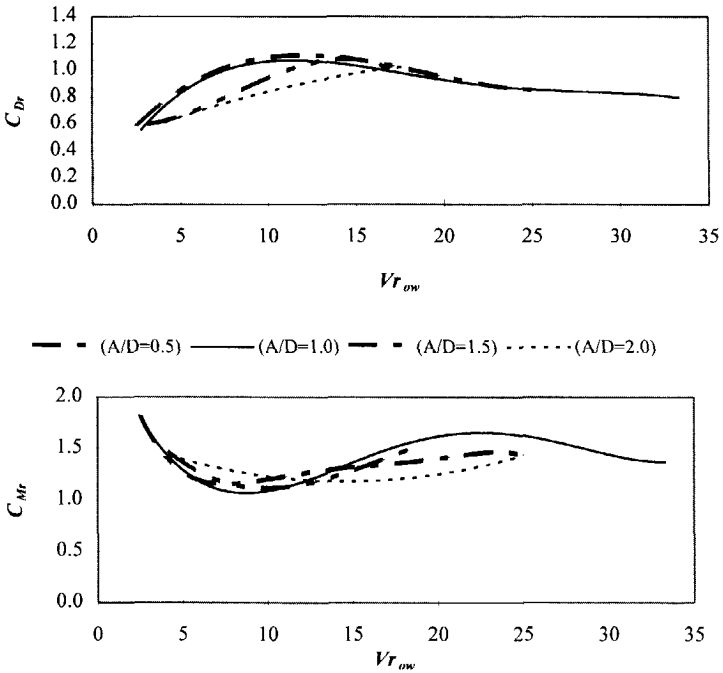


Figure 9.11  In-line Cylinder Oscillation in Waves and Current, $C_{Dr}$ and $C_{Mr}$ Plotted Versus $Vr_{ow}$
Lines: 3rd Order Polynomial Regression Lines Through Data Points

137
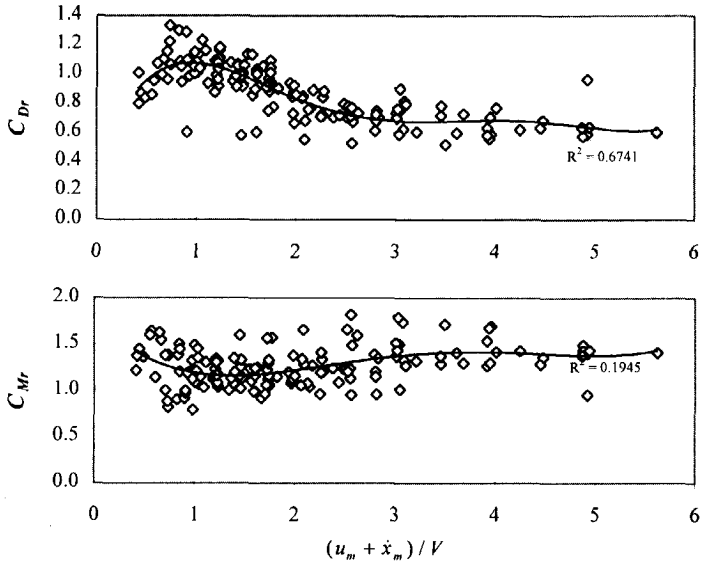
Figure 9.12 In-line Cylinder Oscillation in Waves and Current, $C_{Dr}$ and $C_{Mr}$ Plotted Versus $V_{ratio}$ Lines: 3rd Order Polynomial Regression Lines Through Data Points
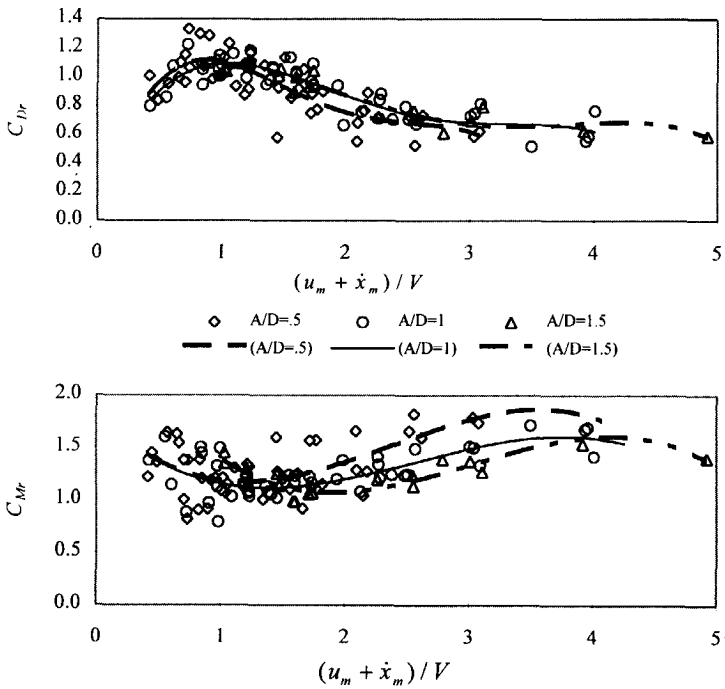


Figure 9.13 In-line Cylinder Oscillation in Waves and Current, $C_{Dr}$ and $C_{Mr}$ Plotted Versus $V_{ratio}$ for Various $A/D$; Lines: 3rd Order Polynomial Regression Lines Through Data Points
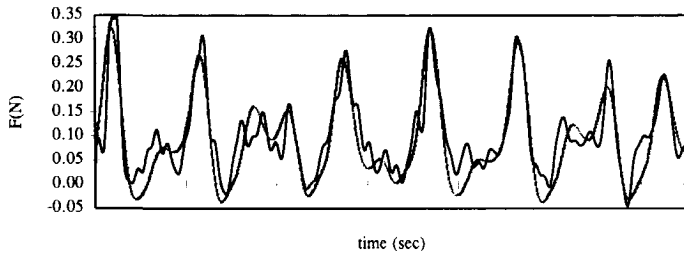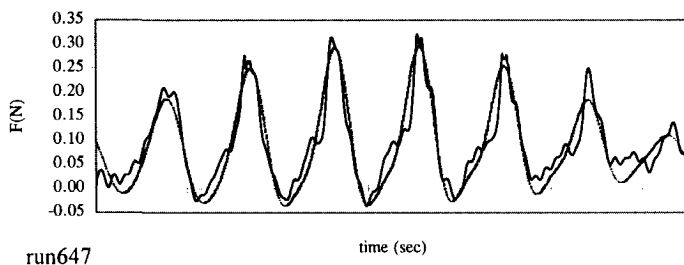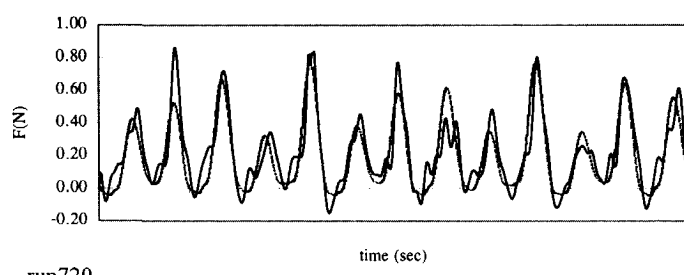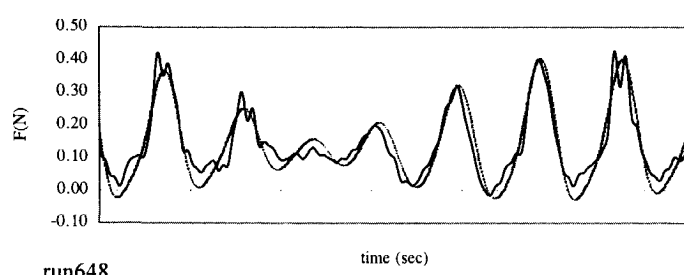
Figure 9.14  Examples of Measured and Predicted Hydrodynamic Force Time Histories Using the
Relative Velocity Model and Smoothed Coefficients
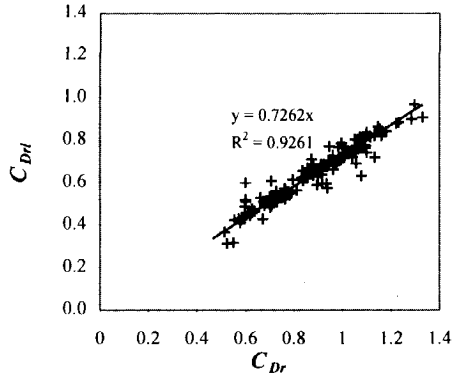
Figure 9.15  In-line Cylinder Oscillation in Waves and Current, Comparison of Drag Coefficients for Model I and II
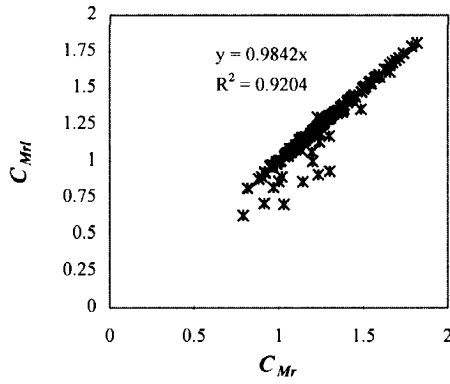


Figure 9.16  In-line Cylinder Oscillation in Waves and Current, Comparison of Inertia Coefficients for Model I and II
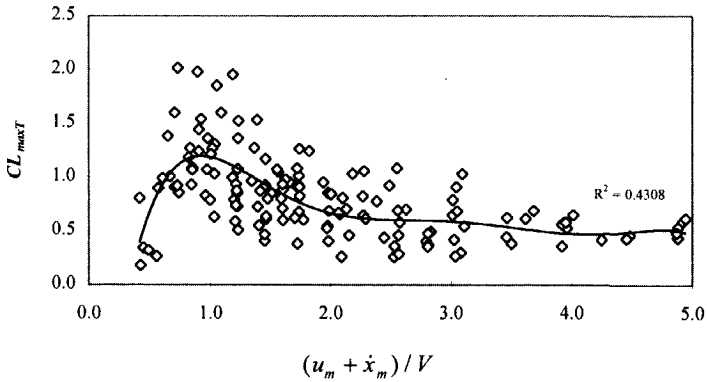


Figure 9.17  In-line Cylinder Oscillation in Waves and Current, Maximum Lift Force Coefficient $C_{l,max}$ Plotted Versus $V_{ratio}$; Solid Line: 4th Order Regression Line Through Data
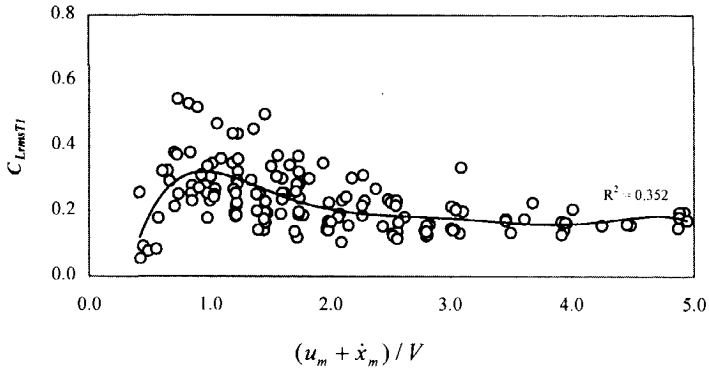
Figure 9.18  In-line Cylinder Oscillation in Waves and Current, RMS Lift Force Coefficient $C_{LrmsT1}$ Plotted Versus $V_{ratio}$; Solid Line: 4th Order Regression Line Through Data Points
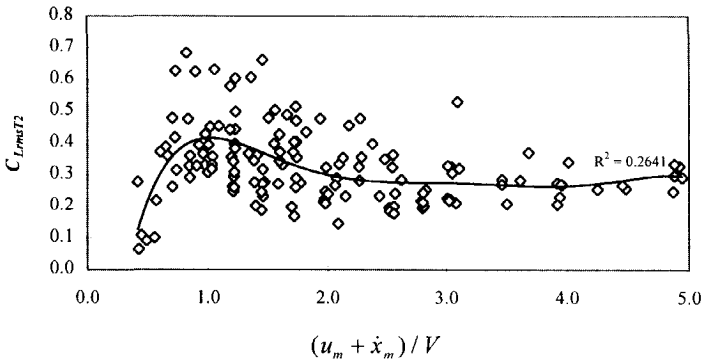


Figure 9.19  In-line Cylinder Oscillation in Waves and Current, RMS Lift Force Coefficient $C_{LrmsT2}$ Plotted Versus $V_{ratio}$; Solid Line: 4th Order Regression Line Through Data Points

# CHAPTER 10

# A Universal Force Model

## 10.1 Introduction

The complex problem of the hydrodynamic interaction between fluid flows and (oscillating) slender cylinders has been studied for different flow conditions separately in the foregoing chapters. For engineering practice, however, it is desirable to combine the separate solutions to provide a universal answer. This chapter discusses the possibility of a universal force model for estimating the hydrodynamic forces on vertical cylinders in combined flow conditions. The results obtained for various flow conditions are compared.

## 10.2 Characteristics of a Universal Solution

A universal load model applicable to any flow condition should have the following characteristics:

- *Specialisation to simpler cases*:
    The parameters involved must allow the model to remain valid for special cases when the flow conditions are simpler.

- *Dependent on common and universally applicable dimensionless parameters*
    The force coefficients should depend on some general nondimensional parameters. These general parameters are also to be appropriate for the simpler cases by degenerating to the similarly simplified nondimensional parameters.

- *Fixed coefficients*
    The coefficients for the universal load model should be applicable for all conditions and combinations of conditions; they should correlate well with the relevant dimensionless parameters.

## 10.3 Promising Model Forms

The common conclusion from the results for the various combinations of single flow conditions is that a model for estimating the hydrodynamic forces must include the total (relative) velocity. Of the various models considered, two models were shown to have the most promise. These two models are:

• An extension of the Morison equation based on the relative velocity approach:

143

$$F = \frac{1}{2}\rho D C_{Dr}|V+u-\dot{x}|(V+u-\dot{x}) + \frac{\pi D^2}{4}\rho C_{Mr}\dot{u} - \frac{\pi D^2}{4}\rho(C_{Mr}-1)\ddot{x} \qquad (10.1)$$

- A postulated linear form of this model:

$$F = \frac{1}{2}\rho D C_{Drl}(V+u_m+\dot{x}_m)(V+u-\dot{x}) + \frac{\pi D^2}{4}\rho C_{Mrl}\dot{u} - \frac{\pi D^2}{4}\rho(C_{Mrl}-1)\ddot{x} \qquad (10.2)$$

Both models satisfy the first criterion for a universal model; the associated velocity and acceleration terms can simply be omitted for the degenerate cases. The degree to which other criteria are met is discussed below by comparing the results obtained for various flow conditions.

## 10.4 Governing Parameters

As already discussed in preceding chapters, the force coefficients in a combined flow field depend upon many dimensionless parameters. The goal here is to find some common parameters that will be equally applicable to the general case of an oscillating cylinder in a wave-current flow field and to the simpler flow conditions.

The results for the general test case discussed in chapter 9 have suggested that a form of Keulegan-Carpenter number and a velocity ratio are the most important parameters. The behaviour of the force coefficients expressed in terms of these parameters for all test cases studied is surveyed in the following section.

## 10.5 Summary of Coefficients Obtained

In order to study the behaviour of the force coefficients - for all test cases - as a function of the most relevant nondimensional parameters in a reasonably transparent manner, the results may be compared in three stages:

1. Comparing results for test cases without a current, being:
   - Cylinder oscillations in still water (O)
   - Fixed cylinder in waves (W)
   - Cylinder oscillations in waves (OW)

2. Comparing results for test cases with a current, being:
   - Cylinder oscillations in current (OC)
   - Fixed cylinder in waves and current (WC)
   - Cylinder oscillations in waves and current (OWC)

3. Comparing results for all test cases collectively.

The most significant parameter for the tests without a current (O, W and OW) is a Keulegan-Carpenter number, while additionally the ratio of the amplitude of (relative) oscillatory velocity to the steady current $V_{ratio}$ is important for the second category.

The force coefficients for the two chosen models are compared first to find the relation between

144

the coefficients in these models. Then, the results for tests cases within each of the above categories are compared in the subsequent sections.

### 10.5.1 Comparison of the Force Coefficients for the Two Models

The force coefficients for the linear version of the relative velocity model (equation 10.2) have been determined for all test cases using the least squares technique. For the test series of cylinder oscillations in still water and the fixed cylinder in waves, the drag coefficients obtained are different from those for the linear form of the Morison equation in each single mode test (model IV in tables 5.2 and 5.5) because a factor of $8/3\pi$ is included in the theoretical linearisation of the original Morison equation. Thus, the drag coefficients from single mode tests (for model IV) have been scaled to correspond to coefficients for the chosen linear load model of equation 10.2.

As shown in figure 10.1, there is a linear relationship between the drag coefficients for the two chosen load models of equations 10.1 and 10.2, $C_{Drl} \approx 0.79 C_{Dr}$; the inertia coefficients are almost identical, $C_{Mrl} \approx C_{Mr}$ (the inertia coefficient values for the tests without waves are plotted as $C_A + 1$ in this figure).

Having such linear relationships between the coefficients for the two models, it is only necessary to discuss the results obtained for the relative velocity model.

### 10.5.2 Tests Without a Current

The combined Keulegan-Carpenter number of $KC_{ow} = KC_o + KC_w$ can be used to compare the results for tests in this category. The drag and inertia coefficients ($C_{Dr}$ and $C_{Mr}$) for these tests are plotted versus $KC_{ow}$ in figure 10.2 in which the inertia coefficient $C_{Mr}$ is plotted as $C_A + 1$ for the pure oscillation tests. Though there are irregularities in the variation of drag and inertia coefficients with $KC_{ow}$, the results for all three test series without current (O, W, OW) are comparable; they show the same trend. Overall, the drag coefficients obtained from the tests with cylinder oscillations in waves are smaller than those from the tests with a fixed cylinder in waves or the tests with cylinder oscillations in still water. The reverse is true for the inertia coefficients obtained from the combined flow field; they are larger than those from the single mode tests. The differences between the families of force coefficients decrease as $KC_{ow}$ increases, by the way. Furthermore, this figure confirms the importance of the (combined) Keulegan-Carpenter number for the flow conditions without a current.

### 10.5.3 Tests With a Current

When a current is added to a flow field, a nondimensional parameter involving current velocity is required in addition to $KC$. As discussed in the preceding chapters, a reduced velocity or a velocity ratio is a suitable additional dimensionless variable for flow conditions with a steady current.

Figure 10.3 shows how the force coefficients correlate with the velocity ratio $V_{ratio} = (u_m + \dot{x}_m)/V$ for all three test cases with a current (OC, WC and OWC). The level of scattering for both force coefficients is high, especially for the inertia coefficient. However, the force coefficients depend

upon the Keulegan-Carpenter number in addition to the velocity ratio; therefore, such scattering in $C_{Dr}$ and $C_{Mr}$ values may be acceptable.

The drag and inertia coefficients obtained from the three test cases with a current are also plotted versus the reduced velocity $Vr_{ow} = Vr_o + Vr_w$ in figure 10.4. A rapid change in coefficient values is observed for the cylinder oscillation plus current tests when $Vr_{ow} \approx 5$. This is associated with the lock-in phenomenon. There are no such rapid changes in $C_{Dr}$ values obtained from the cylinder oscillation in a combined waves plus current flow field; the behaviour of the $C_{Dr}$ curve is relatively smooth. This observation suggests that the lock-in phenomenon may not occur for the same reduced velocity range; the combination of two oscillatory motions (cylinder oscillation and waves) changes the vortex shedding pattern.

As seen in figure 10.4, the correlation of the inertia coefficient values $C_{Mr}$ with $Vr_{ow}$ is relatively better than that of $C_{Mr}$ with $V_{ratio}$. The variation of $C_{Mr}$ with $Vr_{ow}$ is just opposite to that of $C_{Dr}$ with $Vr_{ow}$; when one is high, the other is low and vice versa.

### 10.5.4 All Tests

In order to investigate the possibility of a universal load model, results from all tests are presented in the same plot in figure 10.5. In this figure, a dimensionless parameter combining the Keulegan-Carpenter numbers and the reduced velocities is used:

$$KC_{TC} = KC_o + KC_w + Vr_o + Vr_w \tag{10.3}$$

Figure 10.5a shows the drag coefficient values obtained from all test runs as a function of $KC_{TC}$. Given the fact that only one dimensionless parameter is used in this figure, the results are consistent for the different test cases. The regression lines for the various test series show only small differences but there is a lot of scatter around the regression line(s), especially for low values of $KC_{TC}$. A similar outcome is observed for the inertia coefficient values in figure 10.5b. The heavy solid line in each of these plots is a regression line through all data points regardless of the type of test.

In addition to above comparisons, the force coefficients obtained from all tests are plotted versus $KC_{ow}$ for various reduced velocity values ($Vr_{ow}$) in figure 10.6. The behaviour of the coefficients with these two nondimensional parameters is very similar and meaningful; it appears that $KC_{ow}$ and $Vr_{ow}$ are adequate to determine the force coefficients for all flow conditions studied in the present work.

### 10. 6 Application of the Linear Universal Model

Substituting the linear universal model (equation 10.2) into the equation 8.1 gives a linearised equation of motion:

$$m\ddot{x} + c\dot{x} + kx = \frac{1}{2}\rho D C_{Drl}(V + u_m + \dot{x}_m)(V + u - \dot{x}) + \frac{\pi D^2}{4}\rho C_{Mrl}\dot{u} - \frac{\pi D^2}{4}\rho(C_{Mrl} - 1)\ddot{x} \tag{10.4}$$

This can be rearranged as:

$$m_t\ddot{x} + [c + \frac{1}{2}\rho D C_{Drl}(V + u_m + \dot{x}_m)]\dot{x} + kx = \frac{1}{2}\rho D C_{Drl}(V + u_m - \dot{x}_m)(V + u) + \frac{\pi D^2}{4}\rho C_{Mrl}\dot{u} \qquad (10.5)$$

where $m_t$ is total mass per unit length including the added mass

$$m_t = m + \rho\frac{\pi D^2}{4}(C_{Mrl} - 1) \qquad (10.6)$$

Equation 10.5 is a linear equation with constant coefficients, although there is still a relatively minor degree of iteration involved since the coefficient of the velocity dependent term on the left hand side involves the maximum of the cylinder oscillating velocity $\dot{x}_m$ which in fact depends on the solution of the equation of motion 10.5. However, this is significantly different from iteration at each and every time step for the nonlinear relative velocity model 10.1.

It should be noted that other linearised solutions often involve time-dependent coefficients; in practice these solutions are typically approximated by eliminating the time-dependent coefficients.

The structural damping factor $c$ may be replaced by a quantity that is proportional to the structural dimensionless damping factor $\xi_s$; $c = 2\,m\,\xi_s\,\omega_n$, where $\omega_n$ is the natural frequency of the structure. One may then restate equation 10.5 in terms of a total damping $\xi_t$ as:

$$m_t\ddot{x} + 2m_t\xi_t\omega_n\dot{x} + kx = \frac{1}{2}\rho D C_{Drl}(V + u_m + \dot{x}_m)(V + u) + \frac{\pi D^2}{4}\rho C_{Mrl}\dot{u} \qquad (10.7)$$

where $\xi_t$ is the sum of structural and fluid damping components:

$$\xi_t = \xi_s\frac{m}{m_t} + \frac{C_{Drl}\rho D (V + u_m + \dot{x}_m)}{4 m_t \omega_n} \qquad (10.8)$$

The second term in equation 10.8 is the fluid damping; it increases with the amplitude of the relative velocity.

As already said, equation 10.7 is a linear ordinary differential equation with constant coefficients. It can be solved for the response of the structure by adopting an iterative procedure as follows:

1.  Assume or estimate the maximum response value for the structure
2.  Calculate the maximum structure velocity $\dot{x}_m$.
2.  Determine the force coefficients from the available data.
3.  Solve equation 10.7 exactly to determine the structural response.
4.  Compare the calculated response to the estimated one. If the difference between these is more than a desired value, then select a corrected maximum response value.
5.  Repeat steps one through four until a good match for the response is reached.

## 10.6 Conclusions: Is a Universal Model Possible?

Evidence has been produced which supports that a universal load model in which the force coefficients depend on some general dimensionless parameters is indeed possible.

The results strongly suggest that the linear version of the relative velocity extension of the Morison equation is applicable to all test cases reported in this dissertation. This model, which is linear in its practical application, predicts the hydrodynamic force as well as (or even better than) the full quadratic relative velocity form.

The results further suggest that the appropriate nondimensional parameters for characterising the force coefficients for a combined flow condition are:

1. A general Keulegan-Carpenter number which can be defined as:

$$KC_{ow} = KC_o + KC_w = \frac{u_m T_w + \dot{x}_m T_o}{D} \quad \text{or}$$

$$KC_{TC} = KC_o + KC_w + Vr_o + Vr_w = \frac{(V + u_m)T_w + (V + \dot{x}_m)T_o}{D}$$

2. The ratio between the (relative) oscillatory velocity and the steady current velocity, defined as: $V_{ratio} = \frac{u_m + \dot{x}_m}{V}$ or a combined reduced velocity such as:

$$Vr_{ow} = Vr_o + Vr_w = \frac{V T_w + V T_o}{D}$$

148
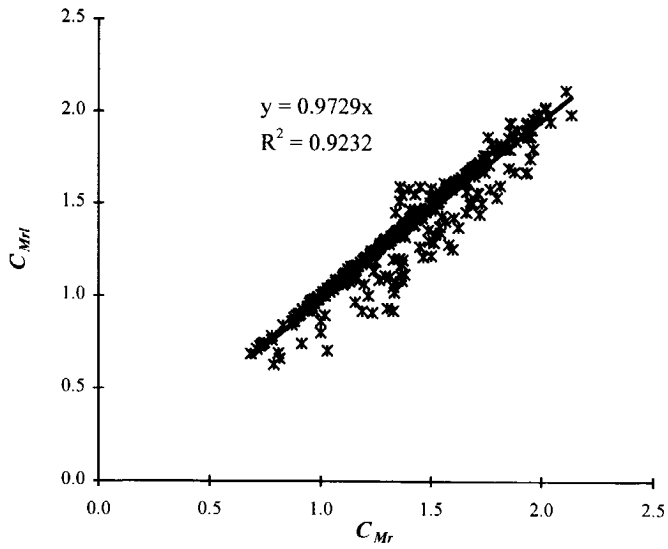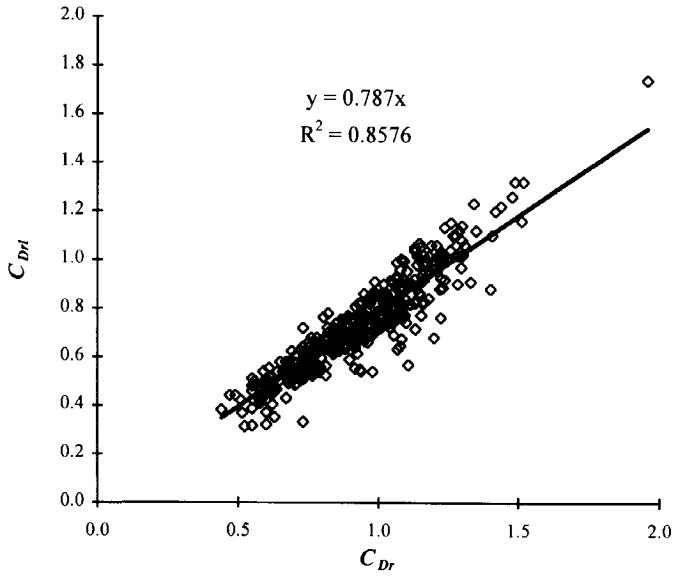
Figure 10.1  All Tests, Comparison Between the Force Coefficients Obtained for the Two Chosen Models

149
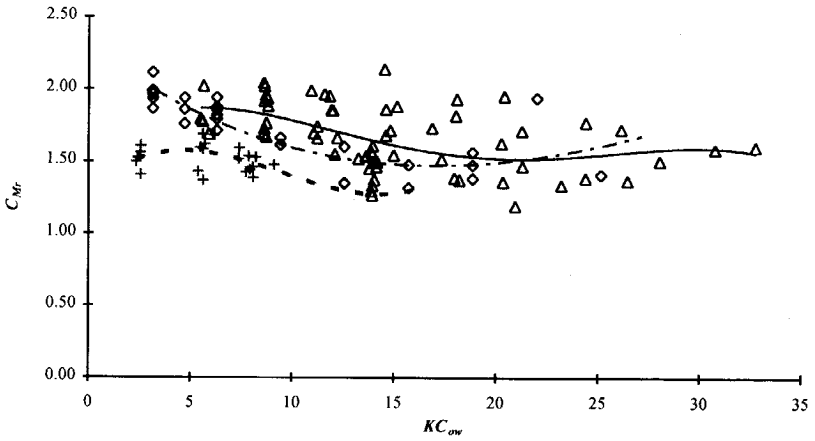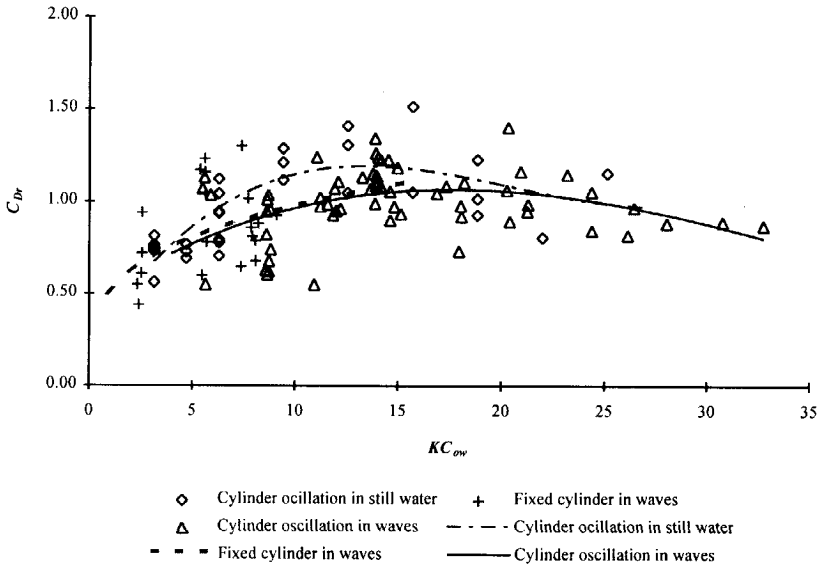
Figure 10.2 Tests Without a Current, Drag and Inertia Coefficients Plotted Versus $KC_{ow}$;
Lines: 3rd Order Polynomial Regression Lines Through Data Points

150
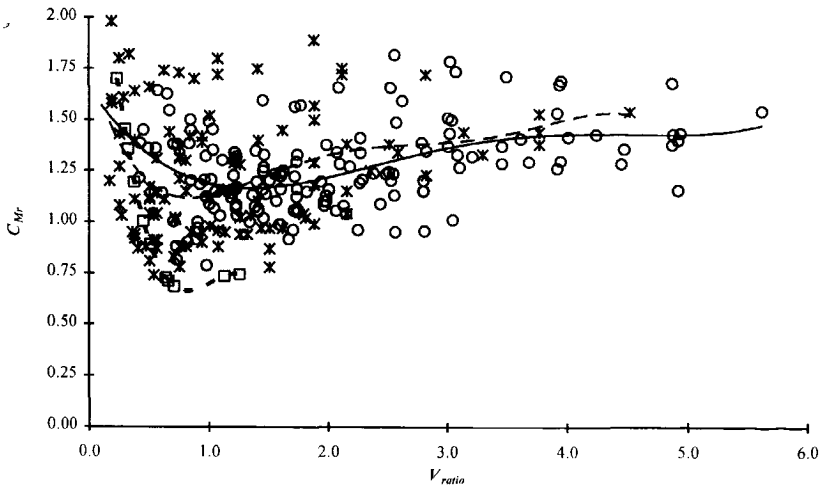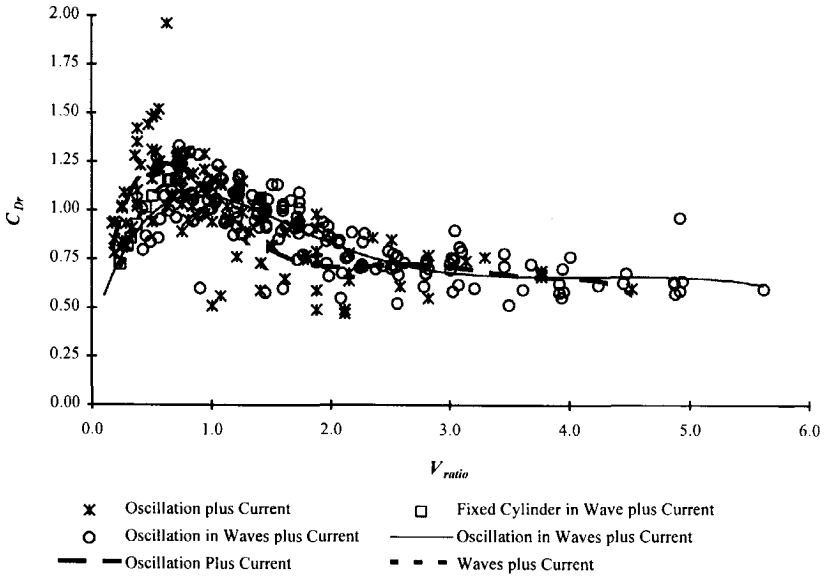
Figure 10.3  Tests With a Current, Drag and Inertia Coefficients Plotted Versus $V_{ratio}$
Lines: 4th Order Polynomial Regression Lines Through Data Points
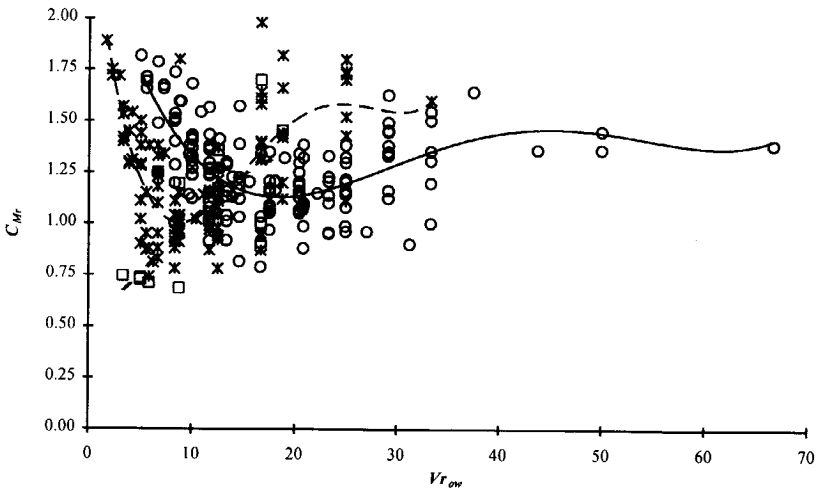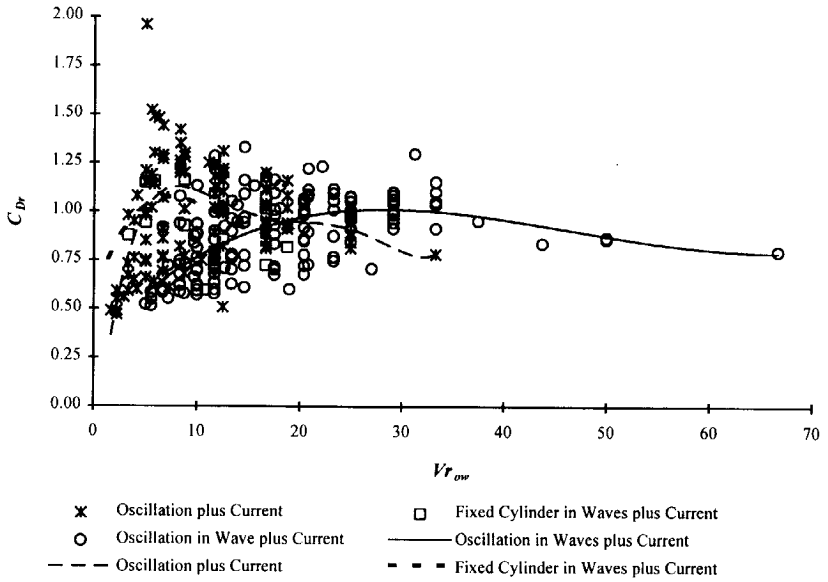
Figure 10.4 Tests with a Current, Drag and Inertia Coefficients Plotted Versus $Vr_{ow}$
Lines: 4th Order Polynomial Regression Lines Through Data Points
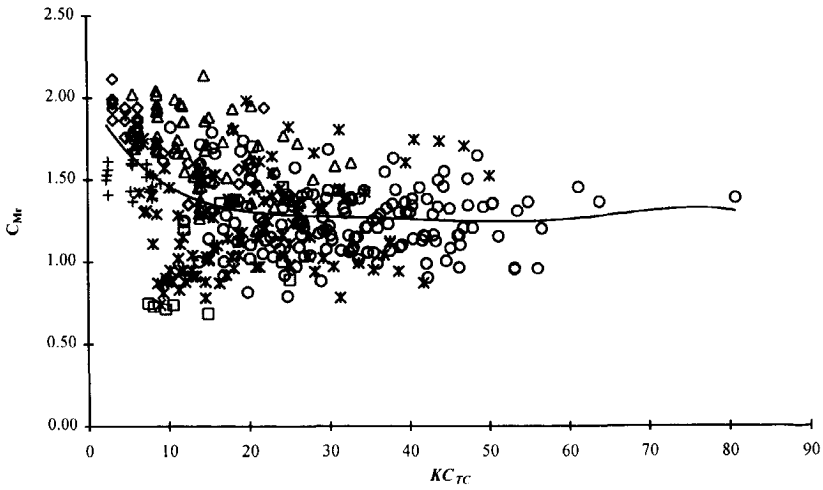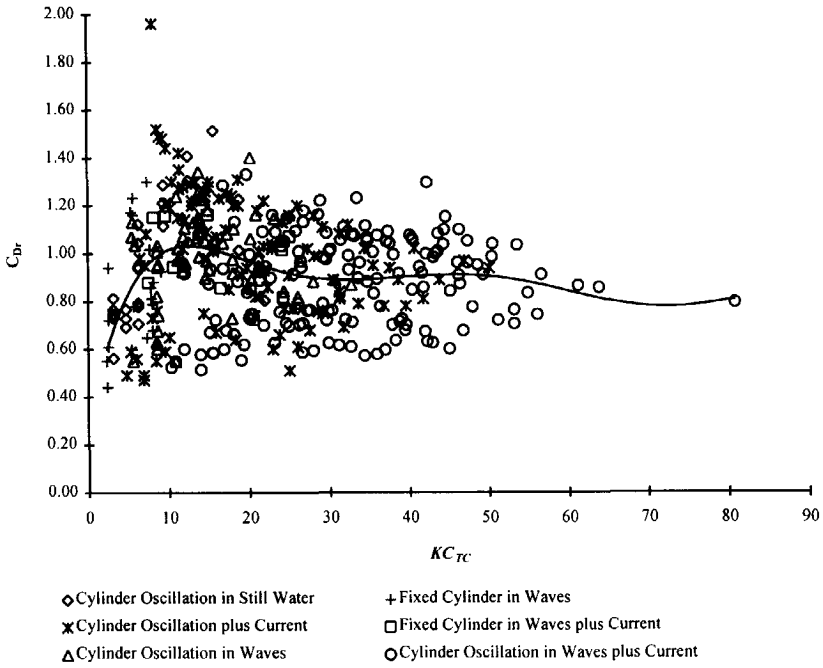
Figure 10.5 All Tests, Drag and Inertia Coefficients Plotted Versus $KC_{TC}$; Solid Lines: 4th Order Polynomial Regression Line Through Data Points for All Tests
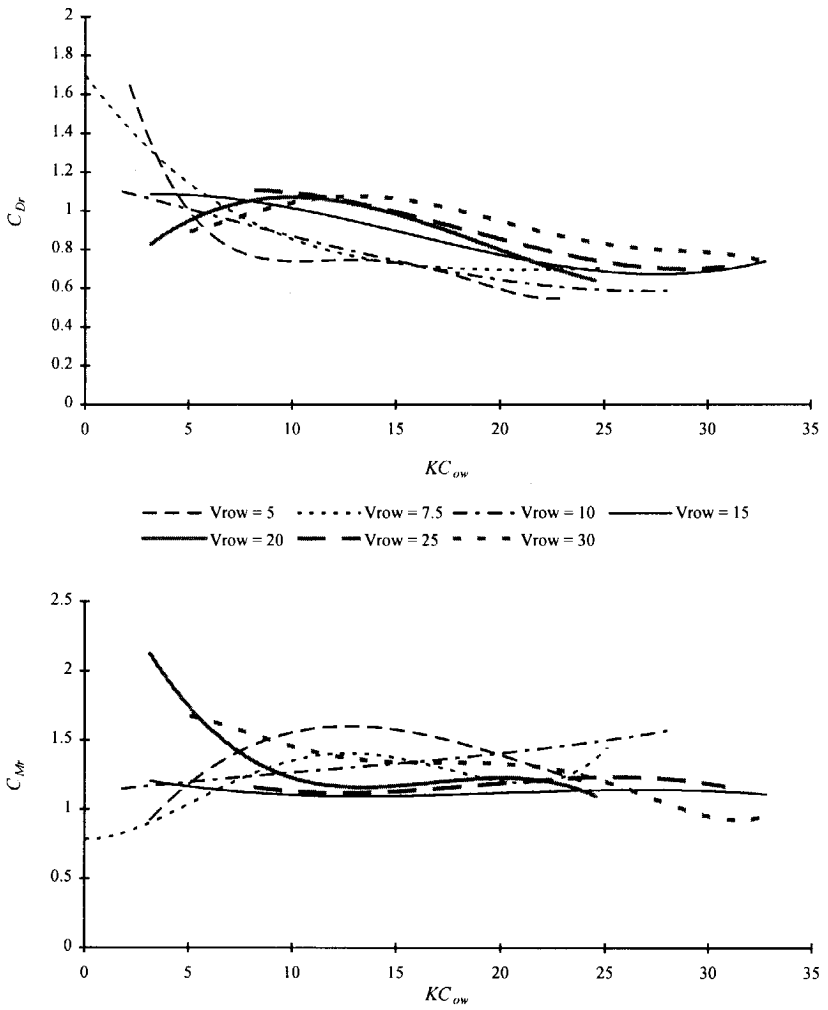
Figure 10.6 All Tests, Drag and Inertia Coefficients Plotted Versus $KC_{ow}$ as a Function of $Vr_{ow}$
Lines: 3rd Order Polynomial Regression Lines Through Data Points

154

# CHAPTER 11

# Conclusions and Recommendations

## 11.1 General

The present study was undertaken to improve the knowledge of total hydrodynamic interaction between a fluid flow (wave and current) on the one hand and slender marine structures on the other. The experimental work has been an attempt to fill some of the vast multi-dimensional parameter space formed by the single mode cases of current only, waves only and oscillation only.

The present experimental work has the following advantages compared to earlier studies:

- All possible flow conditions (that the available laboratory facilities allowed) have been included.
- The same apparatus and test setup have been used for all test cases; any possible systematic error is therefore common to all tests.
- Wide ranges of important dimensionless parameters have been covered.

The specific conclusions corresponding to various test cases have been presented at the end of each relevant chapter. However, the essential overall conclusions of the work will be stated in the next section.

## 11.2 Essential Conclusions

To the best of the author's knowledge, the present work contains the only laboratory-scale results for a combined flow field of waves-current-oscillation. In addition to the presentation of results for the actual force coefficients, computational load models and models for the hydrodynamic interaction forces for various test cases are evaluated against measurements.

It is hoped that these results, combined with other important ideas will help engineers to use the available experimental data for estimating hydrodynamic interactions between slender cylinders and a combined waves and current flow field.

### 11.2.1 Evaluations of the In-line Load Models

Various existing and postulated load models have been examined within the present work. These models are mostly extensions of the Morison equation based on two well-known concepts: the independent flow fields approach (absolute velocity model) and the relative velocity approach. Furthermore, linearised forms of the extended Morison equation have been evaluated to

155

determine the validity of such linearised forms. The results of these evaluations are summarised in the following sections.

### 11.2.1.1 Absolute versus Relative Velocity Model

The suitability of load models based on the assumption of independent flow fields (absolute velocity models) and relative velocity approaches have been evaluated using the following criteria:

- Direct indications from the data
- Quality of fit of the load models
- Coefficient stability

The behaviour of the measured in-line forces against various combinations of variables has been studied to see what the data themselves without any recourse to a force model indicate. The statistical values of the measured forces were used for this purpose. The most important results are as follows:

- The maximum in-line force on the oscillating cylinder in a combined flow field is not equal to the sum of the maximum in-line forces caused by each degenerate flow field separately.

- There is a poor correlation between the steady component of the measured forces $Fm$ and the steady velocity component $V^2$, while there are distinct correlations between $Fm$ and combined velocity variables that include the oscillatory velocities, $u_m$ and $\dot{x}_m$.

- Good correlations are obtained between the root mean square of the oscillatory component of the in-line measured force, $F_{rmsO}$, and velocities that include the steady current velocity.

- The three above observations imply that a proper load model for predicting hydrodynamic interaction force in the combined flow field must include all velocity components. A model based on the relative velocity concept can describe the hydrodynamic interaction of a cylinder with a combined flow field; the independent flow field approach cannot lead to a proper solution.

Even though load models based on the independent flow fields approach were considered improper solutions in the light of direct observations from the data, some extensions of the Morison equation based on this approach have nevertheless been examined. As expected, the results show that these models do not form appropriate load models for a combined flow field for the following reasons:

- The basic assumption made in establishing the absolute velocity form of the modified Morison equation does not seem valid. Indeed, using degenerate coefficients corresponding to two independent flow fields leads to a poor force prediction.
- The absolute velocity models predict the measured forces much less consistently than the relative velocity models when smoothed coefficients are used.
- The force coefficients for the absolute velocity models exhibit more scatter and unusually

156

large values that do not resemble values for simple flow conditions.

In contrast, models based on the relative velocity approach give a much better quality of fit; they have relatively stable coefficients and the coefficient values resemble those for simpler test cases. Another advantage of the relative velocity models is that one deals with fewer coefficients in these models.

### 11.2.1.2 Linear versus Quadratic Form

Attempts have been made to examine linearised forms of the Morison equation for use with various flow fields. The hydrodynamic coefficients for such linearised forms have been determined directly from the data. It has been found that a postulated linear form of the generalised Morison equation based on the relative velocity approach gives the same (or even better) quality of fit as the quadratic form, if the associated value of the linearised drag coefficient is used:

$$F = \frac{1}{2}\rho D C_{Dlr}(V + u_m + \dot{x}_m)(V + u - \dot{x}) + \frac{\pi D^2}{4}\rho C_{Mlr}\dot{u} - \frac{\pi D^2}{4}\rho(C_{Mlr} - 1)\ddot{x}$$

where:
$V$ = the steady current velocity,
$u, \dot{u}$ = instantaneous orbital velocity and acceleration,
$u_m$ = amplitude of orbital velocity,
$\dot{x}, \ddot{x}$ = instantaneous cylinder velocity and acceleration,
$\dot{x}_m$ = amplitude of cylinder velocity,
$C_{Dlr}, C_{Mlr}$ = drag and inertia coefficients in the linearised model.

Besides the quality of fit, this linear relative velocity model has the following advantages:

- In contrast to common practice in linearised solutions, there is no need for approximation or simplification.
- The velocity terms involved are easy to estimate.
- Since it is linear in application, it facilitates a dynamic analysis.

### 11.2.2 Possibility of a Universal Model

One objective of the present work has been to investigate the possibility of a universal load model applicable to all possible flow conditions. This universal load model should degenerate to simpler flow conditions and coefficients should be dependent on common and universal dimensionless parameters. Furthermore, the hydrodynamic coefficients for such a model should be stable and correlate well with the relevant parameters. The results presented here support the possibility of such a universal load model in which the force coefficients depend on some general dimensionless parameters. Both the relative velocity extension of the Morison equation and the linear version of this model satisfy these criteria for a universal model in the flow conditions considered. The results strongly suggest that the linear version of the relative velocity form of the Morison equation extension is applicable to all test cases reported in this dissertation.

157

### 11.2.3 Hydrodynamic Coefficients

The following more specific results have been obtained from the present experimental study concerning the hydrodynamic coefficients of the promising load models (relative velocity and the linear relative velocity models):

- The results have shown that there is a linear relationship between the drag coefficients for the two promising load models, $C_{Dlr} \approx 0.78 C_{Dr}$; the inertia coefficients are almost identical, $C_{Mlr} \approx C_{Mr}$.

- The drag and inertia coefficients for a combined flow field are significantly different from those for a simple flow field when plotted versus conventional dimensionless parameters. This implies that the extension of the Morison equation is not an aspect of the choice of a reference system alone; a different set of coefficients would have to be used to reflect the combination of the two separate flow effects.

- Generally the drag coefficient for the relative velocity extension of the Morison equation is somewhat smaller - in the rage of dimensionless parameters considered - than that for the original Morison equation.

- In the light of the above conclusion, it is obvious that the engineering practice of using the coefficients for regular waves to describe hydrodynamic forces from a combined waves and current flow field cannot be justified.

- There is no single parameter with which the drag and inertia coefficients may be correlated without the need for other parameters. However, the correlation between the force coefficients and some parameters are better than with other parameters. The results suggest that the appropriate nondimensional parameters for a combined flow condition might be a general (total) Keulegan-Carpenter number $KC_{TC}$ and the velocity ratio $V_{ratio}$ (or the reduced velocity $Vr_{ow}$).

### 11.2.4 Transverse Force Coefficients

Due to time and space limitations, the transverse force has not been studied fully in this dissertation. However, some results have been presented to demonstrate the significance of the lift force in a combined flow field. The main conclusions of the transverse force analyses are summarised below:

- The maximum lift force is of the same order of magnitude as the in-line force for intermediate Keulegan-Carpenter numbers in a combined flow field.

- The frequency of the lift force $f_v$ in oscillatory flow plus current depends on the total (relative) velocity, and increases with increasing (total) Keulegan-Carpenter number, $KC_{ov}$.

- Various maximum and rms lift force coefficients have been calculated by normalising the measured transverse forces. For the test case of cylinder oscillation in waves, the coefficients

normalised by the relative velocity term $(u\text{-}\dot{x})_{max}$ show less scatter than other normalisations.

- Both the peak lift coefficient $C_{l,max}$ and the rms lift force coefficient $C_{l,rms}$ depend on both the Keulegan-Carpenter number and the reduced velocity or the velocity ratio. They are generally smaller than the corresponding in-line force coefficients.

## 11.3 Recommendations for Future Work

There are several continuations of this work that can be of interest. The work should be continued along two paths: First further analysis of the available data is required to investigate the validity of the main conclusions presented here for other tested flow conditions, i.e. in-line cylinder oscillation in irregular waves and transverse cylinder oscillation in waves and/or current. Then, some new experiments are to be carried out to extend the range of the dimensionless parameters and to include other flow and cylinder motion conditions.

### 11.3.1 Further Data Analysis

The test series matrix includes 17 different test cases ( 908 test runs) of which only seven cases (503 test runs) have been studied for this dissertation. Table 11.1 shows particulars of the data analysis performed. Not only should the remaining test series be analysed, some additional work on the test series studied is also needed. For example, the lift force for in-line cylinder oscillations has not been treated completely yet. Further information on the behaviour of the lift force in the combined flow fields is very important.

Further parametric analysis of the coefficients obtained may yield a better means of presenting these data in a more universal way. In the ideal case a coefficient such as $C_D$ could be plotted against some universal parameter as a single curve.

Due to randomness of the sea, it is vital to analyse the data for the test series that include irregular waves in order to investigate the suitability of results from regular waves for application to more realistic flow conditions.

| Flow Conditions | Cylinder Oscillations | | | |
|---|---|---|---|---|
| | None | In-line | | Transverse |
| | | In-line | Lift Force | |
| Still water | — | Fully | Partly | Preliminary |
| Current only | Fully | Fully | Partly | Preliminary |
| Regular waves only | Fully | Fully | Partly | Preliminary |
| Regular waves plus current | Fully | Fully | Partly | Preliminary |
| Irregular waves only | Preliminary | Preliminary | Preliminary | Preliminary |
| Irregular waves plus current | Preliminary | Preliminary | Preliminary | Preliminary |

Table 11.1  Overview of Data Analysis

The results of transverse oscillation tests are very important for a better understanding of the vortex induced vibration of slender cylinders in waves and current flow field. These data have not been studied at all.

## 11.3.2 New Experiments

Even though a full matrix of experiment has been carried out, there are further improvements and extensions that are possible. The experimental setup can be modified to enable newer and more complete testing programmes. Some of the suggestions in the section that follows relate to extending capabilities of the test apparatus.

### 11.3.2.1 Extending Nondimensional Parameter Ranges

As discussed in chapter 2, achieving a wider range of parameters in the present experimental study was not possible; the experimental facilities permitted only subcritical - and for some cases critical - flow conditions; higher oscillation frequencies - important for modeling the lock-in phenomenon - were not possible, for example. Since combinations of the relevant parameters are very important for comparison of experimental data and real situations, a complete test programme must include a wider range of such combinations, see sections 2.5 and 4.7.

A new oscillator is needed to be able to model significant physical phenomena and to cover wider ranges of governing parameters. General specifications of the oscillator needed have been summarised in Shafiee-far (1995a).

### 11.3.2.2 Combined In-line and Transverse Oscillations

It is known that vortex shedding imposes two sets of oscillating forces on cylinders: an oscillating transverse lift force at the vortex shedding frequency and a smaller oscillating in-line drag force at twice the frequency of shedding. For a long slender cylinder, the predominant response is in the transverse direction, but there is an oscillating response in the in-line direction as well. The overall motion often resembles a figure eight, "8", when viewed in the axial direction.

Attempts to carry out model scale forced-oscillation tests with combined in-line and transverse oscillations are rare. However, it should not be difficult to design and construct an apparatus capable of combined motions, preferably allowing both regular and irregular oscillations in both directions. The test cylinder should be mounted vertically on the oscillator in such a way that the cylinder can be oscillated in any arbitrary direction in the horizontal plane. The oscillator should have the following specifications:

- high frequency (up to 3 Hz)
- simultaneous oscillations in the x and y directions
- regular and irregular oscillations

The oscillator should handle an appropriate combination of amplitude and frequency in order to cover some interesting ranges of nondimensional parameters - including the lock-in condition.

160

# Notation and Symbols

## Roman Letters

$A$ : Oscillation amplitude
$B$ : Towing tank width
$c$ : Structural damping
$C_A$ : Added mass coefficient
$C_{Al}$ : Added mass coefficient (linearised Morison equation)
$C_{Aa}$ : Added mass coefficient in absolute velocity model (combined flow fields)
$C_{Ao}$ : Added mass coefficient due to cylinder oscillation in the combined flow fields
$C_{Ar}$ : Added-mass coefficient in relative velocity model (combined flow fields)
$C_{AT}$ : Total added mass coefficient (from harmonic analysis)
$C_D$ : Drag coefficient
$C_{Dm}$ : Mean drag coefficient
$C_{Do}$ : Oscillatory drag coefficient due to the cylinder oscillation in combined flow fields
$C_{Ds}$ : Drag coefficient in steady currents
$C_{Dw}$ : Oscillatory drag coefficient due to waves in the combined flow fields
$C_{DT}$ : Total drag coefficient (from harmonic analysis)
$C_{Dl}$ : Drag coefficient (linearised Morison equation)
$C_{Dr}$ : Oscillating drag coefficient in relative velocity model
$C_{Drl}$ : Oscillating drag coefficient in linear version of relative velocity model
$C_{Da}$ : Oscillatory drag coefficient in absolute velocity model
$C_{Dh}$ : Drag coefficient in hybrid model (equation 9.7)
$C_{alm}$ : The nth added-mass coefficient in harmonic load model
$C_{dhn}$ : The nth drag coefficient in harmonic load model
$C_L$ : Lift force coefficient
$C_{L.max}$ : Peak lift force coefficient
$C_{L.maxT}$ : Peak lift force coefficient in a combined flow field (equations 8.15 and 9.10)
$C_{L.maxR}$ : Peak lift force coefficient in a combined flow field (equations 8.16 and 9.11)
$C_{L.rms}$ : RMS lift force coefficient
$C_{L.rmsT}$ : RMS lift force coefficient in a combined flow field (equations 8.17)
$C_{L.rmsT1}$ : RMS lift force coefficient in a combined cylinder oscillation, waves and current flow field, $Fy_{max}$ normalised by $(V+u_m+\dot{x}_m)^2$ (equation 9.12)
$C_{L.rmsT2}$ : RMS lift force coefficient in a combined cylinder oscillation, waves and current flow field, $Fy_{max}$ normalised by $(V+u_{rms}+\dot{x}_{rms})^2$ (equation 9.13)
$C_{L.rmsR}$ : RMS lift force coefficient in a combined cylinder oscillation and waves flow field, $Fy_{rms}$ normalised by $(u-\dot{x})_{max}^2$ (equations 8.18)
$C_{L.rmsR1}$ : RMS lift force coefficient in a combined cylinder oscillation, waves and current flow field, $Fy_{rms}$ normalised by $(V+u-\dot{x})_{max}^2$ (equations 9.14)
$C_{L.rmsR2}$ : RMS lift force coefficient in a combined cylinder oscillation, waves and current flow field, $Fy_{rms}$ normalised by $(V+u-\dot{x})_{rms}^2$ (equations 9.15)
$C_M$ : Inertia coefficient
$C_{Mw}$ : Inertia coefficient due to waves in the combined flow fields

161

| | | |
|---|---|---|
| $C_{Mr}$ | : | Inertia coefficient in relative velocity model |
| $C_{Mrl}$ | : | Inertia coefficient in linear version of relative velocity model |
| $C_{MT}$ | : | Total inertia coefficient (from harmonic analysis) |
| $C_{Ma}$ | : | Inertia coefficient in absolute velocity model |
| $C_{Mh}$ | : | Inertia coefficient in hybrid model (equation 9.7) |
| $d$ | : | Water depth |
| $D$ | : | Cylinder diameter |
| $F_{max}$ | : | Maximum of the in-line measured force |
| $F_{rmsT}$ | : | Root mean square of the total in-line measured force |
| $Fm$ | : | Mean of the in-line measured force |
| $F_{rmsO}$ | : | Root mean square of the oscillatory component of the in-line measured force |
| $Fy_{max}$ | : | Maximum of the transverse measured force |
| $Fy_{rms}$ | : | Root mean square of the transverse measured force |
| $f_v$ | : | Strouhal frequency |
| $f_o$ | : | Oscillation frequency |
| $f_w$ | : | Wave frequency |
| $g$ | : | Acceleration due to gravity |
| $H$ | : | Wave height |
| $Hs$ | : | Significant wave height |
| $k$ | : | Wave number, structural stiffness |
| $K_{ac}$ | : | Nondimensional parameter proportional to acceleration terms of cylinder oscillation and waves ($= uT_o^2/D$) |
| $KC$ | : | Keulegan-Carpenter number |
| $KC_w$ | : | Keulegan-Carpenter number for waves ($=u_mT_w/D$) |
| $KC_o$ | : | Keulegan-Carpenter number for cylinder oscillations ($=\dot{x}_mT_o/D$) |
| $KC_{ov}$ | : | Keulegan-Carpenter number, total flow for current and oscillation ($=(V+\dot{x}_m)T_o/D$) |
| $KC_{wv}$ | : | Keulegan-Carpenter number, total flow for current and waves ($=(V+u_m)T_w/D$) |
| $KC_{ow}$ | : | Sum of the Keulegan-Carpenter numbers for degenerate flows ($=KC_o+KC_w$) |
| $KC_{owvo}$ | : | Keulegan-Carpenter number for cylinder oscillations in waves and current flow field based on cylinder oscillation period ($=(V+u_m+\dot{x}_m)T_o/D$) |
| $KC_{owvw}$ | : | Keulegan-Carpenter number for cylinder oscillations in waves and current flow field based on wave period ($=(V+u_m+\dot{x}_m)T_w/D$) |
| $KC_r$ | : | Keulegan-Carpenter number, relative flow ($=(u-\dot{x})_{max}T_r/D$) |
| $KC_T$ | : | Keulegan-Carpenter number, total flow for oscillation and wave ($=(u_m+\dot{x}_m)T_w/D$) |
| $KC_{TC}$ | : | Combined Keulegan-Carpenter number ($= KC_o+KC_w+Vr_o+Vr_w$) |
| $m$ | : | Mass |
| $m_a$ | : | Added mass |
| $Re$ | : | Reynolds number |
| $Re_w$ | : | Reynolds number due to waves ($=u_mD/\nu$) |
| $Re_o$ | : | Reynolds number due to cylinder oscillation ($=\dot{x}_mD/\nu$) |
| $Re_{ov}$ | : | Reynolds number due to total flow of oscillation and current ($=(V+\dot{x}_m)D/\nu$) |
| $Re_{owv}$ | : | Reynolds number due to total flow of oscillation, waves and current ($=(V+u_m+\dot{x}_m)D/\nu$) |
| $Re_{wv}$ | : | Reynolds number due to total flow of waves and current ($=(V+u_m)D/\nu$) |
| $Re_T$ | : | Reynolds number due to total flow of oscillation and waves ($=(u_m+\dot{x}_m)D/\nu$) |
| $Re_r$ | : | Reynolds number, relative flow ($=(u-\dot{x})_{max}D/\nu$) |
| $s$ | : | distance from the bed |

| | | |
|---|---|---|
| $St$ | : | Strouhal number for steady current, $(= f_v D/V)$ |
| $St_o$ | : | Strouhal number for oscillatory flow, $(= f_v D/\dot{x}_m)$ |
| $St_w$ | : | Strouhal number for waves, $(= f_v D/u_m)$ |
| $St_{ov}$ | : | Strouhal number for total flow - oscillatory flow plus steady current, $(=f_v D/(V+\dot{x}_m))$ |
| $St_{wv}$ | : | Strouhal number for total flow - waves plus steady current, $(= f_v D/(V+u_m))$ |
| $R^2$ | : | The square of the Pearson product moment correlation coefficient through data points, see appendix V. |
| $t$ | : | time |
| $T_0$ | : | Mean zerocrossing period |
| $T_o$ | : | Oscillation period |
| $T_r$ | : | Relative (motion) period |
| $T_p$ | : | Peak spectral period |
| $T_w$ | : | Wave period |
| $u$ | : | Velocity of ambient flow, water particle horizontal velocity due to waves |
| $u_m$ | : | Amplitude of water particle horizontal velocity due to waves |
| $\dot{u}$ | : | Water particle horizontal acceleration due to waves |
| $\dot{u}_m$ | : | Amplitude of water particle horizontal acceleration due to waves |
| $V$ | : | Towing speed or current velocity |
| $V_{ratio}$ | : | Ratio of the maximum (total) oscillatory velocity to the steady velocity $(=(u_m+\dot{x}_m)/V)$ |
| $Vr$ | : | Reduced velocity, $(Vr = VT_w/D$ or $Vr = VT_o/D)$ |
| $Vr_o$ | : | Reduced velocity of the steady flow in comparison with the cylinder oscillation |
| $Vr_{ow}$ | : | Total reduced velocity $(= Vr_o+Vr_w)$ |
| $Vr_w$ | : | Reduced velocity of the steady flow in comparison with flow due to the waves |
| $x$ | : | Cylinder motion |
| $\hat{x}$ | : | Amplitude parameter, $(A/D)$ |
| $\dot{x}$ | : | Velocity of cylinder motion |
| $\ddot{x}$ | : | Acceleration of cylinder motion |
| $\dot{x}_m$ | : | Maximum cylinder oscillatory velocity |
| $\ddot{x}_m$ | : | Maximum cylinder acceleration |
| $z$ | : | Vertical co-ordinate from mean still water level upward |

## Greek Letters

| | | |
|---|---|---|
| $\beta$ | : | Frequency parameter, $(=Re/KC = D^2/T\nu$, or $=Re_o/KC_o = D^2/T_o\nu)$ |
| $\epsilon$ | : | Goodness-of-fit parameter |
| $\eta$ | : | Wave surface elevation |
| $\theta$ | : | Wave phase angle $(= kx - \omega t)$ |
| $\lambda$ | : | Wave length |
| $\rho$ | : | Density of water |
| $\nu$ | : | Kinematic viscosity |
| $\phi$ | : | Phase angle, and potential function |
| $\psi$ | : | Phase angle |
| $\omega$ | : | Angular frequency $(=2\pi/T)$ |
| $\omega_{app}$ | : | Apparent wave angular frequency in a fixed frame of reference in waves plus current flow field $(\omega_{app}=\omega_w+kV)$ |
| $\omega_n$ | : | Natural frequency of structure |

$\omega_w$       : Wave angular frequency ($=2\pi/T_w$)

$\xi_s$       : Structural dimensionless damping factor

$\xi_t$       : Sum of structural and fluid damping components

# References

API RP 2A LRFD, 1993, *Recommended Practice for Planning, Designing and Constructing Fixed Offshore Platforms, Load and Resistance Factor Design, First Edition*, API, USA.

Barnouin, B., Mattout, M. and Sagner, M., 1979, "Experimental study of the validity domain of some formulae for hydrodynamic forces for regular and irregular flows," in *Mechanics of Wave-Induced Forces on Cylinders*, edited by Shaw, T.L, Pitman Advanced Publishing Program.

Bearman, P.W., Lin, X.W., and Mackwood, P.R., 1992, "Measurement and prediction of response of circular cylinders in oscillating flow," *BOSS* 92, London, pp. 297-307.

Bearman, P.W., and Obasaju, E.D., 1989, "Transverse forces on a circular cylinder oscillating in-line with a steady current," *OMAE*, 1989, The Hague, pp. 253-258.

Bearman, P.W., 1988, "Wave Loading Experiments on Circular Cylinders at Large Scale," BOSS 88, Trondheim, pp. 471-487.

Bearman, P.W., Chaplin, J.R., Graham, J.M.R, Hall, P.F., and Klopman, G., 1985, "The loading on a cylinder in post-critical flow beneath periodic and random waves," *BOSS* 85, Delft, pp. 213-225.

Bearman, P.W., Graham, J.M.R. and Obasaju, E.D. 1984, "A model equation for the Transverse forces on Cylinders in Oscillatory Flows," *Applied Ocean Research*, Vol. 6, pp. 166-172.

Bishop, J. R., 1979, "RMS force coefficients derived from Christchurch bay," in *Mechanics of Wave-Induced Forces on Cylinders*, edited by Shaw, T.L, Pitman Advanced Publishing Program, pp. 334-345.

Bishop, R.E.D. and Hassan A.Y., 1964, "The lift and drag forces on a circular cylinder oscillating in a flowing flow," *Proc. Royal Society*, Series A, Vol. 277, 1964.

Blevins, R.D., 1990, *Flow Induced Vibration*, Van Nostrand Reinhold, New York.

Borgman, L.E., 1972, "Statistical models for ocean waves and wave forces," *Advances in Hydroscience*, Academic Press, London, pp. 139-182.

Chakrabarti, S.K., 1987, *Hydrodynamics of Offshore Structures*, Computational Mechanics Publications Southampton, Boston.

Chakrabarti, S.K., 1980, "Inline forces on fixed vertical cylinder in waves," *Journal of Waterway, Coastal and Ocean Division*, ASCE, May 1980, Vol. **106**, pp. 145-155.

Chakrabarti, S.K. and Cotter, D.C., 1984, "Hydrodynamic coefficients of a mooring tower," *J. of Energy Resources Technology*, ASME, Sept. 1984, pp. 449-458.

Chakrabarti, S.K., Wolbert, A.L., and Tam, W.A., 1976, "Wave forces on vertical circular cylinder," *J. of Waterways, Harbors and Coastal Engineering Division*, ASCE, May 1976, Vol. **102**.

Ghanem, R. and Spanos, P., 1992, "Coupled in-line and transverse flow-induced structural vibration: higher order harmonic solutions," OMAE, 1992, Vol. 1-A, pp. 377-384.
Gudmestad, O.T. and Connor, J.J., 1983, "Linearization methods and the influence of current on the nonlinear hydrodynamic drag force," *Applied Ocean Research*, Vol. **5**, No. 4, pp. 184-194.

Hartlen, R.T. and Currie, I.G., 1970, "Lift-oscillator model of vortex-induced vibration," *Journal of the*

*Engineering Mechanics Division*, Proceeding of the ASCE, Vol. **96**, pp. 577-591.

Hogben, N., 1974, "Wave resistance of surface piercing vertical cylinders in uniform currents," National Physical Laboratory, report ship 183, 1974.

Huang, N.E., Chen, D.T., Tung, CC. And Smith, J.R., 1972, "Interactions between steady non-uniform currents and gravity waves with application for current measurements", *J. Physics of Ocean*, Vol. **2**, pp. 420-431.

Isaacson, M., Subbiah, K., and Balwin, J., 1991 "Force coefficient estimation from random wave data," *The First International Offshore and Polar Engineering Conference*, Edinburgh, Scotland, pp. 149-157.

Iwagaki, Y., Asano, T. and Nagai, F., 1983, "Hydrodynamic forces on a circular cylinder in wave-current co-existing fields," *Memories of the Faculty of Engineering*, Kyoto University, XLV, pp. 11-23, 1983.

Iwan, W.D. and Blevins, R.D., 1974, "A model for vortex-induced oscillation of structures," *Journal of Applied Mechanics*, Vol. **41**, pp. 581-586.

Kaplan, F., Jiang, C.W., and Dello Stritto, F.J., 1981, "Determination of offshore structure Morison equation force coefficients via system identification techniques," *Proceeding Hydrodynamics on Ocean Engineering*, Trondheim, Norway, 1981, Vol. 1, pp. 469-489.

Kato, M., Abe, T., Tamiya, M. and Kumakiri, T, 1983, "Drag forces on oscillating cylinders in a uniform flow," *Offshore Technology Conference* 4591, pp. 95-102.

Klopman, G., and Kostense, J. K., 1990, "The loading on a vertical cylinder in random waves at high Reynolds numbers," in A. Torum and O. T. Gudmestad (Eds.), *Water Waves Kinematics* Kluwer Academic Publisher, pp. 679-699..

Koterayama, W. and Nakamura, M., 1986, "Wave forces acting on a moving cylinder," OMAE 1986, Vol. I, Part A, pp. 149-154.

Koterayama, W, 1984, "Wave forces acting on a vertical circular cylinder with a constant forward velocity", *Ocean Engineering* Vol. 11(4), pp. 363-379.

Langley, R.S., 1984, "The linearization of three dimensional drag force in random sea current," *Applied Ocean Research*, Vol. **6**, pp. 126-131.

Laya, E.J., Connor, J.J., and Shyam Sunder, S., 1984, "Hydrodynamic forces on flexible offshore structures," *J. of Engineering Mechanics*, ASCE, March 1984, Vol. **119** , pp. 433-448.

Leira, B.J., 1987, "Multidimensional stochastic linearization of drag forces," *Applied Ocean Research*, Vol. **9**, pp. 150-162.

Li, Y.C., and Kang, H.C., 1992, "Wave-current forces on slender circular cylinder," OMAE 1992, Alberta, Canada, Vol. IA, pp. 117-125.

Lighthill, J., 1986, "Fundamentals concerning wave loading on offshore structures," *J. of Fluid Mechanics*, Vol. **173**, pp. 667-681.

Low, H.T., Chew, Y.T. and Tan, K.T., 1989, "Fluid forces on a cylinder oscillating in-line with a uniform flow," *Ocean Engng.*, Vol. **16**, No. 3, pp. 307-318.

Malhotra, A.K. and Penzien, J., 1970, "Nondeterministic analysis of offshore structures, *J. of*

*Engineering Mechanic Division*, ASCE, Vol. **96**, pp. 985-991.?

Massie, W.W., 1980, "Influence of surface wake on cylinder drag," internal report, Coastal Engineering Group, Civil Engineering Department, Delft University of Technology.

McConnell, K.G. and Park, Y.S., 1982, "The frequency components of fluid-lift forces acting on a cylinder oscillating in still water," *Experimental Mechanics*, Vol. **22**, pp. 216-222.

Mercier, J.A., 1973, "Large amplitude oscillations of a circular cylinder in a low-speed stream," Ph.D. Thesis, Stevens Institute of Technology.

Moe, G., Holden, K., and Yttervoll, P.O., 1994, "Motions of spring-supported cylinders in subcritical water flow," *Proceedings of International Offshore and Polar Engineering Conference*, Osaka, Japan pp 468-475.

Moe, G., 1992, "Prototype measurements of marine risers - A hydrodynamic perspective," Proceedings of the Workshop on Marine Riser Mechanics, Vol. II, pp. 262-274, Michigan.

Moe, G. and Verley, R.L.P., 1980, "Hydrodynamic damping of offshore structures in waves and currents," *Offshore Technology Conference* 3798, Houston, 1980.

Najafian, G. and Burrows, R., 1994, "Critical assessment of the least square error method used in derivation of Morison's force coefficients," *Journal of Offshore Mechanics and Arctic Engineering*, Vol. **116**, February, pp. 1-6.

Otter, A., 1992, "Forces on an oscillating cylinder and related fluid flow phenomena," Ph.D. thesis, University of Twente.

Pantazopoulos, M.S., 1994, "Vortex-induced vibration parameters: Critical review," OMAE 1994, Vol. 1, pp. 199-255.

Peregrine, D.H., 1976, "Interaction of water waves and currents," *Advances in Applied Mechanics*, Vol. **16**, pp. 9-117.

Price, S.J., Paidoussis, M.P. and Synchterz, P.W., 1988, "An experimental investigation of the quasi-steady assumption for bluff bodies in cross-flow," Proceeding of International Symposium on Flow-Induced Vibration and Noise, Chicago, Illinois, pp.91-111.

Ren, Z. and He, J., 1986, "Wave-current coefficients for isolated pile," OMAE 1986, Vol. I, Part A, pp. 144-148.

Sarpkaya, T., 1993, "Offshore hydrodynamics," *Journal of Offshore Mechanics and Arctic Engineering*, Vol. **115**, February, pp. 2-5.

Sarpkaya, T., 1989, "Computational methods with vortices - the 1988 Freeman Scholar Lecture." *Journal of Fluid Engineering*, ASME, Vol. **111**, No. 1, March, pp. 5-52.

Sarpkaya, T. and Storm, M., 1985 "In-line force on a cylinder translating in oscillatory flow," *Applied Ocean Research*. Vol. **7**, No. 4, pp. 188-195

Sarpkaya, T., Bakmis, C. and Storm, M.A., 1984, "Hydrodynamic forces from combined wave and current flow on smooth and rough circular cylinders at high Reynolds numbers," *Offshore Technology Conference* 4830, Houston, pp. 455-462.

Sarpkaya, T., and Isaacson, M., 1981, Mechanics of Wave Forces on Offshore Structures, Van Nostrand

Reinold, New York.

Sarpkaya, T., 1979, "Vortex induced oscillations, a selective review," *J. Applied Mechanics*, ASME Series E. Vol. **46**, pp. 241-258.

Sarpkaya, T., 1976, "Vortex shedding and resistance in harmonic flow about smooth and rough circular cylinders at high Reynolds numbers," Report No. NPS-59SL76021, U.S. Naval Graduate School, Monterey, Calif.

Schlichting, H., 1968, *Boundary-Layer Theory*, McGraw-Hill Book Co., New York, 6th ed.

Shafiee-Far, M., Massie, W.W. and Vugts, J.H., 1996, "The validity of Morison equation extensions," *Offshore Technology Conference* 8064, Houston, 1996.

Shafiee-Far, M., 1995a, "Requirements for the experimental investigation of hydrodynamic interaction of slender cylinders," Workgroup Offshore Technology, Delft University of Technology, 1995.

Shafiee-Far, M., 1995b, "Model experiments on hydrodynamic interaction of slender cylinders," Workgroup Offshore Technology, Delft University of Technology, 1995.

Shafiee-Far, M., 1994a, "Slender Flexible Marine Structures, Part I: Structural Aspects," Workgroup Offshore Technology, Delft University of Technology, 1994.

Shafiee-Far, M., 1994b, "Slender Flexible Marine Structures, Part II: Hydrodynamic Analysis," Workgroup Offshore Technology, Delft University of Technology, 1994.

Shafiee-Far, M., 1994c, "Slender Flexible Marine Structures, Part III: Computational Methods," Workgroup Offshore Technology, Delft University of Technology, 1994.

Skop, R.A. and Griffin, O.M., 1973, "A Model for the vortex-excited resonant response of bluff cylinders," *Journal of Sound and Vibration*, Vol. **27**, pp. 225-233.

Stansby, P.K., El-Khairy, N. and Bullock, G.N., 1983, "Experimental study of forces on a cylinder in oscillatory flow with a cross current," *Applied Ocean Research*, Vol. **5**, No. 4, pp. 195-203.

Stansby, P.K., Bullock, G.N. and Short, I, 1983, "Quasi-2-D forces on a vertical cylinder in waves", *J. Of Waterways, Port, Coastal and Ocean Engineering*, ASCE, Vol. **109**, No. 1, pp. 128-132.

Thomas, G.P. 1979, "Wave-current interactions: an experimental and numerical study," in *Mechanics of Wave-Induced Forces on Cylinders*, edited by Shaw, T.L, Pitman Advanced Publishing Program.

Verley, R.L.P. 1982, "A simple model for vortex-induced forces in waves and oscillating currents" *Applied Ocean Research,* Vol. **4**, No. 2, pp. 117-120.

Verley, R.L.P. 1980, "Oscillations of cylinders in waves and currents," Ph.D. Thesis, Loughbrough University.

Verley, R.L.P. and Johns, D.J., 1983, "Oscillations of cylinders in waves and currents," Hemisphere Publishing Corp., Washington, Vol. 2, paper PH3.6, pp. 690-701.

Vugts, J.H., Bouquet, A.G., 1985 "A nonlinear frequency domain description of wave forces on an element of a vertical pile in random seas," *BOSS* 85, Delft, pp. 239-253.

Vugts, J.H., 1979, "A review of hydrodynamic loads on offshore structures and their formulation," BOSS'79, London, Paper 54.

# APPENDIX I

## Techniques for Determining the Hydrodynamic Coefficients

The determination of hydrodynamic forces on slender cylinders is commonly carried out using the Morison equation, which requires the use of empirical drag and inertia coefficients. The selection of these coefficients for use in hydrodynamic force calculations is an important concern related to the design of offshore structures. Knowledge of these coefficients has developed over the last decades from laboratory experiments and field tests.

In a typical investigation of fluid loading on a slender cylinder, the force on the cylinder, *Fm*, and the ambient flow velocity and/or acceleration, $u$ and $\dot{u}$, are measured; then $C_D$ and $C_M$ in the Morison equation are determined using a suitable method of analysis. Various methods have been purposed and used in the past to estimate $C_D$ and $C_M$ values. However, the suitability of these methods has not received enough attention.

A summary of methods of estimating $C_D$ and $C_M$ values from regular and random waves is given below.

### I.1 Coefficients Determination Techniques from Regular Waves

From various suggested methods, two methods are commonly used to determine force coefficients in waves or oscillatory flows. These methods are:

1.  Least Squares Method: a least squares fitting of the two coefficients to the force;

2.  Fourier averaged method: drag and inertia coefficients are related to the first two Fourier coefficients at the fundamental oscillatory frequency.

### I.1.1  Least Squares Method

The least squares method is the most popular method for estimating the constant force coefficients $C_D$ and $C_M$ by minimizing the square of the difference between the time series of measured and predicted force. Considering the original Morison equation, the error term is:

$$e \ = \ F_m - F_p \ = \ F_m - \frac{1}{2} C_D \rho D u |u| \ - \ C_M \rho \frac{\pi D^2}{4} \dot{u}$$

where $F_m$ is the known measured force.

Squaring both sides of this equation and taking averages gives:

$$\overline{e^2} \ = \ \overline{F_m^2} + \frac{1}{4}\rho^2 D^2 C_D^2 \overline{u^4} \ - \ \rho D C_D \overline{F_m u |u|} \ + \ \frac{1}{4}\pi\rho^2 D^3 C_D C_M \overline{u|u|\dot{u}} + \frac{\pi^2 D^4}{16}\rho^2 C_M^2 \overline{\dot{u}^2} \ - \ \frac{\pi D^2}{2}\rho C_M \overline{F_m \dot{u}}$$

169

Assuming

$$S_1 = \overline{u^4}$$
$$S_2 = \overline{u|u|\dot{u}}$$
$$S_3 = \overline{F_m u|u|}$$
$$S_4 = \overline{\dot{u}^2}$$
$$S_5 = \overline{F_m \dot{u}}$$
$$S_6 = \overline{F_m^2}$$

then above equation reduces to:

$$\overline{e^2} = \frac{1}{4}\rho^2 \; D^2 C_D^2 S_1 + \frac{1}{4}\pi\rho^2 D^3 \; C_D C_M S_2 - \rho D \; C_D S_3 + \frac{\pi^2 D^4}{16}\rho^2 C_M^2 S_4 - \frac{\pi D^2}{2}\rho C_M S_5 + S$$

The error term will be minimum when:

$$\frac{\partial \overline{e^2}}{\partial C_D} = \frac{1}{2}\rho^2 \; D^2 C_D \; S_1 + \frac{1}{4}\pi\rho^2 D^3 \; C_M S_2 - \rho D \; S_3 = 0$$

and

$$\frac{\partial \overline{e^2}}{\partial C_M} = \frac{1}{4}\pi\rho^2 D^3 C_D S_2 + \frac{\pi^2 D^4}{8}\rho^2 C_M S_4 - \frac{\pi D^2}{2}\rho S_5 = 0$$

The simultaneous solution of these equations leads to the following relation:

$$C_D = \frac{2}{\rho D} \cdot \frac{S_3 S_4 - S_2 S_5}{S_1 S_4 - S_2^2} \qquad C_M = \frac{4}{\rho \pi D^2} \cdot \frac{S_2 S_3 - S_1 S_5}{S_2^2 - S_1 S_4}$$

The error between the measured and the calculated forces - particularly in the neighbourhood of the maximum forces - may be further minimised by choosing the square of the measured forces as the weighting factor in the least-squares method:

$$e^2 = F_m^2 (F_m - F_p)^2$$

Then one can find the force coefficients from the following relations:

$$C_D = \frac{2}{\rho D} \cdot \frac{S_{3w} S_{4w} - S_{2w} S_{5w}}{S_{1w} S_{4w} - S_{2w}^2}$$

$$C_M = \frac{4}{\rho \pi D^2} \cdot \frac{S_{2w} S_{3w} - S_{1w} S_{5w}}{S_{2w}^2 - S_{1w} S_{4w}}$$

where:

$$S_{1w} = \overline{F_m^2 u^4}$$
$$S_{2w} = \overline{F_m^2 u |u| \dot{u}}$$
$$S_{3w} = \overline{F_m^3 u |u|}$$

$$S_{4w} = \overline{F_m^2 \dot{u}^2}$$
$$S_{5w} = \overline{F_m^3 \dot{u}}$$

Above solutions for determining the force coefficients - for original Morison equation - can also be used for the relative velocity form of the Morison equation provided that the velocity term $u$ is exchanged with the relative velocity term. However, these solutions are not straightforward to determine the force coefficients for other forms of the Morison equation (those have more than two terms). One may obtain force coefficients for those forms by minimising the error term ($e$) using an iterative numerical process. Such a process has been implemented in the present work for determining the force coefficient for various forms of Morison equation extensions.

## I.2 Fourier-averaged Coefficients

The Fourier-averaged drag and inertia coefficients over a period of time may be calculated by multiplying both sides of the Morison equation once with $u$ and once with $\dot{u}$ to yield:

$$C_D = \frac{2 \int_0^T F(t)u(t)dt}{\rho D \int_0^T |u(t)|[u(t)]^2 dt}$$

$$C_M = \frac{4 \int_0^T F(t)\dot{u}(t)dt}{\rho \pi D^2 \int_0^T [\dot{u}(t)]^2 dt}$$

The force coefficients may also be estimated via individual Fourier-coefficient analysis. From basic Fourier series theory a wave force F(t) can be represented as a series:

$$F(t) = a_0 + \sum_{n=1}^{\infty} a_n \cos(\frac{2\pi nt}{T}) + \sum_{n=1}^{\infty} b_n \sin(\frac{2\pi nt}{T})$$

where the coefficients $a_0$, $a_n$ and $b_n$ are given by

$$a_0 = \frac{1}{T} \int_0^T F(t)dt$$

171

$$a_n = \frac{2}{T} \int_0^T F(t)\cos(\frac{2\pi nt}{T})dt$$

$$b_n = \frac{2}{T} \int_0^T F(t)\sin(\frac{2\pi nt}{T})dt$$

Provided that $a_n$ and $b_n$ are zero for $n \geq 3$, one may deduce $C_D$ and $C_M$ for a cylinder in harmonic oscillatory flow from $a_1$ and $b_1$:

$$C_D = \frac{3\pi}{8} \cdot \frac{a_1}{0.5\rho D u_m^2}$$

$$C_M = \frac{b_1}{0.25\rho\pi D^2 \dot{u}_m}$$

where $u_m$ and $\dot{u}_m$ are amplitude of water particle horizontal velocity and acceleration, respectively.

The drag and inertia coefficients may also be determined based on equivalent energy dissipation, see Otter (1992). It has been demonstrated analytically that the ratio of the drag coefficient obtained by this method to one obtained via the least squares technique equals $27\pi 2/256 = 1.041$.

## I.1.3 Other Suggested Methods

Besides the above methods other methods have also been suggested by various researchers. Some of these methods are briefly explained below.

Bearman et al. (1985) have shown that the force and velocity signals could be well represented by taking the first six Fourier components. Since the time average $u(t)|u(t)|$ is zero the drag and inertia coefficients can be evaluated from the following expressions:

$$C_D = \frac{\overline{2F(t)\,u(t)}}{\rho D\,|u(t)|^3}$$

$$C_M = \frac{\overline{4\,F(t)\,\dot{u}(t)}}{\rho\pi D^2 |\dot{u}(t)|^2}$$

Coefficients derived from these relationships provided a better fit to the force signal than those from using just the first order components. $C_D$ and $C_M$ are calculated on a wave-by-wave basis and are averaged over the length of the record.

Applying the fact that $u|u|\dot{u}$ is also theoretically zero over a wave cycle, Klopman and Kostense (1990) have found the following relations:

172

$$C_D = \frac{2F(t)\,u(t)\,|u(t)|}{\rho D\,u(t)^4}$$

$$C_M = \frac{4\,\overline{F(t)\,\ddot{u}(t)}}{\rho \pi D^2 \,|\ddot{u}(t)|^2}$$

Najafian and Burros (1994) have introduced the 'maximum correlation method', a method that predicts force coefficients with variances of the observed forces to be equal to those of computed forces.

### I.2 Coefficients Determination Techniques from Random Waves

In random waves, hydrodynamic coefficients have been determined on a wave-by-wave basis as for regular waves or by analysis of the entire wave record. In the latter case, the relatively long records of measured forces and water particle kinematics (in the order of 20 min) are assumed to be samples of stationary random processes, Borgman (1972).

A number of methods exist for determination of the drag and inertia coefficients in random waves. These methods may be classified into:

    1. Those that provide a single pair of force coefficients for a given set of signals.
    2. Those that provide variable coefficients.

Isaacson et al. (1991) have referred to the following methods for analysing random wave force data:

*Constant Coefficients*:

1. least squares fit of the force time series
2. least squares fit of the force spectrum
3. method of moments applied to the force probability distribution
4. least squares fit of the peak force
5. method of moments applied to the peak force probability distribution
6. method of maximum likelihood applied to the peak force probability distribution

*Variable Coefficients*:

7. least-squares fit on a wave-by-wave basis
8. cross-spectrum fitting

Some of these methods are based on specific assumptions such as a linearisation of the drag force or a narrow-banded wave spectrum. The methods involving the force spectrum (2 and 8) are generally based on linearisation of the drag term in the Morison equation. On the other hand the methods involving peak force probability distributions (5 and 6) generally assume that the wave height follows a Rayleigh distribution, which is itself based on the assumption of a

173

narrow-banded wave spectrum. Since the Rayleigh distribution may be suitable even for waves which are not narrow-banded, this limitation may not be very severe. The remaining methods (1, 3, 4 and 7) do not require either assumption.

Isaacson et al. (1991) have shown that the least squares fit of the entire time series is the most reliable method with the least scatter in the estimated force coefficients.

Besides the methods mentioned above, there are a number of other methods. For example, Bishop (1979) has developed an analysis technique which yields a mean square wave force related to similar parameters for the wave kinematics:

$$\overline{F^2} = A^2 \overline{u^4} + B^2 \overline{\dot{u}^2}$$

A and B contain the drag and inertia force coefficients:

$$A = \sqrt{C_D} \, \rho \, D$$

$$B = C_M \, \rho \frac{\pi}{4} D^2$$

The values of the force coefficients are obtained by least squares fitting to data sets.

# APPENDIX II

## List of Test Runs

### 1. Towing the Cylinder in Calm Water

| V(m/s) | A (m) | To (s) | Tw (s) | Hw | Run | Date |
|--------|-------|--------|--------|-----|-----|------|
| 0.2 | - | - | | | 43 | 24/6/1994 |
| 0.2 | - | - | - | - | 460 | 10/8/1994 |
| 0.2 | - | - | - | - | 904 | 8/8/1994 |
| 0.35 | - | - | - | - | 44 | 24/6/1994 |
| 0.35 | - | - | - | - | 227 | 11/7/1994 |
| 0.5 | - | - | - | - | 36 | 24/6/1994 |
| 0.5 | - | - | - | - | 40 | 24/6/1994 |
| 0.5 | - | - | - | - | 511 | 19/7/1994 |
| 0.75 | - | - | - | - | 41 | 24/6/1994 |
| 0.75 | - | - | - | - | 228 | 11/7/1994 |
| 1 | - | - | - | - | 37 | 24/6/1994 |
| 1 | - | - | - | - | 38 | 24/6/1994 |
| 1 | - | - | - | - | 39 | 24/6/1994 |
| 1 | - | - | - | - | 79 | 27/6/1994 |
| 1 | - | - | - | - | 194 | 29/6/1994 |
| 1 | - | - | - | - | 195 | 29/6/1994 |
| 1 | - | - | - | - | 196 | 29/6/1994 |
| 1 | - | - | - | - | 230 | 11/7/1994 |
| 1 | - | - | - | - | 231 | 11/7/1994 |
| 1 | - | - | - | - | 241 | 12/7/1994 |
| 1 | - | - | - | - | 264 | 13/7/1994 |
| 1 | - | - | - | - | 325 | 14/7/1994 |
| 1 | - | - | - | - | 415 | 15/7/1994 |
| 1 | - | - | - | - | 441 | 10/8/1994 |
| 1 | - | - | - | - | 442 | 10/8/1994 |
| 1 | - | - | - | - | 461 | 11/8/1994 |
| 1 | - | - | - | - | 484 | 12/8/1994 |
| 1 | - | - | - | - | 510 | 19/7/1994 |
| 1 | - | - | - | - | 553 | 20/7/1994 |
| 1 | - | - | - | - | 592 | 21/7/1994 |
| 1 | - | - | - | - | 651 | 22/7/1994 |
| 1 | - | - | - | - | 704 | 25/7/1994 |
| 1 | - | - | - | - | 749 | 26/7/1994 |
| 1 | - | - | - | - | 750 | 26/7/1994 |
| 1 | - | - | - | - | 785 | 27/7/1994 |
| 1 | - | - | - | - | 814 | 28/7/1994 |
| 1 | - | - | - | - | 822 | 29/7/1994 |
| 1 | - | - | - | - | 858 | 1/8/1994 |
| 1 | - | - | - | - | 867 | 2/8/1994 |
| 1 | - | - | - | - | 875 | 2/8/1994 |
| 1 | - | - | - | - | 880 | 3/8/1994 |
| 1 | - | - | - | - | 887 | 4/8/1994 |
| 1 | - | - | - | - | 903 | 8/8/1994 |
| 1 | - | - | - | - | 916 | 9/8/1994 |
| 1.5 | - | - | - | - | 42 | 24/6/1994 |
| 1.5 | - | - | - | - | 229 | 11/7/1994 |

## 2. Fixed Cylinder in Waves

| V(m/s) | A (m) | To (s) | Tw (s) | Hw | Run | date |
|--------|-------|--------|--------|----|-----|------|
| - | - | - | 1 | H1 | 290 | 13/7 |
| - | - | - | 1 | H1 | 587 | 20/7 |
| - | - | - | 1 | H1 | 593 | 21/7 |
| - | - | - | 1 | H1 | 689 | 22/7 |
| - | - | - | 1 | H1 | 705 | 25/7 |
| - | - | - | 1 | H1 | 876 | 2/8 |
| - | - | - | 1.5 | H2 | 242 | 12/7 |
| - | - | - | 1.5 | H2 | 416 | 15/7 |
| - | - | - | 1.5 | H2 | 566 | 20/7 |
| - | - | - | 1.5 | H2 | 668 | 22/7 |
| - | - | - | 1.5 | H2 | 756 | 26/7 |
| - | - | - | 1.5 | H2 | 787 | 27/7 |
| - | - | - | 1.5 | H2 | 815 | 28/7 |
| - | - | - | 1.5 | H2 | 828 | 29/7 |
| - | - | - | 1.5 | H2 | 868 ` | 2/8 |
| - | - | - | 2 | H3 | 271 | 13/7 |
| - | - | - | 2 | H3 | 351 | 14/7 |
| - | - | - | 2 | H3 | 417 | 15/7 |
| - | - | - | 2 | H3 | 537 | 19/7 |
| - | - | - | 2 | H3 | 555 | 20/7 |
| - | - | - | 2 | H3 | 630 | 21/7 |
| - | - | - | 2 | H3 | 652 | 22/7 |
| - | - | - | 2 | H3 | 716 | 25/7 |
| - | - | - | 2 | H3 | 761 | 26/7 |
| - | - | - | 2 | H3 | 771 | 26/7 |
| - | - | - | 2 | H3 | 772 | 26/7 |
| - | - | - | 2 | H3 | 840 | 29/7 |
| - | - | - | | H4 | 456 | 10/8 |
| - | - | - | | H4 | 881 | 3/8 |
| - | - | - | | H4 | 929 | 9/8 |

## 3. Oscillation in Calm Water

| A/D | V(m/s) | To (s) | Tw (s) | Hw | Run | date |
|-----|--------|--------|--------|----|-----|------|
| 0.5 | 0.05 | 0.504 | - | - | 80 | 27/6 |
| 0.5 | 0.05 | 0.505 | - | - | 233 | 11/7 |
| 0.5 | 0.05 | 0.505 | - | - | 234 | 11/7 |
| 0.5 | 0.05 | 0.525 | - | - | 46 | 24/6 |
| 0.5 | 0.05 | 0.571 | - | - | 73 | 24/6 |
| 0.5 | 0.05 | 0.667 | - | - | 265 | 13/7 |
| 0.5 | 0.05 | 0.672 | - | - | 67 | 24/6 |
| 0.5 | 0.05 | 0.69 | - | - | 47 | 24/6 |
| 0.5 | 0.05 | 0.807 | - | - | 48 | 24/6 |
| 0.5 | 0.05 | 0.807 | - | - | 61 | 24/6 |
| 0.5 | 0.05 | 1 | - | - | 488 | 12/8 |
| 0.5 | 0.05 | 1 | - | - | 267 | 13/7 |

176

| A/D | V(m/s) | To (s) | Tw (s) | Hw | Run | date |
|---|---|---|---|---|---|---|
| 0.5 | 0.05 | 1 | - | - | 485 | 12/8 |
| 0.5 | 0.05 | 1.003 | - | - | 49 | 24/6 |
| 0.5 | 0.05 | 1.394 | - | - | 2 | 24/6 |
| 0.5 | 0.05 | 1.5 | - | - | 269 | 13/7 |
| 0.5 | 0.05 | 2.136 | - | - | 45 | 24/6 |
| 0.75 | 0.05 | 0.667 | - | - | 448 | 10/8 |
| 0.75 | 0.05 | 1 | - | - | 444 | 10/8 |
| 0.75 | 0.05 | 2 | - | - | 443 | 10/8 |
| 1 | 0.05 | 0.566 | - | - | 113 | 27/6 |
| 1 | 0.05 | 0.667 | - | - | 326 | 14/7 |
| 1 | 0.05 | 0.667 | - | - | 452 | 10/8 |
| 1 | 0.05 | 0.668 | - | - | 106 | 27/6 |
| 1 | 0.05 | 0.821 | - | - | 99 | 27/6 |
| 1 | 0.05 | 1 | - | - | 316 | 13/7 |
| 1 | 0.05 | 1 | - | - | 466 | 11/8 |
| 1 | 0.05 | 1 | - | - | 462 | 11/8 |
| 1 | 0.05 | 1.001 | - | - | 92 | 27/6 |
| 1 | 0.05 | 1.353 | - | - | 87 | 27/6 |
| 1 | 0.05 | 1.5 | - | - | 306 | 13/7 |
| 1 | 0.05 | 2 | - | - | 475 | 11/8 |
| 1.5 | 0.05 | 0.811 | - | - | 135 | 28/6 |
| 1.5 | 0.05 | 1 | - | - | 364 | 14/7 |
| 1.5 | 0.05 | 1.002 | - | - | 128 | 28/6 |
| 1.5 | 0.05 | 1.389 | - | - | 121 | 27/6 |
| 1.5 | 0.05 | 1.5 | - | - | 374 | 14/7 |
| 1.5 | 0.05 | 1.702 | - | - | 142 | 28/6 |
| 2 | 0.05 | 1 | - | - | 390 | 15/7 |
| 2 | 0.05 | 1.005 | - | - | 166 | 28/6 |
| 2 | 0.05 | 1.2 | - | - | 160 | 28/6 |
| 2 | 0.05 | 1.388 | - | - | 154 | 28/6 |
| 2 | 0.05 | 1.5 | - | - | 394 | 15/7 |
| 2 | 0.05 | 1.711 | - | - | 148 | 28/6 |
| 2.5 | 0.05 | 1.201 | - | - | 187 | 28/6 |
| 2.5 | 0.05 | 1.39 | - | - | 180 | 28/6 |
| 2.5 | 0.05 | 1.5 | - | - | 428 | 15/7 |
| 2.5 | 0.05 | 1.7 | - | - | 173 | 28/6 |
| 3 | 0.05 | 1.5 | - | - | 418 | 15/7 |
| 4 | 0.05 | 2 | - | - | 479 | 9/8 |
| 3 | 0.05 | 1.206 | - | - | 215 | 29/6 |
| 3 | 0.05 | 1.392 | - | - | 209 | 29/6 |
| 3 | 0.05 | 1.702 | - | - | 203 | 29/6 |
| 3 | 0.05 | 1.991 | - | - | 197 | 29/6 |

177

## 4. Cylinder Oscillating in Longitudinal Direction

| V (m/s) | A (m) | To (s) | Tw (s) | Hw | Run | Date |
|---------|-------|--------|--------|-----|-----|------|
| - | 0.03 | 2 | - | - | 512 | 19/7 |
| - | 0.03 | 1.5 | - | - | 513 | 19/7 |
| - | 0.03 | 1 | - | - | 514 | 19/7 |
| - | 0.03 | 0.668 | - | - | 520 | 19/7 |
| - | 0.03 | 0.5 | - | - | 525 | 19/7 |
| - | 0.03 | 0.667 | - | - | 554 | 20/7 |
| - | 0.06 | 0.667 | - | - | 606 | 21/7 |
| - | 0.06 | 1 | - | - | 612 | 21/7 |
| - | 0.06 | 1.5 | - | - | 618 | 21/7 |
| - | 0.06 | 2 | - | - | 624 | 21/7 |
| - | 0.06 | 1 | - | - | 698 | 22/7 |
| - | 0.06 | 0.667 | - | - | 706 | 25/7 |
| - | 0.09 | 1.5 | - | - | 711 | 25/7 |
| - | 0.09 | 1.5 | - | - | 721 | 25/7 |
| - | 0.09 | 2 | - | - | 729 | 25/7 |
| - | 0.12 | 1 | - | - | 751 | 26/7 |
| - | 0.12 | 1.5 | - | - | 766 | 26/7 |
| - | 0.12 | 2 | - | - | 781 | 26/7 |
| - | 0.15 | 2 | - | - | 796 | 27/7 |
| - | 0.15 | 1.5 | - | - | 809 | 27/7 |
| - | 0.18 | 2 | - | - | 823 | 29/7 |
| - | 0.18 | 1.5 | - | - | 832 | 29/7 |
| - | 0.18 | 1.25 | - | - | 846 | 29/7 |
| - | 0.24 | 2 | - | - | 850 | 29/7 |
| - | 0.21 | 2 | - | - | 862 | 1/8 |
| - | 0.03 | 0.667 | - | - | 888 | 4/8 |
| - | 0.06 | 0.667 | - | - | 890 | 4/8 |
| - | 0.045 | 0.667 | - | - | 906 | 8/8 |
| - | 0.045 | 1 | - | - | 912 | 8/8 |
| - | 0.045 | 1.5 | - | - | 917 | 9/8 |
| - | 0.045 | 2 | - | - | 921 | 9/8 |

## 5. Towing the Cylinder in Waves (Regular and Irregular)

| V(m/s) | A (m) | To (s) | Tw (s) | Hw | Run | date |
|--------|-------|--------|--------|-----|-----|------|
| 0.05 | - | - | 2 | H3 | 272 | 13/7 |
| 0.05 | - | - | 1.5 | H2 | 243 | 12/7 |
| 0.2 | - | - | 1 | H1 | 291 | 13/7 |
| 0.2 | - | - | | H4 | 459 | 10/8 |
| 0.2 | - | - | 2 | H3 | 273 | 13/7 |
| 0.2 | - | - | 1.5 | H2 | 244 | 12/7 |
| 0.35 | - | - | 2 | H3 | 274 | 13/7 |
| 0.35 | - | - | 1 | H1 | 292 | 13/7 |
| 0.35 | - | - | 1.5 | H2 | 245 | 12/7 |
| 0.5 | - | - | 1 | H1 | 293 | 13/7 |

178

| A/D | V(m/s) | To (s) | Tw (s) | Hw | Run | date |
|------|--------|--------|--------|-----|-----|------|
| 0.5 | - | - | 2 | H3 | 275 | 13/7 |
| 0.5 | - | - | 1.5 | H2 | 246 | 12/7 |
| 0.75 | - | - | 1.5 | H2 | 247 | 12/7 |
| 0.75 | - | - | 2 | H3 | 276 | 13/7 |
| 0.2 | - | - | | H4 | 898 | 5/8 |
| 0.2 | - | - | | H4 | 885 | 3/8 |

## 6. Transverse Oscillation while Translating the Cylinder

| A/D | V(m/s) | To (s) | Tw (s) | Hw | Run | date |
|------|--------|--------|--------|-----|-----|------|
| 0.5 | 0.2 | 0.504 | - | - | 81 | 27/6 |
| 0.5 | 0.2 | 0.506 | - | - | 235 | 11/7 |
| 0.5 | 0.2 | 0.571 | - | - | 74 | 24/6 |
| 0.5 | 0.2 | 0.667 | - | - | 500 | 12/8 |
| 0.5 | 0.2 | 0.672 | - | - | 68 | 24/6 |
| 0.5 | 0.2 | 0.809 | - | - | 62 | 24/6 |
| 0.5 | 0.2 | 1 | - | - | 486 | 12/8 |
| 0.5 | 0.2 | 1 | - | - | 493 | 12/8 |
| 0.5 | 0.2 | 1.003 | - | - | 50 | 24/6 |
| 0.5 | 0.2 | 1.5 | - | - | 499 | 12/8 |
| 0.5 | 0.2 | 2 | - | - | 498 | 12/8 |
| 0.5 | 0.35 | 0.504 | - | - | 82 | 27/6 |
| 0.5 | 0.35 | 0.506 | - | - | 236 | 11/7 |
| 0.5 | 0.35 | 0.571 | - | - | 75 | 24/6 |
| 0.5 | 0.35 | 0.672 | - | - | 69 | 24/6 |
| 0.5 | 0.35 | 0.809 | - | - | 63 | 24/6 |
| 0.5 | 0.35 | 1.003 | - | - | 51 | 24/6 |
| 0.5 | 0.35 | 1.394 | - | - | 57 | 24/6 |
| 0.5 | 0.5 | 0.504 | - | - | 83 | 27/6 |
| 0.5 | 0.5 | 0.506 | - | - | 237 | 11/7 |
| 0.5 | 0.5 | 0.571 | - | - | 76 | 24/6 |
| 0.5 | 0.5 | 0.667 | - | - | 266 | 13/7 |
| 0.5 | 0.5 | 0.672 | - | - | 70 | 24/6 |
| 0.5 | 0.5 | 0.809 | - | - | 64 | 24/6 |
| 0.5 | 0.5 | 1 | - | - | 268 | 13/7 |
| 0.5 | 0.5 | 1 | - | - | 487 | 12/8 |
| 0.5 | 0.5 | 1.003 | - | - | 52 | 24/6 |
| 0.5 | 0.5 | 1.394 | - | - | 58 | 24/6 |
| 0.5 | 0.5 | 1.5 | - | - | 270 | 13/7 |
| 0.5 | 0.75 | 0.504 | - | - | 84 | 27/6 |
| 0.5 | 0.75 | 0.506 | - | - | 238 | 11/7 |
| 0.5 | 0.75 | 0.568 | - | - | 77 | 24/6 |
| 0.5 | 0.75 | 0.672 | - | - | 71 | 24/6 |
| 0.5 | 0.75 | 0.809 | - | - | 65 | 24/6 |
| 0.5 | 0.75 | 1.003 | - | - | 53 | 24/6 |
| 0.5 | 0.75 | 1.394 | - | - | 59 | 24/6 |
| 0.5 | 1 | 0.503 | - | - | 85 | 27/6 |
| 0.5 | 1 | 0.568 | - | - | 78 | 24/6 |

| A/D | V(m/s) | To (s) | Tw (s) | Hw | Run | date |
|-----|--------|--------|--------|-----|------|------|
| 0.5 | 1 | 0.809 | - | - | 66 | 24/6 |
| 0.5 | 1 | 0.506 | - | - | 239 | 11/7 |
| 0.5 | 1 | 1.003 | - | - | 54 | 24/6 |
| 0.5 | 1 | 1.394 | - | - | 60 | 24/6 |
| 0.5 | 1.25 | 0.503 | - | - | 86 | 27/6 |
| 0.5 | 1.25 | 1.003 | - | - | 55 | 24/6 |
| 0.75 | 0.2 | 0.667 | - | - | 449 | 10/8 |
| 0.75 | 0.2 | 1 | - | - | 445 | 10/8 |
| 0.75 | 0.35 | 0.667 | - | - | 450 | 10/8 |
| 0.75 | 0.35 | 1 | - | - | 446 | 10/8 |
| 0.75 | 0.5 | 0.667 | - | - | 451 | 10/8 |
| 0.75 | 0.5 | 1 | - | - | 447 | 10/8 |
| 1 | 0.2 | 0.566 | - | - | 114 | 27/6 |
| 1 | 0.2 | 0.667 | - | - | 453 | 10/8 |
| 1 | 0.2 | 0.667 | - | - | 327 | 14/7 |
| 1 | 0.2 | 0.668 | - | - | 107 | 27/6 |
| 1 | 0.2 | 0.81 | - | - | 100 | 27/6 |
| 1 | 0.2 | 1 | - | - | 463 | 11/8 |
| 1 | 0.2 | 1 | - | - | 317 | 13/7 |
| 1 | 0.2 | 1.001 | - | - | 93 | 27/6 |
| 1 | 0.2 | 1.353 | - | - | 88 | 27/6 |
| 1 | 0.2 | 1.5 | - | - | 469 | 11/8 |
| 1 | 0.2 | 1.5 | - | - | 307 | 13/7 |
| 1 | 0.2 | 2 | - | - | 476 | 11/8 |
| 1 | 0.35 | 0.566 | - | - | 115 | 27/6 |
| 1 | 0.35 | 0.667 | - | - | 454 | 10/8 |
| 1 | 0.35 | 0.667 | - | - | 328 | 14/7 |
| 1 | 0.35 | 0.668 | - | - | 108 | 27/6 |
| 1 | 0.35 | 0.808 | - | - | 101 | 27/6 |
| 1 | 0.35 | 1 | - | - | 318 | 13/7 |
| 1 | 0.35 | 1 | - | - | 464 | 11/8 |
| 1 | 0.35 | 1.001 | - | - | 94 | 27/6 |
| 1 | 0.35 | 1.353 | - | - | 89 | 27/6 |
| 1 | 0.35 | 1.5 | - | - | 470 | 11/8 |
| 1 | 0.35 | 1.5 | - | - | 308 | 13/7 |
| 1 | 0.5 | 0.571 | - | - | 116 | 27/6 |
| 1 | 0.5 | 0.667 | - | - | 329 | 14/7 |
| 1 | 0.5 | 0.667 | - | - | 455 | 10/8 |
| 1 | 0.5 | 0.668 | - | - | 109 | 27/6 |
| 1 | 0.5 | 0.823 | - | - | 102 | 27/6 |
| 1 | 0.5 | 1 | - | - | 465 | 11/8 |
| 1 | 0.5 | 1 | - | - | 319 | 13/7 |
| 1 | 0.5 | 1.001 | - | - | 95 | 27/6 |
| 1 | 0.5 | 1.353 | - | - | 90 | 27/6 |
| 1 | 0.5 | 1.5 | - | - | 309 | 13/7 |
| 1 | 0.5 | 1.5 | - | - | 471 | 11/8 |
| 1 | 0.5 | 2 | - | - | 477 | 9/8 |

180

| A/D | V(m/s) | To (s) | Tw (s) | Hw | Run | date |
|-----|--------|--------|--------|-----|-----|------|
| 1 | 0.75 | 0.552 | - | - | 117 | 27/6 |
| 1 | 0.75 | 0.667 | - | - | 330 | 14/7 |
| 1 | 0.75 | 0.668 | - | - | 110 | 27/6 |
| 1 | 0.75 | 0.808 | - | - | 103 | 27/6 |
| 1 | 0.75 | 0.997 | - | - | 96 | 27/6 |
| 1 | 0.75 | 1 | - | - | 320 | 13/7 |
| 1 | 0.75 | 1.353 | - | - | 91 | 27/6 |
| 1 | 0.75 | 1.5 | - | - | 472 | 11/8 |
| 1 | 0.75 | 1.5 | - | - | 310 | 13/7 |
| 1 | 1 | 0.565 | - | - | 118 | 27/6 |
| 1 | 1 | 0.668 | - | - | 111 | 27/6 |
| 1 | 1 | 0.808 | - | - | 104 | 27/6 |
| 1 | 1 | 0.99 | - | - | 97 | 27/6 |
| 1 | 1.25 | 0.565 | - | - | 119 | 27/6 |
| 1 | 1.25 | 0.668 | - | - | 112 | 27/6 |
| 1 | 1.25 | 0.808 | - | - | 105 | 27/6 |
| 1 | 1.25 | 0.998 | - | - | 98 | 27/6 |
| 1 | 1.5 | 0.569 | - | - | 120 | 27/6 |
| 1.5 | 0.2 | 0.811 | - | - | 136 | 28/6 |
| 1.5 | 0.2 | 1 | - | - | 365 | 14/7 |
| 1.5 | 0.2 | 1.002 | - | - | 129 | 28/6 |
| 1.5 | 0.2 | 1.389 | - | - | 122 | 27/6 |
| 1.5 | 0.2 | 1.5 | - | - | 375 | 14/7 |
| 1.5 | 0.2 | 1.702 | - | - | 143 | 28/6 |
| 1.5 | 0.35 | 0.811 | - | - | 137 | 28/6 |
| 1.5 | 0.35 | 1 | - | - | 366 | 14/7 |
| 1.5 | 0.35 | 1.002 | - | - | 130 | 28/6 |
| 1.5 | 0.35 | 1.389 | - | - | 123 | 27/6 |
| 1.5 | 0.35 | 1.5 | - | - | 376 | 14/7 |
| 1.5 | 0.35 | 1.702 | - | - | 144 | 28/6 |
| 1.5 | 0.5 | 0.811 | - | - | 138 | 28/6 |
| 1.5 | 0.5 | 1 | - | - | 367 | 14/7 |
| 1.5 | 0.5 | 1.002 | - | - | 131 | 28/6 |
| 1.5 | 0.5 | 1.389 | - | - | 124 | 27/6 |
| 1.5 | 0.5 | 1.5 | - | - | 377 | 14/7 |
| 1.5 | 0.5 | 1.702 | - | - | 145 | 28/6 |
| 1.5 | 0.75 | 0.811 | - | - | 139 | 28/6 |
| 1.5 | 0.75 | 0.999 | - | - | 132 | 28/6 |
| 1.5 | 0.75 | 1 | - | - | 368 | 14/7 |
| 1.5 | 0.75 | 1.366 | - | - | 125 | 27/6 |
| 1.5 | 0.75 | 1.702 | - | - | 146 | 28/6 |
| 1.5 | 1 | 0.811 | - | - | 140 | 28/6 |
| 1.5 | 1 | 0.999 | - | - | 133 | 28/6 |
| 1.5 | 1 | 1.366 | - | - | 126 | 27/6 |
| 1.5 | 1 | 1.702 | - | - | 147 | 28/6 |
| 1.5 | 1.25 | 0.808 | - | - | 141 | 28/6 |
| 1.5 | 1.25 | 1.367 | - | - | 127 | 27/6 |

| A/D | V(m/s) | To (s) | Tw (s) | Hw | Run | date |
|-----|--------|--------|--------|-----|-----|------|
| 1.5 | 1.25 | 1.001 | - | - | 134 | 28/6 |
| 2 | 0.2 | 1 | - | - | 391 | 15/7 |
| 2 | 0.2 | 1.005 | - | - | 167 | 28/6 |
| 2 | 0.2 | 1.2 | - | - | 161 | 28/6 |
| 2 | 0.2 | 1.388 | - | - | 155 | 28/6 |
| 2 | 0.2 | 1.5 | - | - | 395 | 15/7 |
| 2 | 0.2 | 1.696 | - | - | 149 | 28/6 |
| 2 | 0.35 | 1 | - | - | 392 | 15/7 |
| 2 | 0.35 | 1.005 | - | - | 168 | 28/6 |
| 2 | 0.35 | 1.2 | - | - | 162 | 28/6 |
| 2 | 0.35 | 1.388 | - | - | 156 | 28/6 |
| 2 | 0.35 | 1.5 | - | - | 396 | 15/7 |
| 2 | 0.35 | 1.696 | - | - | 150 | 28/6 |
| 2 | 0.5 | 1 | - | - | 393 | 15/7 |
| 2 | 0.5 | 1.005 | - | - | 169 | 28/6 |
| 2 | 0.5 | 1.2 | - | - | 163 | 28/6 |
| 2 | 0.5 | 1.388 | - | - | 157 | 28/6 |
| 2 | 0.5 | 1.5 | - | - | 397 | 15/7 |
| 2 | 0.5 | 1.696 | - | - | 151 | 28/6 |
| 2 | 0.75 | 1.017 | - | - | 170 | 28/6 |
| 2 | 0.75 | 1.2 | - | - | 164 | 28/6 |
| 2 | 0.75 | 1.388 | - | - | 158 | 28/6 |
| 2 | 0.75 | 1.696 | - | - | 152 | 28/6 |
| 2 | 1 | 1.003 | - | - | 171 | 28/6 |
| 2 | 1 | 1.2 | - | - | 165 | 28/6 |
| 2 | 1 | 1.388 | - | - | 159 | 28/6 |
| 2 | 1 | 1.696 | - | - | 153 | 28/6 |
| 2 | 1.25 | 1.084 | - | - | 172 | 28/6 |
| 2.5 | 0.2 | 1.201 | - | - | 188 | 28/6 |
| 2.5 | 0.2 | 1.39 | - | - | 181 | 28/6 |
| 2.5 | 0.2 | 1.5 | - | - | 429 | 15/7 |
| 2.5 | 0.2 | 1.7 | - | - | 174 | 28/6 |
| 2.5 | 0.35 | 1.201 | - | - | 189 | 28/6 |
| 2.5 | 0.35 | 1.39 | - | - | 182 | 28/6 |
| 2.5 | 0.35 | 1.5 | - | - | 430 | 15/7 |
| 2.5 | 0.35 | 1.7 | - | - | 175 | 28/6 |
| 2.5 | 0.5 | 1.201 | - | - | 190 | 28/6 |
| 2.5 | 0.5 | 1.39 | - | - | 183 | 28/6 |
| 2.5 | 0.5 | 1.5 | - | - | 431 | 15/7 |
| 2.5 | 0.5 | 1.675 | - | - | 176 | 28/6 |
| 2.5 | 0.75 | 1.201 | - | - | 191 | 28/6 |
| 2.5 | 0.75 | 1.39 | - | - | 184 | 28/6 |
| 2.5 | 0.75 | 1.5 | - | - | 432 | 15/7 |
| 2.5 | 0.75 | 1.7 | - | - | 177 | 28/6 |
| 2.5 | 1 | 1.201 | - | - | 192 | 28/6 |
| 2.5 | 1 | 1.39 | - | - | 185 | 28/6 |
| 2.5 | 1.25 | 1.201 | - | - | 193 | 28/6 |

182

| A/D | V(m/s) | To (s) | Tw (s) | Hw | Run | date |
|-----|--------|--------|--------|-----|-----|------|
| 2.5 | 1 | 1.7 | - | - | 178 | 28/6 |
| 2.5 | 1.25 | 1.39 | - | - | 186 | 28/6 |
| 2.5 | 1.25 | 1.7 | - | - | 179 | 28/6 |
| 3 | 0.2 | 1.5 | - | - | 419 | 15/7 |
| 3 | 0.35 | 1.5 | - | - | 420 | 15/7 |
| 3 | 0.5 | 1.5 | - | - | 421 | 15/7 |
| 3 | 0.75 | 1.5 | - | - | 422 | 15/7 |
| 4 | 0.2 | 2 | - | - | 480 | 9/8 |
| 4 | 0.35 | 2 | - | - | 481 | 9/8 |
| 4 | 0.5 | 2 | - | - | 482 | 9/8 |
| 4 | 0.75 | 2 | - | - | 483 | 9/8 |
| 3 | 0.2 | 1.206 | - | - | 216 | 29/6 |
| 3 | 0.2 | 1.392 | - | - | 210 | 29/6 |
| 3 | 0.2 | 1.702 | - | - | 204 | 29/6 |
| 3 | 0.2 | 1.996 | - | - | 198 | 29/6 |
| 3 | 0.35 | 1.206 | - | - | 217 | 29/6 |
| 3 | 0.35 | 1.397 | - | - | 211 | 29/6 |
| 3 | 0.35 | 1.702 | - | - | 205 | 29/6 |
| 3 | 0.35 | 1.996 | - | - | 199 | 29/6 |
| 3 | 0.5 | 1.206 | - | - | 218 | 29/6 |
| 3 | 0.5 | 1.397 | - | - | 212 | 29/6 |
| 3 | 0.5 | 1.702 | - | - | 206 | 29/6 |
| 3 | 0.5 | 1.996 | - | - | 200 | 29/6 |
| 3 | 0.75 | 1.206 | - | - | 219 | 29/6 |
| 3 | 0.75 | 1.397 | - | - | 213 | 29/6 |
| 3 | 0.75 | 1.702 | - | - | 207 | 29/6 |
| 3 | 0.75 | 1.996 | - | - | 201 | 29/6 |
| 3 | 1 | 1.206 | - | - | 220 | 29/6 |
| 3 | 1 | 1.397 | - | - | 214 | 29/6 |
| 3 | 1 | 1.702 | - | - | 208 | 29/6 |
| 3 | 1 | 1.996 | - | - | 202 | 29/6 |

## 7. Transverse Oscillation in Waves (Regular and Irregular)

| A/D | V(m/s) | To (s) | Tw (s) | Hw | Run | date |
|-----|--------|--------|--------|-----|-----|------|
| 0.5 | - | 0.666 | 1 | H1 | 294 | 13/7 |
| 0.5 | - | 1 | 1 | H1 | 298 | 13/7 |
| 0.5 | - | 1.5 | 1 | H1 | 302 | 13/7 |
| 0.5 | 0.05 | 0.667 | 1.5 | H2 | 258 | 12/7 |
| 0.5 | 0.05 | 1 | 1.5 | H2 | 253 | 12/7 |
| 0.5 | 0.05 | 1.5 | 1.5 | H2 | 248 | 12/7 |
| 0.5 | - | 0.667 | 2 | H3 | 286 | 13/7 |
| 0.5 | 0.05 | 1 | 2 | H3 | 282 | 13/7 |
| 0.5 | 0.05 | 1.5 | 2 | H3 | 277 | 13/7 |
| 0.5 | - | 0.667 | | H4 | 490 | 12/8 |
| 0.5 | - | 1 | | H4 | 489 | 12/8 |
| 0.5 | - | 1.5 | | H4 | 491 | 12/8 |
| 0.5 | - | 2 | | H4 | 492 | 12/8 |

| A/D | V(m/s) | To (s) | Tw (s) | Hw | Run | date |
|---|---|---|---|---|---|---|
| 1 | - | 0.667 | 1 | H1 | 331 | 14/7 |
| 1 | - | 1 | 1 | H1 | 321 | 13/7 |
| 1 | - | 1.5 | 1 | H1 | 311 | 13/7 |
| 1 | - | 0.667 | 1.5 | H2 | 336 | 14/7 |
| 1 | - | 1 | 1.5 | H2 | 340 | 14/7 |
| 1 | - | 1.5 | 1.5 | H2 | 344 | 14/7 |
| 1 | - | 0.667 | 2 | H3 | 360 | 14/7 |
| 1 | - | 1 | 2 | H3 | 356 | 14/7 |
| 1 | - | 1.5 | 2 | H3 | 352 | 14/7 |
| 1 | - | 0.667 | | H4 | 457 | 10/8 |
| 1 | - | 1 | | H4 | 467 | 11/8 |
| 1 | - | 1.5 | | H4 | 473 | 11/8 |
| 1 | - | 2 | | H4 | 478 | 9/8 |
| 1.5 | - | 1 | 1 | H1 | 382 | 14/7 |
| 1.5 | - | 1.5 | 1 | H1 | 386 | 14/7 |
| 1.5 | - | 1 | 2 | H3 | 369 | 14/7 |
| 1.5 | - | 1.5 | 2 | H3 | 378 | 14/7 |
| 2 | - | 1 | 1.5 | H2 | 398 | 15/7 |
| 2 | - | 1.5 | 1.5 | H2 | 402 | 15/7 |
| 2 | - | 1 | 2 | H3 | 410 | 15/7 |
| 2 | - | 1.5 | 2 | H3 | 406 | 15/7 |
| 2.5 | - | 1.5 | 1.5 | H3 | 433 | 15/7 |
| 3 | - | 1.5 | 2 | H3 | 423 | 15/7 |

## 8. Transverse Oscillation in Waves while Towing

| A/D | V(m/s) | To (s) | Tw (s) | Hw | Run | date |
|---|---|---|---|---|---|---|
| 0.5 | 0.2 | 0.666 | 1 | H1 | 295 | 13/7 |
| 0.5 | 0.2 | 1 | 1 | H1 | 299 | 13/7 |
| 0.5 | 0.2 | 1.5 | 1 | H1 | 303 | 13/7 |
| 0.5 | 0.35 | 1.5 | 1 | H1 | 304 | 13/7 |
| 0.5 | 0.35 | 0.666 | 1 | H1 | 296 | 13/7 |
| 0.5 | 0.35 | 1 | 1 | H1 | 300 | 13/7 |
| 0.5 | 0.5 | 0.666 | 1 | H1 | 297 | 13/7 |
| 0.5 | 0.5 | 1 | 1 | H1 | 301 | 13/7 |
| 0.5 | 0.5 | 1.5 | 1 | H1 | 305 | 13/7 |
| 0.5 | 0.2 | 1 | 1.5 | H2 | 254 | 12/7 |
| 0.5 | 0.2 | 1.5 | 1.5 | H2 | 249 | 12/7 |
| 0.5 | 0.2 | 0.667 | 1.5 | H2 | 259 | 12/7 |
| 0.5 | 0.35 | 1 | 1.5 | H2 | 255 | 12/7 |
| 0.5 | 0.35 | 1.5 | 1.5 | H2 | 250 | 12/7 |
| 0.5 | 0.35 | 0.667 | 1.5 | H2 | 260 | 12/7 |
| 0.5 | 0.5 | 1 | 1.5 | H2 | 256 | 12/7 |
| 0.5 | 0.5 | 0.667 | 1.5 | H2 | 261 | 12/7 |
| 0.5 | 0.5 | 1.5 | 1.5 | H2 | 251 | 12/7 |
| 0.5 | 0.75 | 1.5 | 1.5 | H2 | 252 | 12/7 |
| 0.5 | 0.75 | 1 | 1.5 | H2 | 257 | 12/7 |
| 0.5 | 0.75 | 0.667 | 1.5 | H2 | 262 | 12/7 |

| A/D | V(m/s) | To (s) | Tw (s) | Hw | Run | date |
|-----|--------|--------|--------|-----|-----|------|
| 0.5 | 0.2 | 1.5 | 2 | H3 | 278 | 13/7 |
| 0.5 | 0.2 | 1 | 2 | H3 | 283 | 13/7 |
| 0.5 | 0.2 | 0.667 | 2 | H3 | 287 | 13/7 |
| 0.5 | 0.35 | 1.5 | 2 | H3 | 279 | 13/7 |
| 0.5 | 0.35 | 1 | 2 | H3 | 284 | 13/7 |
| 0.5 | 0.35 | 0.667 | 2 | H3 | 288 | 13/7 |
| 0.5 | 0.5 | 1.5 | 2 | H3 | 280 | 13/7 |
| 0.5 | 0.5 | 1 | 2 | H3 | 285 | 13/7 |
| 0.5 | 0.5 | 0.667 | 2 | H3 | 289 | 13/7 |
| 0.5 | 0.75 | 1.5 | 2 | H3 | 281 | 13/7 |
| 0.5 | 0.2 | 1.5 | | H4 | 496 | 12/8 |
| 0.5 | 0.2 | 2 | | H4 | 497 | 12/8 |
| 0.5 | 0.2 | 0.667 | | H4 | 495 | 12/8 |
| 0.5 | 0.2 | 1 | | H4 | 494 | 12/8 |
| 1 | 0.2 | 0.667 | 1 | H1 | 332 | 14/7 |
| 1 | 0.2 | 1.5 | 1 | H1 | 312 | 13/7 |
| 1 | 0.2 | 1 | 1 | H1 | 322 | 13/7 |
| 1 | 0.35 | 1.5 | 1 | H1 | 313 | 13/7 |
| 1 | 0.35 | 1 | 1 | H1 | 323 | 13/7 |
| 1 | 0.35 | 0.667 | 1 | H1 | 333 | 14/7 |
| 1 | 0.5 | 1.5 | 1 | H1 | 314 | 13/7 |
| 1 | 0.5 | 1 | 1 | H1 | 324 | 13/7 |
| 1 | 0.5 | 0.667 | 1 | H1 | 334 | 14/7 |
| 1 | 0.75 | 1.5 | 1 | H1 | 315 | 13/7 |
| 1 | 0.75 | 0.667 | 1 | H1 | 335 | 14/7 |
| 1 | -0.2 | 1.5 | 1.5 | H2 | 350 | 14/7 |
| 1 | -0.35 | 1.5 | 1.5 | H2 | 349 | 14/7 |
| 1 | -0.5 | 1.5 | 1.5 | H2 | 348 | 14/7 |
| 1 | 0.2 | 1.5 | 1.5 | H2 | 345 | 14/7 |
| 1 | 0.2 | 1 | 1.5 | H2 | 341 | 14/7 |
| 1 | 0.2 | 0.667 | 1.5 | H2 | 337 | 14/7 |
| 1 | 0.35 | 1 | 1.5 | H2 | 342 | 14/7 |
| 1 | 0.35 | 0.667 | 1.5 | H2 | 338 | 14/7 |
| 1 | 0.35 | 1.5 | 1.5 | H2 | 346 | 14/7 |
| 1 | 0.5 | 1.5 | 1.5 | H2 | 347 | 14/7 |
| 1 | 0.5 | 0.667 | 1.5 | H2 | 339 | 14/7 |
| 1 | 0.5 | 1 | 1.5 | H2 | 343 | 14/7 |
| 1 | 0.2 | 1 | 2 | H3 | 357 | 14/7 |
| 1 | 0.2 | 1.5 | 2 | H3 | 353 | 14/7 |
| 1 | 0.2 | 0.667 | 2 | H3 | 361 | 14/7 |
| 1 | 0.35 | 0.667 | 2 | H3 | 362 | 14/7 |
| 1 | 0.35 | 1 | 2 | H3 | 358 | 14/7 |
| 1 | 0.35 | 1.5 | 2 | H3 | 354 | 14/7 |
| 1 | 0.5 | 1.5 | 2 | H3 | 355 | 14/7 |
| 1 | 0.5 | 1 | 2 | H3 | 359 | 14/7 |
| 1 | 0.5 | 0.667 | 2 | H3 | 363 | 14/7 |
| 1 | 0.2 | 1 | | H4 | 468 | 11/8 |

| A/D | V(m/s) | To (s) | Tw (s) | Hw | Run | date |
|-----|--------|--------|--------|-----|-----|------|
| 1 | 0.2 | 0.667 | | H4 | 458 | 10/8 |
| 1 | 0.2 | 1.5 | | H4 | 474 | 11/8 |
| 1.5 | 0.2 | 1.5 | 1 | H1 | 387 | 14/7 |
| 1.5 | 0.2 | 1 | 1 | H1 | 383 | 14/7 |
| 1.5 | 0.35 | 1.5 | 1 | H1 | 388 | 14/7 |
| 1.5 | 0.35 | 1 | 1 | H1 | 384 | 14/7 |
| 1.5 | 0.5 | 1 | 1 | H1 | 385 | 14/7 |
| 1.5 | 0.5 | 1.5 | 1 | H1 | 389 | 14/7 |
| 1.5 | 0.2 | 1.5 | 2 | H3 | 379 | 14/7 |
| 1.5 | 0.2 | 1 | 2 | H3 | 370 | 14/7 |
| 1.5 | 0.35 | 1 | 2 | H3 | 371 | 14/7 |
| 1.5 | 0.35 | 1.5 | 2 | H3 | 380 | 14/7 |
| 1.5 | 0.5 | 1 | 2 | H3 | 372 | 14/7 |
| 1.5 | 0.5 | 1.5 | 2 | H3 | 381 | 14/7 |
| 1.5 | 0.75 | 1 | 2 | H3 | 373 | 14/7 |
| 2 | 0.2 | 1 | 1.5 | H2 | 399 | 15/7 |
| 2 | 0.2 | 1.5 | 1.5 | H2 | 403 | 15/7 |
| 2 | 0.35 | 1.5 | 1.5 | H2 | 404 | 15/7 |
| 2 | 0.35 | 1 | 1.5 | H2 | 400 | 15/7 |
| 2 | 0.5 | 1 | 1.5 | H2 | 401 | 15/7 |
| 2 | 0.5 | 1.5 | 1.5 | H2 | 405 | 15/7 |
| 2 | 0.2 | 1.5 | 2 | H3 | 407 | 15/7 |
| 2 | 0.2 | 1 | 2 | H3 | 411 | 15/7 |
| 2 | 0.35 | 1 | 2 | H3 | 412 | 15/7 |
| 2 | 0.35 | 1.5 | 2 | H3 | 408 | 15/7 |
| 2 | 0.5 | 1 | 2 | H3 | 413 | 15/7 |
| 2 | 0.5 | 1.5 | 2 | H3 | 409 | 15/7 |
| 2.5 | 0.2 | 1.5 | 1.5 | H3 | 434 | 15/7 |
| 2.5 | 0.35 | 1.5 | 1.5 | H3 | 435 | 15/7 |
| 2.5 | 0.5 | 1.5 | 1.5 | H3 | 436 | 15/7 |
| 3 | 0.2 | 1.5 | 2 | H3 | 424 | 15/7 |
| 3 | 0.35 | 1.5 | 2 | H3 | 425 | 15/7 |
| 3 | 0.5 | 1.5 | 2 | H3 | 426 | 15/7 |
| 3 | 0.75 | 1.5 | 2 | H3 | 427 | 15/7 |

## 9. In-line Oscillation in Waves

| V (m/s) | A (m) | To (s) | Tw (s) | Hw | Run | Date |
|---------|-------|--------|--------|-----|-----|------|
| - | 0.03 | 0.5 | 1 | H1 | 602 | 21/7 |
| - | 0.03 | 1 | 1 | H1 | 598 | 21/7 |
| - | 0.03 | 1 | 1 | H1 | 877 | 2/8 |
| - | 0.03 | 1.5 | 1 | H1 | 594 | 21/7 |
| - | 0.03 | 2 | 1 | H1 | 590 | 20/7 |
| - | 0.03 | 2 | 1 | H1 | 588 | 20/7 |
| - | 0.03 | 0.5 | 1.5 | H2 | 567 | 20/7 |
| - | 0.03 | 0.667 | 1.5 | H2 | 571 | 20/7 |
| - | 0.03 | 1 | 1.5 | H2 | 575 | 20/7 |
| - | 0.03 | 1.5 | 1.5 | H2 | 579 | 20/7 |

186

| A/D | V(m/s) | To (s) | Tw (s) | Hw | Run | date |
|---|---|---|---|---|---|---|
| - | 0.03 | 2 | 1.5 | H2 | 583 | 20/7 |
| - | 0.03 | 0.5 | 2 | H3 | 561 | 20/7 |
| - | 0.03 | 0.667 | 2 | H3 | 556 | 20/7 |
| - | 0.03 | 1 | 2 | H3 | 548 | 19/7 |
| - | 0.03 | 1.5 | 2 | H3 | 543 | 19/7 |
| - | 0.03 | 2 | 2 | H3 | 538 | 19/7 |
| - | 0.03 | 0.667 | | H4 | 889 | 4/8 |
| - | 0.03 | 1 | | H4 | 883 | 3/8 |
| - | 0.03 | 1.5 | | H4 | 884 | 3/8 |
| - | 0.03 | 2 | | H4 | 882 | 3/8 |
| - | 0.045 | 1 | | H4 | 932 | 9/8 |
| - | 0.045 | 1.5 | | H4 | 926 | 9/8 |
| - | 0.045 | 1.5 | | H4 | 930 | 9/8 |
| - | 0.045 | 2 | | H4 | 925 | 9/8 |
| - | 0.045 | 2 | | H4 | 931 | 9/8 |
| - | 0.06 | 0.667 | 1 | H1 | 707 | 25/7 |
| - | 0.06 | 0.667 | 1 | H1 | 664 | 22/7 |
| - | 0.06 | 0.668 | 1 | H1 | 703 | 22/7 |
| - | 0.06 | 1 | 1 | H1 | 699 | 22/7 |
| - | 0.06 | 1.5 | 1 | H1 | 694 | 22/7 |
| - | 0.06 | 2 | 1 | H1 | 690 | 22/7 |
| - | 0.06 | 0.667 | 1.5 | H2 | 669 | 22/7 |
| - | 0.06 | 0.995 | 1.5 | H2 | 673 | 22/7 |
| - | 0.06 | 1 | 1.5 | H2 | 677 | 22/7 |
| - | 0.06 | 1.5 | 1.5 | H2 | 68! | 22/7 |
| - | 0.06 | 2 | 1.5 | H2 | 685 | 22/7 |
| - | 0.06 | 1.5 | 2 | H3 | 660 | 22/7 |
| - | 0.06 | 1.5 | 2 | H3 | 653 | 22/7 |
| - | 0.06 | 2 | 2 | H3 | 639 | 21/7 |
| - | 0.06 | 2 | 2 | H3 | 640 | 21/7 |
| - | 0.06 | 2 | 2 | H3 | 632 | 21/7 |
| - | 0.06 | 2 | 2 | H3 | 634 | 21/7 |
| - | 0.06 | 2 | 2 | H3 | 631 | 21/7 |
| - | 0.06 | 2 | 2 | H3 | 635 | 21/7 |
| - | 0.06 | 2 | 2 | H3 | 636 | 21/7 |
| - | 0.06 | 2 | 2 | H3 | 641 | 21/7 |
| - | 0.06 | 2 | 2 | H3 | 637 | 21/7 |
| - | 0.06 | 2 | 2 | H3 | 638 | 21/7 |
| - | 0.06 | 2 | 2 | H3 | 633 | 21/7 |
| - | 0.06 | 2 | 2 | H3 | 642 | 21/7 |
| - | 0.06 | 2 | 2 | H3 | 644 | 21/7 |
| - | 0.06 | 2 | 2 | H3 | 645 | 21/7 |
| - | 0.06 | 2 | 2 | H3 | 643 | 21/7 |
| - | 0.06 | 0.667 | | H4 | 891 | 4/8 |
| - | 0.06 | 1 | | H4 | 892 | 4/8 |
| - | 0.06 | 1 | | H4 | 896 | 4/8 |
| - | 0.06 | 1.25 | | H4 | 895 | 4/8 |

| A/D | V(m/s) | To (s) | Tw (s) | Hw | Run | date |
|---|---|---|---|---|---|---|
| - | 0.06 | 1.5 | | H4 | 893 | 4/8 |
| - | 0.06 | 2 | | H4 | 901 | 5/8 |
| - | 0.06 | 2 | | H4 | 894 | 4/8 |
| - | 0.06 | 3 | | H4 | 905 | 8/8 |
| - | 0.09 | 1 | 1.5 | H2 | 745 | 25/7 |
| - | 0.09 | 1.5 | 1.5 | H2 | 741 | 25/7 |
| - | 0.09 | 2 | 1.5 | H2 | 737 | 25/7 |
| - | 0.09 | 1 | 2 | H3 | 717 | 25/7 |
| - | 0.09 | 1.5 | 2 | H3 | 725 | 25/7 |
| - | 0.09 | 2 | 2 | H3 | 733 | 25/7 |
| - | 0.12 | 1 | 1.5 | H2 | 757 | 26/7 |
| - | 0.12 | 1.5 | 1.5 | H2 | 777 | 26/7 |
| - | 0.12 | 2 | 1.5 | H2 | 788 | 27/7 |
| - | 0.12 | 1 | 2 | H3 | 762 | 26/7 |
| - | 0.12 | 1.5 | 2 | H3 | 773 | 26/7 |
| - | 0.12 | 2 | 2 | H3 | 792 | 27/7 |
| - | 0.15 | 1.5 | 1.5 | H2 | 816 | 28/7 |
| - | 0.15 | 2 | 1.5 | H2 | 805 | 27/7 |
| - | 0.15 | 2 | 1.5 | H2 | 820 | 28/7 |
| - | 0.15 | 2 | 2 | H3 | 801 | 27/7 |
| - | 0.18 | 1.5 | 1.5 | H2 | 837 | 29/7 |
| - | 0.18 | 2 | 1.5 | H2 | 829 | 29/7 |
| - | 0.18 | 1.5 | 2 | H3 | 841 | 29/7 |
| - | 0.18 | 2 | 2 | H3 | 844 | 29/7 |
| - | 0.21 | 2 | 1.5 | H2 | 869 | 2/8 |
| - | 0.21 | 2 | 2 | H3 | 872 | 2/8 |
| - | 0.24 | 2 | 1.5 | H2 | 859 | 1/8 |
| - | 0.24 | 2 | 2 | H3 | 855 | 29/7 |

## 10. In-line Oscillation While Towing the Cylinder

| V (m/s) | A (m) | To (s) | Tw (s) | Hw | Run | Date |
|---|---|---|---|---|---|---|
| 0.5 | 0.03 | 0.5 | - | - | 528 | 19/7 |
| 0.75 | 0.03 | 0.5 | - | - | 529 | 19/7 |
| 0.35 | 0.03 | 0.5 | - | - | 527 | 19/7 |
| 0.2 | 0.03 | 0.5 | - | - | 526 | 19/7 |
| 0.35 | 0.03 | 0.668 | - | - | 522 | 19/7 |
| 0.5 | 0.03 | 0.668 | - | - | 523 | 19/7 |
| 0.75 | 0.03 | 0.668 | - | - | 524 | 19/7 |
| 0.2 | 0.03 | 0.668 | - | - | 521 | 19/7 |
| 0.75 | 0.03 | 1 | - | - | 518 | 19/7 |
| 0.2 | 0.03 | 1 | - | - | 515 | 19/7 |
| 0.35 | 0.03 | 1 | - | - | 516 | 19/7 |
| 1 | 0.03 | 1 | - | - | 519 | 19/7 |
| 0.5 | 0.03 | 1 | - | - | 517 | 19/7 |
| 0.5 | 0.03 | 1.5 | - | - | 532 | 19/7 |
| 0.35 | 0.03 | 1.5 | - | - | 531 | 19/7 |
| 0.75 | 0.03 | 1.5 | - | - | 533 | 19/7 |

| V (m/s) | A (m) | To (s) | Tw (s) | Hw | Run | Date |
|---------|-------|--------|--------|-----|-----|------|
| 0.2 | 0.03 | 1.5 | - | - | 530 | 19/7 |
| 0.5 | 0.03 | 2 | - | - | 536 | 19/7 |
| 0.2 | 0.03 | 2 | - | - | 534 | 19/7 |
| 0.35 | 0.03 | 2 | - | - | 535 | 19/7 |
| 0.2 | 0.045 | 0.667 | - | - | 907 | 8/8 |
| 0.2 | 0.045 | 0.667 | - | - | 908 | 8/8 |
| 0.75 | 0.045 | 0.667 | - | - | 911 | 8/8 |
| 0.5 | 0.045 | 0.667 | - | - | 910 | 8/8 |
| 0.35 | 0.045 | 0.667 | - | - | 909 | 8/8 |
| 0.35 | 0.045 | 1 | - | - | 914 | 8/8 |
| 0.2 | 0.045 | 1 | - | - | 913 | 8/8 |
| 0.5 | 0.045 | 1 | - | - | 915 | 8/8 |
| 0.2 | 0.045 | 1.5 | - | - | 918 | 9/8 |
| 0.35 | 0.045 | 1.5 | - | - | 919 | 9/8 |
| 0.5 | 0.045 | 1.5 | - | - | 920 | 9/8 |
| 0.35 | 0.045 | 2 | - | - | 923 | 9/8 |
| 0.2 | 0.045 | 2 | - | - | 922 | 9/8 |
| 0.5 | 0.045 | 2 | - | - | 924 | 9/8 |
| 0.5 | 0.06 | 0.667 | - | - | 609 | 21/7 |
| 0.35 | 0.06 | 0.667 | - | - | 608 | 21/7 |
| 0.2 | 0.06 | 0.667 | - | - | 607 | 21/7 |
| 1 | 0.06 | 0.667 | - | - | 611 | 21/7 |
| 0.75 | 0.06 | 0.667 | - | - | 610 | 21/7 |
| 0.2 | 0.06 | 1 | - | - | 613 | 21/7 |
| 0.5 | 0.06 | 1 | - | - | 615 | 21/7 |
| 0.75 | 0.06 | 1 | - | - | 616 | 21/7 |
| 0.35 | 0.06 | 1 | - | - | 614 | 21/7 |
| 1 | 0.06 | 1 | - | - | 617 | 21/7 |
| -0.5 | 0.06 | 1.5 | - | - | 657 | 22/7 |
| 0.75 | 0.06 | 1.5 | - | - | 622 | 21/7 |
| 0.5 | 0.06 | 1.5 | - | - | 621 | 21/7 |
| 1 | 0.06 | 1.5 | - | - | 623 | 21/7 |
| 0.5 | 0.06 | 1.5 | - | - | 656 | 22/7 |
| 0.35 | 0.06 | 1.5 | - | - | 620 | 21/7 |
| 0.35 | 0.06 | 1.5 | - | - | 655 | 22/7 |
| 0.2 | 0.06 | 1.5 | - | - | 654 | 22/7 |
| 0.2 | 0.06 | 1.5 | - | - | 619 | 21/7 |
| 0.75 | 0.06 | 2 | - | - | 628 | 21/7 |
| 0.2 | 0.06 | 2 | - | - | 625 | 21/7 |
| 0.35 | 0.06 | 2 | - | - | 626 | 21/7 |
| 0.5 | 0.06 | 2 | - | - | 627 | 21/7 |
| 1 | 0.06 | 2 | - | - | 629 | 21/7 |
| 0.5 | 0.09 | 1.5 | - | - | 714 | 25/7 |
| 0.5 | 0.09 | 1.5 | - | - | 724 | 25/7 |
| 0.75 | 0.09 | 1.5 | - | - | 715 | 25/7 |
| 0.35 | 0.09 | 1.5 | - | - | 713 | 25/7 |
| 0.35 | 0.09 | 1.5 | - | - | 723 | 25/7 |

| V (m/s) | A (m) | To (s) | Tw (s) | Hw | Run | Date |
|---------|-------|--------|--------|-----|-----|------|
| 0.2 | 0.09 | 1.5 | - | - | 712 | 25/7 |
| 0.2 | 0.09 | 1.5 | - | - | 722 | 25/7 |
| 0.5 | 0.09 | 2 | - | - | 732 | 25/7 |
| 0.35 | 0.09 | 2 | - | - | 731 | 25/7 |
| 0.2 | 0.09 | 2 | - | - | 730 | 25/7 |
| 0.5 | 0.12 | 1 | - | - | 754 | 26/7 |
| 0.75 | 0.12 | 1 | - | - | 755 | 26/7 |
| 0.35 | 0.12 | 1 | - | - | 753 | 26/7 |
| 0.2 | 0.12 | 1 | - | - | 752 | 26/7 |
| 0.35 | 0.12 | 1.5 | - | - | 768 | 26/7 |
| 0.5 | 0.12 | 1.5 | - | - | 769 | 26/7 |
| 0.75 | 0.12 | 1.5 | - | - | 770 | 26/7 |
| 0.2 | 0.12 | 1.5 | - | - | 767 | 26/7 |
| 0.75 | 0.12 | 2 | - | - | 786 | 27/7 |
| 0.35 | 0.12 | 2 | - | - | 783 | 26/7 |
| 0.2 | 0.12 | 2 | - | - | 782 | 26/7 |
| 0.5 | 0.12 | 2 | - | - | 784 | 26/7 |
| 0.5 | 0.15 | 1.5 | - | - | 812 | 27/7 |
| 0.75 | 0.15 | 1.5 | - | - | 813 | 27/7 |
| 0.2 | 0.15 | 1.5 | - | - | 810 | 27/7 |
| 0.35 | 0.15 | 1.5 | - | - | 811 | 27/7 |
| 0.35 | 0.15 | 2 | - | - | 798 | 27/7 |
| 0.75 | 0.15 | 2 | - | - | 800 | 27/7 |
| 0.2 | 0.15 | 2 | - | - | 797 | 27/7 |
| 0.5 | 0.15 | 2 | - | - | 799 | 27/7 |
| 0.2 | 0.18 | 1.25 | - | - | 847 | 29/7 |
| 0.5 | 0.18 | 1.25 | - | - | 849 | 29/7 |
| 0.35 | 0.18 | 1.25 | - | - | 848 | 29/7 |
| 0.5 | 0.18 | 1.5 | - | - | 835 | 29/7 |
| 0.2 | 0.18 | 1.5 | - | - | 833 | 29/7 |
| 0.75 | 0.18 | 1.5 | - | - | 836 | 29/7 |
| 0.35 | 0.18 | 1.5 | - | - | 834 | 29/7 |
| 0.35 | 0.18 | 2 | - | - | 825 | 29/7 |
| 0.2 | 0.18 | 2 | - | - | 824 | 29/7 |
| 0.5 | 0.18 | 2 | - | - | 826 | 29/7 |
| 0.75 | 0.18 | 2 | - | - | 827 | 29/7 |
| 0.75 | 0.21 | 2 | - | - | 866 | 1/8 |
| 0.2 | 0.21 | 2 | - | - | 863 | 1/8 |
| 0.5 | 0.21 | 2 | - | - | 865 | 1/8 |
| 0.35 | 0.21 | 2 | - | - | 864 | 1/8 |
| 0.75 | 0.24 | 2 | - | - | 854 | 29/7 |
| 0.5 | 0.24 | 2 | - | - | 853 | 29/7 |
| 0.2 | 0.24 | 2 | - | - | 851 | 29/7 |
| 0.35 | 0.24 | 2 | - | - | 852 | 29/7 |

190

## 11. In-line Oscillation In Waves while Towing the Cylinder

| V (m/s) | A (m) | To (s) | Tw (s) | Hw | Run | Date |
|---------|-------|--------|--------|-----|-----|------|
| 0.2 | 0.03 | 0.5 | 1 | H1 | 604 | 21/7 |
| 0.2 | 0.03 | 0.667 | 1 | H1 | 601 | 21/7 |
| 0.2 | 0.03 | 1 | 1 | H1 | 599 | 21/7 |
| 0.2 | 0.03 | 1 | 1 | H1 | 878 | 2/8 |
| 0.2 | 0.03 | 1.5 | 1 | H1 | 595 | 21/7 |
| 0.2 | 0.03 | 2 | 1 | H1 | 591 | 20/7 |
| 0.35 | 0.03 | 0.5 | 1 | H1 | 605 | 21/7 |
| 0.35 | 0.03 | 0.667 | 1 | H1 | 602 | 21/7 |
| 0.35 | 0.03 | 0.667 | 1 | H1 | 600 | 21/7 |
| 0.35 | 0.03 | 1 | 1 | H1 | 879 | 2/8 |
| 0.35 | 0.03 | 1 | 1 | H1 | 597 | 21/7 |
| 0.35 | 0.03 | 1.5 | 1 | H1 | 596 | 21/7 |
| 0.75 | 0.03 | 2 | 1 | H1 | 589 | 20/7 |
| 0.2 | 0.03 | 0.5 | 1.5 | H2 | 568 | 20/7 |
| 0.2 | 0.03 | 0.667 | 1.5 | H2 | 572 | 20/7 |
| 0.2 | 0.03 | 1 | 1.5 | H2 | 576 | 20/7 |
| 0.2 | 0.03 | 1.5 | 1.5 | H2 | 580 | 20/7 |
| 0.2 | 0.03 | 2 | 1.5 | H2 | 584 | 20/7 |
| 0.35 | 0.03 | 0.5 | 1.5 | H2 | 569 | 20/7 |
| 0.35 | 0.03 | 0.667 | 1.5 | H2 | 573 | 20/7 |
| 0.35 | 0.03 | 1 | 1.5 | H2 | 577 | 20/7 |
| 0.35 | 0.03 | 1.5 | 1.5 | H2 | 581 | 20/7 |
| 0.35 | 0.03 | 2 | 1.5 | H2 | 585 | 20/7 |
| 0.5 | 0.03 | 0.5 | 1.5 | H2 | 570 | 20/7 |
| 0.5 | 0.03 | 0.667 | 1.5 | H2 | 574 | 20/7 |
| 0.5 | 0.03 | 1 | 1.5 | H2 | 578 | 20/7 |
| 0.5 | 0.03 | 1.5 | 1.5 | H2 | 582 | 20/7 |
| 0.5 | 0.03 | 2 | 1.5 | H2 | 586 | 20/7 |
| 0.2 | 0.03 | 0.5 | 2 | H3 | 562 | 20/7 |
| 0.2 | 0.03 | 0.667 | 2 | H3 | 557 | 20/7 |
| 0.2 | 0.03 | 1 | 2 | H3 | 549 | 19/7 |
| 0.2 | 0.03 | 1.5 | 2 | H3 | 544 | 19/7 |
| 0.2 | 0.03 | 2 | 2 | H3 | 539 | 19/7 |
| 0.35 | 0.03 | 0.5 | 2 | H3 | 563 | 20/7 |
| 0.35 | 0.03 | 0.667 | 2 | H3 | 558 | 20/7 |
| 0.35 | 0.03 | 1 | 2 | H3 | 550 | 19/7 |
| 0.35 | 0.03 | 1.5 | 2 | H3 | 545 | 19/7 |
| 0.35 | 0.03 | 2 | 2 | H3 | 540 | 19/7 |
| 0.5 | 0.03 | 0.5 | 2 | H3 | 564 | 20/7 |
| 0.5 | 0.03 | 0.667 | 2 | H3 | 559 | 20/7 |
| 0.5 | 0.03 | 1 | 2 | H3 | 551 | 19/7 |
| 0.5 | 0.03 | 1.5 | 2 | H3 | 546 | 19/7 |
| 0.5 | 0.03 | 2 | 2 | H3 | 541 | 19/7 |
| 0.75 | 0.03 | 0.5 | 2 | H3 | 565 | 20/7 |
| 0.75 | 0.03 | 0.667 | 2 | H3 | 560 | 20/7 |
| 0.75 | 0.03 | 1 | 2 | H3 | 552 | 19/7 |

| V (m/s) | A (m) | To (s) | Tw (s) | Hw | Run | Date |
|---------|-------|--------|--------|-----|-----|------|
| 0.75 | 0.03 | 1.5 | 2 | H3 | 547 | 19/7 |
| 0.75 | 0.03 | 2 | 2 | H3 | 542 | 19/7 |
| 0.2 | 0.03 | 1.5 | | H4 | 886 | 3/8 |
| 0.2 | 0.045 | 1.5 | | H4 | 928 | 9/8 |
| 0.2 | 0.045 | 1.5 | | H4 | 934 | 9/8 |
| 0.2 | 0.045 | 2 | | H4 | 933 | 9/8 |
| 0.2 | 0.045 | 2 | | H4 | 927 | 9/8 |
| 0.2 | 0.06 | 0.667 | 1 | H1 | 708 | 25/7 |
| 0.2 | 0.06 | 0.667 | 1 | H1 | 665 | 22/7 |
| 0.2 | 0.06 | 1 | 1 | H1 | 700 | 22/7 |
| 0.2 | 0.06 | 1.5 | 1 | H1 | 695 | 22/7 |
| 0.2 | 0.06 | 2 | 1 | H1 | 691 | 22/7 |
| 0.35 | 0.06 | 0.667 | 1 | H1 | 666 | 22/7 |
| 0.35 | 0.06 | 0.667 | 1 | H1 | 709 | 25/7 |
| 0.35 | 0.06 | 1 | 1 | H1 | 701 | 22/7 |
| 0.35 | 0.06 | 1 | 1 | H1 | 662 | 22/7 |
| 0.35 | 0.06 | 1.5 | 1 | H1 | 696 | 22/7 |
| 0.35 | 0.06 | 2 | 1 | H1 | 692 | 22/7 |
| 0.5 | 0.06 | 0.667 | 1 | H1 | 667 | 22/7 |
| 0.5 | 0.06 | 0.667 | 1 | H1 | 710 | 25/7 |
| 0.5 | 0.06 | 1 | 1 | H1 | 702 | 22/7 |
| 0.5 | 0.06 | 1 | 1 | H1 | 663 | 22/7 |
| 0.5 | 0.06 | 1.5 | 1 | H1 | 697 | 22/7 |
| 0.5 | 0.06 | 2 | 1 | H1 | 693 | 22/7 |
| 0.2 | 0.06 | 0.667 | 1.5 | H2 | 670 | 22/7 |
| 0.2 | 0.06 | 0.995 | 1.5 | H2 | 674 | 22/7 |
| 0.2 | 0.06 | 1 | 1.5 | H2 | 678 | 22/7 |
| 0.2 | 0.06 | 1.5 | 1.5 | H2 | 682 | 22/7 |
| 0.2 | 0.06 | 2 | 1.5 | H2 | 686 | 22/7 |
| 0.35 | 0.06 | 0.667 | 1.5 | H2 | 671 | 22/7 |
| 0.35 | 0.06 | 0.995 | 1.5 | H2 | 675 | 22/7 |
| 0.35 | 0.06 | 1 | 1.5 | H2 | 679 | 22/7 |
| 0.35 | 0.06 | 1.5 | 1.5 | H2 | 683 | 22/7 |
| 0.35 | 0.06 | 2 | 1.5 | H2 | 687 | 22/7 |
| 0.5 | 0.06 | 0.667 | 1.5 | H2 | 672 | 22/7 |
| 0.5 | 0.06 | 0.995 | 1.5 | H2 | 676 | 22/7 |
| 0.5 | 0.06 | 1 | 1.5 | H2 | 680 | 22/7 |
| 0.5 | 0.06 | 1.5 | 1.5 | H2 | 684 | 22/7 |
| 0.5 | 0.06 | 2 | 1.5 | H2 | 688 | 22/7 |
| -0.35 | 0.06 | 1.5 | 2 | H3 | 658 | 22/7 |
| -0.2 | 0.06 | 1.5 | 2 | H3 | 659 | 22/7 |
| 0.2 | 0.06 | 1 | 2 | H3 | 661 | 22/7 |
| 0.2 | 0.06 | 2 | 2 | H3 | 646 | 21/7 |
| 0.35 | 0.06 | 2 | 2 | H3 | 647 | 21/7 |
| 0.5 | 0.06 | 2 | 2 | H3 | 648 | 21/7 |
| 0.75 | 0.06 | 2 | 2 | H3 | 649 | 21/7 |
| 1 | 0.06 | 2 | 2 | H3 | 650 | 21/7 |

| V (m/s) | A (m) | To (s) | Tw (s) | Hw | Run | Date |
|---------|-------|--------|--------|-----|-----|------|
| 0.2 | 0.06 | 1 | | H4 | 897 | 4/8 |
| 0.2 | 0.06 | 1.5 | | H4 | 899 | 5/8 |
| 0.2 | 0.06 | 2 | | H4 | 900 | 5/8 |
| 0.2 | 0.06 | 3 | | H4 | 902 | 5/8 |
| 0.2 | 0.09 | 1 | 1.5 | H2 | 746 | 25/7 |
| 0.2 | 0.09 | 1.5 | 1.5 | H2 | 742 | 25/7 |
| 0.2 | 0.09 | 2 | 1.5 | H2 | 738 | 25/7 |
| 0.35 | 0.09 | 1 | 1.5 | H2 | 747 | 25/7 |
| 0.35 | 0.09 | 1.5 | 1.5 | H2 | 743 | 25/7 |
| 0.35 | 0.09 | 2 | 1.5 | H2 | 739 | 25/7 |
| 0.5 | 0.09 | 1 | 1.5 | H2 | 748 | 25/7 |
| 0.5 | 0.09 | 1.5 | 1.5 | H2 | 744 | 25/7 |
| 0.5 | 0.09 | 2 | 1.5 | H2 | 740 | 25/7 |
| 0.2 | 0.09 | 1 | 2 | H3 | 718 | 25/7 |
| 0.2 | 0.09 | 1.5 | 2 | H3 | 726 | 25/7 |
| 0.2 | 0.09 | 2 | 2 | H3 | 734 | 25/7 |
| 0.35 | 0.09 | 1 | 2 | H3 | 719 | 25/7 |
| 0.35 | 0.09 | 1.5 | 2 | H3 | 727 | 25/7 |
| 0.35 | 0.09 | 2 | 2 | H3 | 735 | 25/7 |
| 0.5 | 0.09 | 0.997 | 2 | H3 | 720 | 25/7 |
| 0.5 | 0.09 | 1.5 | 2 | H3 | 728 | 25/7 |
| 0.5 | 0.09 | 2 | 2 | H3 | 736 | 25/7 |
| 0.2 | 0.12 | 1 | 1.5 | H2 | 758 | 26/7 |
| 0.2 | 0.12 | 1.5 | 1.5 | H2 | 778 | 26/7 |
| 0.2 | 0.12 | 2 | 1.5 | H2 | 789 | 27/7 |
| 0.35 | 0.12 | 1 | 1.5 | H2 | 759 | 26/7 |
| 0.35 | 0.12 | 1.5 | 1.5 | H2 | 779 | 26/7 |
| 0.35 | 0.12 | 2 | 1.5 | H2 | 790 | 27/7 |
| 0.5 | 0.12 | 1 | 1.5 | H2 | 760 | 26/7 |
| 0.5 | 0.12 | 1.5 | 1.5 | H2 | 780 | 26/7 |
| 0.5 | 0.12 | 2 | 1.5 | H2 | 791 | 27/7 |
| 0.2 | 0.12 | 1 | 2 | H3 | 763 | 26/7 |
| 0.2 | 0.12 | 1.5 | 2 | H3 | 774 | 26/7 |
| 0.2 | 0.12 | 2 | 2 | H3 | 793 | 27/7 |
| 0.35 | 0.12 | 1 | 2 | H3 | 764 | 26/7 |
| 0.35 | 0.12 | 1.5 | 2 | H3 | 775 | 26/7 |
| 0.35 | 0.12 | 2 | 2 | H3 | 794 | 27/7 |
| 0.5 | 0.12 | 1 | 2 | H3 | 765 | 26/7 |
| 0.5 | 0.12 | 1.5 | 2 | H3 | 776 | 26/7 |
| 0.5 | 0.12 | 2 | 2 | H3 | 795 | 27/7 |
| 0.2 | 0.15 | 1.5 | 1.5 | H2 | 817 | 28/7 |
| 0.2 | 0.15 | 2 | 1.5 | H2 | 806 | 27/7 |
| 0.35 | 0.15 | 1.5 | 1.5 | H2 | 818 | 28/7 |
| 0.35 | 0.15 | 2 | 1.5 | H2 | 807 | 27/7 |
| 0.35 | 0.15 | 2 | 1.5 | H2 | 821 | 28/7 |
| 0.5 | 0.15 | 1.5 | 1.5 | H2 | 819 | 28/7 |
| 0.5 | 0.15 | 2 | 1.5 | H2 | 808 | 27/7 |

| V (m/s) | A (m) | To (s) | Tw (s) | Hw | Run | Date |
|---------|-------|--------|--------|-----|-----|------|
| 0.2 | 0.15 | 2 | 2 | H3 | 802 | 27/7 |
| 0.35 | 0.15 | 2 | 2 | H3 | 803 | 27/7 |
| 0.5 | 0.15 | 2 | 2 | H3 | 804 | 27/7 |
| 0.2 | 0.18 | 1.5 | 1.5 | H2 | 838 | 29/7 |
| 0.2 | 0.18 | 2 | 1.5 | H2 | 830 | 29/7 |
| 0.35 | 0.18 | 1.5 | 1.5 | H2 | 839 | 29/7 |
| 0.35 | 0.18 | 2 | 1.5 | H2 | 831 | 29/7 |
| 0.2 | 0.18 | 1.5 | 2 | H3 | 842 | 29/7 |
| 0.2 | 0.18 | 2 | 2 | H3 | 845 | 29/7 |
| 0.35 | 0.18 | 1.5 | 2 | H3 | 843 | 29/7 |
| 0.2 | 0.21 | 2 | 1.5 | H2 | 870 | 2/8 |
| 0.35 | 0.21 | 2 | 1.5 | H2 | 871 | 2/8 |
| 0.2 | 0.21 | 2 | 2 | H3 | 873 | 2/8 |
| 0.35 | 0.21 | 2 | 2 | H3 | 874 | 2/8 |
| 0.2 | 0.24 | 2 | 1.5 | H2 | 860 | 1/8 |
| 0.35 | 0.24 | 2 | 1.5 | H2 | 861 | 1/8 |
| 0.2 | 0.24 | 2 | 2 | H3 | 856 | 29/7 |
| 0.35 | 0.24 | 2 | 2 | H3 | 857 | 29/7 |

194

# APPENDIX III

## Influence of Surface Wake

A current passing a vertical cylinder disturbs the pressure field around the cylinder and generates a run-up at the "front" of the cylinder and a corresponding drawdown "behind" the cylinder resulting in an additional drag force acting locally on the cylinder. This additional force will, of course, act only near the water surface. For a cylinder of finite length, the wake pressure distribution will also influence the three-dimensional flow pattern near the submerged cylinder end. The influences of surface wakes on cylinder drag has been studied in the past, see, e.g. Massie (1980) and Hogben (1974). Many investigators have worked with a surface piercing cylinder of finite length upon which they have measured or calculated a total force as a function of submerged length. However, in these investigations the wake pressure distribution will influence the three-dimensional flow pattern and therefore the influences of submerged length and pressure wake are combined.

In the present study, the hydrodynamic forces have been measured on two or three short segments of a vertical cylinder. To examine the effect of the free surface wake, a simple model given by Massie (1980) has been used. In this model it is assumed that the total force measured on a segment is the sum of its form drag force and its surface wake drag:

$$F = F_w + F_D$$

where: $F_w$ is the surface wake force, a function of submergence, and $F_D$ is the form drag force. This can also be expressed in terms of drag coefficients by dividing each term by $1/2 \rho V^2 D$ which then yields:

$$C_R = C_w + C_D$$

$C_w$ depends on a submergence parameter, $SP$. This submergence parameter itself depends on three independent variables, $V$, $D$, and $z$:

$$C_w = K \cdot SP$$

$$SP = \frac{f(Fr_s)}{Fr_D^2}$$

Where K is a constant, $Fr_S$ and $Fr_D$ are submergence and diameter Froude numbers respectively:

$$Fr_s = \frac{V}{\sqrt{gz}}$$

$$Fr_D = \frac{V}{\sqrt{gD}}$$

Massie (1980) has used a dimensionless submergence, $z/D$, and the diameter Froude number, $Fr_D$, for tabulating the submergence parameter. Using the table and graph given in Massie (1980), the submergence parameters, $SP$, are determined for the three rings of the cylinder, see table III-1. Assuming $K=1.0$, the results indicate that the effect of surface wakes on ring no. 1 is negligible

195

while it is considerable on ring no. 3. Table III-2 lists measured and corrected drag coefficients for the lower rings (no. 1 and no. 2) when V=1 m/s.

The difference between (averaged) measured mean drag coefficients of ring no.1 and ring no. 2 for $V = 1$ m/s was 0.092. This is much more than the difference between SP values given in table III.1 for the same velocity. Having such a difference indicates that: either the constant K is more than unity (K≈2.14) or other factors have also affected the measured forces, e.g. end effects.

Even with K = 2.14, the influence of free surface on ring no.1 (which has been used in the present work) is negligible for $V \le 0.5$ m/s which form the bulk of the test runs.

| $Fr_D$ | 0.26 | 0.46 | 0.65 | 0.98 | 1.2 | 1.96 |
|---|---|---|---|---|---|---|
| $V$ m/s | 0.20 | 0.35 | 0.50 | 0.75 | 1.0 | 1.5 |
| SP values: | | | | | | |
| ring no. 3 | - | 0.008 | 0.065 | 0.131 | 0.155 | 0.09 |
| ring no. 2 | - | - | 0.027 | 0.060 | 0.087 | 0.077 |
| ring no. 1 | - | - | - | 0.023 | 0.044 | 0.065 |

Table III-1  The values of the submergence parameter at different levels

| Ring | $C_R$ | $C_W$ | $C_D$ | $C_D/C_R$ |
|---|---|---|---|---|
| 1 | 1.110 | 0.087 | 1.068 | 0.96 |
| 2 | 1.202 | 0.044 | 1.119 | 0.93 |

Table III-2 Measured and corrected mean drag coefficients, $V$≈1 m/s

# APPENDIX IV

## Determination of the Relative Period

The relative period is the period of the combined flow field resulting from the cylinder oscillation in waves. The velocity of forced sinusoidal cylinder motion can be expressed as:

$$\dot{x}(t) = A_o \omega_o \sin(\omega_o t - \phi_o)$$

And, the horizontal water particle velocity due to waves as:

$$u(t) = A_w \omega_w \sin(\omega_w t - \phi_w)$$

Then the relative velocity is:

$$V_{rel}(t) = u(t) - \dot{x}(t) = A_w \omega_w \sin(\omega_w t - \phi_w) - A_o \omega_o \sin(\omega_o t - \phi_o)$$

The relative period $T_r$ is defined as the time interval for which the velocity in the combined flow field reaches the same value, that is to say the time for which:

$$V_{rel}(t + T_r) = V_r(t)$$

So:

$$u(t + T_r) - \dot{x}(t + T_r) = u(t) - \dot{x}(t)$$

Using the following relationship:

$$\sin(p) - \sin(q) = 2\sin(\frac{p-q}{2})\cos(\frac{p+q}{2})$$

one may write:

$$2A_w \omega_w \sin(\frac{\omega_w T_r}{2}) \cos(\omega_w t + \frac{\omega_w T_r}{2} - \phi_w) - 2A_o \omega_o \sin(\frac{\omega_o T_r}{2})\cos(\omega_o t + \frac{\omega_o T_r}{2} - \phi_o) = 0$$

or in a simplified way:

$$f(t)\sin(\frac{\omega_w T_r}{2}) - g(t)\sin(\frac{\omega_o T_r}{2}) = 0$$

where $f(t)$ and $g(t)$ are independent functions. This relationship should be satisfied for all t. Thus, it is necessary that:

$$\frac{\omega_w T_r}{2} = n_1 \pi$$

$$\frac{\omega_o T_r}{2} = n_2 \pi$$

where $n_1$ and $n_2$ are the two lowest possible integers. Therefore, the relative period $T$ may be calculated as:

$$T_r = n_1 T_w$$
$$T_r = n_2 T_o$$

This is in turn a definition of the least common multiple for two integers. To determine the relative period, one needs to find the least common multiple of the periods of motion.

# APPENDIX V

## Correlation Coefficients

In the present work, the $R^2$ correlation coefficient has been used to reflect the extent of a linear relationship between two data sets as well as to evaluate the suitability of the regression lines. The $R^2$ coefficient returns the square of the Pearson product moment correlation coefficient through data points (in known y's and x's). The Pearson product moment correlation coefficient, $R$, is a dimensionless index that ranges from -1.0 to 1.0 inclusive, i.e. $0 \leq R^2 \leq 1$.

The $R^2$ value can be interpreted as the proportion of the variance in $y$ attributable to the variance in $x$. The equation for the $R$ value is:

$$R = \frac{n(\sum xy) - (\sum x)(\sum y)}{\sqrt{[n\sum x^2 - (\sum x)^2][n\sum y^2 - (\sum y)^2]}}$$

Note that *the $R^2$* correlation coefficient is also the square of the normal correlation coefficient ($\rho$) which is usually used to determine the relationship between two properties, i.e $R^2 = \rho^2$. The equation for this correlation coefficient is:

$$\rho_{xy} = \frac{Cov(x,y)}{\sigma_x \cdot \sigma_y}$$

where:

$$-1 \leq \rho_{xy} \leq 1$$

and:

$$Cov(x,y) = \frac{1}{n}\sum_{i=1}^{n}(x_i - \mu_x)(y_i - \mu_y)$$

$$\sigma_x = \sqrt{\frac{n\sum x^2 - (\sum x)^2}{n^2}}$$

$$\mu_x = \frac{1}{n}\sum x$$

Thus one may convert the $R^2$ correlation coefficients obtained to the normal correlation coefficients as:

$$\rho = \sqrt{R^2}$$

Since $R^2 \leq 1$, the normal correlation coefficients would be larger than the reported values for $R^2$.

**Curriculum Vitae**

Mehdi Shafiee-Far was born on October 23, 1958 in Ghom, Iran. He started his study in Civil Engineering at the Faculty of Engineering of Tabriz University, Tabriz, Iran in 1976. When all universities in Iran were closed for three years during his third study year, he worked in a construction company and a government organization for developments of rural areas. He was involved in construction of roads and hydraulic structures. He received his B.Sc. degree from the reopened Tabriz University in 1984.

After graduation he joined a consulting engineering company where he worked in various capacities designing and supervising construction of hydraulic structures till 1987.

In 1988 he obtained a M.Sc. Degree from the Department of Civil Engineering, Iran University of Science and Technology, Tehran.

In 1988-1989 he attended a postgraduate course in Coastal and Offshore Engineering at the International Institute of Hydraulic and Environmental Engineering (IHE) in Delft, The Netherlands and obtained the Diploma of Hydraulic Engineering.

In May 1990 he came to IHE for the second time and obtained a Master of Science degree in Hydraulic Engineering (study branch of Coastal and Offshore Engineering) in February 1991. He returned to the consulting engineering company in Iran and worked as project manager for more than a year.

From April 1992 he has worked as a Research Fellow with the Offshore Technology Group of the Delft University of Technology in Delft, The Netherlands. During his thesis work, he has written several reports and articles and participated and gave presentations in several conferences and seminars in The Netherlands, Belgium, Great Britain, Norway and the United States of America.